SENSIBLE HEAT FLUX AND EVAPORATION FOR SPARSE VEGETATION USING TEMPERATURE-VARIANCE AND A DUAL-SOURCE MODEL

by

MICHAEL G. ABRAHA

Submitted in fulfillment of the academic requirements of the degree of

Doctor of Philosophy

in Agrometeorology
Soil-Plant-Atmosphere-Continuum Research Unit
School of Environmental Sciences
Faculty of Science and Agriculture
University of KwaZulu-Natal
Pietermaritzburg
South Africa

March, 2010

Preface

The research contained in this dissertation was carried out in the Discipline of Agrometeorology, School of Environmental Sciences, Faculty of Science and Agriculture, University of KwaZulu-Natal, Pietermaritzburg. The research undertaken here was financially supported by the Water Research Commission and University of KwaZulu-Natal.

The duration of this study was from January 2005 to October 2009.

The contents of this work have not been submitted in any form to another university and, except where the work of others is acknowledged in the text, the results are the authors own investigation.

The research was completed under the supervision of:
MJ Savage, Senior Professor of Agrometeorology, School of Environmental Sciences

As the candidate's supervisor, I agree to the submission of this thesis for examination.

Professor MJ Savage:
Signed ……
Date …….

DECLARATION 1 - Plagiarism

I ..... declare that

(i) The research reported in this dissertation, except where otherwise indicated, is my original work.

(ii) This dissertation has not been submitted for any degree or examination at any other university.

(iii) This dissertation does not contain other persons' data, pictures, graphs or other information, unless specifically acknowledged as being sourced from other persons.

(iv) This dissertation does not contain other persons' writing, unless specifically acknowledged as being sourced from other researchers. Where other written sources have been quoted, then:
a) their words have been re-written but the general information attributed to them has been referenced;
b) where their exact words have been used, their writing has been placed inside quotation marks, and referenced.

(v) Where I have reproduced a publication of which I am an author, co-author or editor, I have indicated in detail which part of the publication was actually written by myself alone and have fully referenced such publications.

(vi) This dissertation does not contain text, graphics or tables copied and pasted from the Internet, unless specifically acknowledged, and the source being detailed in the dissertation and in the References sections.

Signed: ……

DECLARATION 2 - publications in preparation

1. Abraha MG, Savage MJ (2009) Sensible heat flux estimation using temperature-variance over different surfaces. In preparation.

2. Abraha MG, Savage MJ (2009) Seasonal water-use assessment of *Jatropha curcas* using temperature-variance and surface renewal methods. In preparation.

3. Abraha MG, Savage MJ (2009) Validation of a three-dimensional solar irradiance interception model for tree crops. In preparation.

4. Abraha MG, Savage MJ (2009) Evaporation estimation over sparse vegetation using single- and dual-source models. In preparation.

5. Abraha MG, Savage MJ (2009) Estimating sensible heat flux from radiometric temperature over sparse tree crops. In preparation.

Collection, analysis and interpretation of the data used in all the above mentioned manuscripts, as well as the organization and write-up is accomplished by the author of this dissertation. The contribution of my supervisor, Professor MJ Savage, was in providing helpful comments and suggestions as well as proofreading of the manuscripts.

ACKNOWLEDGMENTS

I wish to express my warmest and heartfelt gratitude to Prof. MJ Savage for his invaluable ideas and suggestions, and support during the supervision.

I would also like to extend my special thanks to - Mrs. J Manickum for facilitating field and office works, Ms. Bernie Hoosen and Ms. Thembeka Latha for administrative works, and Mrs. Meryl Savage for her hospitality and most needed assistance.

My sincere appreciation also goes to current and former students of Agrometeorology Discipline, University of KwaZulu-Natal (UKZN), N Moyo, E Nile, G Odhiambo and M Mengistu; and S Ghezehei of the Department of Plant Production and Soil science, University of Pretoria for the highly valued discussions and comments.

Funding from UKZN, Water Research Commission (WRC) and Council for Scientific and Industrial Research (CSIR) is gratefully acknowledged.

Assistance from the CSIR staff, and particularly, Prof. CS Everson, Alistair Clulow, Lelethu Sinuka and Joshua Xaba in facilitating field related activities is gratefully acknowledged.

Special thanks are due to my friends Y Ghile, G Adhanom, D Russom, M Frezghi, A Hailu, Eden Frezghi, T Mabhaudhi, Senait Tecle and Mebrahtu Amaha; and friends at home (Eritrea) M Ageba, M Ghebregiorgis, M Yohannes, T Tekeste, Y Tecle, G Ristu and E Melake for their support and encouragement.

I would also like to thank my parents and siblings for the moral support and patience during my study; and to the Heavenly Father for His love, goodness and grace!

ABSTRACT

The high population growth rate and rapid urbanization that the world is experiencing today has aggravated the competition for the already scarce resource – water – between the agricultural sector and the other economic sectors. Moreover, within the agricultural sector, water is increasingly being used for commercial plantations as opposed to growing food crops, threatening food security. Therefore, it is very important that this scarce resource is managed in an efficient and sustainable manner, for now and future use. This requires understanding the process of evaporation for accurate determination of water-use from agricultural lands. In the past, direct measurements of evaporation have proven difficult because of the cost and complexity of the available equipments, and level of expertise involved. This justifies a quest for relatively simple, accurate and inexpensive methods of determining evaporation for routine field applications. Estimation of sensible heat flux (H) from high frequency air temperature measurements and then calculating latent energy flux (λE) and hence evaporation as a residual of the shortened surface energy balance equation, assuming that closure is met, is appealing in this sense. Concurrent net irradiance (R_n) and soil heat flux (G) measurements can be conducted with relative ease for use in the energy balance equation. Alternately, evaporation can also be mathematically modelled, using single- or multi-layer models depending on vegetation cover, from less expensive routine meteorological observations. Therefore, the ultimate objective of this study is to estimate and model H and λE, and thereby evaporation, accurately over sparsely vegetated agricultural lands at low cost and effort.

Temperature-variance (TV) and surface renewal (SR) methods, which use high-frequency (typically 2 to 10 Hz) air temperature measurements, are employed for estimation of H. The TV method is based on the Monin and Obukhov Similarity Theory (MOST) and uses statistical measures of the high frequency air temperature to estimate H, including adjustments for stability. The SR method is based on the principle that an air parcel near the surface is renewed by an air parcel from above and, to determine H, it uses higher order air temperature differences between two consecutive sample measurements lagged by a certain time interval. Single- and double-layer models that are based on energy and resistance combination theory were also used to estimate evaporation and H from sparse vegetation. Single- and double-layer models that were extended to include inputs of

radiometric temperature in order to estimate H were also used. The transmission of solar irradiance to the soil beneath in sparse canopies is variable and depends on the vegetation density, cover and apparent position of the sun. A three-dimensional radiation interception model was developed to estimate this transmission of solar irradiance and was used as a sub-module in the double-layer models. Estimations of H from the TV (H_{TV}), SR (H_{SR}) and double-layer models were compared against H obtained from eddy covariance (H_{EC}), and the modelled λE (single- and double-layer) were compared with that obtained from the shortened energy balance involving H_{EC}. Besides, long-term λE calculated from the shortened energy balance using H_{TV} and H_{SR} were compared with those calculated using H_{EC}.

Unshielded and naturally-ventilated fine-wire chromel-constantan thermocouples (TCs), 75 μm in diameter, at different heights above the ground over sparse *Jatropha curcas* trees, mixed grassland community and bare fallow land were used to measure air temperature. A three-dimensional sonic anemometer mounted at a certain height above the ground surface was also used to measure virtual temperature and wind speed at all three sites. All measurements were done differentially at 10-Hz frequency. Additional measurements of R_n, G and soil water content (upper 60 mm) were also made.

The Jatropha trees were planted in a 3-m plant and inter-row spacing in a 50 m × 60 m plot with the surrounding plots planted to a mixture of Jatropha trees and Kikuyu grass. Average tree height and leaf area index measurements were taken on monthly and bimonthly basis respectively. An automatic weather station about 10 m away from the edge of the Jatropha plot was also used to obtain solar irradiance, air temperature and relative humidity, wind speed and direction and precipitation data. Soil water content was measured to a depth of 1000 mm from the surface at 200 mm intervals. Soil and foliage surface temperatures were measured using two nadir-looking infrared thermometers with one mounted directly above bare soil and the other above the trees.

The three-dimensional solar irradiance interception model was validated using measurements conducted on different trees and planting patterns. Solar irradiance above and below tree canopies was measured using LI-200 pyranometer and tube solarimeters respectively. Leaf area density (*LAD*) was estimated from *LAI*, canopy shape and volume

measurements. It was also determined by scanning leaves using either destructive sampling or tracing method.

The performance of the TV method over sparse vegetation of *J. curcas*, mixed grassland community and fallow land was evaluated against H_{EC}. Atmospheric stability conditions were identified using (i) sensor height (z) and Obukhov length (L) obtained from EC and (ii) air temperature difference between two thermocouple measurement heights. The H_{TV} estimations, adjusted and not adjusted for skewness (actual and estimated) of air temperature (s_k), for unstable conditions only and for all stability conditions were used. An improved agreement in terms of slope, coefficient of determination (r^2) and root mean square error (*RMSE*), almost over all surfaces, was obtained when the temperature difference rather than the z/L means of identifying stability conditions was used. The agreement between the H_{TV} and H_{EC} was improved for estimations adjusted for actual s_k than not adjusted for s_k. Improved agreement was also noted when H_{TV} was adjusted using estimated s_k compared to not adjusting for s_k over *J. curcas*. The TV method could be used to estimate H for surfaces with varying homogeneity with reasonable accuracy.

Long-term water-use of a fetch-limited sparse vegetation of *J. curcas* was determined as a residual of the shortened surface energy balance involving H_{TV} and H_{SR} and compared with those estimated using H_{EC}. Concurrent measurements of R_n and G were also performed. The long-term water-use of *J. curcas* trees calculated from the shortened surface energy balance involving H_{TV} and H_{SR} agreed very well when compared with those obtained from H_{EC}. The seasonal H_{TV} and H_{SR} also agreed very well when compared with H_{EC}. Changes in structure of the canopy and environmental conditions appeared to influence partitioning of the available energy into H and λE. The seasonal total evaporation for the EC, TV and SR methods amounted to 626, 640 and 674 mm respectively with a total rainfall of 690 mm. Footprint analysis also revealed that greater than 80% of the measured flux during the day originates from within the surface of interest. The TV and SR methods, therefore, offer a relatively low-cost means for long-term estimation of H, and λE, hence the total evaporation, using the shortened surface energy balance along with measurements of R_n and G.

Evaporation and biomass production estimations from tree crops requires accurate representation of solar irradiance transmission through the canopy. A relatively simple three-dimensional, hourly time-step tree-canopy radiation interception model was

developed and validated using measurements conducted on isolated trees, hedgerows and tree canopies arranged in tramline mode. Measurements were obtained using tube solarimeters placed 0.5 m from each other starting from the base of a tree trunk in four directions, along and perpendicular to the row up to mid-way between trees and rows. Model-simulations of hourly radiant transmittance were in good agreement with measurements with an overall r^2 of 0.91; Willmott's index of agreement of 0.96; and general absolute standard deviation of 17.66%. Agreement between model-estimations and measurements, however, was influenced by distance and direction of the node from the tree trunk, sky conditions, symmetry of the canopy, and uniformity of the stand and leaf distribution of the canopy. The model could be useful in planning and management applications for a wide range of tree crops.

Penman-Monteith (PM) equation and the Shuttleworth and Wallace (SW) model, representing single- and dual-source models respectively, were used to determine the total evaporation over a sparse vegetation of *J. curcas* from routine automatic weather station observations, resistance parameters and vegetation indices. The three-dimensional solar irradiance interception model was used as a sub-module in the SW model. The total evaporation from the sparse vegetation was also determined as a residual of the shortened surface energy balance using measurements of R_n, G and H_{EC}. The PM equation failed to reproduce the 'measured' daily total evaporation during periods of low *LAI*, with improved agreement with increased *LAI*. The SW model, however, produced total evaporation estimates that agreed very well with the 'measured' with a slope of 0.96, r^2 of 0.91 and *RMSE* of 0.45 mm for a *LAI* ranging from 0 (no leaves) to 1.83 m^2 m^{-2}. The SW model also estimated soil evaporation and plant transpiration separately, and about 66 % of the cumulative evaporation was attributed to soil evaporation. These findings suggest that the PM equation should be replaced by the SW model for surfaces that assume a range of *LAI* values during the growing season.

The *H* was estimated using (i) SW model that was further developed to include surface radiometric temperature measurements; (ii) one-layer model, but linked with a two-layer model for estimation of excess resistance, that uses surface radiometric temperature; and (iii) the SW model (unmodified). The agreement between modelled and measured *H*, using 10-min data, was in general reasonably good with *RMSE* (W m^{-2}) of 45.11, 43.77 and 39.86 for the three models respectively. The comparative results that were achieved from

(iii) were not translated into the daily data as all models appeared to have a tendency to underestimate *H*. The resulting *RMSE*s for the daily *H* data for the three models were (MJ m^{-2}) 1.16, 1.17 and 1.18 respectively. It appears that similar or better agreement between measured and estimated *H* can be forged without the need for surface radiometric temperature measurements.

The study showed, in general, that high frequency air temperature measurements can be used to estimate *H* with reasonable accuracy using the simple and relatively low-cost TV and SR methods. Moreover, these methods can be used to calculate λE, hence *ET*, as a residual of the shortened surface energy balance equation along with measurements of R_n and *G* assuming that energy balance closure is met. The simple and low-cost nature of these methods makes replication of measurements easier and their robust nature allows long-term measurements of energy fluxes. The study also showed that *H* and λE can be modeled using energy and resistance combination equations with reasonable accuracy. It also reiterated that the SW-type models, which treat the plant canopy and soil components separately, are more appropriate for estimation of *H* and λE over sparse vegetation as opposed to the PM-type models.

TABLE OF CONTENTS

LIST OF SYMBOLS

For different symbols sharing the same description, the chapter in which they are used is included in the description column.

a	amplitude of air temperature ramp (^oC)
A, A_c, A_s	total available energy flux for the canopy, the vegetation and the soil respectively (W m^{-2})
B^{-1}	dimensionless bulk parameter
C	extinction coefficient of the crop (dimensionless) (Chapter 2)
c_*	turbulent scale for the scalar concentration
c_d	mean drag coefficient for the individual vegetative elements
c_p	specific heat capacity of air at constant pressure (MJ kg^{-2} c^{-1})
d	zero plane of displacement for vegetation (m)
D	vapour pressure deficit at reference height (kPa)
D_o	vapour pressure deficit at canopy source height (kPa)
d_p	'preferred value' of the zero plane of displacement for vegetation (0.63h) (m)
e	water vapour pressure (kPa)
e_o	water vapour pressure at canopy source height (kPa)
e_z	water vapour pressure at reference height (kPa)
ET_q	equation of time correction (hours)
$e_w(T)$	saturated vapour pressure at temperature T ($T = T_z$, T_o)
f (x, z-d)	footprint of a scalar flux or concentration for measurements at height z
$F(x, z\text{-}d)$	scalar flux or concentration at height z
g	acceleration of gravity (m s^{-2})
G/G_s	soil heat flux (W m^{-2})
G_c	stomatal conductance of the canopy (m s^{-1})
g_s	stomatal conductance of a leaf (m s^{-1})
G_w	aerodynamic and stomatal conductance to sensible heat transfer in series (m s^{-1})
h	vegetation height (m)
H, H_c, H_s	total sensible heat flux for the canopy, the vegetation and the soil respectively (W m^{-2})
h_a	hour angle of the sun (radians)
I_s	incoming solar irradiance (W m^{-2})
k	extinction coefficient of the crop (dimensionless) (Chapter 5)
K	eddy diffusion coefficient (m^2 s^{-1})
k	von Kármán's constant (dimensionless)
K_h	eddy diffusion coefficient at the top of the crop (m^2 s^{-1})
L	Monin Obukhov length (m)
LAD	leaf area density (m^2 m^{-3})
LAI	leaf area index (m^2 m^{-2})
lat	latitude of a location on the earth's surface (radians)
LC	longitudinal correction (hours)
L_d	down coming long wave irradiance (W m^{-2})
L_u	outgoing long wave irradiance (W m^{-2})

n	eddy diffusivity decay constant in the crop (dimensionless)
q_*	turbulent scale for specific humidity (kg kg^{-1})
R_a^a	aerodynamic resistance between canopy source and reference height (s m^{-1})
R_a^s	aerodynamic resistance between the soil and vegetative components (s m^{-1})
R_a^c	bulk boundary layer resistance of the vegetative component (s m^{-1})
R_s^c	bulk stomatal resistance of the vegetative component (s m^{-1})
R_s^s	surface resistance of the soil component (s m^{-1})
R_{nc}	total net radiation flux absorbed by the vegetative elements (W m^{-2})
R_a	aerodynamic resistance (s m^{-1})
R_{am}	aerodynamic resistance to momentum (s m^{-1})
R_b	excess resistance (s m^{-1})
r_b	mean leaf boundary layer resistance per unit surface area of vegetation (s m^{-1})
R_c	canopy resistance (s m^{-1})
R_h	aerodynamic resistance to sensible heat transfer (s m^{-1})
R_l	mean leaf irradiance (W m^{-2})
rI_s	reflected solar irradiance (W m^{-2})
R_n	total net radiation flux (W m^{-2})
R_{ni}	isothermal net radiation
R_{ns}	total net radiation flux transmitted into the soil (W m^{-2})
r_o	cuticular resistance (s m^{-1})
r_r	excess resistance (s m^{-1})
r_s	mean stomatal resistance per unit surface area of vegetation (s m^{-1})
$s + l$	ramping period of air temperature ramp (s)
s_k	skewness of air temperature (^{o}C)
$S^n(r)$	air temperature structure function at time lag r, order n
T_*	turbulent temperature scale (K)
T_a	air temperature (^{o}C)
T_c	foliage surface temperature (^{o}C)
T_i	sample air temperature at time i (^{o}C)
T_o	air temperature at canopy source height (^{o}C)
T_r	radiometric surface temperature (^{o}C)
T_s	soil surface temperature (^{o}C)
T_z	air temperature at reference height (^{o}C)
u	longitudinal wind speed (m s^{-1})
u_*	friction velocity (m s^{-1})
u_h	wind speed at canopy top (m s^{-1})
u_z	wind speed at reference height (m s^{-1})
v	lateral wind speed (m s^{-1})
V	volume of a parcel of air (m^3)
w	vertical wind speed (m s^{-1})
w_l	average canopy leaf width (m)
z	reference height, where measurements are taken, above the ground (m)
z'_o	roughness length of the soil or understorey crop (m)
Z_o	'preferred value' of the roughness length of the bare substrate ($0.13h$) (m)

z_o	roughness length of the crop (m)
z_{oh}	roughness length for sensible heat flux (m)
z_{om}	roughness length for momentum (m)
z_r	measurement height above the crop canopy (m)
Δ	derivative of the saturated vapour pressure with respect to temperature (kPa C^{-1})
Ψ_m, Ψ_h	stability correction factor for momentum and sensible heat transfer respectively
α	calibration factor for surface renewal
β	elevation angle of the sun above the horizon (radians)
δ	declination angle of the sun (radians)
ε	emissivity (dimensionless)
ϕ	azimuth angle of the sun (radians)
γ	psychrometric constant (kPa K^{-1})
λ	latent heat of vapourization (MJ kg^{-1})
λE, λE_c,λE_s	total latent energy flux for the canopy, the vegetation and the soil respectively (W m^{-2})
θ	zenith angle of the sun (radians) (in Chapter 5)
θ	soil water content (m^3 m^{-3}) (in Chapters 2, 6 and 7)
ρ	air density (kg m^{-3})
σ_c	concentration fluctuation of a scalar entity
σ_T	standard deviation of air temperature (^oC)
ζ	dimensionless stability parameter

LIST OF TABLES

LIST OF FIGURES

1 INTRODUCTION

The 2008 Revision (United Nations, 2009a) on world population revealed that the current (2009) 6.8 billion population is projected to reach 7 billion early in 2012 and 9.1 billion by 2050, growing at about 57.5 million per year. The developing countries will account for almost entirely the additional 2.3 billion, with their population projected to rise from the current 5.6 billion to 7.9 billion in 2050. The population growth rate of the least developed countries is the highest in the world accounting for 2.3% increase per year, with the population expected to double from the current 0.84 billion to 1.7 billion in 2050. The study also predicts rapid urbanization, accompanied by large internal migration from rural areas to cities, in these developing countries. This is of great concern when viewed in the context of the impacts it will have on agriculture and other economic sectors regarding the scarce resource water. Increasing population and urbanization would mean more and more fresh water being diverted to cities for industrial and urban uses, competing and leaving the agricultural sector to do with less water for crop production despite increased demand. The wastes that are generated by the industrial and urban areas may also pollute water sources reducing water quality and restricting its use for agriculture. Notwithstanding this, about 14% of the world population, living in the developing countries which are predicted to host the biggest share of the population growth in the years to come, is still underfed (United Nations, 2006, 2009b). Moreover, globally there is a shift of production from grains towards more profitable fruits, vegetables, other high value crops, commercial plantations and bioenergy products. This would aggravate the already prevalent problem of producing and providing more food for the increasing world population and threatens national and/or regional food security.

In light of all mentioned above, however challenging it might be, it appears appropriate to value the water in economic (monetary) terms that aims to maximize benefits across the range of water uses in a way that ensures efficient and sustainable utilization of the resource, while recognizing the needs of the poor and disadvantaged members of the society, for current and future generations (United Nations, 2006). In South Africa, agriculture and forestry face increased competition for the scarce resource water by urban and industrial uses. Recently in South Africa, as in many parts of the world, the introduction of *Jatropha curcas*, an exotic deciduous tree plant belonging to the family

Euphorbiaceae grown for its oil-rich seeds which are regarded as a promising option for biofuel, has been initiated. These trees can be planted as sole stands or in combination with other crops as part of an agroforestry system. Large-scale cultivation of such exotic trees should consider, among other things, its water-use. Similar issues have been recognized nationally, and led to the 1998 Republic of South Africa National Water Act which refers, among other things, to the possible charging and allocation of fresh water in the case of activities that result in stream flow reduction. This requires a thorough knowledge and understanding of the hydrological cycle components and processes involved, of which evaporation or water-use by agricultural or tree crops is the most crucial and arguably the most difficult to measure, for their routine determination and quantification with reliable accuracy and precision.

A number of techniques and models have been developed through time to measure or estimate total evaporation from different surfaces. These may differ in the medium that they consider as a means for evaporation determination which could be the soil, plant, atmosphere or a combination thereof. Moreover the techniques can differ in their accuracy, simplicity and robustness, measurement sampling, spatial representation, computational and expertise requirement, cost, etc.

The difference in profile soil water content over a period of time could give an estimation of evaporation. But this method does not work well under conditions of frequent and large precipitation events, and large drainage rates, lateral flows and water tables located close to the surface (Brutsaert, 2005). Evaporation has also been determined using a lysimeter, a large container filled with soil, water and plants to mimic the surrounding area. This device records weights at regular time intervals and allows calculation of water lost as soil evaporation and plant transpiration over a period of time. It is considered as a standard for evaporation measurement but its expensive and often-difficult-to-construct, non-portable and destructive nature has restricted its use (Savage *et al*., 1997). Furthermore, after long dry periods, the loss of water by evaporation within the lysimeter may not match that outside the non-permeable lysimeter walls (M J Savage pers. comm. 2009). Evaporation can also be calculated as a residual in the water balance equation assuming independent measurements or estimates of the components guarantee closure of the equation. However simple in principle it might look, it is very difficult to independently determine the component parts with reliable accuracy, and hence is seldom used.

The rate of sap flow measurement in plants, obtained using heat (or isotopes) as a tracer, can also be used to determine the rate of plant transpiration. These techniques are limited in a sense that they can be applied only to mono-specific stands of trees, are mostly intrusive and cause wounds that distort flows, and require felling of trees in order to acquire sap-wood area and wound information necessary for evaporation estimation (Savage *et al*., 2000). Besides, additional measurements of soil evaporation may be required to obtain total evaporation in case the trees do not fully and uniformly cover the soil.

Techniques that gather information from the atmosphere to determine evaporation and other energy fluxes fall under micrometeorological studies. These techniques usually use the energy and mass equations to deduce the energy fluxes. Common to almost all these micrometeorological techniques is that they require steady state conditions, uniform surface with extensive fetch that are limited by measurement height. Eddy covariance, Bowen ratio, scintillometry, flux-gradients, flux-variance, surface renewal, etc. techniques fall under this category. Although all the above techniques are point-measurements, except for surface scintillometry which gives area-averaged energy flux, their measurements have footprint representativity.

Eddy covariance (Swinbank, 1951) is a direct measurement of energy fluxes based on the measurement of fluctuations of the vertical wind velocity and scalar concentration - water vapour concentration in the case of evaporation. It is the most commonly used technique by researchers, considered as a standard, to determine energy and material fluxes. However, there are strict requirements that need to be met for successful measurement of these fluxes. The sensors' frequency response should be greater or equal to 10 Hz, the instrument should be properly aligned, it requires high level of expertise to analyse and interpret data, the data requires extensive post-measurement corrections, etc. The instrument is also very expensive, ranging from US $3000 to $20000 per instrument (Snyder *et al*., 2008). These reasons have mainly limited the application of the eddy covariance to research experiments only. The eddy covariance technique can also be used to determine sensible heat flux, momentum flux density and trace gas fluxes in a similar fashion.

Bowen ratio (Bowen, 1926) energy balance (BREB) is a micrometeorological technique for an indirect determination of evaporation using measurements of mean air temperature and water vapour pressure at two levels. BREB requires additional measurements of net irradiance and soil heat flux. The latent heat, or evaporation, becomes undefined when the Bowen ratio (β) approaches -1, which usually happens either during the morning or evening (Savage *et al*., 2009). This results in inevitable exclusion of data. Condensation of dew on sensors also prevents any meaningful measurement of air temperature and water vapour pressure. The full set of BREB is less expensive than eddy covariance, but still expensive for routine evaporation determination (Savage *et al*., 1997).

Surface layer or large aperture scintillometry is a Monin-Obukhov similarity theory (MOST) based approach that determines area-averaged sensible heat flux. It propagates radiation at high frequency (typically 1 kHz and 8 Hz respectively) and detects the radiation intensity fluctuations caused by the atmosphere refractive scattering of turbulent eddies in the path of the propagated radiation for determining the sensible heat flux. However, the technique fails to indicate the direction of energy fluxes and may require friction velocity and correction for Bowen ratio (β) which might necessitate additional measurements (Savage *et al*., 2004).

Flux-gradient methods are low-cost and MOST-based micrometeorological techniques which require mean water vapour pressure measurements at two levels. These approaches are based on first order closure of Fick's law and determine evaporation as a product of an exchange coefficient and concentration gradient of the water vapour pressure. They involve a great deal of empiricism in the form of "universal" non-dimensional stability correction factors which have assumed slightly different forms and/or values in the past (Prueger and Kustas, 2005).

Flux-variance technique, first proposed by Tillman (1972) for sensible heat flux, is a MOST-based approach that determines evaporation on the basis of a single-height measurement above the surface of interest. It involves high frequency (2 to 10 Hz) measurements of the scalar of interest and second (and third) order statistics calculated thereof to estimate energy fluxes. The attraction of this technique lies in its cost effectiveness and simplicity of computation. There is mixed information in the literature concerning the "universal" constants used in this technique with some arguing that site-

specific constants should be determined depending on the type of the surface. Another limitation is that the technique works well mainly in the unstable atmospheric stability conditions although there is evidence that it can also be reasonably extended to the neutral and stable part of the stability conditions. There is also general consensus in the literature that this technique estimates momentum and sensible heat fluxes from vertical wind velocity and air temperature (temperature-variance) measurements respectively with reliable accuracy but not the latent energy flux (the term latent energy is preferred to latent heat since the process is a phase-change with little change in temperature). An alternative solution is to solve for the latent energy flux, and thereby evaporation, as a residual of the shortened surface energy balance equation, with concurrent measurements or estimation of net irradiance and soil heat flux.

Another technique that involves a single-height high frequency (2 to 10 Hz) measurement of a scalar for estimation of energy fluxes is the surface renewal (Paw U *et al*., 1995). The main advantages of this technique include: its low-cost, ability to estimate energy fluxes across all stability conditions, and applicability in both inertial and roughness sub-layers since it is independent of MOST. However, the method is computationally demanding and requires calibration of a coefficient that is used in the technique by regressing estimates against independent - usually eddy covariance - standard measurements. This technique has mostly been used for estimation of sensible heat flux and calculation of evaporation would also require solving for the latent energy flux as a residual of the shortened surface energy balance equation.

Quite a number of models have also been developed over time to determine evaporation from different surfaces. The classic Penman-Monteith (Monteith, 1965) known as the ‘Big leaf’ model or its variants are the most widely used. These are physically-based single-layer models that involve a combination of radiation and resistance parameters to determine evaporation from measurements of solar irradiance, minimum and maximum air temperatures, minimum and maximum relative humidity or dew point temperature, and wind speed. The Penman-Monteith equation can also be used as grass reference evaporation with prescribed daylight and night-time stomatal conductance values. Evaporation can then be calculated as the product of the grass reference evaporation and a crop factor determined based on crop species and growth stage (Allen *et al*., 1998).

The Penman-Monteith models were basically derived for horizontally homogeneous surfaces (Monteith, 1965) and fail to accurately estimate evaporation rates from sparse canopies. For heterogeneous or sparse canopies, the Penman-Monteith equation has been extended to multi-layer and multi-source models so that the contribution of evaporative loss originating from the soil and plant can be modelled separately and accurately (e.g., Shuttleworth and Wallace, 1985; Choudhury and Monteith, 1988). These models have also been modified to accommodate inputs of canopy and soil surface temperatures. The main weather parameter that creates variability in such surfaces is the solar irradiance intercepted by the canopy and that transmitted to the soil or understorey as it is used to estimate the net irradiance above and below the canopy, an input required by the multi-layer models, and as such deserves special attention.

Therefore, the main aim of this study is to evaluate the reliability of the low-cost meteorological techniques in determining water-use of a sparse vegetation of sole stands of *Jatropha curcas*. For this purpose the temperature-variance and surface renewal techniques and the multi-layer models were chosen. The temperature-variance and surface renewal were used to estimate the sensible heat flux, and then latent energy flux, and hence evaporation, was calculated as a residual of the shortened surface energy balance equation with concurrent measurements of net irradiance and soil heat flux.

Specific objectives of this study include:

1. To investigate the applicability of the temperature-variance technique in estimating sensible heat flux with and without third order statistics of high frequency air temperature measurements under different atmospheric stability conditions over rough sparse vegetation of *Jatropha curcas*, and homogenous mixed grassland community and fallow bare soil. The application of the surface renewal method over different surfaces in South Africa has been done elsewhere and will not be duplicated here.

2. Evaluation of the estimation of long-term sensible heat flux from a fetch-limited *J. curcas* plot using temperature-variance and surface renewal techniques and the latent energy flux, and hence the total evaporation, calculated as a residual term of

the shortened surface energy balance involving measurements of net irradiance and soil heat flux.

3. Validation of a three-dimensional radiation interception model using a variety of regularly spaced tree crops with planting patterns including isolated trees, hedgerows and trees arranged in a tramline mode against field measurements.

4. To evaluate the applicability of a multi-source model in estimating the latent energy flux, and thereby the evaporation arising from sole stands of *J. curcas* trees and the soil beneath against those calculated as a residual of the shortened surface energy balance from measurements of net irradiance, soil and sensible heat fluxes assuming that energy balance closure is met. Moreover, the performance of the Penman-Monteith equation for the same field is assessed.

5. To investigate the use of single- and multi-source models for estimation of sensible heat flux, using surface radiometric temperature as input, over sparse vegetation of *J. curcas*. Additionally sensible heat flux estimates using a multi-source model without the need for surface radiometric temperature measurements are evaluated.

2 THEORETICAL BACKGROUND AND LITERATURE REVIEW

2.1 ATMOSPHERIC BOUNDARY LAYER

2.1.1 Introduction

The earth's surface is closely coupled to the layer of air directly above it by turbulent exchange processes (Dabberdt *et al*., 1993). There is a continuous interaction between these two media. Knowledge of these interactions is very important in order to understand the dynamics of the biosphere-atmosphere interface and quantify the exchange processes that occur therein. The weather and climate and distribution of trace gases in the lower atmosphere are influenced to a large extent by these interactions (Pielke *et al*., 1998) and hence its importance to all life forms on the earth's surface is apparent.

The lowest layer of the atmosphere that is directly influenced by the effects of the earth's surface where momentum, heat, and mass are transferred via mechanisms of turbulent transfer and mixing and responds accordingly with a time scale of an hour or less is referred to as the atmospheric (planetary) boundary layer (ABL) (Panofsky and Dutton, 1984; Stull, 1988; Garratt, 1992; Arya, 2001). The depth of the ABL varies both in time (on the order of an hour or less) and space from tens of meters to several kilometres in response to the diurnal heating and cooling cycle. During the day, following sunrise, the underlying surface warms and produces a convective layer immediately above which grows through the morning reaching heights of 1 to 2 km by mid afternoon. Under such situations, unstable conditions influenced by strong surface heating prevail in the ABL. In contrast, during the night, following sunset, the underlying surface cools rapidly due to radiative heat loss, turbulence weakens and the ABL depth shrinks to about 50 to 200 m. This situation is characterized by stable conditions where the surface becomes cooler than the air. Neutral conditions are rarely realized but may closely be approximated under conditions of strong wind and overcast sky (Garratt, 1992; Kaimal and Finnigan, 1994; Arya, 2001)

The ABL can be divided roughly into two layers, the inner (wall or surface) and outer (Ekman) layers (Fig. 2.1). In the outer region, transport processes are little affected by the

nature of underlying surface, but are sensitive to the Coriolis force due to the earth's rotation. In contrast, transport processes in the inner region (surface layer) are mainly dependent on the nature of the underlying surface while they are insensitive to the earth's rotational effect. The region above these two layers is called the free atmosphere where transport processes are not affected by surface heating and friction (Garratt, 1992; Kaimal and Finnigan, 1994).

The surface layer comprises the lower part of the ABL and is relatively easily accessible for surface flux measurements. The exchange processes within the atmosphere in this layer are almost always turbulent (Panofsky and Dutton, 1984; Kaimal and Finnigan, 1994; Arya, 2001). The surface layer is divided into two sublayers (Garratt, 1992): the roughness (interfacial) sublayer and inertial (constant flux) sublayer. The roughness sublayer is the lower part of the surface layer comprising the layer of air within and just above the roughness elements. The roughness sublayer begins at the earth's surface and extends from the ground vertically upwards to a distance of about 1.5 (Arya, 2001), 5/3 (Sellers *et al*., 1986), and 1.5 to 3.5 (Brutsaert, 1982; Prueger and Kustas, 2005) times the length of the roughness elements. In this layer, turbulence is strongly affected by the structure of the individual surface roughness elements (Brutsaert, 1982; Mahrt, 2000), e.g., the uneven height of plants, the spacing between plants, the clumping of trees, leaves and branches, buildings or edges of fields (Mahrt, 2000). These elements usually create horizontal variability in the flow and accordingly hinder the sampling and measurement of a representative surface flux from a single point measurement (Mahrt, 2000). The inertial sublayer is the top part of the surface layer sitting on the roughness sublayer. This layer is characterized with a strong vertical gradient controlling the transfer of momentum, mass, and heat through it. The vertical variations of vertical fluxes in this layer do not change appreciably and can be assumed constant, and hence lend themselves to observations from the surface and masts or towers erected to this layer (Pasquill, 1972; Brutsaert, 1982; Rosenberg *et al*., 1983; Panofsky and Dutton, 1984; Dabberdt *et al*., 1993; Kaimal and Finnigan, 1994; Arya, 2001). Relations between fluxes and their vertical profiles, that consider both the mechanical and thermal turbulence that exist in this layer, were first proposed by Monin and Obukhov (1954) and their theory is commonly recognized as the Monin-Obukhov Similarity Theory (MOST).

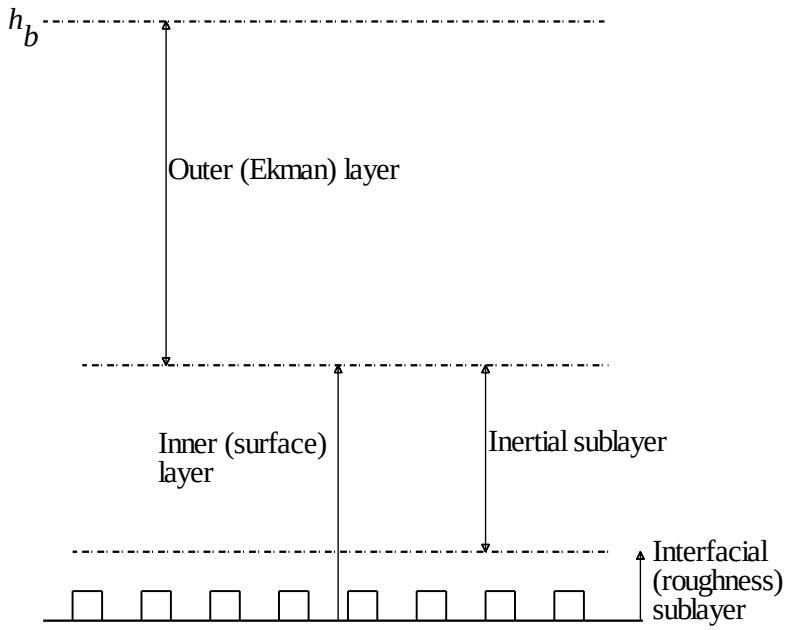

Fig. 2.1 Schematic atmospheric boundary-layer structure for aerodynamically rough flow in neutrally stratified conditions (after Garratt, 1992) where h_b is the boundary layer depth

2.1.2 Monin-Obukhov Similarity Theory (MOST)

MOST is based on the assumption that flow is steady, horizontally homogeneous and quasistationary (Arya, 2001). MOST states that the mean flow and turbulence characteristics in the surface layer depend only on four independent variables: the height above the surface z, the friction velocity u_*, turbulent temperature scale T_* in K (now modified MOST also includes turbulent scale for specific humidity in kg kg^{-1}, q_*, as well), and the buoyancy variable g/T (where g is the acceleration of gravity and T (K) is the air temperature) (Garratt, 1992; Kaimal and Finnigan, 1994; Arya, 2001). These four independent variables can be expressed in terms of three basic dimensions (length, time and temperature) and can be combined into one dimensionless variable. The variable chosen to describe the dimensionless characteristic of turbulence by Monin and Obukhov (1954) was the buoyancy parameter and is commonly known as the dimensionless stability parameter, ζ:

$$\zeta = z/L \quad \text{or} \quad \zeta = \frac{z-d}{L} \tag{2.1}$$

where z is the height where flow measurements are observed, d the zero plane displacement height (m), and

$$L = -\frac{\overline{T}}{kg} \cdot \frac{\rho c_p}{H} \cdot u_*^3 \qquad (2.2)$$

is Obukhov length of stability (m), $\overline{T}$ the average air temperature (K), k von Kármán's constant (0.41), ρ the mean density of air (1.14 kg m^{-3}), c_p the specific heat capacity of air at constant pressure (1011 J kg^{-1} K^{-1}) and H the sensible heat flux. More recently this definition has been modified to include the buoyancy effects of evaporation (Businger and Yaglom, 1971). The dimensionless stability parameter ζ has become a more rigorous theoretical means of identifying stability in atmospheric sciences. Table 2.1 summarizes the general properties of z/L and stability conditions. It has been documented that, above flat homogeneous surface, the statistics of atmospheric variables, such as gradients, variances, and covariances, become universal functions of ζ when normalized by appropriate scaling parameters (e.g., u_*, T_*, q_*) and serve as a foundation for quantification of fluxes (Monin and Yaglom, 1971; Panofsky and Dutton, 1984; Kaimal and Finnigan, 1994).

The other variables in which flow and turbulence characteristics are dependent upon are defined:

$$u_* = \left[\left(\overline{u'w'} \right)^2 + \left(\overline{v'w'} \right)^2 \right]^{0.25} \qquad (2.3)$$

where u, v and w denote the longitudinal, lateral and vertical wind speeds respectively and the primes denote fluctuation from the mean over certain sampling period of time (e.g., $u' = u - \overline{u}$) with overbars representing component means,

$$T_* = \frac{H}{\rho c_p u_*}, \text{ and} \qquad (2.4)$$

Table 2.1 Summary of the stability classes using the dimensionless stability parameter ζ (after Panofsky and Dutton (1984) and Deardorff (1978))

Class	Range in $\zeta = (z - d)/L$	Description
Convective	$\zeta < -0.05$	Heat convection dominant
Unstable	$-0.05 \leq \zeta < -0.02$	Mechanical turbulence dominant
Neutral	$-0.02 \leq \zeta < 0.02$	Purely mechanical turbulence
Slightly-stable	$0.02 \leq \zeta < 0.2$	Mechanical turbulence slightly damped by temperature stratification
Strongly-stable	$\zeta > 0.2$	Mechanical turbulence severely reduced by temperature stratification

$$q_* = \frac{E}{\rho u_*} \tag{2.5}$$

where E is the water vapour mass flux density (kg s^{-1} m^{-2}).

Quantifying the air-surface exchange processes can be accomplished by (Dabberdt *et al*., 1993): (i) micrometeorological techniques that measure the transport processes in the atmospheric surface layer; (ii) budget analysis which is based on the evaluation of the component terms that can potentially change the mean concentration of a variable with time and then estimate the flux through the use of ambient mass balance; and (iii) enclosure techniques which derive fluxes from measurements of change in mean concentration using chambers placed over the surface. For many agricultural applications, micrometeorological techniques are preferred since they are non-intrusive, can be applied on a semi-continuous basis, and can provide aerially averaged fluxes from point measurements (Meyers and Baldocchi, 2005). But these techniques work under the assumption of stationary flow, horizontally homogeneous surface conditions, and flat terrain in equilibrium with upwind surface or "footprint" (discussed below) (Meyers and Baldocchi, 2005). These conditions, however, exist seldom in nature and hence deviations from these assumptions should be considered in the interpretation of collected data.

2.1.3 Footprint

During the past few decades, micrometeorological techniques have been intensively used to study scalar fluxes and/or trace gas concentrations. These techniques usually rely on the assumption that the surface of interest is horizontally homogeneous and uniform with adequate fetch. A 100:1 fetch-to-height ratio had been widely used to ensure that the

measured fluxes/concentrations have the surface of interest as their source. While this ratio may be adequate for tall rough canopies, it may not be so for short crops or smooth surfaces (Leclerc and Thurtell, 1990). The idea is even more complicated when realizing that surface conditions are mostly inhomogeneous in nature with varying source strength of the entity to be measured. A number of studies have attempted to address this problem by quantifying the 'flux footprint' which describes the contribution per unit emission, of each element of the upwind surface area source to the vertical scalar flux or concentration measured at a height *z* (Horst and Weil, 1992). This contribution depends on the upwind distance from the source area to the observation point (*x*), observation height (*z*), atmospheric stability and roughness length (Schuepp *et al*., 1990; Leclerc and Thurtell, 1990).

Several theoretical approaches have been developed in the past to determine the footprint function. These can be classified into four general categories (Vesala *et al*., 2008): (i) analytical models, (ii) Lagrangian stochastic particle dispersion models, (iii) large eddy simulations, and (iv) ensemble-averaged closure models. Some models are constructed from a combination of these approaches. These models vary in the principle they are based on, underlying assumptions, limitations, level of complexity, computational intensity, etc.

Analytical models are based on simulation of the Eulerian random velocity field (Vesala *et al*., 2008). These models are simple to use, however, with most analytical models applicable only in horizontally homogeneous surfaces as they rely on the inverted plume assumption and work better in neutral stability conditions (Schmid, 2002).

The Lagrangian models are based on Lagrangian trajectory simulation and assume that the diffusion of a passive scalar can be represented by the trajectories of a finite number of particles that are completely independent of each other (Schmid, 2002). The Lagrangian models could be of two types: forward and backward Lagrangian models. The forward Lagrangian models, as with the analytical models rely on the inverted plume assumption, and hence are applicable only to horizontally homogeneous surfaces (Schmid, 2002). Whereas the backward Lagrangian models can be used in a range of homogeneity flows since they do not rely on the inverted plume assumption (Schmid, 2002; Vesala *et al*., 2008). However, the performance of both Lagrangian models depends on how well the turbulence is represented, which may be difficult to obtain especially in cases with

spatially varying sources (Leclerc *et al*., 1997). Besides, the Lagrangian models are computationally intensive. To overcome this problem, Hsieh *et al*. (2000) developed an analytical model based on numerical results obtained from forward Lagrangian models. Kljun *et al*. (2004) also provided an algebraic footprint estimation using a simple parameterization based on a backward Lagrangian model.

The large-eddy simulation (LES) and closure model approaches are based on ensemble-averaged Navier-Stokes equations and closure assumptions (Vesala *et al*., 2008). In the LES models, the large eddies are directly resolved at subgrid-scales assuming that most of the fluxes are contained in them. The model uses certain boundary conditions in order to determine the flux footprint (Leclerc *et al*., 1997). The closure model makes use of turbulent diffusion equations to estimate the contribution of each cell to the measured flux (Sogachev and Lloyd, 2004). Both models can simulate the turbulence statistics and the scalar flux field under any given condition, which is lacking in the Lagrangian models. They are also quite useful in estimating the footprint from heterogeneous surfaces (Sogachev and Lloyd, 2004; Vesala *et al*., 2008). But the LES models are computationally intensive, even more so than their Lagrangian counterparts, which may become prohibitive in their application for routine field experiments. However, they are extremely valuable in validating the other simpler footprint models as they provide a more realistic representation of the flow responsible for the scalar fluxes (Schmid, 2002; Vesala *et al*., 2008). The closure model is a recent development in the field of flux footprint and boasts of low computing cost resources. Sogachev and Sedletski (2006) have developed a simplified 'Footprint calculator' to facilitate the utilization of this approach.

All these flux footprint models could be very useful in designing an experiment, setting distance in the downwind direction from the edge of a surface and optimum height above the surface for placement of a sensor. Analyzing data post-measurement also aides in determining the spatial extent and contribution of upwind surface area source to the measured vertical flux at a certain height above the ground during the measurement time. The choice of the model should consider surface condition (homogeneity or lack of), atmospheric stability, ease of application, and computational intensity of the model.

2.1.4 Radiation and energy balance in the ABL

The condition of the ABL is dictated to a large extent by the diurnal heating and cooling of the earth's surface in response to solar irradiance. Solar irradiance, the ultimate source of all the available energy on the earth's surface, in the absence of clouds, is transmitted through the atmosphere to reach the surface without appreciably affecting the air temperature of the ABL. Over land, the sun's rays heat the surface which in turn heats the air in contact with it by conduction setting up a convective current of air. In the absence of solar irradiance, however, the surface cools rapidly due to radiative heat loss to space thwarting the supply of energy to the turbulent motion resulting in contraction of the ABL (Kaimal and Finnigan, 1994).

The influence of solar irradiance on the biosphere-atmosphere interaction can be accounted for by considering the mass and energy conservation law in which gains balance losses. This can be accomplished either in terms of the radiation or energy balance. In both cases, the equations are balanced against net irradiance (R_n). In the radiation balance, R_n is given as the difference between incoming and outgoing irradiances at or near the earth's surface. For a flat extensive homogeneous surface, R_n is the sum of the differences between incoming (I_s) and reflected (rI_s) shortwave irradiances; and incoming (L_d) and emitted (L_u) longwave irradiances. I_s has the sun and atmosphere as its source, rI_s is reflected from the surface, L_d and L_u are emitted from the atmosphere and surface respectively. All components have W m^{-2} as their unit.

$$R_n = I_s - rI_s + L_d - L_u \tag{2.6}$$

Micrometeorological techniques usually consider energy fluxes to account for the mass and energy exchanges that occur at the biosphere-atmosphere interface. Knowledge of these exchanges in the soil-plant-atmosphere system is important to understand and model the agricultural, hydrological, ecological and climatological processes that occur over a variety of surface conditions (Choudhury and Monteith, 1988; de Bruin *et al.*, 1993; Prueger and Kustas, 2005). The flux of radiative energy input (or its absence) above a surface causes, neglecting advected energy and physical and biochemical energy storage terms, heating or cooling of the surface, evaporation/condensation of water from/to the

surface, and heating or cooling of the soil surface by conduction. In balancing the energy flux components, two sign conventions are widely used in the literature to define energy terms directed towards and away from the surface. In this and the rest of the sections, radiative fluxes (R_n) directed towards the surface will assume positive values, while nonradiative fluxes (all except R_n) will be negative, and vice versa. The shortened surface energy balance equation is mathematically represented as:

$$R_n = G + H + \lambda E \tag{2.7}$$

where G is the soil heat flux (W m^{-2}), H the sensible heat flux (W m^{-2}), λ the latent energy of vapourization (J kg^{-1}) and E the water vapour flux density (kg s^{-1} m^{-2}). Partitioning of the net irradiance into the component parts is imperative for estimation of total evaporation from variety of surface conditions. Furthermore, it is essential to partition the total evaporation in vegetated canopies into evaporation from the soil and transpiration from the green vegetation for purposes of irrigation scheduling, crop growth and yield predictions, evaluation of water extraction by roots and optimal spacing of agricultural crops or trees, modelling the transport of chemicals in the soil, etc (Boast, 1986). This requires understanding of the processes of heat, water and moment exchange and transfer within the soil-plant-atmosphere system. The processes by which these energy components are exchanged between the soil, plant and atmosphere is complex and non-linear (Allen, 1998).

The R_n and G terms can either be independently measured or estimated from standard meteorological observations but direct measurements of H and λE, in practice, have proven difficult due to cost and complexity of the equipments used. This urges a search for alternative methods of estimating these energy components accurately with less effort and cost.

In the past, several methods that estimate H from measurements of air temperature using instruments that are deployed at or above a surface of interest have been forged. Such methods enable the latent energy flux (λE) to be calculated as a residual of the shortened surface energy balance equation (Eq. (2.7)) assuming that closure is met (discussed below). The fluxes λE and H can alternately be mathematically modelled from routine or less

expensive micrometeorological observations. Sections 2.2 and 2.4 are devoted to the estimation of H from high frequency air temperature measurements and mathematical modelling of λE and H over rough sparse vegetation, respectively.

2.1.5 Surface energy balance closure

The surface energy balance is based on the fundamental principle of conservation of mass and energy where gains must balance losses (Twine *et al*., 2000; Wilson *et al*., 2002; Kanda *et al*., 2004; Barr *et al*., 2006; Oncley *et al*., 2007). The shortened surface energy balance is said to be closed when its independently measured components satisfy Eq. (2.7), or more appropriately when surface energy fluxes ($H + \lambda E$) equal the available energy ($R_n - G$). When field measurements fail to comply with the above, then this is referred to as the lack of surface energy balance closure.

Several field experiments had been conducted in the past to investigate surface energy balance closure (e.g., Twine *et al*., 2000; Wilson *et al*., 2002; Kanda *et al*., 2004; Barr *et al*., 2006; Oncley *et al*., 2007; Castellvi *et al*., 2008) and indicate a surface imbalance usually associated with the surface energy fluxes ($H + \lambda E$) underestimated by 10 to 30% compared to the available energy ($R_n - G$). Several reasons for lack of closure have been discussed by Mahrt (1998) and reviewed by Twine *et al*. (2000) and Kanda *et al*. (2004). These were generally related to (1) uncertainties in observational conditions such as sites and instruments including – (a) errors related to frequency response, alignment, and flow distortions, (b) inconsistency of the source areas sampled by the turbulent fluxes and radiation sensors, and (c) heterogeneities of surface conditions; and (2) turbulent structures in the atmosphere including – (a) flux divergence between the measurement height and the ground, (b) insufficient averaging periods related to the non-stationarity of the flow, and (c) turbulent dispersive fluxes arising from the existence of organized planetary boundary-layer turbulent structures. The instruments for measuring R_n and G, often ignored assuming that the error they introduce is small (e.g., Twine *et al*., 2000), could contribute to lack of closure. Lack of closure is also not confined to heterogeneous and/or fetch-limited surfaces as imbalances have also been reported over so called ideal surfaces with extensive homogeneous flat surfaces (e.g., Twine *et al*., 2000).

The surface energy balance closure issue is of great concern especially where long-term measurements of energy fluxes such as water vapour and CO_2 are concerned. Interpretation of such underestimated fluxes could lead to inaccurate conclusions on water management and carbon sequestration respectively. Therefore, it is important that the reasons for the lack of closure be known and accounted for. But more often than not, imbalances are inevitable and the norm is to check whether the errors are within an acceptable range or not.

2.2 ESTIMATION OF SENSIBLE HEAT FLUX FROM AIR TEMPERATURE

Several micrometeorological methods have been developed to measure and estimate the mass and energy exchange in the soil-plant-atmosphere system. Among these eddy covariance (EC), flux-gradient and Bowen ratio methods can be mentioned. The EC method (Swinbank, 1951) is the most commonly-used method for direct measurement of these fluxes. However, the cost of the equipment and expertise required to run the system has confined its use mainly for research purposes. This prompts for simple, accurate, less expensive and robust alternative instrumentation that can determine these fluxes for routine field applications. Methods that use high frequency air temperature measurements are appealing with this regard. A thermocouple for high frequency air temperature measurement costs about $100, whereas the price of a sonic anemometer, for direct measurement of fluxes, varies between $3000 and $20000 (Snyder *et al*., 2008).

Compared to instrumentation for EC, these temperature-based methods are simple, low cost and robust, requiring little maintenance (Weaver, 1990; Lloyd *et al*., 1991; Castellvi *et al*., 2006). These attributes make spatial replication easy (Castellvi *et al*., 2006), enable estimation of fluxes over large areas by installation of a number of instruments at different sites, and hence can serve as ground truth observations for regional flux measurements made from satellites and aircrafts (Lloyd *et al*., 1991; Kustas *et al*., 1994; Sugita and Kawakubo, 2003). It has also been documented that these methods could be applied close to the surface making access to instrumentation over tall canopies easier (Castellvi *et al*., 2006). Their robust nature also makes the approaches attractive for long term, unattended measurement of fluxes at remote sites. Moreover, compared to EC method, these approaches do not require as high sampling frequency (Katul *et al*., 1995, 1996; Hsieh *et al*., 1996), distortion corrections (de Bruin *et al*., 1993; Katul *et al*., 1995, 1996),

favourable wind direction (Katul *et al*., 1995; 1996), and careful sensor positioning and alignment (Weaver, 1990; Lloyd *et al*., 1991; Katul *et al*., 1995, 1996; Hsieh *et al*., 1996). The absence of the need for sensor positioning and alignment also makes these approaches suitable for the sensors to be suspended from a balloon (Lloyd *et al*., 1991) and aircraft (Weaver, 1990) for estimation of average fluxes over large areas.

2.2.1 Temperature-variance (TV) method

The flux-variance method is a simple and relatively inexpensive technique that uses the Monin-Obukhov Similarity Theory (MOST) along with statistical measures of the scalar of interest. This method has been pioneered by Tillman (1972) for estimation of sensible heat flux (*H*) from homogenous surfaces under dry and unstable atmospheric conditions. The method used to estimate *H* is referred to as temperature-variance (TV) method as it uses the standard deviation of high frequency, typically 2 to 10 Hz air temperature measurements (Katul *et al*., 1995), without the need for turbulence measurement of wind velocity. Since its inception, the TV method has been quite successfully applied to determine *H* over various surfaces (e.g., Wesely, 1988; Weaver, 1990; Lloyd *et al*., 1991; de Bruin *et al*., 1993; Padro, 1993; Vugts *et al*., 1993; Kustas *et al*., 1994; Albertson *et al*., 1995; Katul *et al*., 1995, 1996; Hsieh *et al*., 1996, 2008; Unland *et al*., 1996; Wesson *et al*., 2001; Sugita and Kawakubo, 2003; Prueger *et al*., 2004; Castellvi and Martínez-Cob, 2005; Guo *et al*., 2009). The flux-variance method has also been applied to vertical wind speed and water vapour in order to estimate momentum and latent energy flux exchanges respectively (e.g., Wesely, 1988; Weaver, 1990; de Bruin *et al*., 1993; Padro, 1993; Vugts *et al*., 1993; Katul *et al*., 1995, 1996; Sugita and Kawakubo, 2003; Hsieh *et al*., 2008; Guo *et al*., 2009). The method has also been extended for estimation of CO_2 fluxes (e.g., Hsieh *et al*., 2008; Guo *et al*., 2009).

The conclusions drawn by comparing flux-variance estimations of energy fluxes against measurements from EC over a variety of surfaces, climatic and atmospheric stability conditions have been mixed (Katul *et al*., 1995, 1996). For example, Lloyd *et al*. (1991) - over bare soil, mature millet, fallow savannah and tiger bush; de Bruin *et al*. (1993) - over a uniform terrain; and Albertson *et al*. (1995) - over a uniform dry lake bed, obtained good agreements between *H* estimated from the TV method, using universal constants employed in the similarity function, and *H* measured from EC. Weaver (1990) and Wesson *et al*.

(2001) also found reasonably accurate results using the method with universal constants over uniform surfaces. However, when they applied the method over non-uniform surfaces the agreement between estimated and measured fluxes were found to deteriorate and necessitated calibration of the constants in order to match the independent measurements of *H* from EC. Kustas *et al*. (1994) and Hsieh *et al*. (1996) also adjusted the constants based on correlations between estimated and measured *H*, for studies conducted over non-uniform surfaces. In line with this, Katul *et al*. (1995) found systematic overestimation of latent energy flux over non-uniform surface, but the estimated *H* did not show any systematic error although the scatter of the points along the one-to-one line was rather large. Padro (1993) applied the TV method over fully leaved deciduous forest, leafless deciduous forest and wetland and found an improved agreement when the constants were calibrated based on surface conditions and the scalar being considered. But he also acknowledged that comparable estimates could be obtained using the simplified version for the free convective stability conditions based on Wyngaard (1971) which requires only a single universal constant. Hsieh *et al*. (2008) derived the constants for sensible heat and latent energy fluxes for grassland, rice paddy and forest and found them to be similar for the first two sites but different for the last site.

Most of the above studies opted to use a simplified equation of the TV method in the free convective limit, in order to avoid the inclusion of stability parameters and estimate *H* only on the basis of a single-level high frequency air temperature measurement made above the surface of interest (Sugita and Kawakubo, 2003). But this equation does not perform well in the stable and near-neutral regions resulting in uncertain results (e.g., Weaver, 1990; Katul *et al*., 1995; Castellvi and Martínez-Cob, 2005).

All the findings obtained from research conducted in the past point to the need for calibration of the method using independent measurements of fluxes, especially for non-uniform surfaces. Care should also be exercised in selecting equations of the method among the various existing formulations, as they differ in type of input data requirement and application to different atmospheric stability conditions. The questions that need to be asked when using the method should include: Which version of the equation should be used? How should the constants be determined? Should the equation include a stability parameter? If so, how should it be determined? For instance, using the free convective limit equation for stable atmospheric stability conditions does not require knowledge of the

friction velocity but it could result in very poor results in the stable and near stable atmospheric conditions. Obviously there are some other versions of the equation that require determination of the stability parameter, more specifically friction velocity or the Obukhov length of stability. These can be obtained from high frequency three-dimensional wind velocity measurements, estimated from vertical measurements of wind speed using the similarity theory (e.g., Katul *et al*., 1995) or estimated by iterative procedures (Hsieh *et al*., 1996). The original version of the equation used by Tillman (1972) used skewness of air temperature to determine the stability parameter. This version of the equation, similar to the equation used by Wyngaard (1971), requires only a single-level high frequency air temperature measurement above the surface. Following is the development and derivation of the temperature-variance method.

On the basis of the MOST, the standard deviation of the concentration fluctuation of a scalar entity, σ_c, above a flat homogeneous surface can be expressed as a dimensionless function of atmospheric stability, $-z/L$ (Monin and Yaglom, 1971):

$$\frac{\sigma_c}{c_*} = f\left(-z/L\right) \tag{2.8}$$

where c_* is the turbulent scale for the scalar concentration, z the measurement height above the ground (m) and L the Obukhov length of stability (m) given in Eq. (2.2). The sensible heat flux related to the profiles of wind speed and air temperature by the equation:

$$H = \rho c_p u_* T_* \tag{2.9}$$

where u_* and T_* are given in Eqs (2.3) and (2.4) respectively. Tillman (1972) exploited the relationship between the normalized standard deviation of air temperature, σ_T / T_*, and function of atmospheric stability, $f(-z/L)$, to arrive at an expression for the complete unstable region:

$$\frac{\sigma_T}{T_*} = c_1\left(c_2 - \frac{z}{L}\right)^{-1/3} \tag{2.10}$$

The free convective limit ($z/L \leq -0.2$), also appears to scale well with $(-z/L)^{1/3}$, and Wyngaard *et al*. (1971) showed that Eq. (2.10) reduces to - which also appears to have good applicability for the general unstable range (Tillman, 1972):

$$\frac{\sigma_T}{T_*} = c_1\left(-z/L\right)^{-1/3} \tag{2.11}$$

It has been noted that the free convective limit was not well defined by Wyngaard *et al*. (1971) (Katul *et al*., 1995; Hsieh *et al*., 1996) and Katul *et al*. (1995) suggested that $z/L \leq -0.04$ be used to identify the stability conditions for applying the simplified free convective equation of Wyngaard *et al*. (1971). For the stable and neutral limits (Table 2.1), $-z/L$ approaches zero and σ_T / T_* tends to a constant value, c_3. From Eq. (2.10) it follows that for the near neutral and neutral conditions:

$$c_2 = \left(\frac{c_1}{c_3}\right)^3 \tag{2.12}$$

where c_1 and c_2 are similarity constants given as 0.95 and 0.05 by Tillman (1972) based on the work of Wyngaard *et al*. (1971). The coefficient c_3 is not well defined and had assumed values of 1.77 (Tillman, 1972), 1.85 (Weseley, 1988), 2.2 (Weaver, 1990) and 2 (de Bruin *et al*., 1993) and 2.5 (Padro, 1993) for the neutral and stable portion of the stability range.

Tillman (1972) observed, based on MOST, that functions of dimensionless higher order moments such as skewness of air temperature (s_k) are determined by z/L.

$$s_k = \frac{1}{\sigma_T^{\,3}}\left[\frac{1}{n}\sum_{i=1}^{n}\left(T_i - \overline{T}\right)^3\right] \tag{2.13}$$

where T_i is the air temperature value at time i, and n the number of observations within a certain averaging period. After plotting s_k versus z/L in a linear and semi-log form, Tillman (1972) expressed z/L as a function of s_k:

$$\frac{z}{L} = -A\exp\left(Bs_k\right), \text{ for } -3 < \frac{z}{L} \leq -0.01 \tag{2.14}$$

where A and B are constants given as 0.0137 and 4.39 respectively. This indicates that s_k could be used in estimating the stability parameter of the atmosphere from a single scalar variable of air temperature. Eqs (2.2), (2.9) and (2.10) – for the whole unstable region and Eqs (2.2), (2.9) and (2.11) – for the free convective zone, respectively, can be combined following Tillman (1972) to relate H with σ_T and $\overline{T}$ only as follows:

$$H = \rho c_p \left[\left(\frac{\sigma_T}{c_1}\right)^3 \left(\frac{kgz}{\overline{T}}\right)\left(\frac{c_2 - z/L}{-z/L}\right)\right]^{1/2} \text{ for } \frac{z}{L} < 0 \tag{2.15}$$

$$H = \rho c_p \left[\left(\frac{\sigma_T}{c_1}\right)^3 \left(\frac{kgz}{\overline{T}}\right)\right]^{1/2} \text{ for } \frac{z}{L} < -0.2 \tag{2.16}$$

Yet Eq. (2.15) would require knowledge of u_* in order to determine the stability parameter z/L. Substituting the expression of z/L from Eq. (2.14) into Eq. (2.15), however, can overcome the necessity for determination of u_*:

$$H = \rho c_p \left[\left(\frac{\sigma_T}{c_1}\right)^3 \left(\frac{kgz}{\overline{T}}\right)\left(\frac{c_2 + A\exp\left(Bs_k\right)}{A\exp\left(Bs_k\right)}\right)\right]^{1/2} \tag{2.17}$$

Originally the TV method, since it is based on MOST, was meant to be used along with measurements conducted in the inertial sublayer, but many studies have demonstrated its validity in the roughness sublayer as well (e.g., Weaver, 1990; Lloyd *et al.*, 1991; Padro, 1993; Albertson *et al.*, 1995; Katul *et al.*, 1995, 1996; Hsieh *et al.*, 1996; Wesson *et al.*, 2001; Castellvi *et al.*, 2004; Castellvi and Martínez-Cob, 2005). In fact, Castellvi and Martínez-Cob (2005) evaluated the performance of the TV method in both layers and found more accurate results in the roughness sublayer than in the inertial sublayer. Measurements conducted in the roughness sublayer are proportional to z whereas measurements conducted in the inertial sublayer are proportional to $z - d$ (Chen *et al.*, 1997b). But the height of the roughness layer in vegetated surfaces is ill defined (e.g., 5h/3

(Sellers *et al*., 1986), ~1.5*h* (Arya, 2001), and 1.5*h* to 3.5*h* (Brutsaert, 1982; Prueger and Kustas, 2005), *h* being the height of the vegetation canopy). Also the roughness layer does not end suddenly and abruptly but rather gradually. The accuracy of the estimates of *H* from the TV method, therefore, could be affected by uncertainties in displacement length when the height input changes from *z* to *z* - *d* in the inertial sublayer close to the interface of the two sublayers. It is apparent that *H* calculated from the TV method using TCs mounted on either side of the interface region would differ markedly despite the proximity of the two sensors, especially for tall vegetation. To avoid such uncertainties, measurements in the transition zone should be avoided, certain functions should be introduced to smoothen the sudden drop of the height input or different formulation of the equations should be used for this zone.

In the same manner as for *H*, similar relations could also be forged for u_* (Tillman, 1972):

$$u_* = \frac{H}{\rho c_p \left(\frac{\sigma_T}{c_1} \right) \left[c_2 + A \exp\left(B s_k \right) \right]^{1/3}} \tag{2.18}$$

2.2.2 Surface renewal (SR) method

Paw U and Brunet (1991) introduced the surface renewal (SR) method for analysis and estimation of scalar fluxes over vegetated canopies. It is a simple and relatively inexpensive technique that is based on the principle that an air parcel near the surface is renewed (hence the name surface renewal) by an air parcel from above. The theory behind the SR method on the canopy surface-atmosphere interface is well documented (e.g., Paw U *et al*., 1995; Katul *et al*., 1996; Snyder *et al*., 1996). An air parcel that penetrates or sweeps into the surface from above resides at the canopy surface and gradually heats or cools because of heat exchange between the parcel and the canopy elements. The parcel stays there until another parcel displaces it instantly after which it rapidly leaves the canopy surface into the atmosphere. This process involves ramp-like structures (rapid increase and decrease of a scalar), which are the result of turbulent coherent structures that are known to exhibit ejections and sweeps under shear conditions (Gao *et al*., 1989; Raupach *et al*., 1989; Paw U *et al*., 1992).

The air temperature ramps created by the turbulent coherent structures consist of amplitude (*a*), quiescent period (*s*) for which there is no change in air temperature with time, and ramping period (*l*) for which there is a change in air temperature with time. The amplitude (a) is positive for unstable and negative for stable atmospheric conditions. If an air temperature sensor were placed at the canopy surface-atmosphere interface (assuming the surface was warmer than the air parcel - unstable atmospheric conditions), a rapid decrease of air temperature during the sweeping phase, followed by a quiescent period and then a gradual increase during the ramping period and finally a rapid decrease during the ejection time would be recorded. For surfaces cooler than the air parcel - stable atmospheric conditions, the record of air temperature would show a rapid increase, followed by a quiescent period and then by a gradual decrease and finally a rapid increase during the sweeping, ramping and ejection phases respectively. This is presented schematically in Fig. 2.2 (Snyder *et al*., 1996).

Paw U *et al*. (1995) used heat transfer theory between the air parcel and canopy elements to derive sensible heat flux (*H*) and expressed it as a change with time of heat energy content of an air parcel of volume *V*:

$$H = \alpha \rho c_p \frac{dT}{dt}\left(\frac{V}{A}\right) \tag{2.19}$$

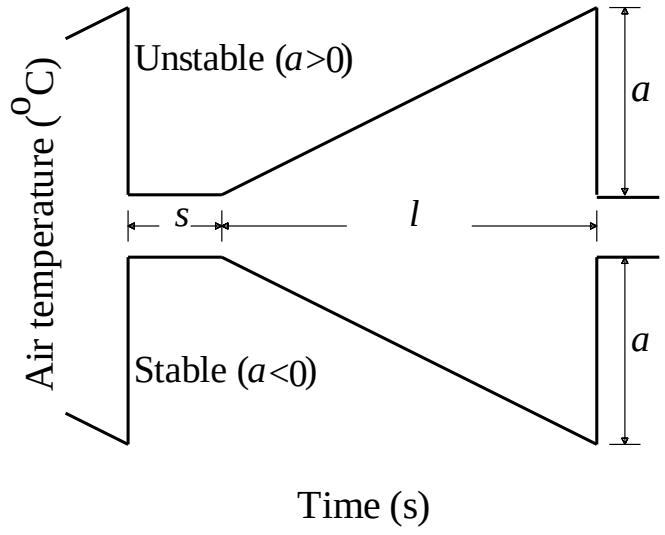

Fig. 2.2 Idealized schematic of the temperature ramps with amplitude a > 0 for unstable and a < 0 for stable atmospheric conditions where *s* and *l* represent the quiescent and ramping periods respectively

where α is a weighting factor and *dT/dt* the change of air temperature with time and *V/A* the volume per unit horizontal area of the air parcel. The term *V/A* is simplified to give the height in the vertical direction – taken as the measurement height *z*. The above equation requires measurements of the total derivative of air temperature with respect to time (*dT/dt*), but fixed air temperature sensors can only measure the partial derivative; hence the equation assumes that *dT/dt* is approximately equal to $\partial T / \partial t$ (Paw U *et al*., 1995). But this assumption may not be valid under strong local advection such as at a height close to the surface-atmosphere interface (Snyder *et al*., 1996). The above equation also assumes that internal advection for the given parcel of air is small and negligible. Application of Eq. (2.19) requires low pass filtering techniques to smooth the temperature data in order to eliminate internal advection effects (Paw U *et al*., 1995) which proved to be cumbersome because of the necessity to choose filter functions and use of numerical methods to identify scalar increases or decreases (Paw U *et al*., 2005).

Snyder *et al*. (1996) simplified and made Eq. (2.19) more applicable by assuming that the ratio of the average ramp amplitude to the average ramp duration (*a/l*) is an estimate of *dT/dt*. But the resulting equation has to be multiplied by the relative time for heating *l*/(*s*+*l*) to account for the quiescent period - for which there is no change in air temperature. Therefore, Eq. (2.19) can be rewritten as:

$$H = \alpha \rho c_p z \frac{a}{s+l} \tag{2.20}$$

Snyder *et al*. (1996) also used the air temperature structure function ($S^n(r)$) and statistical moments as suggested by van Atta (1977) to deduce the amplitude (*a*) and the ramp period (*s*+*l*) from:

$$S^n(r) = \frac{1}{m-j} \sum_{i=1+j}^{m} (T_i - T_{i-j})^n \tag{2.21}$$

where *n* is the power of the function, *m* the number of data points in the time interval measured at frequency *f* (Hz), and *j* the number of sample lags between data points corresponding to a time lag $r = j/f$ and T_i the temperature sample at a time *i*. According to the structure function theory, the time lag (*r*) must be much less than *s* + *l*. Finally, an

estimate of the mean value for amplitude (a) during the time interval is determined by solving the structure function equation for the real roots. The amplitude (a) is described by a cubic function as follows:

$$a^3 + pa + q = 0 \tag{2.22}$$

where the coefficients p and q are described as:

$$p = 10S^2(r) - \frac{S^5(r)}{S^3(r)} \tag{2.23}$$

$$q = 10S^3(r) \tag{2.24}$$

Finally, the ramp period $s + l$ is calculated from

$$s + l = -\frac{a^3 r}{S^3(r)} \tag{2.25}$$

Estimation of H using the SR method requires only a single-level high frequency (2 to 10 Hz) air temperature measurement that is fast enough to capture the ramp-like structures. The measurements can be conducted within, at or above the canopy. The method is deemed to be applicable under all stability conditions, although sometimes the structure function equation fails to find real solutions to the equations under stable conditions resulting in loss of data (Snyder *et al.*, 2008). The biggest problem of the method is also the need for calibration against independent measurements of H to determine the weighing factor α, e.g., by regressing direct measurements of H from EC versus SR estimations. The slope of the regression line forced through the origin represents α. The regression coefficient α is meant to account for unequal heating of air parcels below the measurement height and other potential deviations arising from the assumptions used in formulating the method (Snyder *et al.*, 1996; Spano *et al.*, 1997a, b, 2000; Drexler *et al.*, 2004). It generally depends on the measurement height, lag time (r), canopy structure and thermocouple size (Snyder *et al.*, 1996; Spano *et al.*, 1997a, b, 2000; Duce *et al.*, 1998). Once determined, α is fairly stable, almost invariant and does not change from site to site regardless of weather conditions unless the canopy structure changes (Paw U *et al.*, 1995;

Snyder *et al*., 1996, 2008; Spano *et al*., 2000). A consistent α value of 0.5, using air temperature measurements conducted at canopy height, for coniferous forests, orchards, and maize canopies (Paw U *et al*., 1995); and 1.0 for short turf grass using measurements conducted at several heights above the canopy (Snyder *et al*., 1996) were reported to give best estimates of *H*.

In general, the lag time (*r*) and the measurement height (*z*) should be tailored to suit the surface structure and thermocouple size; then, α can be calibrated against independent measurements. Spano *et al*. (2000), for a sparse grape vineyard canopy, found that calibration was not required if the measurements were performed at about 90% of the canopy height. Calibration of α might also be avoided if the canopy were separated into layers, as opposed to the conventional single-layer treatment of the canopy. The *H*s obtained from each individual layer are added to give the total canopy *H*. Spano *et al*. (2000) found *H* estimated in this manner, for their canopy type, to be comparable with independently measured *H*. This approach is appealing as it eliminates the need for calibration of the SR method, but more research and investigation over different surface structures are required to ascertain its validity.

In general, the SR method has been successfully applied over a range of surfaces (e.g., Paw U *et al*., 1995; Snyder *et al*., 1996, 2008; Duce *et al*., 1997; Spano *et al*., 1997a, b, 2000; Zapta and Martínez-Cob, 2001; Savage *et al*., 2004; Mengistu, 2008). The method has been in constant development and refinement since its introduction, and several versions of the SR method for estimation of *H* exist. The methods that use the earlier version of SR do not require u_* for estimation of *H* (e.g., Paw U *et al*., 1995; Snyder *et al*., 1996, 1997; Spano *et al*., 1997a, b, 2000; Zapta and Martínez-Cob, 2001). The method has been modified to quantify the change in air temperature following a ramp period instead of considering a sharp decrease in air temperature followed by a quiescent period (Chen *et al*., 1997a). Using this approach, Chen *et al*. (1997b) found good agreement between estimated and measured *H* over straw mulch, forest and bare soil. Castellvi (2004) also included similarity theory to the SR method to arrive at an expression that does not require calibration of the weighing factor α. But both methods require u_* or the Obukhov stability length that has either to be observed using instruments other than air temperature sensors or estimated iteratively.

Although the field set up of the method is easy, the programming and mathematical computations that are involved in the method are rather complex. This, added with the method being relatively new, has proved to be prohibitive in its adoption especially by agriculturalists, over the past few years. Published works of this method are few and far apart, and mainly restricted to a few familiar names in the literature apart from the group which initiated the method. Paw U *et al*. (1995) also stressed that the method can be used for any scalar concentration but so far the works that have been done focus on air temperature for estimation of *H*, and studies on the other scalars are deficient.

2.3 EDDY COVARIANCE (EC) METHOD

The mean vertical gradients of fluxes are almost entirely the result of turbulent mixing and can be defined in terms of turbulent (or eddy) components of velocities and of the properties being transferred (Kaimal and Finnigan, 1994). The mean flux across any plane is directly proportional to the covariance between the wind component normal to that plane and the entity in question (Swinbank, 1951; Kaimal and Finnigan, 1994). Eddy covariance (EC) is a direct means of measuring mean vertical turbulent fluxes above extensive surfaces of homogeneous medium using fast response sensors (≥ 10 Hz) for measurement of vertical wind speed (*w*) and a scalar entity of interest (*s*), and their fluctuations (Swinbank, 1951). Thus, measurements of high frequency air temperature (*T*) and vertical wind velocity (*w*) allow the estimation of sensible heat flux (*H*) by eddy covariance:

$$H = \rho c_p \overline{w'T'} \tag{2.26}$$

The primes denote fluctuation from the mean over certain sampling period of time ($w' = w - \overline{w}$, and $T' = T - \overline{T}$, with overbars representing component means), and the bar over $w'T'$ represents average observations over an appropriate sampling period, typically 30 to 60 min, to capture all of the eddy motions that contribute to the flux (Meyers and Baldocchi, 2005). EC requires, like most micrometeorological methods, minimum fetch-to-height ratio to ensure that mean fluxes from the source of interest, and not from other sources, are being sampled. Placement of sensors above surface is also crucial for accurate mean flux measurements using EC. Savage *et al*. (1995), in research conducted over homogeneous grass surface, found no significant differences in *H* measurements with

sensors placed at 0.50, 1.0 and 1.25 m above the grass surface. Placement of sensors below the 0.5 m margin, however, resulted in reduction of *H* measurements. They attributed this to larger fraction of eddies of small size being detected between the sonic anemometer transducers. Other necessary considerations of the method that need attention were summarized by Foken and Wichura (1995) and include: flow distortion by the sensor and masts, sensor separation, coordinate correction for sensor misalignment, adjustment for density fluctuations, etc.

This method has been in use and constant development especially in terms of the relevant instrumentation and data acquisition system. However, it still requires expensive, sensitive and complex instruments in sonic anemometry to measure the vertical component of wind velocity and the scalar of interest at high frequency. Nevertheless, as it gives a direct measure of a scalar flux (*H* in our case), it has been widely used as a standard against which other alternative methods are compared (e.g., Lloyd *et al*., 1991; Albertson *et al*., 1995; Katul *et al*., 1995, 1996; Paw U *et al*., 1995; Hsieh *et al*., 1996; Snyder *et al*., 1996, 1997; Spano *et al*., 1997; Wesson *et al*., 2001; Castellvi and Martínez-Cob, 2005; Castellvi *et al*., 2006). The method, however, requires a number of post-measurement corrections to remove potential sources of error and more often than not shows lack of closing the energy balance equation (Ham and Heilman, 2003). Numerous field experiments conducted on energy balance closure using the EC indicate that the surface energy fluxes ($H + \lambda E$) are underestimated by 10 to 30% compared to the available energy ($R_n - G$). Twine *et al*. (2000) speculated that the proportion of underestimation for $H + \lambda E$ might be similar but Savage (2009) found that there was no underestimation in EC *H* compared with independently measured *H* using a dual-beam surface layer scintillometer in a mesic grassland. All the difficulties associated with the EC method have prohibited its usefulness for routine agricultural applications and confined its use mainly for research purposes.

2.4 ENERGY AND MASS EXCHANGE MODELLING OVER VEGETATION SURFACES

Vegetation-atmosphere models are often used to simulate the exchange of energy and mass fluxes between the biosphere and the atmosphere. Two approaches are used in modelling these fluxes depending on the way they treat the canopy (Raupach and Finnigan, 1988). One approach treats the canopy as a single-layer of vegetation overlying the soil leading to

single-layer models (e.g., Monteith, 1965), commonly known as ‘big leaf’ models. These models simulate the exchange of fluxes between the biosphere and the atmosphere by assuming that the canopy is analogous to an individual leaf. The other approach divides the canopy into multiple layers, assuming the canopy varies with height but identical conditions are experienced within each layer, yielding to multi-layer models (e.g., Norman and Campbell, 1983). These models require a greater number of parameters compared to the single-layer models, and, in fact, they have been criticized as being over-parameterized (Raupach and Finnigan, 1988; Baldocchi and Meyers, 1998). But Baldocchi and Meyers (1998) refute this by demonstrating that model parameters for a multi-layer vegetation-atmosphere model are constrained by one another and can be readily attained through the aid of biogeochemical and eco-physiological principles. On the other hand, the parameters of the single-layer models, especially the bulk resistances, are difficult to acquire and relate to measurable physiological or physical quantities (Raupach and Finnigan, 1988) and are often tuned to fit to flux observations in the field (Monteith, 1965).

Plant canopies may also display horizontal heterogeneity as in mixed cropping systems (e.g., intercropping, agroforestry, and forests), isolated tree crowns, row crops, crops in their earlier growth stages, etc. (Norman and Welles, 1983; Sinoquet, 1993). The interaction of such canopies with the atmosphere should consider not only the vertical but also the horizontal variability, as the horizontal components considered may contribute differently but considerably towards the energy and mass exchange. Multi-layer models that account for horizontal variability in plant canopies have been developed (e.g., Shuttleworth and Wallace, 1985; Choudhury and Monteith, 1988). These models treat the exchange of energy and mass as occurring at the soil and the plant (double-source), but the ‘big leaf’ type models distinguish between the fluxes associated with the soil and plant components crudely, if they ever do (Raupach and Finnigan, 1988; De Pury and Farquahar, 1997).

2.4.1 Penman-Monteith ‘Big leaf’ models

Evaporation losses could be measured directly from the plant and soil components, estimated from soil water content or calculated using micrometeorological methods. The micrometeorological methods may vary depending on the principle involved, measurement requirements, sophistication of instruments used, complexity of processing calculations,

etc. The Penman-Monteith (hereafter PM) equation is a simple biophysical model for estimating latent energy flux (λE), and hence evaporation, from single-level meteorological measurements (Monteith, 1965). The PM equation is used for estimation of daily evaporation using inputs of daily (or hourly) weather variables including: solar irradiance, minimum and maximum air temperatures, minimum and maximum relative humidity or dew point temperature, and wind speed. The equation combines energy balance and resistance-based heat and mass transfer equations, hence it is termed as the combination equation (Fig. 2.3). The λE from the PM equation is estimated as (Monteith, 1965):

$$\lambda E = \frac{\Delta(R_n - G_s) + \rho c_p D / R_a^a}{\Delta + \gamma(1 + R_a^c / R_a^a)} \tag{2.27}$$

where Δ is the slope of the saturation water vapour pressure function of the reference and mean canopy source height temperatures (kPa K^{-1}), D the atmospheric water vapour pressure deficit (kPa), R_a^a the aerodynamic resistance (s m^{-1}), R_a^c the canopy resistance (s m^{-1}) and γ the psychrometric constant (kPa K^{-1}). The other symbols assume their former definitions.

Although the PM equation is probably the most widely used means of estimating evaporation rates, it does have certain shortcomings (Raupach and Finnigan, 1988). The PM equation attempts to include the control exerted by plants on evaporation through canopy resistance (R_a^c).This resistance is not well-defined, especially in sparse canopies, as it represents the soil and the plant resistances and becomes difficult to relate it to simple measurable variables either physically or empirically. This resistance merely becomes a surface resistance and most big leaf models attempt to fine tune its values by comparing the model against measured fluxes. It also ignores canopy gradients and does not account for counter-gradient transfers. The equation was derived for horizontally homogeneous soil or vegetation surfaces (Monteith, 1965) and fails to accurately estimate evaporation rates from sparse canopies and partition fluxes associated with the soil and plant components (Shuttleworth and Wallace, 1985).

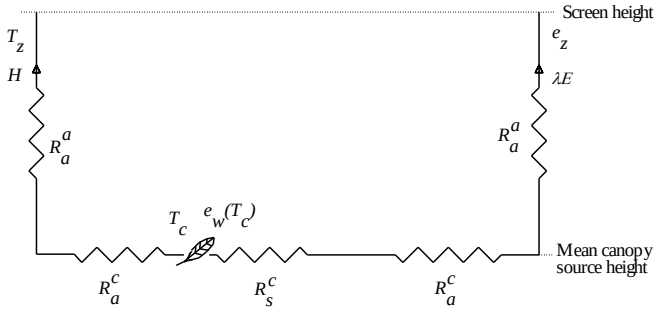

Fig. 2.3 Schematic diagram of resistances and fluxes in the 'big-leaf' PM evaporation model

2.4.2 Multi-source models for sparse vegetation

Most micrometeorological methods measure only a single integrated flux from a vegetated canopy or bare soil. The contribution of evaporation from vegetation and from the soil may vary depending on crop cover; therefore, it becomes important to distinguish between the two especially in heterogeneous or sparse vegetation (Kabat *et al*., 1997). This prompted the development of models that consider separate mass and energy transfer as occurring at the plant canopy and the soil substrate (e.g., Shuttleworth and Wallace, 1985; Choudhury and Monteith, 1988).

Two approaches are employed for computing mass and energy transfer from sparse vegetation: coupled and uncoupled (patch) models. In the coupled approach, the sources of the fluxes from the plants and soil are assumed to be superimposed, interacting with each other, hence the total flux is additive (Lhomme and Chehbouni, 1999). Shuttleworth and Wallace (1985) were among the first to note and develop theoretical equations for such environments and test their significance in a diagnostic approach with prescribed resistance values. Shuttleworth and Gurney (1990) further improved the model by replacing the former aerodynamic transfer sub-model with a new one, and reformulating the model to allow the calculation of canopy resistance from measurements of foliage temperature. Choudhury and Monteith (1988) also formulated a similar model to the Shuttleworth and Wallace (hereafter called SW) model but with four layers. The SW model is by far the most widely used. It has been modified to accommodate two-storey vegetation (Dolman, 1993), two-component canopies (Wallace, 1997), and inputs from radiometric surface temperatures (Lhomme *et al*., 1994a, b, 1997; Norman *et al*., 1995; Kustas and Norman, 1999).

In the uncoupled or patch approach the sources of the fluxes are placed side by side in the form of a mosaic or patch work assuming that the sources are large enough to yield independent fluxes. Hence, the fluxes are vertical and non-interacting, with the total flux being a weighted average from the sources (Lhomme and Chehbouni, 1999). The choice between the two approaches is a matter of horizontal heterogeneity scale: the coupled models are used to treat small-scale horizontal heterogeneity, and the uncoupled model - large-scale horizontal heterogeneity (Blyth and Harding, 1995; Lhomme and Chehbouni, 1999).

2.4.2.1 Dual-source: coupled model of Shuttleworth and Wallace (1985)

The SW model derives the fluxes from the available energy and resistance-based heat and mass transfer at the vegetation and soil components (Fig. 2.4). The available energy for the canopy (A), soil (A_s) and vegetation (A_c) are, respectively, given by:

$$A = R_n - G_s = \lambda E + H \tag{2.28}$$

$$A_s = R_{ns} - G_s = \lambda E_s + H_s \tag{2.29}$$

$$A_c = A - A_s \tag{2.30}$$

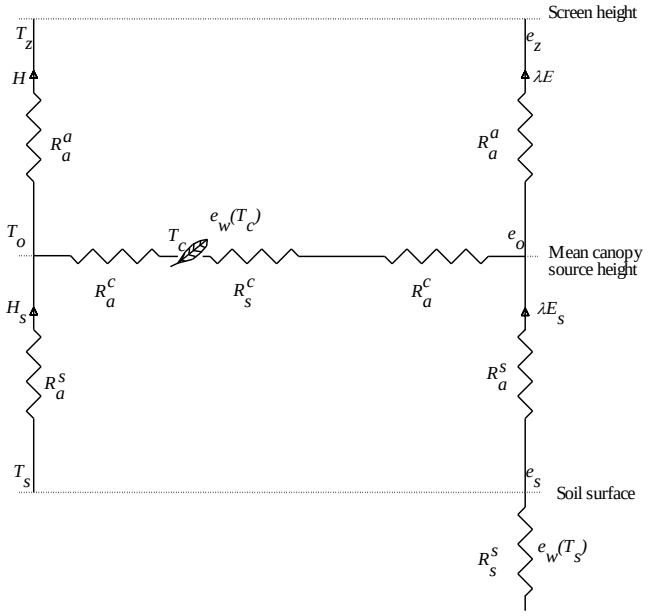

Fig. 2.4 Schematic diagram of resistances and fluxes in the two-layer evaporation model of Shuttleworth and Wallace (1985)

where the subscripts *s* and *c* refer to soil and vegetation respectively. The heat and mass transfer equations for sensible heat (H) and latent (λE) energy fluxes are also, respectively, given by:

$$T_z - T_o = \frac{-HR_a^a}{\rho c_p} \tag{2.31}$$

$$e_z - e_o = \frac{-\lambda E R_a^a \gamma}{\rho c_p} \tag{2.32}$$

where T_z and T_o are the air temperatures at reference and canopy source heights respectively, e_z and e_o the vapour pressures at reference and canopy source heights respectively and R_a^a the aerodynamic resistance between canopy source and reference heights.

The water vapour pressure deficits at a reference (D) and mean canopy (D_o) heights are, respectively, defined as:

$$D = e_w(T_z) - e_z \tag{2.33}$$

$$D_o = e_w(T_o) - e_o \tag{2.34}$$

where $e_w(T_z)$ and $e_w(T_o)$ are the saturated water vapour pressures at T_z and T_o respectively. The introduction of Δ into the mean canopy height water vapour pressure yields:

$$D_o = e_w(T_z) - [e_w(T_z) - e_w(T_o)] - e_o \tag{2.35}$$

Substituting Eqs (2.28), (2.31) and (2.32) into Eq. (2.35) results in a relationship between D and D_o:

$$D_o = D + [\Delta A - (\Delta + \gamma)\lambda E]\frac{R_a^a}{\rho c_p} \tag{2.36}$$

Together, these equations form PM-type equations for separate calculation of evaporation from the soil and the vegetation in the canopy:

$$\lambda E_s = \frac{\Delta A_s + \frac{\rho c_p}{R_a^s}\left(D + [\Delta A - (\Delta + \gamma)\lambda E]\frac{R_a^a}{\rho c_p} \right)}{\Delta + \gamma(1 + \frac{R_s^s}{R_a^s})} \tag{2.37}$$

$$\lambda E_c = \frac{\Delta(A - A_s) + \frac{\rho c_p}{R_a^c}\left(D + [\Delta A - (\Delta + \gamma)\lambda E]\frac{R_a^a}{\rho c_p} \right)}{\Delta + \gamma(1 + \frac{R_s^c}{R_a^c})} \tag{2.38}$$

where R_s^c is the bulk stomatal resistance of the vegetative component, R_s^s the surface resistance of the soil component, R_a^c the bulk boundary layer resistance of the vegetative component, and R_a^s the aerodynamic resistance between the soil and canopy source height. All resistances have s m^{-1} as their unit.

Finally the total latent energy flux from the system, λE, is the sum of the soil and vegetative evaporation, and the resultant equation is arranged in the form:

$$\lambda E = C_s PM_s + C_c PM_c \tag{2.39}$$

The PM_s and PM_c are PM-type combination equations for surfaces with bare soil and fully-covered vegetation respectively:

$$PM_s = \frac{\Delta A + \{\rho c_p D - \Delta R_a^s (A - A_s)\}/(R_a^a + R_a^s)}{\Delta + \gamma\left(1 + \frac{R_s^s}{(R_a^a + R_a^s)}\right)} \tag{2.40}$$

$$PM_c = \frac{\Delta A + \left(\rho c_p D - \Delta R_a^c A_s\right)/(R_a^a + R_a^c)}{\Delta + \gamma\left(1 + \frac{R_s^c}{(R_a^a + R_a^c)}\right)} \tag{2.41}$$

The C_s and C_c coefficients in Eq. (2.39) are given by:

$$C_s = \left(1 + \frac{R_s R_a}{R_c (R_s + R_a)}\right)^{-1} \tag{2.42}$$

$$C_c = \left(1 + \frac{R_c R_a}{R_s (R_c + R_a)}\right)^{-1} \tag{2.43}$$

where R_a, R_s and R_c are given by:

$$R_a = (\Delta + \gamma) R_a^a \tag{2.44}$$

$$R_s = (\Delta + \gamma) R_a^s + \gamma R_s^s \tag{2.45}$$

$$R_c = (\Delta + \gamma) R_a^c + \gamma R_s^c \tag{2.46}$$

The net irradiance above the canopy is partitioned between the vegetation (R_{nc}) and the soil surface (R_{ns}) using the exponential Beer's law:

$$R_{ns} = R_n \exp(-C \cdot LAI) \tag{2.47}$$

$$R_{nc} = 1 - [R_n \exp(-C \cdot LAI)] \tag{2.48}$$

where C is the extinction coefficient of the crop and LAI the leaf are index. Exponential models are derived on the assumption of a horizontally homogeneous closed canopy with randomly mixed foliage elements. Therefore, its application on heterogeneous or sparse crops with the component parts too separated in space and/or with foliage elements within the canopy organized in non-random manner may violate the basic assumption of the exponential models (Lhomme and Chehbouni, 1999). This needs to be replaced by a radiation interception model that accounts for radiation penetration through heterogeneous canopies (Kustas and Norman, 1999).

2.4.2.2 Dual-source: uncoupled (patch) models

The uncoupled or patch model is applied to a patchwork terrain with small ratio of vegetation height to patch size. The patches act independent of one another and the total available energy flux (*A*) is partitioned based on contributions from the fractional cover of the patches (Lhomme and Chehbouni, 1999):

$$A = (1-\alpha)A_s + \alpha A_c \tag{2.49}$$

where α denotes fractional cover of the vegetation patch. The same is also true for the total sensible and latent energy fluxes. The model combines the energy balance equations with the classic Ohm's law equations to give the PM-type equation for calculating the sensible heat and latent energy fluxes from the soil and vegetative components:

$$\lambda E_s = \frac{\Delta A_s + \rho c_p D / R_a^s}{\Delta + \gamma\left(1 + \frac{R_s^s}{R_a^s}\right)} \tag{2.50}$$

$$\lambda E_c = \frac{\Delta A_c + \rho c_p D / R_a^c}{\Delta + \gamma\left(1 + \frac{R_s^c}{R_a^c}\right)} \tag{2.51}$$

2.4.3 Resistance formulations

Knowledge of the resistance parameters is key to understanding combination equations for an accurate estimation of evaporation. The required resistance parameters are usually the aerodynamic, plant canopy and soil surface resistances. The aerodynamic resistances are usually related to the height of the plant above the ground and density of the vegetative part of the plant which influence the wind speed, size and diffusivity of eddies within the canopy. The plant canopy resistances are functions of the degree of stomatal opening, which in turn are affected by photosynthetically active irradiance, ambient CO_2 concentration, leaf temperature, leaf water vapour pressure deficit, leaf water status, etc. The soil surface resistance is influenced by variations in temperature and water vapour

pressure of the soil surface and directly beneath in relation to that of the air or the canopy, and the degree of soil wetness. Theoretical solutions and experimental difficulties encountered in acquiring these parameters will be discussed in following sections.

2.4.3.1 Penman-Monteith 'Big leaf' models

The PM 'big leaf' models require knowledge of the aerodynamic and boundary layer canopy resistances *a priori* in order to physically describe the total evaporation. The aerodynamic resistance for a canopy is given as (Thom, 1971):

$$R_{am} = R_h = \frac{1}{ku_*}\ln\left(\frac{z-d}{z_{om}}\right) + \Psi_m(\zeta) \tag{2.52}$$

where R_{am} and R_h are the aerodynamic resistances to momentum and sensible heat transfer respectively, k the von Kármán's constant, u_* the friction velocity, z measurement height, d the zero plane of displacement, z_{om} the roughness length for momentum and Ψ_m the stability correction factor for momentum transfer. But the resistance to heat exchange is greater than the corresponding resistance to momentum in plant canopies because the source of heat is located lower in the plant canopy compared to the sink of momentum (Thom, 1972). This is expressed as an excess resistance (R_b) that is added to R_{am} in order to obtain a corrected value of R_h. Thus,

$$R_h = R_{am} + R_b \tag{2.53}$$

R_b is related to friction velocity and von Kármán's constant as follows (Thom, 1972):

$$R_b = B^{-1}/u_*, \text{ with } kB^{-1} = \ln\left(z_{om}/z_{oh}\right) \Rightarrow R_b = \frac{\ln\left(z_{om}/z_{oh}\right)}{ku_*} \tag{2.54}$$

z_{oh} is the roughness length for sensible heat flux. Therefore R_h is given by:

$$R_h = \frac{1}{ku_*}\left(\ln\left(\frac{z-d}{z_{om}}\right)+\ln\left(\frac{z_{om}}{z_{oh}}\right)+\left(\Psi_m(\zeta)-\Psi_h(\zeta)\right)\right) \qquad (2.55)$$

Canopy resistance, R_a^c, is assumed to be equal to the resistances of all individual stomates in a canopy arranged in parallel. Shuttleworth and Wallace (1985) described R_a^c as an inverse function of *LAI*:

$$R_a^c = {r_s}/{2LAI} \qquad (2.56)$$

where r_s is the mean stomatal resistance per unit surface area of vegetation and *LAI* is the total leaf area index of the vegetative canopy.

In a sense, this R_a^c in the PM equation is meant to account for the control that the plants exert on water vapour transfer from the canopy to the atmosphere. Empirical equations that relate the stomatal resistance (r_s) to variables that can be independently measured have been developed in the past. For example, Jarvis (1976) developed an empirical relationship that estimates r_s as a function of photosynthetically active irradiance, leaf temperature, leaf water vapour deficit, leaf water potential, soil moisture conditions and CO_2 concentration. Equations like the Jarvis (1976) or related ones have been employed in many evaporation models (e.g., Dolman *et al.*, 1993; Stannard, 1993; Blyth and Harding, 1995; Huntingford *et al.*, 1995). Determination of the r_s value will be dealt with in the next section.

The significance of the PM equation lies on how accurately these bulk resistances are determined from their single leaf counterparts or estimated from other relationships, which may not be an easy task to accomplish. This is the reason why most of the time these parameters are determined from independent measurements of available energy fluxes, water vapour pressure deficit and air temperature at a reference height (Raupach and Finnigan, 1988).

2.4.3.2 Dual-source models

2.4.3.2.1 Aerodynamic resistances

Height of the plant above the ground and density of the vegetative part of the plant are among the key factors that influence wind speed, size and diffusivity of eddies within the canopy and thereby the transfer of heat and water vapour below and above the canopy. The SW model employs two aerodynamic resistances: between the substrate and the mean canopy height, R_a^s and between the mean canopy height and reference height, R_a^a. Shuttleworth and Wallace (1985), for a fully developed canopy ($LAI \geq 4$), assumed that:

(i) the effective source of energy flux occurs at $d + z_o$, with $d = 0.63h$ and $z_o = 0.13h$,

(ii) the eddy diffusion coefficient, K, above the canopy is given by (Thom, 1971),

$$K = ku_*(z-d), \quad (z > h) \tag{2.57}$$

with u_*, in neutral conditions of stability, given by:

$$u_* = \frac{ku_z}{\ln\left(z-d/z_o\right)} \tag{2.58}$$

where u_z is the mean wind speed at a reference height.

(iii) the eddy diffusion coefficient decreases with height (Thom, 1971), thus

$$K = K_h \exp\left(-n\left(1-z/h\right)\right) \quad \left(z < h\right) \tag{2.59}$$

where K_h is the value of K at the top of the crop given by $ku_*(h - d)$, and n the eddy diffusivity decay constant for a closed canopy. The reciprocal of the eddy diffusion coefficient was integrated over the heights zero to $d + z_o$, and $d + z_o$ to z to derive an expression for the R_a^s and R_a^a respectively for bare soil and closed canopy, and it was assumed that R_a^s and R_a^a vary linearly with LAI values in between. In this regard, d and z_o

are implicitly defined in the transition between the two limits. In common with Choudhury and Monteith (1988), Shuttleworth and Gurney (1990) explicitly defined d and z_o, as functions of LAI by fitting simple functions to curves derived from second-order closure of in-canopy turbulent transfer in Shaw and Pereira (1982):

$$d = 1.1h\ln(1+X^{1/4}) \tag{2.60}$$

$$z_o = \begin{cases} z'_o + 0.3hX^{1/2} & 0 \le X \le 0.2 \\ 0.3h(1-d/h) & 0.2 < X \le 1.5 \end{cases} \tag{2.61}$$

where z'_o is the roughness length of the substrate, and

$$X = c_d LAI \tag{2.62}$$

where c_d is the effective value of the mean drag coefficient for the individual vegetative elements making up the canopy. Shuttleworth and Gurney (1990) retained the three assumptions of Shuttleworth and Wallace (1985) but set the effective source of energy to $d_p + Z_o$, where $d_p = 0.63h$ and $Z_o = 0.13h$, as preferred values over $d + z_o$. The impact of this on estimated values of surface resistance was found to be very small, but Shuttleworth and Gurney (1990) recommended that this explicit description of $d + z_o$ be used in evaporation models.

Considering the above assumptions and integrating the reciprocal of the eddy diffusion coefficient and the decay of the eddy diffusion coefficient equations, over the heights zero to $d_p + Z_o$ and $d_p + Z_o$ and z respectively, R_a^s and R_a^a can be expressed as (Shuttleworth and Gurney, 1990):

$$R_a^s = \frac{h\exp(n)}{nK_h}\left[\exp(-nz'_o/h) - \exp\left(-n(z_o+d)/h\right)\right] \tag{2.63}$$

$$R_a^a = \frac{1}{ku_*}\ln\left(\frac{z-d}{h-d}\right) + \frac{h}{nK_h}\left[\exp\left\{n\left(1-\frac{Z_o+d_p}{h}\right)\right\} - 1\right] \tag{2.64}$$

Choudhury *et al*. (1986), assuming that the roughness length for momentum and sensible heat are equal, also expressed R_a^a for non-neutral conditions in the following way:

$$R_a^a = \frac{\ln^2\left((z-d)/z_o\right)}{k^2 u_z \left(1+\eta\right)^p} \tag{2.65}$$

where p = 0.75 and 2 for unstable and stable conditions respectively and,

$$\eta = 5\left(z-d\right)\left(T_s - T_a\right)/T_a u_z^{\,2} \tag{2.66}$$

where T_s and T_a are the surface and air temperatures respectively.

2.4.3.2.2 Crop canopy resistance

The transfer of water vapour and heat between individual leaves and the canopy air stream is affected by thickness and size of the leaf, degree of stomatal opening and the temperature and water vapour pressure of air and wind speed in the vicinity of the leaves. Shuttleworth and Wallace (1985) and Shuttleworth and Gurney (1990), assuming that the eddy diffusion of momentum and energy through the canopy is similar and energy transfer within the canopy occurs only by molecular diffusion through a laminar layer around the leaves, described the bulk boundary layer resistance, R_a^c, as:

$$R_a^c = r_b \big/ 2LAI \tag{2.67}$$

where r_b is the mean leaf boundary layer resistance per unit surface area of vegetation.

Shuttleworth and Wallace (1985) used a prescribed typical value, achieved from the literature, of 25 s m^{-1} for r_b. Shuttleworth and Gurney (1990) and Lhomme *et al*. (1994a, b, 1997), following Choudhury and Monteith (1988), used a relationship for estimating r_b based on average canopy (w_l) and wind speed at the top of the canopy (u_h):

$$r_b = \left(\frac{100}{n}\right)\left(\frac{w_l}{u_h}\right)^{1/2}\left[1-\exp\left(\frac{-n}{2}\right)\right]^{-1} \tag{2.68}$$

Shuttleworth and Gurney (1990) argued that the representation of the bulk stomatal resistance of the canopy as a variation of *LAI* in Shuttleworth and Wallace (1985) was an unrealistically simple presentation of the biological aspect. Instead, they derived it as a function of solar irradiance incident on the leaves, cuticular and stomatal resistances of the individual leaves. They assumed the solar irradiance, $I'(LAI')$, at a certain depth in the canopy, above which the leaf area index is LAI', although this may vary depending on the type of canopy, can be written as:

$$I'(LAI') = I_s \exp(-C \cdot LAI') \tag{2.69}$$

The solar irradiance at the top of the canopy is I_s, and C is the attenuation constant. The mean irradiance of the leaf, R_l, at any depth in the canopy, is equivalent to the attenuation of the vertical flux and, from Eq. (2.69), is:

$$R_l = \frac{-\partial I'(LAI')}{\partial LAI'} = C\, I'(LAI') \tag{2.70}$$

Expressing the stomatal resistance (r_s) in terms of stomatal conductance (g_s) for a single leaf, in which r_s is equal to the reciprocal of g_s, given by:

$$g_s = r_0 + \frac{c_1 R_l}{1 + c_2 R_l} \tag{2.71}$$

where r_0 is the cuticular resistance, assumed to be light independent, c_1 and c_2 are constants that may change significantly with species and canopies. The stomatal conductance of the canopy (G_c), assuming r_0, c_1 and c_2 are independent of leaf position, is set equal to that of the leaves acting in parallel with a total leaf area of *LAI*:

$$G_c(R, LAI) = \int_0^{LAI} g_s(LAI')\, dLAI' \tag{2.72}$$

Then, by combining and integrating Eqs (2.70), (2.71) and (2.72) Shuttleworth and Gurney (1990) arrived at an expression for G_c:

$$G_c(I_s, LAI) = r_0 LAI + \left(\frac{c_1}{c_2 C}\right)\ln\left(\frac{1+c_2 C I_s}{1+c_2 C I_s \exp(\alpha' LAI)}\right) \qquad (2.73)$$

2.4.3.2.3 Soil surface resistance

Shuttleworth and Wallace (1985) and Shuttleworth and Gurney (1990) used only prescribed values of R_s^s corresponding to wet, intermediate and dry soil. Shuttleworth and Gurney (1990) noted that the most inhibiting factor to the usefulness of the SW model may be the poor definition of R_s^s, whose value may remain unknown or poorly measured for practical applications. Others have expressed R_s^s as a function of soil water content and elapsed time, with soil evaporation occurring progressively from a wet soil beneath a dry soil (e.g., Choudhury and Monteith, 1988; Stannard, 1993). Kabat *et al.* (1997) estimated R_s^s based on the Ritchie (1972) approach, which describes bare soil evaporation in two distinct phases, as limited by available energy and available soil water respectively.

2.4.3.3 Resistance computation and parameterization

The most challenging part of the evaporation models is perhaps determining the resistance parameters. Measurement of the resistance parameters in the field is quite difficult and laborious. As described above, these parameters may be estimated from physically-based methods or empirical relationships, but computation and parameterization of the resistances often suffer from lack of a commonly-accepted method.

The aerodynamic resistances are often computed by integrating the reciprocal of the eddy diffusion coefficient and inverting the combination equation or, where stability corrections are required, solving for friction velocity and aerodynamic resistances iteratively. But the classical logarithmic wind profile equation is not applicable for the transfer of sensible heat flux because the transfer of heat encounters greater aerodynamic resistance than the transfer of momentum (Thom, 1972). This translates to the sensible heat flux as having a

lower effective source than the effective sink of momentum. The roughness length and surface temperature associated with sensible heat then become two unknowns in the energy balance and resistance equation. This has prompted researchers to add an extra aerodynamic resistance as a corrective term to the combination equations in estimating the sensible heat flux.

The crop canopy resistances may be measured with a great deal of hard labour at a leaf scale. This may be relatively easy when a plant is composed of only few leaves, as in most grasses, but when the leaves are many, sampling errors are inevitable. These problems have led many researchers to relate such measurements to independent variables. The most commonly used empirical relationship is that of Jarvis (1976) or variants of related procedures drawn thereof which compute stomatal resistance by optimizing parameters of the model using a particular period dataset assuming the variables remain constant (e.g., Dolman, 1993; Stannard, 1993; Blyth and Harding, 1995; Huntingford *et al*., 1995). Lhomme *et al*. (1997) used trial and error to adjust stomatal resistance based on best fit between calculated and measured surface temperatures. Bulk boundary-layer resistance of the canopy is mostly computed following Choudhury and Monteith (1988) who integrated the leaf boundary-layer conductance over the canopy height, assuming *LAI* to be uniformly distributed with height. Stannard (1993) found that the Choudhury and Monteith derivation not to work well for extremely small *LAI*, instead he proposed a method that computes it as a function of turbulent intensities, leaf width, thermal diffusivity of air and the Nusselt number. Huntingford *et al*. (1995) also computed it as functions of the Stanton number and *LAI*. Assuming the resistance values are achieved either from measurements or other relations at the leaf scale successfully, then how these could be scaled up to canopy level resistance is yet another challenge that needs to be overcome. Since these are surface resistances, the common procedure that is followed is to relate them to *LAI* of the canopy (Shuttleworth and Wallace, 1985).

The soil surface resistance also adds another hurdle to the challenge. The value of soil surface resistance may be easily estimated when the soil is in the extreme limits of wetness (saturated or dry condition); it may also be ignored when the soil is fully covered by the vegetation canopy. The difficulty of determining the soil surface resistance arises when the soil surface has intermediate wetness and is not fully covered. Most efforts directed towards solving this problem attempt to relate it to measurable variables of soil water

content or potential along with elapsed time (e.g., Choudhury and Monteith, 1988; Dolman, 1993; Stannard, 1993; Kabat *et al.*, 1997). Norman *et al*. (1995) estimated soil surface resistance as a function of wind speed at a height above the soil surface where the effect of the soil surface roughness is minimal, typically 0.05 to 0.2 m.

Considering the difficulty of measuring the resistance terms, some researchers opted to infer some of these resistance parameters from independent measurements of sensible heat or latent energy fluxes. Some of the resistance parameters clearly depend on weather, structural and soil water conditions and they could be determined by considering measurements over a short period of time (usually in the order of days) assuming that these variables remain constant for that period of time. Such parameters tend to be restricted to the type of conditions for which they are obtained, with limited application outside the conditions under which they are derived. It would be difficult to translate or transfer such parameters to a similar crop separated in time or space. Considering seasonal crops (involving a lot of structural and climatic change) and/or perennial vegetation, the parameters may not be unique for each stage of growth and climatic factors. The mean value of the resistance parameter for a certain growth period or soil water condition will also depend on sensitivity of the model to such parameters.

2.4.4 Net irradiance transmission

Net irradiance of the canopy system can be measured either using net radiometers or estimated from solar irradiance measurements above (and below) the canopy. The net irradiance absorbed by the soil (R_{ns}) is given by a Beer's law relationship of the form:

$$R_{ns} = R_n \exp(-C \cdot LAI) \tag{2.74}$$

and the net irradiance absorbed by the foliage is given:

$$R_{nc} = R_n - R_{ns} = R_n \left[1 - \exp(-C \cdot LAI)\right] \tag{2.75}$$

The use of Beer's law formulation for net irradiance attenuation for sparse canopies using dual-source models has been criticized as inadequate by Kustas and Norman (1999).

Accordingly, they modified the formulations of net irradiance by considering the net shortwave and net longwave irradiances separately for both the soil and vegetation canopy. They also suggested a modification to the equation so that foliage clumping, which is a common occurrence in sparse vegetation, would be accounted for.

2.4.5 Applications

Since the birth of the SW model, several experiments have been conducted to test the validity of the model using independent measurements of total evaporation for various crops over a range of *LAI*. Model outputs from both the SW model and PM equation were also compared for similar conditions. Wallace *et al*. (1990) used the PM equation and SW model to estimate transpiration from sparse dryland millet from measurements of stomatal conductance and *LAI*. They reported a systematic difference in calculated transpiration from the two formulations during the early growth stage of the crop, when the crop was short with low leaf area index. Lafleur and Rouse (1990) and Farahani and Bausch (1995) conducted a field study to assess the seasonal performance of the PM equation and SW model against Bowen ratio energy balance (BREB) measurements over a wetland sedge and maize respectively. The SW model estimates were found to be superior and in good agreement with hourly and daily BREB observations over the sedge and with seasonal cumulative evaporation measurements of maize compared to PM equation estimates, especially during early stages of vegetation growth. Kato *et al*. (2004) also reported similar findings when they compared estimated total evaporation using the PM equation and SW model against BREB observations over row crops of sorghum with varying *LAI*. Stannard (1993) compared the PM, SW and modified Priestley-Taylor models for very sparse wildland vegetation ($LAI < 2$) in semiarid rangeland against measurements from eddy covariance. The SW and modified Priestley-Taylor models were in a better agreement with the eddy covariance measurements compared to the PM equation.

Common to all the above experiments was that the difference between the PM equation and SW model estimates was larger when the vegetation was sparse or at its early growth stage. The difference became progressively smaller as the vegetation grew in height and size with an associated increase in *LAI* and coverage of the ground. These findings indicate that the two models are similar at the limit of a closed canopy and this certifies that there is a need for the PM equation to be superceded by multi-source models for season-long

measurements and/or conditions that span a range of *LAI* with the soil not fully covered for some of the time. The performance of the two models is similar when the canopy closes because the SW model reduces to the PM equation as the canopy grows and covers the ground. The poor performance of the PM equation in the early growth stage or sparse vegetation case was simply because the surface resistance ascribed to the model did not consider the fluxes that may arise from the bare soil. Large values of sensible heat flux when the soil is dry and large values of latent energy flux when the soil is wet are usually common and these tend to modify the in-canopy water vapour pressure deficit (Wallace *et al*., 1990), which is not included in the PM equation, and alter the total evaporation from the system.

Dolman (1993) developed a coupled model, an extension to the SW model, and showed that the model could simulate the observed λE for a one-canopy layered tropical forest, a two-canopy layered tropical savannah, and a one-canopy layered agricultural crop interacting directly with the soil surface. This model, along with the big leaf and uncoupled models, has been applied to the Sahelian vegetation by Blythe and Harding (1995), Huntingford *et al*. (1995) and Kabat *et al*. (1997). Although these authors showed that there was reasonably good agreement between model estimates and observed λE, the flux formulations used in their coupled model was criticized by Lhomme and Chehbouni (1999) for being in contradiction with the basic layer approach equations.

With the development of the dual-source SW model, remotely-sensed radiometric surface temperatures have been successfully used to estimate *H* over sparse and heterogeneous vegetation, and hence the λE as a residual term of the shortened surface energy balance equation along with simultaneous measurements/estimations of R_n and *G* (Lhomme *et al*., 1994a). But an excess resistance (kB^{-1}) due to the replacement of aerodynamic temperature by a radiometric one is often used as a corrective term along with the combination equations in estimating the *H*. This 'radiometric' kB^{-1} is different from its aerodynamic counterpart and has been a subject of several studies in the past (e.g., Kustas *et al*., 1989; Lhomme *et al*., 1994a, b, 1997, 2000; Chehbouni *et al*., 1997; Troufleau *et al*., 1997). Little, if any, convergence has been reached on a commonly-accepted way of determining the 'radiometric' kB^{-1} and it remains largely as a fitting parameter (Troufleau *et al*., 1997).

Kustas *et al*. (1989), in a study of the energy balance of sparse vegetation composed of bushes and bare soil in arid climate using airborne infrared thermometer observations, concluded that the value of kB^{-1} may range from 1 to 10. They proposed parameterization of the excess resistance, kB^{-1}, as a function $u_z(T_r - T_a)$. Troufleau *et al*. (1997), however, found that the parameterization of kB^{-1} as proposed by Kustas *et al*. (1989) to be valid only for high *H* values. Stewart *et al*. (1994) also reported values of kB^{-1} ranging from 3.4 to 12.4 for eight semiarid sites. Lhomme *et al*. (1994a, b), on the other hand, used a statistical relationship that linked radiative-air temperature differences to soil-foliage temperature differences in order to estimate *H* over sparse millet crop and Sahelian fallow savannah. They found that the model-estimated *H* compared reasonably well with measurements obtained by the BREB method. Lhomme *et al*. (1997) and Troufleau *et al*. (1997) showed that the radiometric kB^{-1} was not constant, as is often assumed, for a given canopy but varied with the vegetation, surface resistances and meteorological conditions. Empirical relationships that relate radiative-aerodynamic surface temperature differences to radiative-air temperature differences (Troufleau *et al*., 1997), radiative-aerodynamic surface temperature difference to radiative-air temperature gradient and *LAI* (Chehbouni *et al*., 1997) and analytical solutions (Lhomme *et al*., 1997) focused towards improving the estimation of the parameter radiometric kB^{-1} resulted in a good agreement between predicted and measured *H* over sparse vegetations. Lhomme *et al*. (2000) also proposed a polynomial function for deriving a generic value of kB^{-1} as a function of *LAI*, for various view angle classes. But all these parameterizations are at their preliminary stage and remain largely experimental.

Norman *et al*. (1995) used single- and two-layer approaches with parallel arrangement of resistances and inputs of radiometric surface temperature to estimate *H* over sparse vegetation in semiarid and subhumid sites. Modelled total *H*, λE, and *G* agreed reasonably well with measured experimental data. They found that there was no improvement in using two-layer models over the single-layer models for the dataset they used. But they have underlined that there was no need of tuning certain parameters against measured data in the two-layer model as was the case in the single-layer model. Later Kustas and Norman (1999) showed that the partitioning of the fluxes between the soil and vegetation using the Norman *et al*. (1995) model for row crops was not realistic. Accordingly they modified the formulations of net irradiance (to allow for the effect of clumping in sparse vegetation) and

aerodynamic resistances, and adjusted the magnitude of the Priestley-Taylor coefficient for transpiration, resulting in an improved agreement with observations.

Most of the field measurements that tend to validate the single- and dual-source models were focused only in measuring the total flux from the canopy and not as arising from the soil and the plant canopy. It is difficult to partition the soil and the vegetation component fluxes in fields with incomplete cover because the system is too complex to allow separate measurement of fluxes. Perhaps that is why most of the experiments conducted so far compare measured versus model-estimated total fluxes and not the component fluxes. This is also not possible where remote sensing is applied to measure *H* of the system because radiometric surface temperature measurements are area-weighed mean of the soil and plant component temperatures, not of the soil or plant alone. Kustas and Norman (1999) attempted to partition the soil and vegetation fluxes but they only compared them against outputs from another model and not against field measurements.

The spacing between rows and the distance between plants play a decisive role in the mass and energy transfer in the soil-plant-atmosphere-continuum system. Separation of the soil and vegetation fluxes may have a tremendous implication in early growth stage of crops, row crops with incomplete cover, agroforestry systems, afforestation and reforestation programs. This could be used in water resource management in general as in agriculture and hydrology. It could also be taken a step further both in space and time dimensions to infer regional influence of vegetation on the atmosphere and vice versa both in the present and future time.

3 SENSIBLE HEAT FLUX ESTIMATION USING TEMPERATURE-VARIANCE OVER DIFFERENT SURFACES

ABSTRACT

Direct measurement of the exchange of mass and energy between the land surface and atmosphere is often constrained by the investment required in instruments and expertise. In this study, the performance of a temperature-variance (TV) method, based on statistical measures of air temperature at different heights, varying surface inhomogeneity, from a sparse vegetation of *Jatropha curcas*, mixed grassland community to a fallow land, was evaluated for its suitability to reproduce the direct measurements of sensible heat flux (H) and friction velocity using eddy covariance. Atmospheric stability conditions were identified using (i) sensor height (z) and Obukhov length (L) from eddy covariance and (ii) air temperature difference between two thermocouple measurement heights. Formulations of the TV method involving actual and estimated skewness of air temperature and no skewness of air temperature for unstable conditions only and for all stability conditions were used. The estimated H from TV method using the temperature difference to identify stability conditions yielded an improved agreement in terms of slope, coefficient of determination and root mean square error compared to H estimated using the z/L means of identifying stability conditions over sparse vegetation. The agreement between the estimated and measured H appeared to be good when actual skewness of air temperature was included compared to using no skewness or the inclusion of estimated skewness of air temperature. The inclusion of estimated skewness of air temperature over not using skewness also showed significant improvement in estimation of H for the sparse vegetation of *J. curcas*. The agreement between the friction velocity as estimated from the TV method and measured by eddy covariance appeared to be poor. The TV method could be used to estimate H for surfaces with varying homogeneity with reasonable accuracy.

Keywords: Sensible heat flux; temperature-variance; air temperature skewness; atmospheric stability conditions

3.1 INTRODUCTION

The exchange of mass and energy between the land surface and the atmosphere is important in agricultural, hydrological, ecological and climatological processes (Choudhury and Monteith, 1988; de Bruin *et al*., 1993; Prueger and Kustas, 2005). Several methods have been developed to measure and estimate mass and energy exchanges in the soil-plant-atmosphere system. Among these, eddy covariance (EC) is the most commonly used method for direct measurement of these fluxes. However, the cost of the equipment and expertise required to run the system, correct the measurements and process the data has confined its use mainly to research applications. This prompts for simple, accurate, less expensive and robust alternative instrumentation that can determine these fluxes for routine field applications. The temperature-variance (TV), also referred to as flux-variance, method is a simple and relatively inexpensive technique that uses the Monin and Obukhov (1954) Similarity Theory (MOST) along with statistical measures of air temperature to estimate sensible heat flux (H) from temperature fluctuations only, without the need for turbulence measurement of wind velocity. This method has been pioneered by Tillman (1972) for homogeneous surfaces under dry and unstable atmospheric conditions. Since its inception, it has been successfully applied to determine H over a range of surface homogeneities (e.g., Wesely, 1988; Weaver, 1990; Lloyd *et al*., 1991; de Bruin *et al*., 1993; Padro, 1993; Kustas *et al*., 1994; Albertson *et al*., 1995; Katul *et al*., 1995, 1996; Hsieh *et al*., 1996, 2008; Unland *et al*., 1996; Wesson *et al*., 2001; Castellvi and Martínez-Cob, 2005; Guo *et al*., 2009).

The TV method uses a simplified relation derived for the free convection condition ($z/L \leq$ -0.04 where z is the measurement height above the ground and L the Obukhov length) (Wyngaard *et al*., 1971) to estimate H for unstable conditions, with versions of the method extended to the neutral and stable zones (e.g., Tillman, 1972; Albertson *et al*., 1995; Wesson *et al*., 2001; de Bruin and Hartogensis, 2005). Some workers have sought the application of the full equation developed by Tillman (1972) but were constrained by the inability to determine the stability parameter, or more specifically the friction velocity, u_*, easily and accurately. This problem was solved either iteratively (e.g., Kustas *et al*., 1994; Hsieh *et al*., 1996) or using additional measurements, most notably eddy covariance (EC), for determining u_*. But the introduction of sensors other than those for high frequency air

temperature measurements to determine the atmospheric stability condition negates the simplicity of the TV method. The classic work by Tillman (1972) has used skewness of air temperature to estimate the stability parameter for the inertial sublayer and has reported an improved agreement between the measured and estimated *H*. Savage (2007) has also used skewness of air temperature to adjust TV-estimated *H* over a grassland site but resulted in consistent bias when compared to *H* obtained using EC. None of the other work that followed Tillman (1972) have exploited the applicability of skewness of air temperature in determining *H* using the TV method.

This study investigates the applicability of the TV method with and without skewness of air temperature under different atmospheric stability conditions using high frequency air temperature measurements at different heights over rough sparse vegetation of *J. curcas*, and homogeneous mixed grassland community and fallow bare soil. This study also assesses the determination of stability conditions of the atmosphere using air temperature difference between two thermocouples (TCs) located at different heights, and sensor height (z) and Obukhov length (L) measurements from the EC method for use in the TV method. The TV method estimates of *H* were compared against those obtained using EC.

3.2 THEORY

Using MOST (Monin and Obukhov, 1954), the standard deviation of the concentration fluctuation of a scalar entity, σ_c, above a flat homogeneous surface can be expressed as a dimensionless function of atmospheric stability, $-z/L$ (Monin and Yaglom, 1971):

$$\frac{\sigma_c}{c_*} = f\left(-z/L\right) \tag{3.1}$$

where c_* is the turbulent scale for the scalar concentration and L is given by:

$$L = -\frac{\overline{T}}{kg} \cdot \frac{\rho c_p}{H} \cdot u_*^{\,3} \tag{3.2}$$

where $\overline{T}$ is the average air temperature (K), k the von Kármán constant (0.41), g the acceleration of gravity (9.7968 m s^{-2}), ρ the mean density of air (1.14 kg m^{-3}), c_p the specific heat capacity of air at constant pressure (1011 J kg^{-1} K^{-1}), u_* the friction velocity and H the sensible heat flux related to the profiles of wind speed and temperature through

$$H = \rho c_p u_* T_* \tag{3.3}$$

where T_* is the turbulent scale for temperature (K). Tillman (1972) exploited the relationship between the normalized standard deviation of air temperature, σ_T / T_*, and a function of atmospheric stability, $f(-z/L)$, to arrive at an expression that satisfies the near-neutral and free convection limits for the inertial sublayer. The free convection limit ($z/L \leq -0.04$), appears to scale well with $(-z/L)^{1/3}$, and Wyngaard *et al.* (1971) obtained the following relationship, which also appears to have good applicability for the general unstable range (Tillman, 1972):

$$\frac{\sigma_T}{T_*} = c_1 \left(-z/L\right)^{-1/3} \tag{3.4}$$

For the near neutral limit, $-z/L$ approaches zero and σ_T / T_* tends to a constant value, c_3. An expression that satisfies both the near-neutral and free convection limits is then given by (Tillman, 1972):

$$\frac{\sigma_T}{T_*} = c_1 \left(c_2 - \frac{z}{L}\right)^{-1/3} \tag{3.5}$$

From this it follows that for the near-neutral and neutral conditions:

$$c_2 = \left(\frac{c_1}{c_3}\right)^3 \tag{3.6}$$

where c_1 and c_2 are similarity constants given as 0.95 and 0.05 respectively by Tillman (1972) based on the work of Wyngaard *et al.* (1971), and c_3 is given as 1.77 (Tillman,

1972) and more recently as 2 (de Bruin *et al*., 1993) for the near-neutral and stable portion of the stability range.

MOST also indicates that functions of dimensionless higher order moments such as skewness of air temperature (s_k) are determined by z/L. Hence s_k could be used in estimating the stability parameter of the atmosphere from a single scalar variable of air temperature (Tillman, 1972):

$$s_k = \frac{1}{\sigma_T^{\,3}}\left[\frac{1}{n}\sum_{i=1}^{n}\left(T_i - \overline{T}\right)^3\right] \tag{3.7}$$

$$\frac{z}{L} = -A\exp\left(Bs_k\right), \text{ for } -3 < \frac{z}{L} \le -0.01 \tag{3.8}$$

where T_i is the sample air temperature at time i, n the number of air temperature observations in the averaging period, and A and B constants given as 0.0137 and 4.39 respectively. Eqs (3.2), (3.3) and (3.5) – for the whole unstable region and Eqs (3.2), (3.3) and (3.4) – for the free convection zone, respectively, can be combined following Tillman (1972) to relate H with σ_T and $\overline{T}$ only, independent of u_*, as follows:

$$H = \rho c_p\left[\left(\frac{\sigma_T}{c_1}\right)^3\left(\frac{kgz}{\overline{T}}\right)\left(\frac{c_2 - z/L}{-z/L}\right)\right]^{1/2} \text{ for } \frac{z}{L} < 0 \tag{3.9}$$

$$H = \rho c_p\left[\left(\frac{\sigma_T}{c_1}\right)^3\left(\frac{kgz}{\overline{T}}\right)\right]^{1/2} \text{ for } \frac{z}{L} < -0.2 \tag{3.10}$$

Substituting the expression of z/L from Eq. (3.8) into Eq. (3.9) gives:

$$H = \rho c_p\left[\left(\frac{\sigma_T}{c_1}\right)^3\left(\frac{kgz}{\overline{T}}\right)\left(\frac{c_2 + A\exp\left(Bs_k\right)}{A\exp\left(Bs_k\right)}\right)\right]^{1/2} \tag{3.11}$$

Originally the TV method, since it is based on MOST, was meant to be used along with measurements conducted in the inertial sublayer, but many works have demonstrated the validity of the method in the roughness sublayer as well (e.g., Weaver, 1990; Lloyd *et al*., 1991; Padro, 1993; Albertson *et al*., 1995; Katul *et al*., 1995, 1996; Hsieh *et al*, 1996; Wesson *et al*., 2001; Castellvi and Martínez-Cob, 2005). In fact, Castellvi and Martínez-Cob (2005) evaluated the performance of the TV method in both sublayers and found more accurate results in the roughness sublayer than in the inertial sublayer. Measurements of H conducted in the roughness sublayer are proportional to $z^{½}$ whereas measurements conducted in the inertial sublayer are proportional to $(z - d)^{½}$ (Chen *et al*., 1997b). In this study, the height of roughness sublayer is taken as $5h/3$ (Sellers *et al*., 1986) and z and $z - d$ are used for measurements below and above the $5h/3$ height respectively. The method is also believed to have little applicability under near-neutral and stable conditions (e.g., Llyod *et al*., 1990; Katul *et al*., 1995; Unland *et al*., 1996 and Castellvi and Martínez-Cob, 2005). However, from similarity theory, the fact that σ_T/T_* tends to approach a constant in the near-neutral and stable region can be used (Tillman, 1972) to estimate H from TV method in these stability regions.

In the same manner as for H, similar relations could also be forged for u_* for unstable conditions (Tillman, 1972),

$$u_* = \frac{H}{\rho c_p \left(\frac{\sigma_T}{c_1}\right)\left[c_2 + A\exp\left(Bs_k\right)\right]^{1/3}} \tag{3.12}$$

3.3 MATERIALS AND METHODS

Unshielded and naturally-ventilated fine-wire chromel-constantan thermocouples (TCs), 75 μm in diameter, were mounted at different heights above the ground over sparse vegetation, mixed grassland community and bare fallow land representing different surface homogeneities. Each unit consisted of a pair of TCs arranged in parallel to ensure continuity and minimize loss of data as the TCs could get broken once in a while. A three-dimensional sonic anemometer (Model 81000, RM Young, Traverse City, MI), mounted at a certain height above the ground surface, was also used to measure high frequency virtual

temperature and wind speed at all the sites. The coordinate system was rotated post-data collection, based on a 30-minute observation period, to ensure that the lateral and vertical wind speeds are zero (Kaimal and Finnigan, 1994). This was done to remove errors that might be introduced due to instrumentation alignment (tilt errors) and air flow irregularities (Lee *et al.*, 2006). The sensors were connected to a CR5000 datalogger (Campbell Scientific Inc., Logan, UT). All measurements were done differentially at 10-Hz frequency. The data were subsequently processed over two- and 30-minute time periods. Details of the surfaces, sensor heights and period of measurement are given in Table 3.1.

The Jatropha trees were planted in a 3-m plant and inter-row spacing in a 50 m × 60 m plot with the surrounding plots planted to a mixture of Jatropha trees and Kikuyu grass. The fetch distance from the prevailing wind direction was 40 m. The grassland consisted of mixed grass communities and was situated in an area with 140 m by 100 m with about 85 m fetch in the direction of the prevailing wind direction. The fallow land was bare apart from straw that was left over from a soybean harvested four months prior to the measurements. The dimensions of the fallow land were >300 m by 160 m with a fetch distance of about 230 m from the prevailing wind direction.

Eqs (3.10) and (3.11) were used to calculate *H* from high frequency air temperature measurements made by TCs at different heights (both in the roughness and inertial sublay-

Table 3.1 Details of crops, site, sensor and vegetation heights, and period of measurement

Crop	Site and area	Location	Height (m)			Period of measurement (day of year)
			TC	3-D sonic	Vegetation	
Jatropha (*J. curcas*)	Ukulinga, Pietermaritzburg 0.3 ha	29°40′11″S 30°24′50″E 781 masl	1.20 (1.20) / 2.15 (1.75) / 3.00 (2.35) / (3.8)	2.3	1.0 (1.2)	322-331, 2005 (206-213, 2006)
Mixed grass community	Ukulinga, Pietermaritzburg 1.4 ha	29°67′49″S 30°40′12″E 840 masl	0.8 / 1.8	2.0	0.4	316-333, 2008
Fallow land	Baynesfield > 4.8 ha	29°45′25″S 30°18′2″E 910 masl	0.3 / 0.5	1.2	-	207-228, 2008

ers according to the 5*h*/3 definition of the roughness sublayer height adopted) and their standard deviations. The TV method was originally developed for dry and unstable atmospheric conditions (Tillman, 1972). The issue of identifying stability conditions is, therefore, of utmost importance when determining *H* using this method. The atmospheric stability conditions are given by $z/L < 0$ for unstable, $z/L \approx 0$ for neutral and $z/L > 0$ for stable conditions. It is difficult to determine the *z/L* term from high frequency air temperature measurements only, but it can be easily determined from high frequency wind velocity measurements using the EC system. Qualitative atmospheric stability conditions could be indicated by the difference between two air temperature measurements at different heights. An air temperature measurement, corrected for dry adiabatic lapse rate, at a lower height that exceeds that of an air temperature measurement at a higher height indicates unstable atmospheric condition, and vice versa (Kaimal and Finnigan, 1994). Neutral conditions are indicated by similar air temperature measurements at the two heights. Therefore, the *z/L* calculated from the EC measurements and air temperature difference between two thermocouple measurement heights were used as the two criteria to identify stability condition of the atmosphere for estimating *H* using Eq. (3.11) of the TV method.

The literature finds that the c_1 coefficient varies between 0.95 and 1.1, and a value of 1 is usually taken as universal. Therefore $c_1 = 1$ is used in this study and adjusted to take into account the von Kármán constant, $k = 0.41$. Under near-neutral and stable conditions, a constant coefficient, $c_3 = -2$ is used in Eq. (3.11) following de Bruin *et al*. (1993) with the c_2 coefficient recalculated from Eq. (3.6) equal to 0.35.

The skewness term in Eq. (3.11) was also estimated from a linear relationship between s_k and σ_T. The slope and intercept were established and used along with σ_T in place of s_k for determining *H*. This third option was used as well for estimating *H*. This was needed because σ_T could be easily calculated but s_k values were not always available.

Graphical and statistical methods were used to compare the *H* estimated from TV (H_{TV}) against those obtained from EC (H_{EC}). Graphs depicting distributions of H_{TV} versus H_{EC} on a one-to-one line were used for a quick means of visual evaluation. The statistical indices used also included slope and intercept of a least-squares regression between the estimated

and measured H; the coefficient of determination (r^2), and total root mean square error (*RMSE*).

3.4 RESULTS AND DISCUSSION

Two-minute estimations of H from high frequency air temperature measurements using TCs at different heights were conducted and then averaged over 30 minutes. The H from TV (H_{TV}) were compared against H from eddy covariance (H_{EC}) computed every 30 min for different atmospheric stability conditions.

3.4.1 Sensible heat flux and skewness of air temperature

Since this work adds skewness of air temperature (s_k) to the conventional way of estimating H from the TV method, it is worthy to have an appreciation of the relationship between H and s_k. Skewness is a measure of symmetry or lack of symmetry for certain dataset distribution. Skewness is zero for normally distributed dataset, negative for left skewed distribution (left tail is longer) and positive for right skewed distribution (right tail is longer). A negative skewness of air temperature for a certain period of time indicates that most of the air temperature data for that period of time are less than the mean – implying cooling of the air (e.g., during the evening following sunset). A positive skewness of air temperature, on the other hand, indicates that most of the air temperature data are greater than the mean – implying warming of the air. A zero or near zero values of skewness of air temperature also indicate that the air temperature distribution is symmetric with respect to the mean. Two days two-minute H_{EC} (computed from a three-dimensional sonic anemometer) and s_k (calculated from measurements of high frequency air temperature using fine-wire TC at the same height as the sonic anemometer) were used to depict the relation between the two (Fig. 3.1). H was conventionally assumed to have a positive value when it is directed away from the surface and negative value when directed towards the surface. The trend of H and s_k were similar during the day (unstable condition), but the values of s_k seemed more uncertain during the night while values of H were almost constant with close to zero values throughout the night (stable condition). This relationship shows that values of s_k could be invoked in determining the stability condition of the atmosphere especially during unstable conditions, and hence H.

3.4.2 Sensible heat flux estimation

3.4.2.1 Sparse vegetation: J. curcas

Data for about nine consecutive clear sky days in late autumn of 2005 and winter of 2006, representing high and low solar irradiance loads respectively, were used to test the applicability of the TV method over sparse vegetation of *J. curcas* under unstable conditions only and under all atmospheric stability conditions. The vegetation height, *h*, was, on average, about 1 and 1.2 m in the late autumn of 2005 and winter of 2006 respectively. The estimated H_{TV} were compared against the measured H_{EC}.

3.4.2.1.1 Sensible heat flux under unstable conditions

Identifying the unstable conditions on the basis of *z/L* criterion from EC measurements returned more unstable instances than using the air temperature difference between two measurement heights for the same period. In the site where the measurements were conducted, unstable conditions usually prevail during the day, whereas stable conditions prevail during the night with early morning and early evening being the transition periods. Identifying the unstable conditions using the air temperature difference between two measurement heights agreed with the above statement very well, whereas the *z/L* criterion

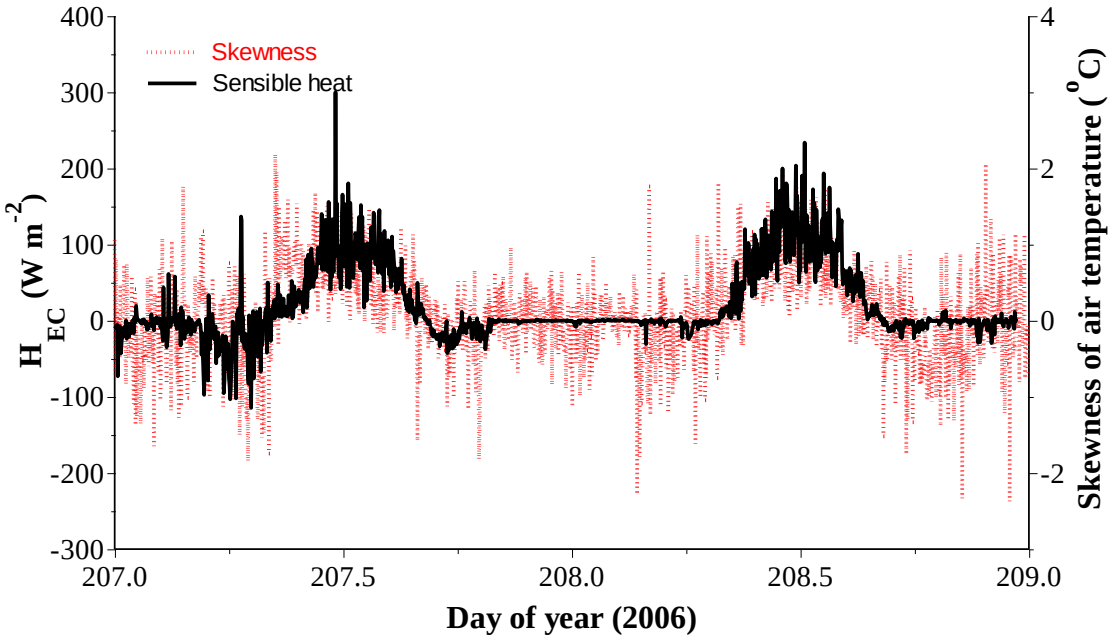

Fig. 3.1 Diurnal variation of H_{EC} and skewness of air temperature over *J. curcas*

indicated unstable conditions during the night as well. The statistical indices achieved by comparing the estimated and measured H were also better in the case where stability conditions were identified using the air temperature difference between two measurement heights rather than using the z/L criterion (Tables 3.2 and 3.3).

The H_{EC} values close to zero were not reproduced well by the TV method when the z/L criterion of identifying atmospheric stability condition was used (Fig. 3.2). This was because the coefficients assigned for these estimations were for unstable conditions and accordingly not compatible with the near-neutral and neutral stability conditions. The statistics achieved by comparing the measured and estimated H, with and without s_k are given in Table 3.2. The slope, for the respective measurement heights, was closer to one when s_k was used, but the graphs showed more scatter in the near-neutral and neutral zone

Table 3.2 Statistical results achieved from comparing 30-min averages of unstable H_{TV} estimates, identified using z/L criterion and calculated with and without actual s_k, and H_{EC} measurements for *J. curcas* (doy 205 to 212, 2006) n = 251

Measurement height (m)	Slope	Intercept (W m^{-2})	r^2	*RMSE* (W m^{-2})
Without skewness				
1.20	0.49	31.45	0.33	37.18
1.75	0.50	31.45	0.28	42.36
2.35	0.40	31.66	0.25	37.79
3.80	0.51	32.58	0.31	39.04
With actual skewness				
1.20	0.55	40.40	0.25	48.59
1.75	0.60	46.68	0.23	56.93
2.35	0.47	37.01	0.24	43.18
3.80	0.63	31.45	0.33	45.51

Table 3.3 Statistical results achieved from comparing 30-min averages of unstable H_{TV} estimates, identified using the air temperature difference criterion and calculated with and without s_k, and H_{EC} measurements for *J. curcas* (doy 205 to 212, 2006) n = 157

Measurement height (m)	Slope	Intercept (W m^{-2})	r^2	*RMSE* (W m^{-2})
Without skewness				
1.20	0.62	9.77	0.86	26.08
1.75	0.65	10.51	0.86	24.55
2.35	0.52	9.22	0.85	32.66
3.80	0.58	13.14	0.80	28.17
With actual skewness				
1.20	0.72	12.85	0.86	20.95
1.75	0.77	13.37	0.86	20.05
2.35	0.59	12.06	0.83	27.51
3.80	0.69	17.11	0.76	25.31

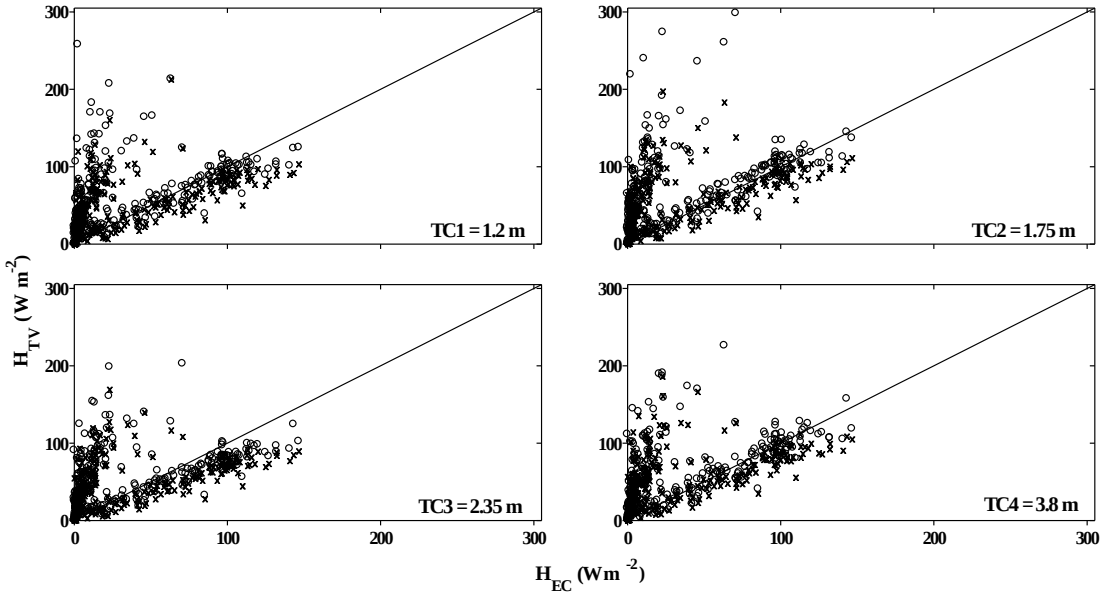

Fig. 3.2 Half-hourly averages of unstable H_{TV} estimates, identified using the *z/L* criterion and calculated with (○) and without (×) actual s_k, plotted against H_{EC} measurements over *J. curcas* (doy 205 to 212, 2006)

of stability conditions when s_k was included and consequently the r^2 and *RMSE* were inferior to the case where s_k was not used. The sign of the s_k values in the neutral and near neutral zone are not clearly defined and may have contributed towards the relatively poor r^2 and *RMSE*. Castellvi and Martínez-Cob (2005) also found similar results for the near-neutral and neutral stability conditions. Weaver (1990) had indicated that the TV method does not reproduce well the small flux measurements since they are susceptible to large errors, and even suggested that they might require determination of separate local coefficients. It should be noted as well that the relations on which the TV method is founded were meant to work only in the free convection and unstable zones for the inertial sublayer.

When the air temperature difference between two measurement heights was used as a criterion of identifying the stability condition, the *H* from the TV method usually return values greater than zero (unstable) but few zero and negative (neutral and stable) *H* values were observed in the corresponding measurements from EC. Consequently, the agreement between the two methods in the instances where zero and negative *H* values were measured by the EC method was not good (Fig. 3.3). Yet the statistical indices achieved following this procedure were by far better than when stability conditions of the atmosphere were identified using the *z/L* criterion (Table 3.3). This shows that the air temperature difference means of identifying stability conditions matches well with the free

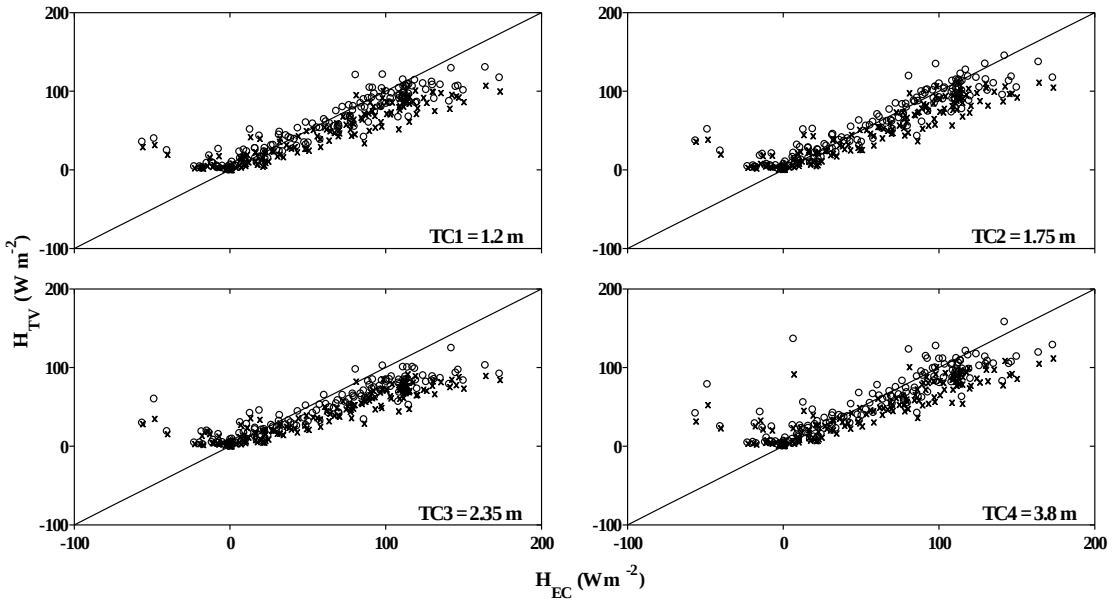

Fig. 3.3 Half-hourly averages of unstable H_{TV} estimates, identified using air temperature difference criterion and calculated with (○) and without (×) actual s_k, against H_{EC} over *J. curcas* (doy 205 to 212, 2006)

convective zone in which Eq. (3.10) is valid. It should be noted, however, that the data points resulting from the air temperature difference method of identifying unstable atmospheric conditions were less in magnitude than using the *z/L* criterion (Tables 3.2 and 3.3). A better agreement was also observed when s_k was included in the estimation of *H* along with the air temperature difference to identify stability conditions for the respective measurement heights (Fig. 3.3 and Table 3.3). The slope and *RMSE* were improved by the inclusion of s_k while the r^2 did not change much. These results also indicate that inclusion of s_k in the TV method improves the accuracy of the estimated *H*.

3.4.2.1.2 Sensible heat flux under stable and unstable conditions

The TV method could also be extended to near-neutral and stable conditions assuming that the σ_T / T_* approaches a constant (Tillman 1972; de Bruin *et al.*, 1993; Albertson *et al.*, 1995; Wesson *et al.*, 2001). Eq. (3.11) was used to determine *H* for unstable, neutral and stable atmospheric conditions. Atmospheric stability conditions were identified using the air temperature difference between two measurement heights following the results of Section 3.4.2.1.1. For the near-neutral and stable atmospheric conditions a $c_3 = 2$ was used following de Bruin *et al*. (1993) with the stability part of the equation equated to one and the c_2 coefficient recalculated according to Eq. (3.6). One-to-one graphs depicting the

agreement between 30 minute H averages computed from the TV method (using no s_k, actual s_k and estimated s_k) and those determined from the EC method are presented in Figs 3.4, 3.5 and 3.6. The statistical indices resulting from the comparisons are also presented in Table 3.4.

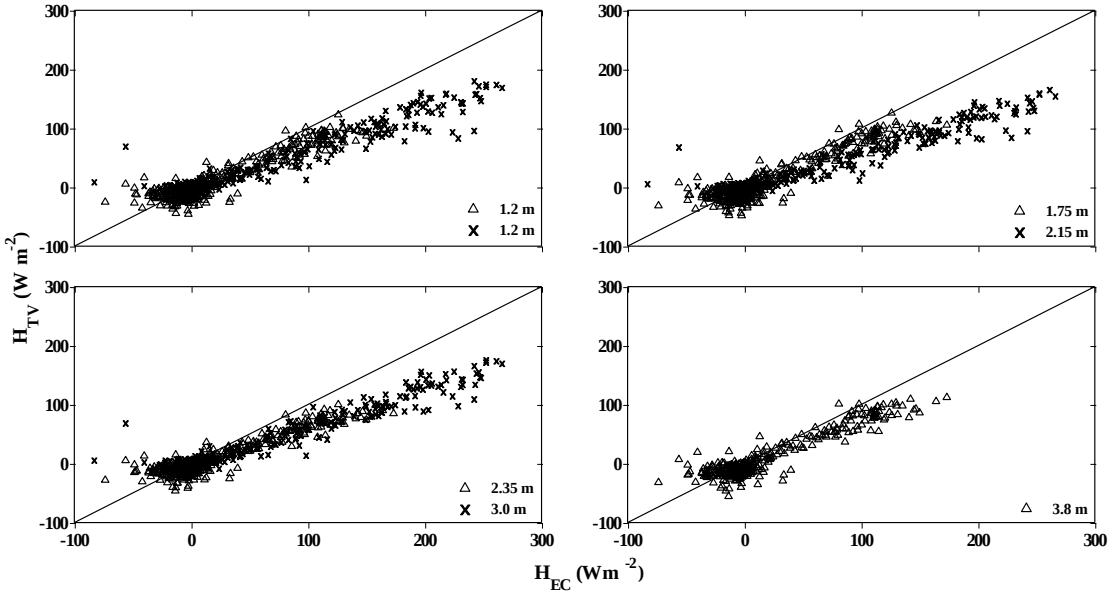

Fig. 3.4 Half-hourly averages of H_{TV} estimates calculated without s_k, with stability conditions identified using air temperature difference criterion, plotted against H_{EC} measurement over *J. curcas* – the ×s and Δs represent data from late autumn of 2005 and winter of 2006 respectively

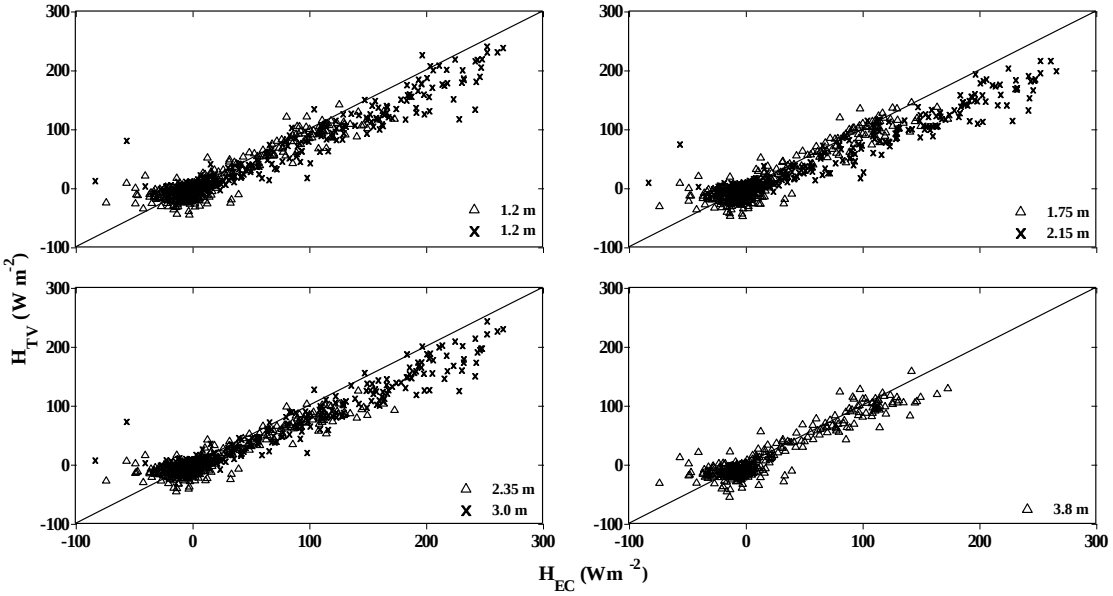

Fig. 3.5 Half-hourly averages of H_{TV} estimates calculated with actual s_k, with stability conditions identified using air temperature difference criterion, plotted against H_{EC} measurements over *J. curcas* - the ×s and Δs represent data from late autumn of 2005 and winter of 2006 respectively

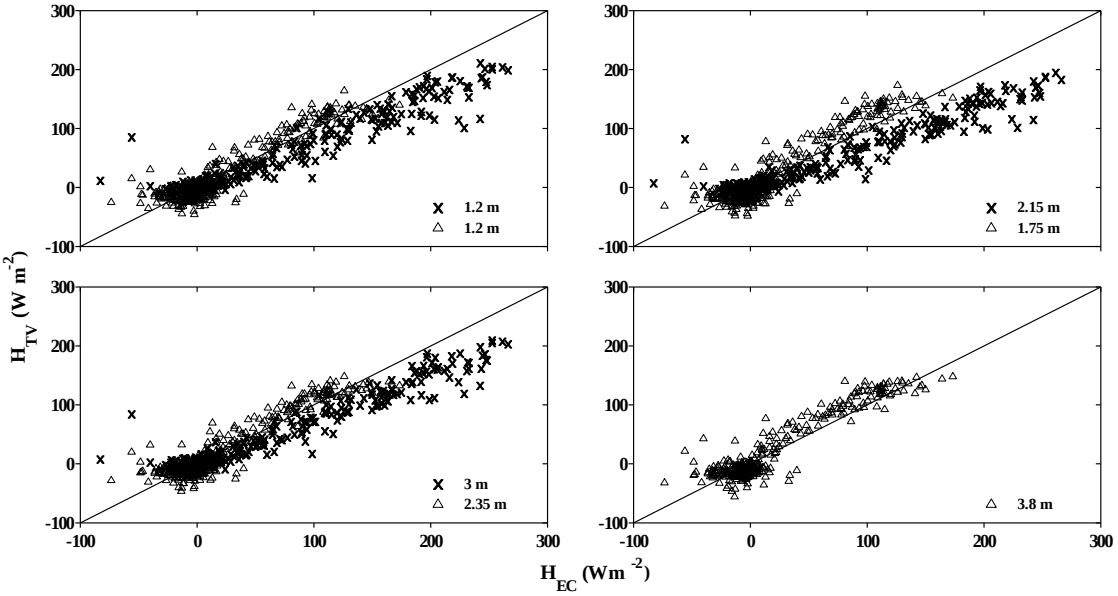

Fig. 3.6 Half-hourly averages of H_{TV} estimates calculated using estimated s_k, with stability conditions identified using air temperature difference criterion, plotted against H_{EC} measurements over *J. curcas* - the ×s and Δs represent data from late autumn of 2005 and winter of 2006 respectively

Table 3.4 Statistical results achieved from comparing 30-min average H_{TV} estimates from all stability conditions calculated without, with actual and estimated s_k values and H_{EC} measured during November 2005 and July 2006 for *J. curcas*

s_k	Period	Measurement height (m)	Slope	Intercept (W m^{-2})	r^2	*RMSE* (W m^{-2})	*n*
Without s_k	18-27 Nov, 2005	1.22	0.62	0.99	0.93	36.96	408
		2.15	0.56	0.78	0.94	41.88	408
		3.00	0.60	0.81	0.94	37.84	408
	24-31 July, 2006	1.20	0.74	-4.67	0.87	20.98	358
		1.75	0.78	-5.43	0.87	20.45	358
		2.35	0.63	-5.02	0.85	25.09	358
		3.80	0.73	-3.87	0.88	20.68	358
Actual s_k	18-27 Nov, 2005	1.22	0.79	1.11	0.94	23.97	408
		2.15	0.72	0.91	0.94	28.98	408
		3.00	0.78	0.94	0.95	24.72	408
	24-31 July, 2006	1.20	0.86	-3.20	0.88	18.04	358
		1.75	0.91	-3.92	0.88	17.88	358
		2.35	0.73	-3.73	0.87	20.88	358
		3.80	0.86	-2.32	0.88	17.56	358
Estimated s_k	18-27 Nov, 2005	1.22	0.74	2.14	0.93	27.36	408
		2.15	0.67	1.52	0.94	32.68	408
		3.00	0.73	1.64	0.94	27.60	408
	24-31 July, 2006	1.20	1.04	-0.49	0.88	18.34	358
		1.75	1.14	-0.03	0.88	21.51	358
		2.35	1.01	0.82	0.88	17.86	358
		3.80	1.05	1.73	0.88	18.98	358

The r^2 achieved by using no s_k value and using actual and estimated s_k were more or less similar for all the datasets presented. But the deviation of the slope from one was more pronounced when s_k was not incorporated, with somewhat mixed results when estimated s_k values were used. Also, larger *RMSE* (less favourable) were observed in both cases compared to the H estimated using actual s_k values. These results indicate that inclusion of the actual s_k values improve the accuracy of the estimation of H using the TV method from such a rough and heterogeneous surface. The statistical indices also indicated that the H values estimated using estimated s_k values yielded a better agreement than using no s_k compared against H_{EC}. These findings suggest that actual s_k values should be used whenever available, and estimated s_k should be used in their absence as opposed to not using s_k values at all for estimation of H using the TV method.

It was clear from Figs 3.4, 3.5 and 3.6 that the H during the late autumn, where there was larger solar irradiance load, was larger in magnitude than during winter. The agreement between estimated H_{TV} using the actual s_k and measured H_{EC} appear to be good across the range of H values calculated except for a slight underestimation of higher values which were observed in the late autumn (Fig. 3.5). Where estimated s_k values were used in the TV method, more scatter of points below the one-to-one line during late autumn and above the line during winter were observed (Fig. 3.6). When no s_k values were involved, the TV method appears to consistently underestimate the H during both seasons (Fig. 3.4). Some authors (e.g., Weaver, 1990; Padro, 1993; Katul *et al.*, 1995; Hsieh *et al.*, 1996) have also found a consistent bias when the H estimated from TV method was plotted on a one-to-one line against those measured using the EC method. This had led them to suggest that the coefficients used in the TV method should be modified depending on the surface conditions where the measurements are made. Such adjustment would make the TV method requiring calibration with the EC method for each surface and crop stage used. In this study, the bias appeared to be less when the actual s_k values were used (Fig. 3.5) – suggesting that, perhaps part of the adjustment could be done by the inclusion of s_k into the TV equation.

The agreement between the estimated H_{TV} and measured H_{EC} seemed different for the range of the atmospheric stability conditions encountered. The unstable H values were well distributed, although slightly biased towards the strong unstable conditions. The near-neutral and stable H values appeared to have uncertain relationship with the points

congested all over this region with a tendency of overestimation towards strong stable conditions.

It was also noted that the statistics achieved by comparing the H_{TV} computed from the sensors mounted above the roughness sublayer mark, defined as $5h/3$ in this study, against H_{EC} was not good compared to the other sensors mounted within the roughness sublayer. This was prominent especially if the sensors were mounted not far above the $5h/3$ mark (e.g., 2.15 m and 2.35 m in 2005 and 2006 respectively). The main reason for this was because of the change in input of the height from z to $z - d$. It was found that the statistics achieved from the measurements conducted above this height becomes similar to the ones achieved from the other sensors if z were used instead of $z - d$. This shows that H calculated from the TV method using TCs mounted on either side of the 'defined' interface region could differ markedly despite the proximity of the two sensors, and hence the accuracy of the estimates may be compromised because of the definition of the atmospheric sublayer heights. To avoid such ambiguities in the estimations, these sublayers should be defined very well, avoid measurements in the 'transition' zone, introduce certain functions that smoothen the sudden drop of the height input or use different sets of equations for this zone.

Most studies that have been done on the estimation of H using the TV method usually focus over extensive and homogeneous surfaces under unstable atmospheric conditions. But H has also been estimated using the TV method over heterogeneous surfaces (e.g., Weaver 1990; Lloyd *et al.*, 1991; Kustas *et al.*, 1994; Katul *et al.*, 1995; Castellvi and Martínez-Cob, 2005). Weaver (1990) found that the TV relation for estimating H is not universal for non-uniform surfaces, thus requiring calibration of the coefficients depending on the surface type. Stability conditions were determined from profile measurements of wind speed. Lloyd *et al*. (1991), on the other hand, have used Eq. (3.10) of the TV method over different surface types to successfully reproduce the direct measurements of H_{EC} with universal coefficients. They specifically found slopes of 1.04 and 1.05, r^2 of 0.90 and 0.96, and standard error of estimate (*SEE*) equal to 17.5 and 44.9 W m^{-2} for relatively rough surfaces of fallow savannah and Tiger bush respectively. Kustas *et al*. (1994) reported a *RMSE* of 26.5 W m^{-2} by comparing H_{TV} against H_{EC} for unstable conditions over a heterogeneous sparse shrub and grass mixed sites. They estimated u_* iteratively in order to determine stability conditions. Katul *et al*. (1995) also found, using Eq. (3.10), a slope of

0.89, r^2 of 0.68 and *SEE* of 49.4 W m^{-2} by comparing H_{TV} against H_{EC} for a naturally rough non-uniform terrain composed of uneven-aged forest. Castellvi and Martínez-Cob (2005) also used the TV method over a heterogeneous olive orchard using two measurement heights above the canopy. They reported a r^2 of 0.73 for both heights, slope of 0.90 and 0.73, and *RMSE* of 46.6 and 53.1 W m^{-2} for the upper and lower measurement heights respectively. Stability conditions were determined from mean horizontal wind speed measurements. The statistical indices obtained in our study using Eq. (3.11) for unstable conditions are better in terms of the *SEE* (data not shown) and *RMSE*, and comparable in terms of r^2 reported in the above studies (Table 3.3). But it is noted that the slopes obtained in our study for some of the measurement heights deviate from unity more than the above studies report (Table 3.3).

Wesson *et al*. (2001) applied the TV method to all stability conditions to determine *H* over pine forest, grass-covered forest clearing and a dry-bed lake assuming σ_T / T_* equals a constant value, c_3. They reported a slope ranging between 0.90 and 1.09, and *RMSE* of 20.49 and 39.68 W m^{-2}. The results obtained in our study using a similar method (Table 3.4) from different measurement heights suggest a similar *RMSE* over a heterogeneous surface. The slopes in our study vary depending on the inclusion or nature of s_k used in the TV method. In general, the formulation that used actual and estimated s_k yielded slopes comparable to the ones reported by Wesson *et al*. (2001) especially in winter, while the other formulations resulted in slopes that deviate from unity more than Wesson *et al*. (2001) reported for all stability conditions (Table 3.4).

3.4.2.2 Homogeneous surfaces: mixed grassland community and fallow land

For comparison with the *J. curcas* results, *H* was also estimated using the TV method over homogeneous surfaces of mixed grassland and bare fallow land and compared against EC measurements. Data collected for about two weeks from sunrise to sunset were used for analysis assuming that mostly unstable atmospheric conditions would prevail during daylight. Yet neutral and stable conditions might occur during the day as well and hence both the air temperature difference between two measurement heights and the *z/L* criteria were used to identify atmospheric stability conditions. The data for stable atmospheric conditions were then excluded from the analysis. The *H* under both criteria of identifying

stability conditions was also estimated with and without using s_k. Finally, the H estimated using the TV method was compared against those obtained from the EC method.

3.4.2.2.1 Mixed grassland community

In general, the agreement between the estimated H_{TV} and measured H_{EC} for this site exhibited more scatter than in the sparse vegetation (Section 3.4.2.1) for similar number of data points. The H estimated using the z/L criterion of determining atmospheric stability condition showed less scatter than those that used the air temperature difference between two measurement heights (Figs 3.7 and 3.8). Accordingly, some of the statistics achieved from the former criterion showed improved agreement between estimated and measured H, especially where r^2 is concerned (Table 3.5). This could be simply because of the fewer number of data points considered in the z/L criterion than those considered in the air temperature difference criterion. The extra data points considered in the air temperature difference criterion are probably from the neutral and near neutral region of the atmospheric stability condition, which were filtered out in the z/L criterion. Besides the failure to reproduce the magnitude of the stable atmospheric conditions using air temperature difference criterion was also apparent (data not shown). Inclusion of s_k improved all the statistics compared to not using s_k except when the z/L criterion of identifying stability condition was used for the TC mounted at 1.8 m.

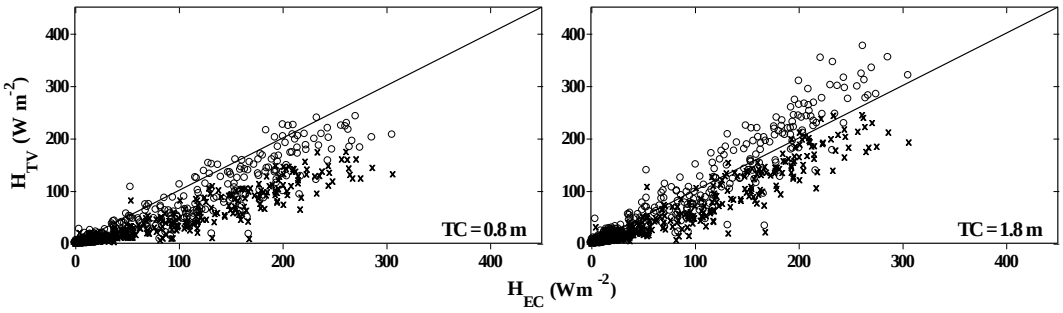

Fig. 3.7 Half-hourly averages of H_{TV} for daylight hours calculated with (○) and without (×) actual *sk*, with stability conditions identified using air temperature difference criterion, plotted against H_{EC} for a mixed grassland community (doy 316-333)

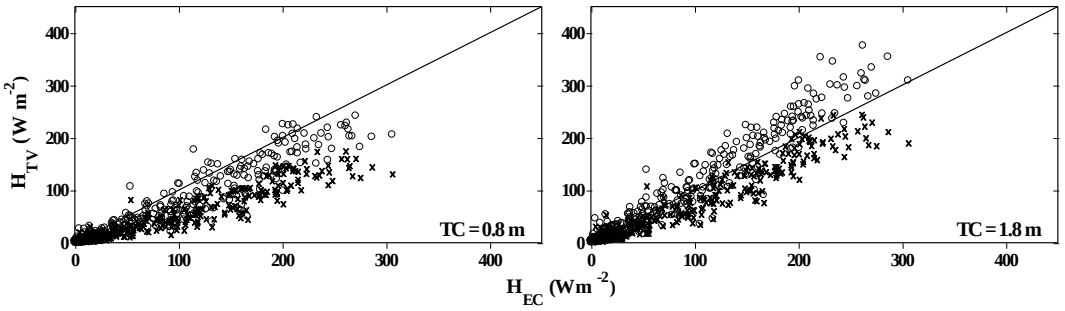

Fig. 3.8 Half-hourly averages of H_{TV} estimates for daylight hours calculated with (○) and without (×) actual s_k, with stability conditions identified using *z/L* criterion, plotted against H_{EC} method for a mixed grassland community (doy 316-333)

When the stability condition was determined using the air temperature difference between two measurement heights, the H_{TV} estimated from the TC mounted at 0.8 m (with and without s_k) underestimated (Fig. 3.7, Table 3.5). While the *H*-TVestimated from the TC mounted at 1.8 m showed variable results: when s_k was used, the higher values of *H* were overestimated, whereas when s_k was not used, there was a consistent underestimation (Fig. 3.7). Similar observations were also noted when the *z/L* criterion of determining stability condition was used albeit showing less outliers (Fig. 3.8). Overall, the H_{TV} estimated from the TC measurements mounted at 1.8 m with and without s_k using both means of identifying stability conditions showed improved agreement.

As in the sparse vegetation, there was little difference in r^2 between H_{TV} determined with and without s_k under the respective means of identifying stability conditions, but the slope and *RMSE* varied. Inclusion of s_k had the effect of increasing the slope, although this may be unde sirable if it increased far beyond one. The s_k had also the effect of decreasing *RMSE* (desirable) especially for the TC mounted at 0.8 m.

Table 3.5 Statistical results achieved from comparing 30-min average H_{TV} estimates computed with and without s_k values and H_{EC} over mixed grassland community during daylight hours (doy 316-333)

Stability criterion	s_k	Measurement height (m)	Slope	Intercept (W m^{-2})	r^2	*RMSE* (W m^{-2})	*n*
Air temperature difference	Actual	0.8	0.79	-6.69	0.88	36.70	381
	s_k	1.8	1.14	-9.48	0.91	29.84	381
	without	0.8	0.54	-4.52	0.88	56.25	371
	s_k	1.8	0.79	-5.94	0.90	34.59	371
z/L	Actual	0.8	0.81	-3.72	0.89	33.69	321
	s_k	1.8	1.17	-4.78	0.93	30.68	321
	without	0.8	0.56	-2.42	0.90	56.48	321
	s_k	1.8	0.81	-2.31	0.93	30.26	321

The height at which the TCs were mounted might be responsible for the differences in statistics achieved from the comparisons, signalling appropriate choice of height of sensors and calibration against standard methods. It should be noted that there was one meter difference between the two TCs, and the upper one (mounted at 1.8 m) was too separated in distance from the vegetation surface. An improved agreement was achieved when z was used instead of $z - d$ for the lower TC (mounted at 0.8 m) indicating lack of a well-defined height for the roughness sublayer. It has been reported that the H_{TV} estimates from sensors mounted in the roughness sublayer yield more accurate results than sensors mounted in the inertial sublayer (Castellvi and Martínez-Cob, 2005). It is noted that the sensor heights used in this study were in the inertial sublayer according to the $5h/3$ definition of the roughness sublayer.

3.4.2.2.2 Fallow land

The fallow land was previously planted to soybean and remnants of the straw were visible on the ground during the time the study was conducted. The TCs were mounted at 0.3 and 0.5 m above the ground surface. Comparison of estimated H_{TV} with the stability condition identified using the air temperature difference between two measurement heights and the z/L criteria was similar as in the mixed grassland community, although the magnitude of H was less in this case (Figs 3.9 and 3.10).

When stability conditions were determined using the air temperature difference criterion, all the H_{TV} estimates showed a tendency to underestimate the measured but the H_{TV} estimated using s_k from the TC mounted at 0.5 m (Fig. 3.9). The underestimation was more pronounced when s_k was not used. Therefore, the TC mounted at 0.5 m with s_k followed by the TC mounted at 0.3 m with s_k showed improved agreements at this site (Table 3.6). As in the mixed grassland community, similar results were observed when H was estimated using the z/L criterion of determining stability condition, with the only difference being more pronounced overestimation at lower values of H (Fig. 3.10).

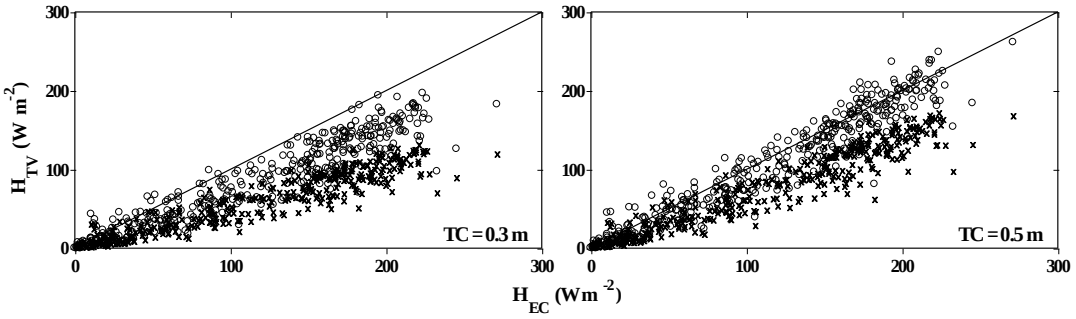

Fig. 3.9 Half-hourly averages of H_{TV} estimates for daylight hours calculated with (○) and without (×) actual s_k, with stability conditions identified using air temperature difference criteria, plotted against H_{EC} measurements for a fallow land (doy 207-228)

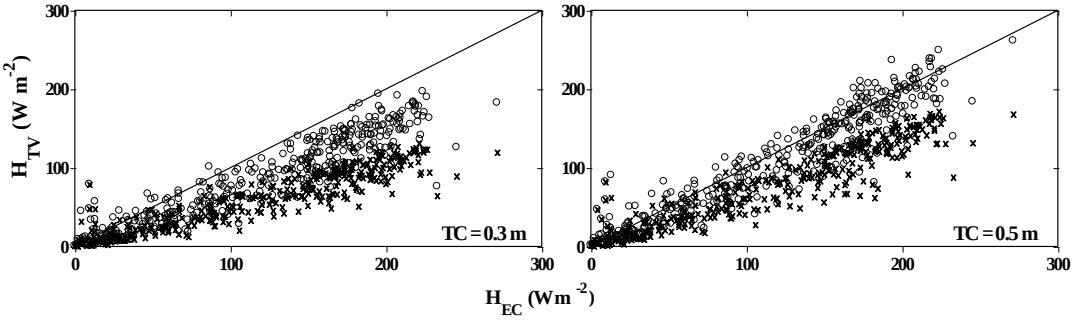

Fig. 3.10 Half-hourly averages of H_{TV} estimates for daylight hours calculated with (○) and without (×) actual s_k, with stability conditions identified using z/L criteria, plotted against H_{EC} for a fallow land (doy 207-228)

Several studies had also been conducted over similar surfaces. For instance, Lloyd *et al*. (1991) and Hsieh *et al*. (2008), using Eq. (3.10), evaluated the TV method over homogeneous surfaces of millet field and grassland community respectively. They reported slopes of 0.84 and 0.83, r^2 of 0.89 and 0.64, and *SEE* (W m^{-2}) equal to 19.1 and 23.91 respectively. In general, the results for the mixed grass community (Table 3.5), especially for the cases where s_k was included using both means of identifying stability conditions, were comparable with the above reports. The *SEE* (W m^{-2}) ranged between 21.77 and 27.79 (data not shown) for the cases where s_k was included, and between 14.49 and 20.01 for the cases where s_k was not included. *SEE* explains the unsystematic or random part of the *RMSE* and thus it should not be surprising to see that the *SEE* for the cases where s_k was included to be greater than for the cases where s_k was not included. In fact, for best estimation, this error should approach the total *RMSE* and the bias or systematic error of the total *RMSE* should approach zero (Willmott, 1981). Lloyd *et al*. (1991), Albertson *et al*. (1995) and Katul *et al*. (1995) also applied Eq. (3.10) of the TV method over extensive bare soil and reported slopes of 0.97, 0.88 and 0.89; r^2 of 0.95, 0.88 and 0.92; and *SEE* (W m^{-2}) of 27.7, 27.5 and 27.4 respectively. Again, comparable results were found for the bare

soil (Table 3.6) for the cases where s_k was included using both means of identifying stability criteria. The *SEE* (W m^{-2}) in this case generally ranged between 12.76 and 21.41 for cases including and excluding s_k using both means of identifying stability conditions. Although the EC system is considered as the standard for measuring energy fluxes, surface energy balance closure studies have shown that it underestimates the surface fluxes (H + λE) by about 10 to 30% (e.g., Twine *et al*., 2000; Wilson *et al*., 2002; Barr *et al*., 2006; Oncley *et al*., 2007; Castellvi *et al*., 2008). If this is correct for H, then the comparison between H_{TV} and H_{EC} need to be adjusted accordingly. But Savage (2009), in a mesic grassland study, had compared H_{EC} against independent H measurements of MOST based surface layer scintillometry and found that the EC did not underestimate H. This suggests that the underestimation may have mainly been in λE.

It should also be noted that the TCs might get broken occasionally, for example due to rain storms, strong winds, birds, etc, and also corrode with time, and hence require regular checkups during field visits (e.g., fortnightly). If the air temperature measurements at different TC heights were chosen to serve as a means of identifying stability criterion, then two or more TCs mounted at different heights, as opposed to the customary single height TC, above the surface of the canopy would be required for the TV method to work under all stability conditions. This might increase the number of TCs required, hence the cost of measurement, but it is still by far less expensive compared to the EC system.

Table 3.6 Statistical results achieved from comparing 30-min average H_{TV} estimates computed with and without s_k values H_{EC} over a fallow land during daylight hours (doy 207-228)

Stability criterion	s_k	Measurement height (m)	Slope	Intercept (W m^{-2})	r^2	*RMSE* (W m^{-2})	*n*
Air temperature difference	Actual	0.3	0.75	-2.77	0.89	40.65	371
	s_k	0.5	0.97	-5.10	0.93	20.79	371
	without	0.3	0.51	-0.57	0.88	68.85	370
	s_k	0.5	0.69	-2.72	0.91	46.74	370
z/L	Actual	0.3	0.74	-0.53	0.88	41.21	369
	s_k	0.5	0.94	--2.16	0.90	23.63	369
	without	0.3	0.50	1.51	0.86	69.29	369
	s_k	0.5	0.67	0.02	0.87	48.89	369

Modern dataloggers with high processing speed can actually calculate s_k directly from high frequency air temperature measurements, allowing real time or online estimation of H, making it possible for the latent energy flux (λE) to be calculated as a residual term of the shortened surface energy balance equation provided measurements of net irradiance and soil heat flux are carried out using the same datalogger. This offers the opportunity for an online calculation of water-use of a system with reasonable accuracy at relatively less cost.

3.4.3. Friction velocity estimation

Friction velocity, u_*, was also predicted using Eq. (3.12) from high frequency measurements of air temperature and its standard deviation and skewness. Atmospheric stability conditions were identified using air temperature difference between two measurement heights. Only data for daytime unstable atmospheric conditions were considered. The agreement between the friction velocities predicted using the TV method from the different measurement heights and those calculated from the EC was poor for all three sites used in this study (Fig. 3.11). A large scatter in general and a negative bias towards larger values of u_* in particular was observed. de Bruin *et al*. (1993) have found a good agreement between u_* computed using an equation similar to Eq. (3.12) and that measured with the EC method for a flat extensive homogeneous surface containing sparse vegetation of grasses and herbs. Their sensors were mounted at about eleven metres above the ground. The large scatter and bias in our case could be due to the closer proximity of the sensors to the vegetation. An improved agreement was observed for TCs mounted at a relatively higher height (Fig 3.11(a) and (b) in our study). Most other studies estimate u_* from the similarity function using measurements of high frequency vertical wind speed and the resulting standard deviation. For example, Katul *et al*. (1995) reported a good agreement between measured and estimated u_*, using the standard deviation of vertical wind speed, for three sites representing a wide range of roughness, atmospheric stability and climate conditions.

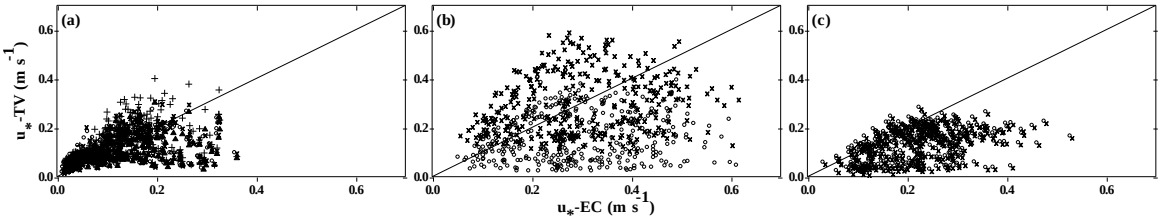

Fig. 3.11 Half-hourly averages of u_* estimated using Eq. (3.12) for unstable atmospheric conditions, with stability conditions identified using air temperature difference criterion, plotted against those obtained from EC for (a) *J. curcas*, (b) grassland, and (c) bare fallow land - the symbols represent (○) TC1, (×) TC2, (+) TC3, and (Δ) TC4- their corresponding heights are given in Table 1

3.5 CONCLUSIONS

Sensible heat flux (H) from a variety of surfaces can be estimated with reasonable accuracy from high frequency measurements of air temperature without the need for measuring turbulence of wind velocity. The temperature-variance (TV) method, using universal constants, was employed to estimate H, over sparse vegetation, mixed grassland community and fallow land, without and with actual and estimated skewness of air temperature (s_k) based on the atmospheric stability conditions. The atmospheric stability conditions were identified using sensor height (z) and Obukhov length (L) measurements from the eddy covariance (EC) and air temperature difference between two thermocouple measurement heights. The air temperature difference criterion showed an improved agreement - in terms of slope, coefficient of determination (r^2) and root mean square error ($RMSE$) – in estimates of unstable H using the TV method compared to z/L criterion over sparse vegetation of *J. Curcas*. The corresponding independent H measurements were conducted using eddy covariance (EC) in both cases. The near-neutral H values estimated from the TV method were not reproduced very well. H_{TV} estimated using actual s_k data resulted in better agreement in terms of slope and $RMSE$ for almost all surfaces compared to not using and/or using estimated s_k within the respective means of identifying stability condition of the atmosphere when compared with H_{EC}. There was little change observed in the r^2 whether actual or estimated or no s_k at all was used. The H determined using estimated s_k from relations between the actual s_k and standard deviation of air temperature also showed an improved agreement over the H estimated without using s_k. This suggests that actual s_k should be used when available, and estimated s_k in its absence than not using s_k at all in the estimation of H using the TV method. Estimation of the friction velocity using the TV method agreed poorly with those calculated from the EC method. The TV

method presents a reasonably accurate and less expensive means of estimating *H* over variety of surfaces.

Acknowledgments

Dr. M Mengistu and Mr. N Moyo - for kindly allowing use of the Ukulinga data for Jatropha and grass respectively, and the Baynesfield Estate – for use of the field facilities at Baynesfield are gratefully acknowledged.

4 SEASONAL WATER-USE ASSESSMENT OF *Jatropha curcas* USING TEMPERATURE-VARIANCE AND SURFACE RENEWAL METHODS

ABSTRACT

Water-use of a system is a complex process that is influenced by the exchange of energy and mass between the surface and the atmosphere. This study was conducted to determine the long-term water-use of a fetch-limited sparse vegetation of *Jatropha curcas* trees using relatively low-cost methods. The sensible heat flux (H) was estimated using temperature-variance (TV) and surface renewal (SR) methods that use only high frequency air temperature measurements without the need for vertical wind speed measurements. Eddy covariance (EC) was also used to determine H. The latent energy flux (λE), and hence the total evaporation, was calculated as a residual of the shortened surface energy balance using measured net irradiance and soil heat flux, and the H determined from the EC, TV and SR methods. Partitioning of the available energy into H and λE was influenced by seasonal changes in the structure of the canopy which in turn responded to changes in environmental conditions. During the dry season H was greater than λE, and vice versa in the wet season. The seasonal H estimated using the TV and SR methods agreed well when compared against those determined using the EC method. The long-term water-use of *J. curcas* trees calculated from the shortened surface energy balance involving the H estimated from the TV and SR methods also agreed very well when compared with those obtained from EC. The seasonal total evaporation for the EC, TV and SR methods were 626, 640 and 674 mm respectively with the rainfall being 690 mm. Footprint analysis was also conducted under all atmospheric stability conditions and revealed that greater than 80% of the measured flux during the day originates from within the surface of interest. The TV and SR methods offer a relatively low-cost means for long-term estimation of H, and the λE, and hence the total evaporation, calculated as a residual of the shortened surface energy balance along with measurements of net irradiance and soil heat flux.

Keywords: temperature-variance; surface renewal; sensible heat flux; latent energy flux; evaporation; shortened energy balance

4.1 INTRODUCTION

Agroforestry systems, whereby trees/shrubs and crops are planted in combination, are destined to reduce the risks associated with agriculture by producing a range of benefits to resource poor farmers including food, fodder and fuel wood in a sustainable manner (Nair, 1991). The trees in agroforestry systems play a role in maintaining soil physical properties through their deeper roots and in some cases restore the soil fertility through nitrogen fixation (leguminous trees) and/or extracting nutrients from deeper depths and shedding their litter on the ground. But there is a contention that such systems consume more resources, especially water, than crops grown separately, and productivity might decrease in cases where such resources are limiting (Nair, 1991).

Jatropha curcas is an oil-rich drought tolerant tree plant belonging to the family Euphorbiaceae (Heller, 1996). It has drawn the interests of scientists and farmers because of its many attributes and potential uses (Openshaw, 2000) and adaptation to a wide range of environmental conditions (Heller, 1996). *J. curcas*, regarded as a promising option for biofuel, is used in manufacturing soap, has medicinal value and like many other trees can be used as means of soil and land protection and CO_2 fixation (Heller, 1996; Gübitz *et al*., 1999; Openshaw, 2000; Francis *et al*., 2005). It is a vigorous, low-growing tree plant, native to Central and South America, but also widely cultivated in the tropics and sub-tropics of Asia and Africa (Heller, 1996; Gübitz *et al*., 1999; Openshaw, 2000; Francis *et al*., 2005). It has few known pests and diseases, and can grow under eroded or marginal soils with low water supply (precipitation ranging from 200 to over 1500 mm per annum) and nutrients (Openshaw, 2000). It is deciduous in nature and sheds its foliage during the dry season. Few studies have attempted to investigate the use of Jatropha trees for various purposes, but reliable scientific information in its water-use is currently lacking. The promotion of cultivation of *J. curcas* on a large scale in a new climatic and soil conditions like South Africa should consider, among other things, its water-use.

Water-use of a system is a complex process that is influenced by the exchange of energy and mass between the surface and the atmosphere. The prevailing atmospheric conditions determine the amount of energy that is available to the surface. This energy is mainly partitioned into fluxes of sensible and latent heat energy and determines the heat and water

vapour content of the atmosphere (Wilson and Baldocchi, 2000). Consequently, this partitioning influences the hydrologic cycle, vertical structure of the atmospheric boundary layer, and many aspects of weather and climatological processes on a regional and global scale (Pielke *et al*., 1998; Wever *et al*., 2002; Wilson *et al*., 2002; Humphreys *et al*., 2003). Hence, an accurate means of obtaining these energy fluxes on a regular basis is vital.

The morphology of the tree crops, which may change from time to time in response to changes in climatic variables, plays a major role in the partitioning of these energy fluxes. Several studies conducted on different ecosystems have indicated that there is significant variability in the partitioning of these fluxes between seasons and years (e.g., Wilson and Baldocchi, 2000; Wever *et al*., 2002; Humphreys *et al*., 2003; Wang *et al*., 2004; Hao *et al*., 2007). Therefore, long-term measurements that capture the energy fluxes arising from the combined effects of different phenological stages and environmental conditions are important for a better understanding and accurate quantification these energy components.

The eddy covariance (EC) method (Swinbank, 1951) offers a direct means of measuring these energy fluxes. However, the cost of the equipment and expertise required for reliable measurements has confined its use mainly to research applications. There is, therefore, a need for simple, accurate, less expensive and robust alternative instrumentations that allow these fluxes to be measured for routine field applications. Methods that involve the measurement of high frequency temperature, *viz* temperature-variance and surface renewal methods, to estimate the sensible heat flux (H) component have gained wide-spread attention in the last two decades. The temperature-variance (TV), also referred to as flux-variance, method (Tillman, 1972) is based on the Monin and Obukhov (1954) Similarity Theory (MOST). Surface renewal (SR) is based on the principle that an air parcel near the surface is renewed by an air parcel from above (Paw U *et al*., 1995).

This study, therefore, quantifies and compares long-term H from a fetch-limited *J. curcas* plot as estimated from EC, TV and SR methods and the latent energy flux (λE), and hence the total evaporation, calculated as a residual term of the shortened surface energy balance involving measurements of net irradiance and soil heat flux.

4.2 THEORY

4.2.1 Surface energy balance

The shortened energy balance of a flat homogeneous surface can be written as:

$$R_n = H + \lambda E + G \tag{4.1}$$

where R_n is the net irradiance, H the sensible heat flux, λE the latent energy flux and G the soil heat flux, with all having W m^{-2} as their unit. This equation defines an energy component, apart from R_n, to be positive when directed away from the surface and negative when directed towards the surface. Closure of the energy balance is said to be met when independently measured components satisfy Eq. 4.1. The λE term, and thereby the total evaporation, can be calculated as a residual of the shortened surface energy balance equation by rearranging Eq. 4.1, assuming closure is met.

4.2.2 Eddy covariance (EC) method

Eddy covariance (EC) allows a direct measurement of H above extensive surfaces of homogeneous medium using high frequency vertical wind velocity (w) and air temperature (T) measurements (Swinbank, 1951):

$$H = \rho c_p \overline{w'T'} \tag{4.2}$$

where ρ is the density of air (1.14 kg m^{-3}), c_p the specific heat capacity of air at constant pressure (1011 J kg^{-1} K^{-1}), w the vertical wind velocity and T the sonic temperature. The primes denote fluctuation from the mean over certain sampling period of time, typically 30 to 60 minutes to capture all of the eddy motions that contribute to the flux (Meyers and Baldocchi, 2005).

4.2.3 Temperature-variance (TV) method

The TV method is a simple and relatively inexpensive technique that uses MOST (Monin and Obukhov, 1954) along with statistical measures of air temperature to estimate *H*, without the need for measuring friction velocity. This method has been pioneered by Tillman (1972) and has been successfully applied to determine *H* over a range of surfaces (e.g., Wesely, 1988; Weaver, 1990; Lloyd *et al*., 1991; de Bruin *et al*., 1993; Padro, 1993; Kustas *et al*., 1994; Albertson *et al*., 1995; Katul *et al*., 1995, 1996; Hsieh *et al*., 1996, 2008; Unland *et al*., 1996; Wesson *et al*., 2001; Sugita and Kawakubo, 2003; Prueger *et al*., 2004; Castellvi and Martínez-Cob, 2005; Guo *et al*., 2009).

Tillman (1972) proposed the following relations to estimate *H* for the whole unstable region and for the free convection zone, respectively.

$$H = \rho c_p \left[\left(\frac{\sigma_T}{c_1} \right)^3 \left(\frac{kgz}{\overline{T}} \right) \left(\frac{c_2 + A\exp\left(Bs_k\right)}{A\exp\left(Bs_k\right)} \right) \right]^{1/2} \tag{4.3}$$

$$H = \rho c_p \left[\left(\frac{\sigma_T}{c_1} \right)^3 \left(\frac{kgz}{\overline{T}} \right) \right]^{1/2} \quad \text{for } \frac{z}{L} < -0.2 \tag{4.4}$$

where σ_T is standard deviation of air temperature, *k* the von Kármán constant (0.41), *g* the acceleration of gravity (m s^{-2}), *z* the measurement height above the ground (m), $\overline{T}$ the average air temperature (K), s_k the skewness of air temperature, *L* the Obukhov length (m) and c_1 and c_2 are similarity constants given as 0.95 and 0.05 by Tillman (1972) based on the work of Wyngaard *et al*. (1971), and c_3 is given as 1.77 (Tillman, 1972) and more recently as 2 (de Bruin *et al*., 1993) for the near-neutral and stable portion of the stability range. The derivation of the above equations is well documented in Tillman (1972).

Atmospheric stability conditions were identified using the air temperature difference between two observations at different heights. An air temperature measurement, corrected for dry adiabatic lapse rate, at a lower height that exceeds that of an air temperature

measurement at a higher height was taken as unstable atmospheric condition, and vice versa (Kaimal and Finnigan, 1994).

4.2.4 Surface renewal (SR) method

The SR method is a simple and relatively inexpensive technique that is based on the principle that an air parcel near the surface is renewed by an air parcel from above (Paw U *et al*., 1995). This process involves ramp-like structures (rapid increase and decrease of a scalar), which are the result of turbulent coherent structures that are known to exhibit ejections and sweeps under shear conditions (Gao *et al*., 1989; Raupach *et al*., 1989; Paw U *et al*., 1992). The theory of heat exchange between a surface and the atmosphere using the SR method is described in detail in Paw U *et al*. (1995), Snyder *et al*. (1996, 1997) and Paw U *et al*. (2005). The exchange of heat energy between a surface and the atmosphere is expressed as:

$$H = \alpha \rho c_p z \frac{a}{s+l} \tag{4.5}$$

where α is a weighting factor, a the amplitude of the air temperature ramps and (s + l) the total ramping period, where s, the quiescent period, refers to the time when there is no change in air temperature, and l, the ramping period, refers to the time when there is a change in air temperature. The amplitude (a) and the ramping period (s + l) were deduced using analytical solutions of van Atta (1977) for air temperature structure function:

$$S^n(r) = \frac{1}{m-j} \sum_{i=1+j}^{m} (T_i - T_{i-j})^n \tag{4.6}$$

where n is the power of the function, m the number of data points in the time interval measured at frequency f (Hz), j the number of sample lags between data points corresponding to a time lag $r = j/f$ and T_i the sample air temperature at time i. Time lags of 0.5 and 1.0 s were used in this study. Second, third and fifth order of the air temperature structure parameter are required to solve for a and (s + l).

Eq. (4.5) was used to estimate H using the measurement height (z) and weighting factor (α) obtained by calibration, usually by regressing independent measurements of H from the EC method versus H from the SR method. The weighting factor α depends on measurement height, canopy architecture and thermocouple size (Snyder *et al*., 1996; Spano *et al*., 1997a, b, 2000; Duce *et al*., 1998). Once determined, it is fairly stable, almost invariant and does not change from site to site regardless of weather conditions unless the surface roughness changes (Paw U *et al*., 1995; Snyder *et al*., 1996, 2008; Spano *et al*., 2000).

4.2.5 Footprint

Micrometeorological techniques conducted over a fetch-limited area usually require a footprint analysis to ensure that the sampled fluxes/concentrations have the surface of interest as their source. Flux footprint describes the contribution per unit source strength, of each element of the upwind surface area source to the vertical scalar flux or concentration measured at a height z (Horst and Weil, 1992). The relationship between flux density (H in this case) $F(x, z\text{-}d)$ and footprint $f(x, z\text{-}d)$ is given by:

$$F(x, z-d) = \int_{-\infty}^{x} S(x)\, f(x, z-d)\, dx \qquad (4.7)$$

where S (W m^{-3} for H) is the source strength at a distance x (m), usually in the upwind direction, from the measurement height z (m) above the ground surface for roughness elements characterized with zero plane displacement height d.

Hsieh *et al*. (2000) developed an approximate analytical model for footprint estimation based on a combination of Lagrangian stochastic dispersion model and dimensional analysis as follows:

$$f(x, z-d) = \frac{1}{k^2 x^2} D z_u{}^P |L|^{1-P} \exp\left(\frac{1}{k^2 x} D z_u{}^P |L|^{1-P}\right) \qquad (4.8)$$

and the cumulative fraction of flux density to surface source flux density ratio is estimated by:

$$\frac{F(x,z-d)}{S_o} = \exp\left(\frac{-1}{k^2 x} D z_u{}^P |L|^{1-P}\right) \quad (4.9)$$

where D and P are similarity constants with D assuming values of 0.28, 0.97 and 2.44 and P 0.59, 1 and 1.33 for unstable, neutral and stable conditions respectively, and z_u a scaling parameter formed by combining the measurement height z, later extended to include z - d by Savage *et al*. (2004), and the roughness length z_o:

$$z_u = \frac{(z-d)^2}{z-(z_o-d)}\left[\ln\left(\frac{z-d}{z_o}\right)-1+\frac{z_o}{z-d}\right] \quad (4.10)$$

4.3 MATERIALS AND METHODS

The study was conducted over sole stands of *J. curcas* trees (50 m × 60 m) at Ukulinga (29°40′11″S, 30°24′50″E, altitude 781 m), KwaZulu-Natal, South Africa. The Jatropha trees were planted in a 3 m × 3 m row and tree spacing. The trees were pruned in mid-spring of 2007 when they were devoid of leaves and then allowed to grow during the hot and rainy summer weather. Average tree height measurements were taken every month using a scaled rod and ranged between 1 and 2.25 m, and leaf area index, measured using LAI-2000 (LI-COR, Lincoln, NE) on a bimonthly basis, ranged between no leaves (winter) and 2.2 (summer) m^2 m^{-2} during the time of the experiment. The prevailing wind at the site was from south east direction, and the fetch distance from the prevailing wind was 40 m. The data used in this study were collected from 20 July 2007 to 19 July 2008.

Wind velocity components and virtual temperature were measured using a three-dimensional sonic anemometer (Model 81000, RM Young, Traverse City, MI) mounted at 2.3 m above the ground. High frequency air temperature measurements for use in the TV and SR methods were made using fine-wire chromel-constantan thermocouples mounted at 1.4, 1.8, 2.3 and 2.7 m above the soil surface. Each unit consisted of a bare, unshielded and naturally-ventilated pair of 75 µm thermocouples arranged in parallel. All sensors were mounted on arms that extended out of a lattice mast that was located at the centre of the plot and were connected to a CR5000 datalogger (Campbell Scientific Inc., Logan, UT).

All measurements were done differentially at 10 Hz frequency. The data were subsequently averaged over two- and 30-minute time periods.

Additional sensors for measuring the remaining energy balance components were also used. The net irradiance was measured using a NR LITE net radiometer (Kipp and Zonen, Delft, The Netherlands) at 3.0 m above the ground when the canopy was short comprising few leaves. Another net radiometer (model Q*7.1, REBS, Seattle, WA), mounted at the same height but facing directly the bare soil, was added when the crop increased in size and height. The average net irradiance was then used in the analysis. These ensured that both the vegetation and the soil were adequately sampled. The soil heat flux was also measured using two soil heat flux plates (HFT-S, REBS, Seattle, WA) placed at a depth of 80 mm below the soil surface, with one of them placed directly below a tree and the other one between trees. A system of parallel thermocouples at depths of 20 and 60 mm were used for measuring the soil heat stored above the soil heat flux plates (Tanner, 1960). Volumetric soil water content in the first 60 mm was also measured using a CS616 time domain reflectometer (TDR). The measurements were sampled every 10 s with a Campbell CR23X and 10-minute averages were computed.

An automatic weather station about 10 m away from the edge of the Jatropha plot was also used to obtain solar irradiance (LI-200 pyranometer), air temperature and relative humidity (CS500 Vaisala), wind speed and direction (Model 03001, RM Young) and precipitation (tipping bucket rain gauge, Texas electronics, Dallas, TX) data. A Campbell CR10X datalogger was used to scan measurements every 10 s and log averages every 10 min.

4.4 RESULTS AND DISCUSSION

4.4.1 Weather variables

Environmental variables play a major role in determining the exchange of energy and matter between a surface and the atmosphere (Wilson and Baldocchi, 2000; Wang *et al*., 2004; Hao *et al*., 2007). Therefore, it is important to understand the pattern of these variables with time in order to fully appreciate these energy exchanges. The diurnal variation of environmental variables for the site from July 20, 2007 to July 19, 2008 is

presented in Fig. 4.1. The combined effect the environmental variables have on the grass reference evaporation (ET_o) (Allen *et al.*, 1998) of the site is depicted in Fig. 4.1(a). The ET_o was, to a greater extent, regulated by available solar irradiance (Fig. 4.1(c)) and hence the similar pattern of solar irradiance and ET_o. The major environmental variable that brings about a change to the weather and climate of the site is the distribution and amount of precipitation. The area is a subtropical humid climate having a summer rainfall distribution concentrated mainly between September and April (Fig. 4.1(b)). The mean annual precipitation for the site is 725 mm per annum and the amount that was received during the study period was 690 mm, which was below average. The diurnal variation in

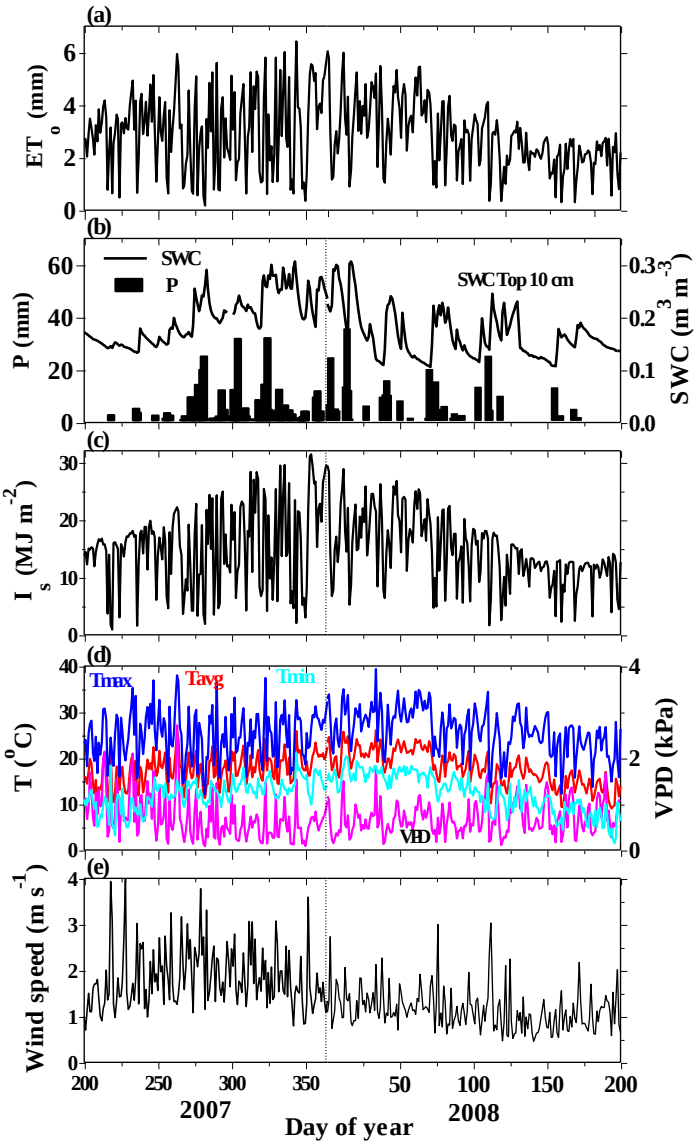

Fig. 4.1 Seasonal variation of daily (a) grass reference evapotranspiration, (b) total precipitation (mm) and soil water content (m^3 m^{-3}- upper 100 mm), (c) solar irradiance (MJ m^{-2}), (d) maximum, average and minimum air temperatures (^oC) and water vapour pressure deficit (kPa) and (e) average wind speed (m s^{-1}) for 2007/2008

the measured soil water content was also related to the distribution of daily precipitation (Fig 4.1(b)) and ranged between 0.11 m^3 m^{-3} to 0.31 m^3 m^{-3}. Fig. 4.1(c) also shows the daily solar irradiance distribution during the study period. It exhibited a bell shaped pattern with its peak in the wet season. The mean air temperature also showed similar pattern to the solar irradiance distribution but with its peak slightly shifted to the right - due to the lag in heating/cooling the surface and atmosphere (Fig. 4.1(d)). Warmer air temperatures were associated with the wet season.

The water vapour pressure deficit, which is a function of air temperature and water vapour pressure, followed somewhat opposite pattern to the average air temperature (Fig. 4.1(d)). Hence, a lower water vapour pressure deficit values were observed during the wet season. The daily mean wind speed had a different pattern compared to the rest of the weather variables. It was higher during the dry season and then decreased gradually during the wet season to reach its lowest in spring and ranged, on average, between 0.4 and 4 m s^{-1} (Fig. 4.1(e)).

4.4.2 Energy balance

The energy balance components were computed for the day-time from sunrise to sunset. Fig. 4.2 shows the pattern of the energy balance components using a moving average with a period of ten days (R_n, G, and H were measured whereas λE was calculated as a residual of the energy balance from EC measurements of H). The Jatropha trees are deciduous in nature and are characterized by leaf senescence during the dry season and emergence in the wet season. The leaf area index (LAI) for the Jatropha plot during the study period is given in Fig. 4.3. The pattern of the energy components responded to the changes in the structure of the canopy and prevailing environmental conditions. The R_n followed similar pattern to the daily solar irradiance. It showed a "Λ" shape with its peak during the wet season. The R_n was utilized in heating the soil surface, vegetation and the atmosphere and also evaporating water. A larger proportion of the R_n was used to heat the soil and atmosphere in the dry season (winter) than to evaporate water. This was because of the little transpiration from the trees as they had shed their foliage and also very low soil evaporation due to the poor availability of soil water during the dry season. This pattern was reversed with the onset of rain, and as the wet season progressed, λE increased in ma-

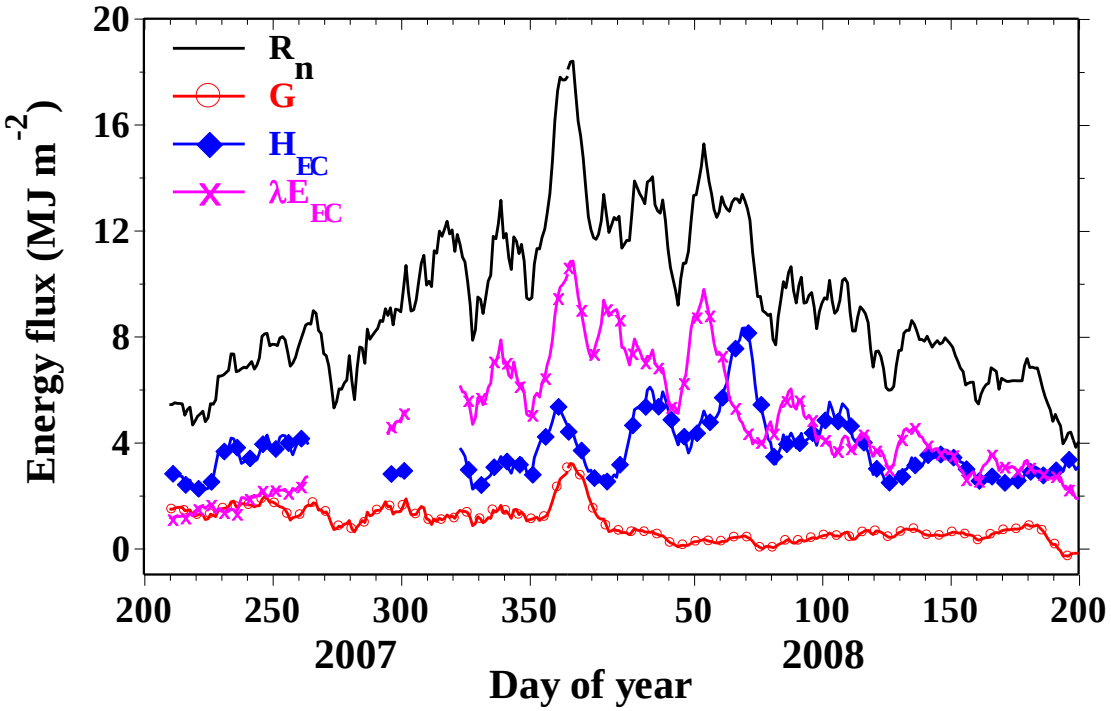

Fig. 4.2 Seasonal variation of daily energy balance components over *J. curcas* during 2007/2008 using a moving average with a period 10

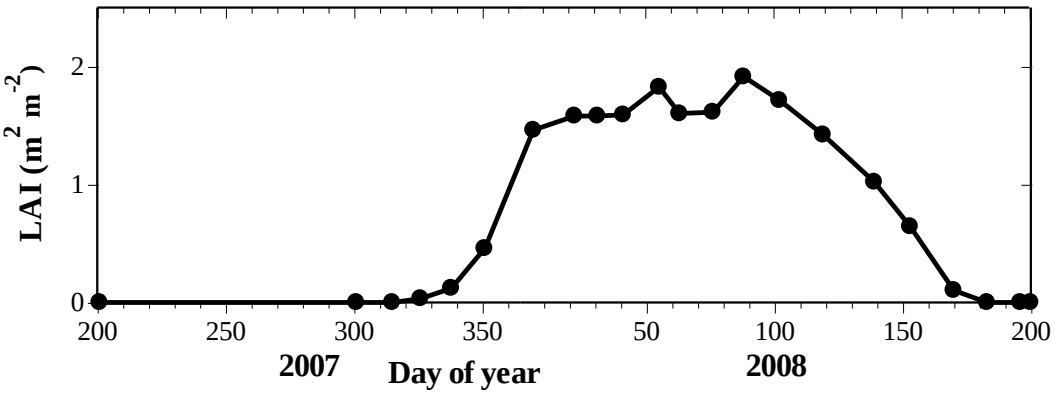

Fig. 4.3 Leaf area index (m^2 m^{-2}) of the Jatropha stand during the study period

gnitude and became greater than *H*. This was because most of the energy was consumed in evaporating water from the foliage structures that had emerged and the soil which had become relatively wetter. Increases in λE in response to increase in R_n occurred, especially following a significant amount of precipitation. Towards the end of the wet season, both *H* and λE started declining responding in opposite manner to the infrequent wet days observed. During the dry season, λE had decreased in value and became almost constant throughout.

In summary, H was greater than λE in the dry season, but λE was by far greater than H in the wet season. These, in general, show the strong influence exerted by the surface (vegetation and soil) and precipitation on the partitioning of the available energy into H and λE. Wilson and Baldocchi (2000) and Wilson *et al*. (2000) also reported similar response of H and λE to leaf emergence and senescence in deciduous forests. A similar pattern between H and air temperature was noted with its peak to the right of the R_n's peak. The G values were always lower than all the other energy components except in the dry season for some time when it had similar values to λE, and in the wet season when it was close to H.

4.4.3 Comparison of TV and SR against EC using season long data

Since the canopy structure of the Jatropha stand changed seasonally in response to environmental conditions, the height of the TC's used for calculation of H using the TV and SR methods had to be changed accordingly. The α and lag time used in the SR method might change as well. This required calibration of the SR method when the stand structure changed, although an attempt was made to use a conservative value of α that did not vary much. The TV method did not require calibration or change of any parameter since it used universal MOST constants. The variable heights and constants used during the experiment along with crop characteristics are given in Table 4.1.

The pattern of the half-hourly H as estimated from the EC, TV and SR methods along with the measured R_n and G for selected cloudless unstable days representing the four seasons is presented in Fig. 4.4. This illustration confirms that the available energy used for heating the surface and atmosphere, and to evaporate water are different for the four seasons. The

Table 4.1 Details of leaf area index, average tree and sensor heights during the study period for all three methods, and the SR parameters used

year	day of year	average tree height (m)	*LAI* (m^2 m^{-2})	sensor height (m)			SR parameters	
				EC	TV	SR	α-value	lag time (s)
2007	200-263	1.20 – 1.85	0	2.3	1.8	1.8	1	1
2007/2008	285-21	1 – 1.85	0 – 1.8	2.3	2.3	1.8	1	1
2008	22-88	1.85 – 1.94	1.8 – 2.2	2.3	2.7	2.7	0.7	0.5
	89-150	1.94 – 2.25	2.2 – 0.9	2.3	2.7	2.7	0.7	1
	151-200	2.25 – 1.98	0.9 – 0.3	2.3	2.7	2.7	0.7	0.5

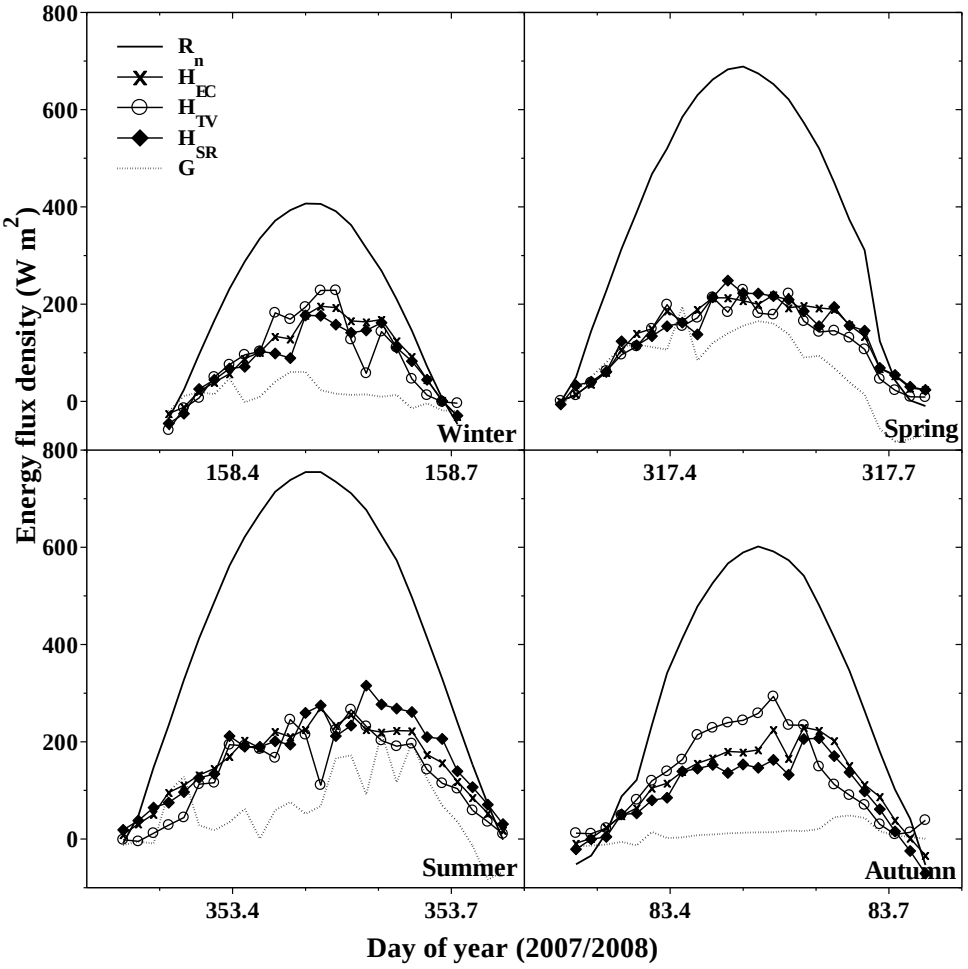

Fig. 4.4 Diurnal variation of half-hourly *H* estimates from the EC, TV and SR methods and the measured net irradiance (R_n) for selected cloudless days during unstable conditions representing different seasons in 2007/2008 over *J. curcas* (Autumn is in the year 2008, the rest in 2007)

highest R_n occurred during the wet season (summer) and the lowest during the dry season (winter). The *H* was the main consumer of the available energy in the dry seasons (winter and autumn).

Fig. 4.4 also illustrates the variation of the energy fluxes during the day. The TV method appeared to underestimate lower values (summer) and overestimate higher values of *H* (autumn) compared to the EC method for the selected days (Fig. 4.4). Whereas H_{SR} closely followed H_{EC}.

Fig. 4.5 shows the daily *H* as estimated from the (a) TV and (b) SR methods against the EC method along with the statistics used to evaluate the correlation. The TV method showed more scatter around the one-to-one line with a greater tendency to underestimate *H*. The

SR method, however, showed very well distributed points along the one-to-one line. The coefficient of determination (r^2) and the root mean square error (*RMSE*), although acceptable in both cases, were better in the case where the SR method was used. Similar patterns were also observed for the λE (Fig. 4.6), although the tendency was to overestimate in the case of the λE calculated using the H from the TV (H_{TV}) method. This was simply because the H was subtracted from the available energy to obtain the λE. Again, the r^2 and *RMSE* were better in the case of the λE calculated using the H_{SR} estimates.

4.4.4 Seasonal water-use

The total water-use by the Jatropha trees as estimated by the EC, SR and TV method is shown in Fig. 4.7. The available energy and daily precipitation are also depicted in units of mm. The total water-use followed the pattern of the available energy and precipitaion. It appears, in Fig. 4.7, that the agreement between the three methods in estimating the daily evapotranspiration (ET) was quite good. But presentation of the above data on a cumulative basis reveals small differences between the estimates of evapotranspiration with time. Three separate months, representing different seasons, were also chosen for illustration (Fig. 4.8). In August, when the trees were devoid of leaves, the evapotranspiration was very low with the soil surface as its main source. The overestimation of ET by the TV method, followed by the SR method compared to EC method is conspicuous. The cumulative ET for the EC, SR and TV methods during August were 20.7, 23.1 and 26.9 mm respectively. The daily average ET, from the respective methods, for this month were 0.67, 0.75 and 0.86 mm. December exhibited the largest ET of the three selected months; and the slight underestimation by the SR method and overestimation by the TV method is clear. The estimated monthly ET by the EC, SR and TV methods were 99.3, 97.0, 105.6 mm respectively. And the respective daily averages for this month were 3.2, 3.1 and 3.4 mm. Finally, in March, with an intermediate ET, the SR and TV methods produced ET that closely matched the ET from EC with the monthly estimations of 61.6, 62.7 and 63.5 mm from the EC, SR and TV methods respectively. The daily average ET for this month was approximately 2.0 mm for all three methods. These three months also illustrate the seasonal variation of evapotranspiration. Overall, the seaso-

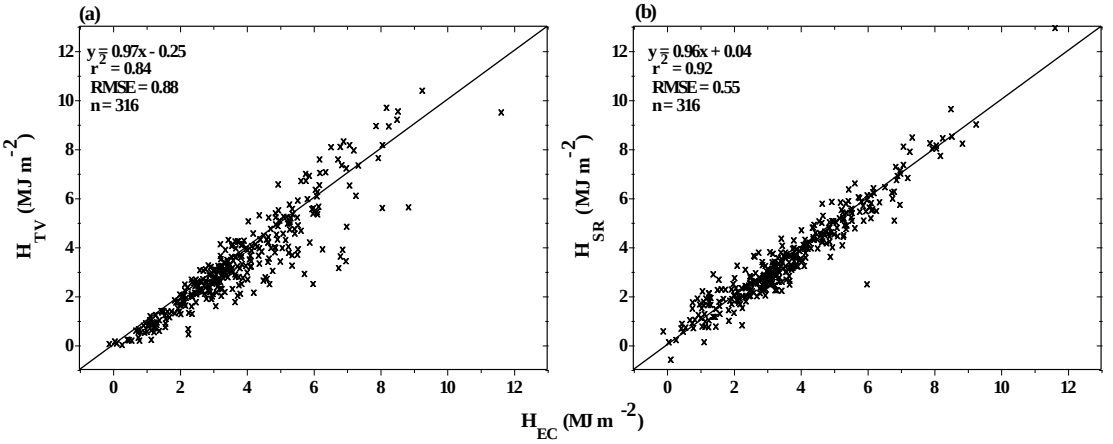

Fig. 4.5 The agreement between seasonal *H* estimated from the (a) TV and (b) SR methods against the EC method over *J. curcas* during 2007/2008 (r^2- coefficient of determination, *RMSE*- root means square error and *n* - the number of observations)

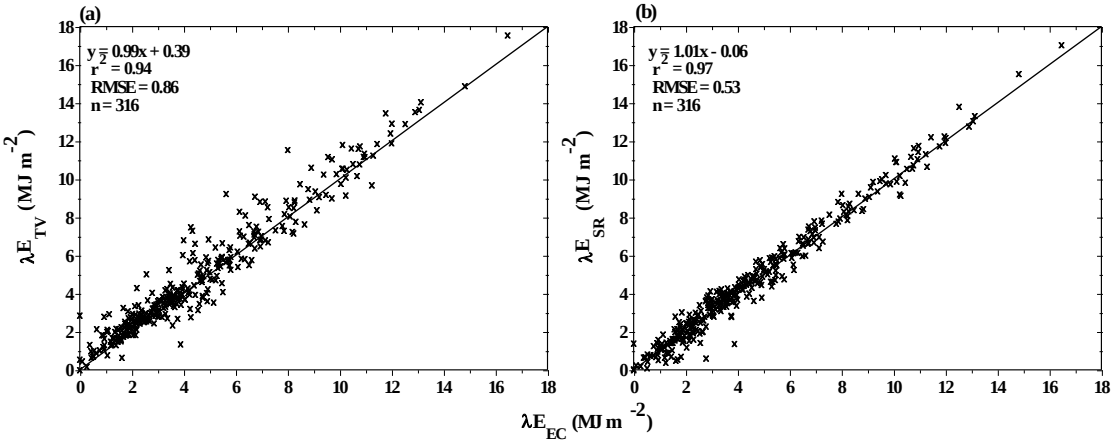

Fig. 4.6 The agreement between seasonal *λE* from the (a) TV and (b) SR methods against the EC method over *J. curcas* during 2007/2008. *λE* was calculated as a residual of the shortened surface energy balance where the *H* was obtained from the TV, SR and EC methods

nal total evaporation for the EC, TV and SR methods was 626, 640 and 674 mm respectively with the rainfall amount being 690 mm.

In 2006, 30-min average ET of *J. curcas* during peak time of the day in summer were found to be about 0.2 mm higher compared with ET of *Pennisetum clandestinum* (Kikuyu grass) at the same site, with similar ET for the rest of the day (M G Mengistu pers. comm., 2009). Seasonal evaporation mesurements during the year 1992 using two Bowen ratio energy balance (BREB) and lysimeter in montane grassland catchment of the Drakenberg mountains, Cathedral Peak, South Africa were 1311.4 mm with annual rainfall amount of 975 mm (Savage *et al.*, 1997). These reports indicate that *J. curcas* does not increase water consumption at field scale compared to grassland sites.

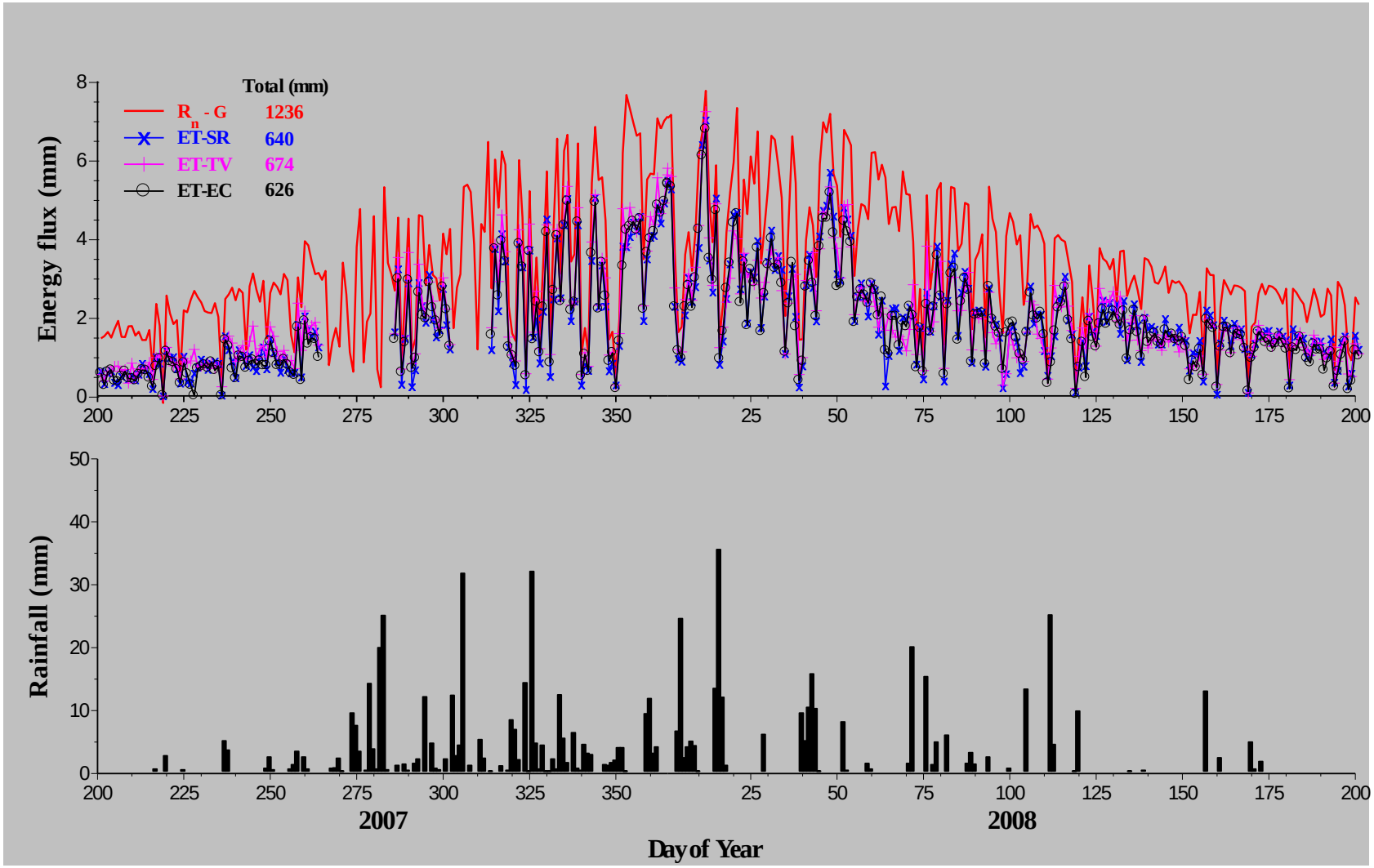

Fig. 4.7 Diurnal variation in evapotranspiration estimates (mm) using the EC, SR and TV methods, the available energy (mm) and rainfall (mm) for day of year 200 (2007) to 200 (2008)

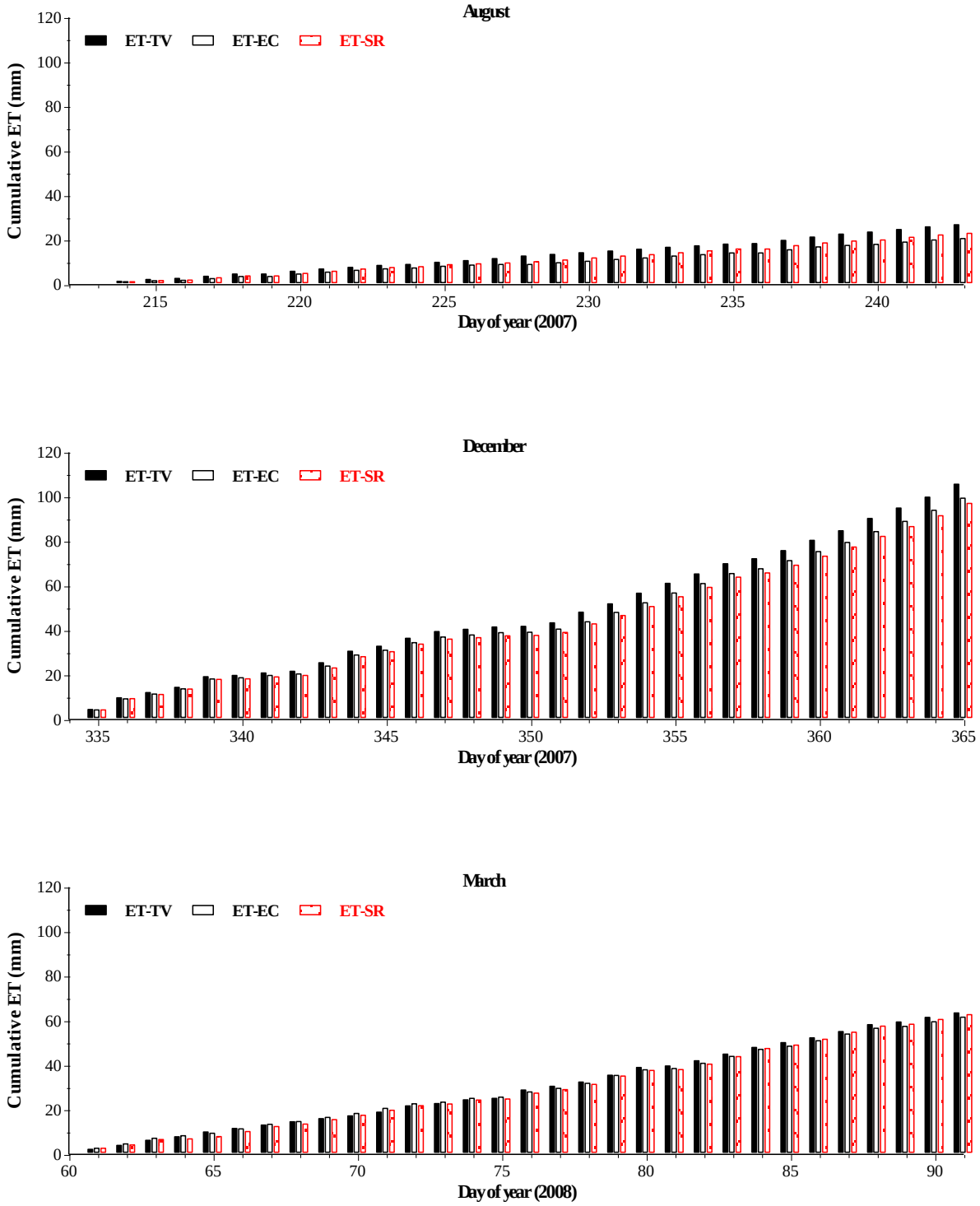

Fig. 4.8 Daily cumulative evapotranspiration (mm) for selected months of August (2007), December (2007) and March (2008). ET- evapotranspiration

Uncertainties related to surface energy balance closure and EC underestimation of surface energy fluxes (H and λE) are discussed in Chapter 2, Section 2.1.5, 2.3; and Chapter 3, Section 3.4.2.

4.4.5 Footprint analysis

Footprint $f(x, z\text{-}d)$ and the ratio of flux density $F(x, z\text{-}d)$ to surface flux density S_o were estimated using Hsieh *et al*. (2000) model for selected 30-min average during the day. A measurement height z = 2.3 m above the ground surface and roughness length z_o = 0.11 and 0.18 m were used. The peak location of the footprint x_{peak} and the 80% fetch to measurement height ratio were also estimated for the dominating wind direction (Fig. 4.9(a) and (b)). The estimations were conducted for all stability conditions as defined by Deardorff (1978).

It is apparent from Fig 4.9(a) that the peak location varies for the different stability conditions. The more unstable the atmospheric condition, the closer is the peak location of the footprint towards the measurement position. As the atmospheric condition became more and more stable the distance of the x_{peak} from the measurement position increased. The shape of the footprint estimation was also long and narrow in the unstable atmospheric conditions becoming shorter and wider as the atmospheric condition becomes more and more stable. The more unstable the atmospheric condition was the more the percentage contribution towards the measured flux from the surface of interest (Fig. 4.9(b)). In the convectionally unstable atmosphere greater than 90% and in the unstable, neutral and slightly stable atmospheric conditions greater than 80% and in the strongly stable condition about 70% of the measured fluxes had originated from the surface of interest. The 70% contribution in strongly stable conditions should not be of great concern especially where H is considered. This is because most of the stability conditions were convectively unstable or unstable during the day, with neutral conditions occurring early in the morning or late in the evening. It is rare to find (strongly/slightly) stable atmospheric conditions during the day. Besides the magnitude of H during such atmospheric conditions, especially slightly stable, is usually small and hence the error encountered due to sampling would be minimal.

Kljun *et al*. (2004) have developed a simple parameterisation for flux footprint prediction based on backward Lagrangian model and compared estimates from their model against those of Hsieh *et al*. (2000) and found a satisfactory agreement for slightly convective, neutral and slightly stable conditions. However, for measurement heights greater than 20 m, they found that the peak location as estimated by the two approaches to differ consider-

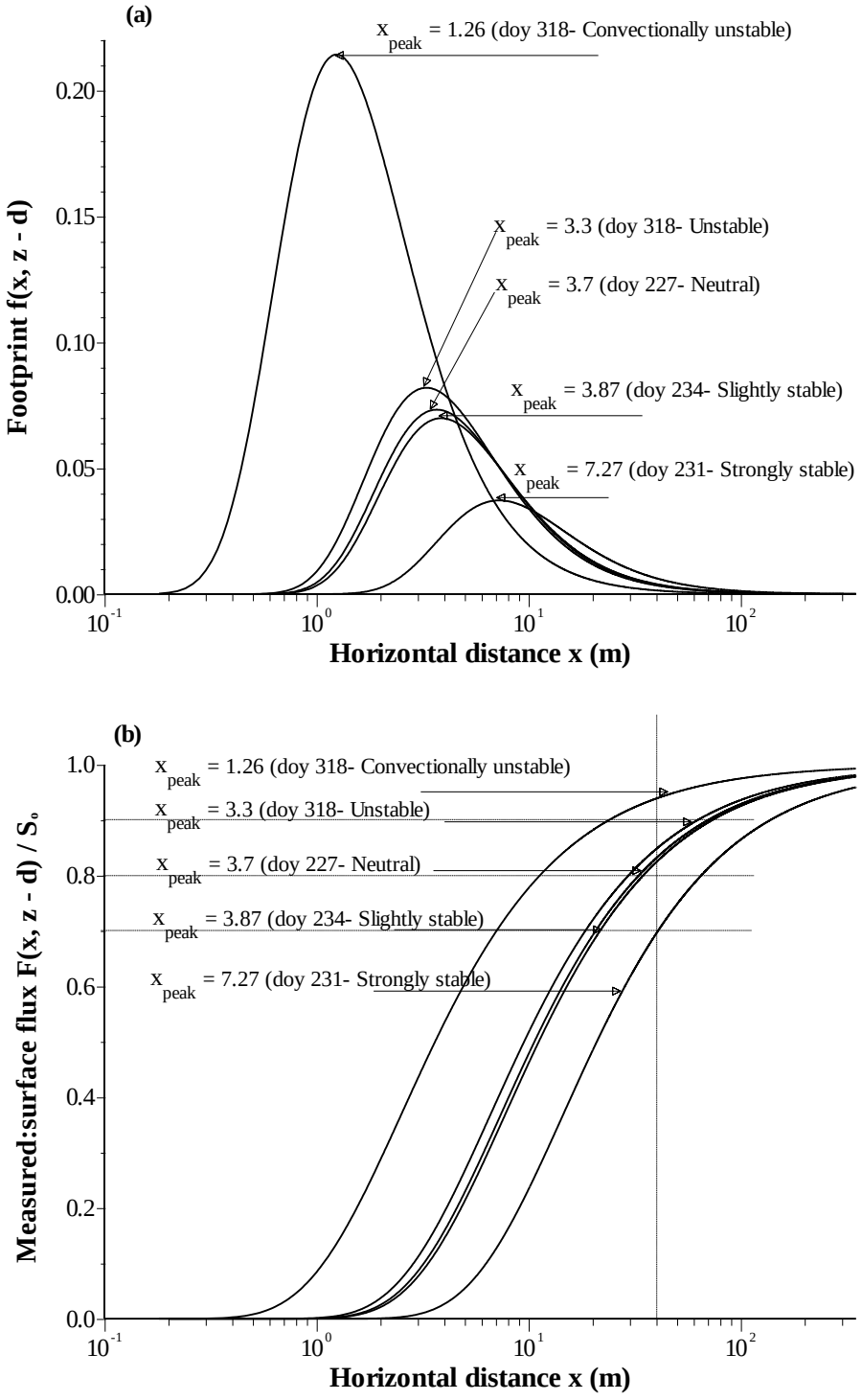

Fig. 4.9(a) Estimated footprint and peak location of footprint for selected days (2007) and different atmospheric stability conditions based on 30-min EC measurements at 2.30 m above the ground and horizontal distance (x) from the measurement position, and (b) the ratio of the flux density $F(x, z - d)$ to surface source flux density S_o for the same stability conditions and days as in (a), with the dashed lines representing the downwind fetch distance (x-axis) and the 70, 80 and 90% of $F(x, z - d)$ to S_o ratio (y-axis)

ably for strongly convective, forced convective, stable and strongly stable conditions. Kljun *et al*. (2004) did not state which way the peak location estimated from Hsieh *et al*. (2000) shifted compared to their peak location estimation. For the site understudy, footprint estimates for the unstable region from the Hsieh *et al*. (2000) and Kljun *et al*. (2004) models were compared (this was not possible for the other stability regions using the Kljun *et al*. (2004) because of restrictions imposed in the inputs). The evolution of the footprint and the peak location were different as estimated from both models. The footprint using the Hsieh *et al*. (2000) model was zero until certain distance downwind from the measurement position and starts to pick up sharply to its peak at 3.3 m from the measurement position; whereas in the Kljun *et al*. (2004) the footprint was above zero even a few meters in the upwind direction from the measurement position (-5 m) but picks up slowly and reached its peak at about 14.5 m in the downwind direction. The estimated peak footprint was also slightly higher from the latter model. But both models –for the given atmospheric stability condition indicated that greater than 90% of the measured flux originated from within the surface area of interest.

These footprint fluxes, for all possible atmospheric stability conditions, can serve as indicators to describe the extent of the surface area contributing towards the measurement of *H* for a given roughness length and wind direction. A point that needs to be stressed here is that these simplified methods of footprint predictions have not been rigorously tested against measurements but rather against comprehensive forms of their Lagrangian parents and other analytic footprint models.

4.5 CONCLUSIONS

This study investigated the seasonal water-use of *Jatropha curcas* using the eddy covariance (EC), surface renewal (SR) and temperature-variance (TV) methods. These methods estimate sensible heat flux (*H*), and evapotranpiration (*ET*) was calculated as a residual of the shortened energy balance term involving measurements of net irradiance and soil heat flux. The seasonal estimates of *ET* from the three methods agreed reasonably well. When the SR and TV methods were compared against the EC method, the SR method performed better than the TV method. This should not be surprising as the SR method is calibrated in response to changes in vegetation structure, whereas the TV

method used fixed constants. The computations involved in the TV method are relatively simple and can be written into a datalogger program code with little difficulty to aid in estimation of online evapotranpiration from the shortened energy balance equation along with appropriate measurements of net irradiance and soil heat flux.

The study also reiterated that *ET* was mainly governed by the available energy, amount of precipitation and vegetation canopy structure. Maximum *ET* amounts were observed during summer (rainy season) when the net irradiance was at its peak and the vegetation growth was vigorous. Contrary to this, minimum *ET* was observed in winter (dry season) when net irradiance was at its lowest and trees had shed most of their leaves. The seasonal *ET* total for the EC, TV and SR methods was 626, 673 and 640 mm respectively with rainfall totalling 690mm. The footprint analysis also revealed that greater than 80% of the measured surface fluxes under most atmospheric stability conditions originated from the surface of interest. It can be concluded that *H* can be routinely estimated with reasonable accuracy using relatively low-cost methods that can in turn be used for estimating long-term water-use from vegetation surfaces using the shortened surface energy balance along with measurements of net irradiance and soil heat flux assuming that closure is met.

5 VALIDATION OF A THREE-DIMENSIONAL SOLAR IRRADIANCE INTERCEPTION MODEL FOR TREE CROPS

ABSTRACT

Solar irradiance is a fundamental factor in estimating evapotranspiration and dry matter production from agricultural fields. A three-dimensional, hourly time-step tree-canopy radiation interception model is validated for four different tree crops including *Jatropha curcas*, *Leucaena leucocephela*, *Macadamia integrifolia* and *Acacia mearnsii*. Planting patterns varied from isolated trees to hedgerows to trees arranged in tramline mode. The model used considers the earth-sun relationship, the geometry of the plant canopy, planting pattern, row orientation and solar irradiance transfer equations to simulate canopy radiant transmittance through tree crops. The model assumes that trees are elliptical in shape with uniform leaf distribution, and that solar irradiance attenuation within the canopy follows Beer's law. Transmittance of direct and diffuse irradiance is calculated separately. In order to determine the solar irradiance at a certain point at the ground, the model calculates the path length traversed through the tree canopy. Radiation can be obstructed by neighbouring trees, so five rows of trees with five trees within each row with the tree of interest at the centre were considered. Inputs of geographic location, altitude, row orientation, row and tree spacing, canopy size, leaf area density and incident solar irradiance are required. In order to validate the model, measurements were taken using tube solarimeters placed 0.5 m from each other starting from the base of a tree trunk in four directions, along and perpendicular to the row up to mid-way between trees and rows. For the validation experiments, a total of between five and 22 tube solarimeters were used. Model validation was carried out for each node using a wide range of input parameters. Model-simulations of hourly radiant transmittance were in good agreement with measurements with an overall coefficient of determination, r^2 = 0.91; Willmott's index of agreement, d = 0.96; and general absolute standard deviation, *GASD* = 17.66%. Agreement between model-simulations and measurements, however, was influenced by distance and direction of the node from the tree trunk, sky conditions, symmetry of the canopy, and uniformity of the stand and leaf distribution of the canopy. The three-dimensional solar irradiance interception model will be useful in planning and management applications for a wide range of tree crops.

Keywords: Solar radiation interception/transmission; Leaf area density; Model; Canopy

5.1 INTRODUCTION

The quantity and quality of solar irradiance intercepted by and that penetrates through the plant canopy to reach the soil surface is an important factor that affects photosynthesis, plant transpiration and soil water evaporation (Mann *et al*., 1980; Annandale *et al*., 2004). Thus, accurate numerical representation of this process in crop growth and soil water balance models is of fundamental importance (Annandale *et al*., 2004). Solar irradiance transfer through plant canopies is primarily determined by (Ross, 1975) (i) the incident solar irradiance above the plant canopy, (ii) optical properties (absorption and scattering) of the canopy and the underlying ground surface, and (iii) canopy architecture including geometry and distribution of plants on the ground, size, orientation and distribution of leaves within the canopy, etc.

Many models have been proposed for estimating transmission of solar irradiance through canopies following the classic work of Monsi and Saeki (1953). Extensive reviews of radiation models have also been documented (e.g., Lemeur and Blad, 1974; Norman, 1975; Myneni *et al*., 1989). However, validation of such models, the focus of this study, needs to be undertaken for a wide range of canopy types. Validation studies are time consuming, requiring many measurements in time and space. Perhaps, this could be the reason why extensive validation, incorporating a range of canopy types, for such models has been rarely undertaken.

The abstraction of the canopy as a turbid medium coupled with radiative transfer equations has enabled researchers to describe the transmission of solar irradiance through the plant canopy and characterize the radiation regime below. Most radiative transfer models, that are used in crop growth and soil water balance models, however, assume a one-dimensional, horizontally homogeneous plant canopy stand (Myneni *et al*., 1989). But plant canopies display horizontal heterogeneity or discontinuity especially for mixed cropping systems (e.g., intercropping, agroforestry, and forests), isolated tree crowns, crops arranged in rows, crops in their earlier growth stages, etc. (Norman and Welles, 1983; Sinoquet, 1993). Interaction of such plant canopies with the directional nature of the solar beam irradiance creates spatial and temporal variation in the quantity and quality of

radiation transmitted through plant canopies (Baldocchi and Collineau, 1994). This makes it very difficult to find a representative extinction coefficient in one-dimensional models for discontinuous canopies. Either a two- or three-dimensional solar radiation model, depending on the arrangement of the plant canopies, can characterize the transmission of solar radiation through such plant canopies by describing leaf grouping in tree crowns better. This is made possible by making more assumptions pertaining to canopy geometry and/or foliage statistical distribution within the canopy (e.g., Norman and Welles, 1983; Annandale *et al*., 2004).

A two-dimensional solar irradiance transfer model may be sufficient to characterize the radiation regime for hedgerow canopies but may be inadequate for canopies which exhibit horizontal discontinuity in both the X and Y-axes because of lack of correct representation of the canopy geometry. Both one- and two-dimensional radiation interception models, in this sense, may overestimate the amount of irradiance intercepted by the plant canopy and underestimate that reaching the soil surface for heterogeneous or discontinuous plant canopies. This may lead to inaccurate estimation of dry matter production, canopy transpiration and soil water evaporation when used in conjunction with crop growth and soil water balance models.

Three-dimensional solar irradiance transfer models, although require more input data than one- or two-dimensional model, may be more appropriate for accurate estimation and characterization of the radiation regime in discontinuous plant canopy stands. The three-dimensional model may also allow testing of how grouping in tree crowns affect radiation interception. A three-dimensional model also reduces to a two-dimensional model when the individual plants of the canopy grow into each other along the row, and reduce to a one-dimensional model when the plants grow and cover the ground uniformly. However, it should be noted that simpler radiation interception models can also be successfully used in discontinuous canopies provided the extinction coefficient is adequately represented as a function of leaf grouping or clumping (Duursma and Mäkelä 2007; Sinoquet *et al.* 2007).

Other approaches have taken radiation interception a step further by trying to simulate the foliage elements, branching nature, geometrical shape, planting pattern, etc. of the stand architecture in an attempt to forge a real representation of the vegetation (e.g., Sinoquet *et al*., 1991; Chen *et al*., 1994). This, compared to the former approach, requires many more

input parameters and is a complex and computationally demanding procedure (Dauzat, 1993).

In this study, we used a three-dimensional sub-hourly or hourly time step tree-crop canopy solar irradiance transfer model, which considers the earth-sun relationship, the geometry of the plant canopy, planting pattern, row orientation and solar irradiance transfer equations. The model uses simplified expressions for radiation scattering and considers the canopy as a uniform single entity compared to other more complex models that divide the canopy into multi-layer sub-canopies of variable leaf distribution. To test the validity of the model, model-estimations of radiant transmittances for a variety of regularly spaced tree crops with planting patterns including isolated trees, hedgerows and trees arranged in a tramline mode were compared with field measurements.

5.2 MODEL DESCRIPTION

A three-dimensional solar irradiance transfer model is developed based on the model of Charles-Edwards and Thornley (1973). The code is in turn based on a modification of a two-dimensional version of this model developed by Annandale *et al*. (2004). The model used here is similar to other previously developed radiation transfer models (Norman and Welles, 1983; Wang and Jarvis, 1990; Green *et al*., 2003), but with some expressions simplified. Flow chart of the model is given in Fig. 5.1. The model assumes that plant canopies are ellipsoidal in shape with small uniformly distributed leaves, and that radiation attenuation through the canopy follows Beer's law. An ellipsoidal canopy shape is chosen because of its adaptability to various other shapes. The fractional radiation transmission (τ) through plant canopies is described as (Norman and Welles, 1983; Campbell and Norman, 1998):

$$\tau = \exp\left(-k \cdot LAD \cdot s \cdot \sqrt{\alpha}\right) \qquad (5.1)$$

where k is the extinction coefficient for which an ellipsoidal leaf angle distribution was assumed (Campbell, 1986), LAD (m^2 m^{-3}) the leaf area (one-sided) density, s (m) the canopy path length through which radiation has to travel to reach a certain point on a horizontal surface, and α the absorptivity of individual leaves for solar irradiance which is

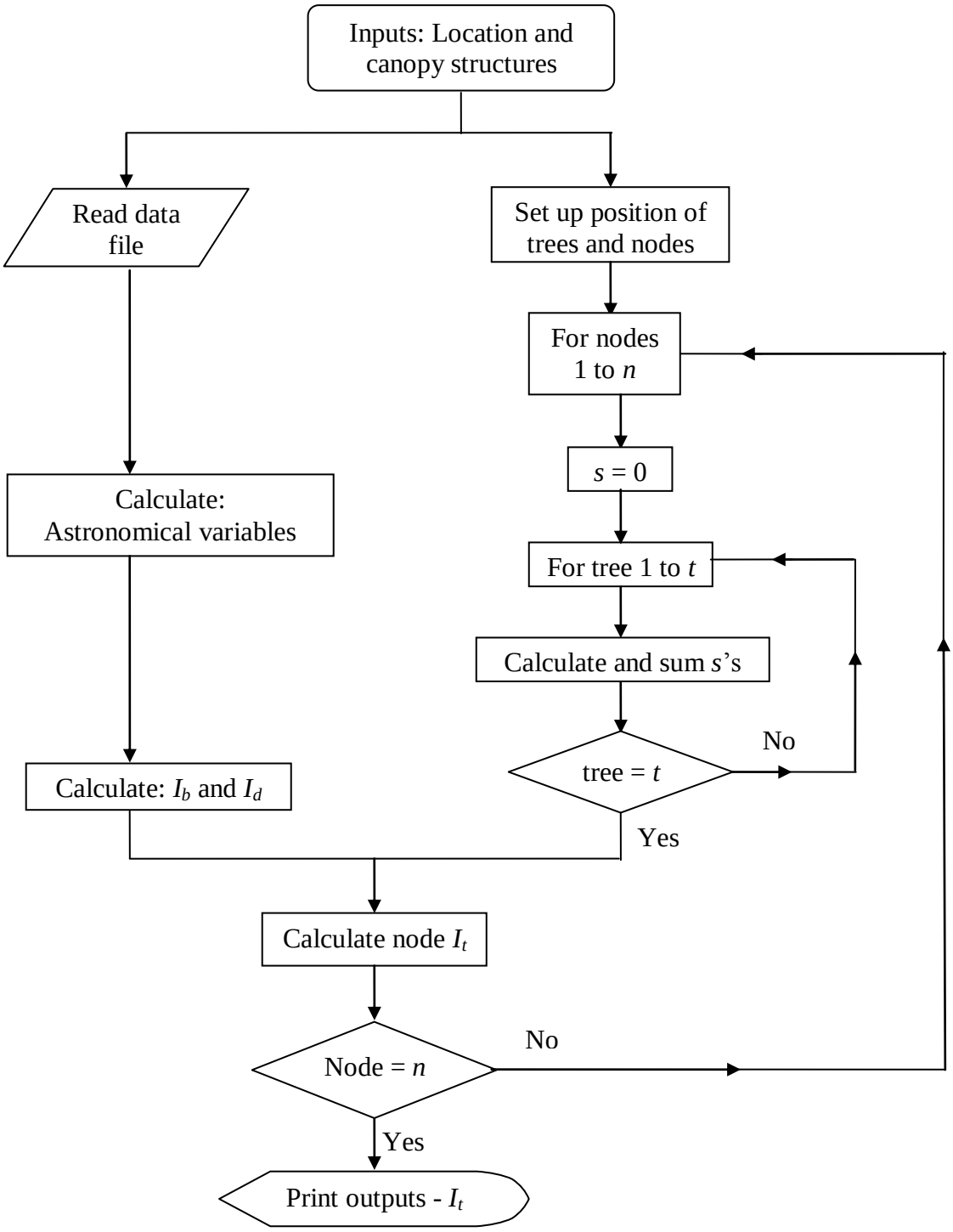

Fig. 5.1 Flow chart of the three-dimensional radiation interception model (*n* = maximum number of nodes, *s* = path length through the tree canopy, *t* = maximum number of trees, I_b, I_d and I_t are direct, diffuse and transmitted irradiances respectively)

taken as 0.5 (Campbell and Norman, 1998). The α term takes radiation scattering (reflection and transmission) within the canopy into account (Annandale *et al*., 2002).

The model calculates the canopy path length (*s*) through which radiation has to travel in order to reach a certain point on a horizontal plane, which could be at or above the ground. The plane is divided into 0.5 m horizontal square grids with the tree of interest at the centre. The path length, *s*, is calculated for each of these grid points. For calculating the path length, *s*, the location of the sun in the sky, the row orientation, and the location and geometry of the plant canopy are crucial.

The location of the sun in the sky for a given location on earth at a given day of year and time of day is described in terms of its elevation angle above the horizon (β) or zenith angle (θ) and its azimuth angle (ϕ). Procedures for calculating the location of the sun in the sky are widely documented (e.g., Swift 1976; Campbell and Norman, 1998). The elevation angle of the sun is determined based on latitude of the location on earth, day of year and time of day.

$$\beta = \arcsin\left(\sin lat \cdot \sin\delta + \cos lat \cdot \cos\delta \cdot \cos h_a\right) \tag{5.2}$$

where *lat* is the latitude (radians) of the location on earth (north positive), and δ and h_a are the declination and hour angle of the sun in radians, respectively. Declination of the sun, δ, can be calculated from day of year, *doy* (with January 1st as day of year one) as:

$$\delta = \arcsin\left(0.39785 \cdot \sin\left(4.869 + 0.01721 \cdot doy + 0.03345 \cdot \sin\left(6.224 + 0.01751 \cdot doy\right)\right)\right) \tag{5.3}$$

The hour angle, h_a, can also be calculated as:

$$h_a = 0.2618 \cdot \left(t - \left(12 - LC - ET_q\right)\right) \tag{5.4}$$

where *t* (hours) is the local time, *LC* longitudinal correction which is +4 minutes (1/15 hours) for every degree east of standard meridian and -4 minutes for every degree west of standard meridian, and ET_q (hours) the equation of time correction as a function of day of year. ET_q can be calculated from:

$$ET_q = [-104.7\sin f + 596.2\sin 2f + 4.3\sin 3f - 12.7\sin 4f - 432.9\cos f - 2\cos 2f + 19.3\cos 3f]/3600 \quad (5.5)$$

where f (radians) is calculated as:

$$f = 4.8786 + 0.0172 \cdot doy \quad (5.6)$$

The elevation, β, and zenith, θ, angles of the sun are complementary angles and therefore θ can be calculated as:

$$\theta = (\pi / 2) - \beta \quad (5.7)$$

The azimuth angle of the sun, ϕ, is measured with respect to due north, increasing in the clockwise direction and can be calculated from:

$$\phi = \arccos\left(\frac{\cos\theta \sin lat - \sin\delta}{\sin\theta \cos lat}\right) \quad (5.8)$$

The azimuth angle should be adjusted to take row orientation into account. The plots, including the tree canopies, were defined using X, Y and Z coordinates (three-dimensional). The tree canopy shape was also described using canopy dimensions (across and along the row and in vertical directions), bare stem height and leaf area density.

Charles-Edwards and Thornley (1973) combined the information retrieved from the location of the sun with the geometry of the plant in order to calculate the path length, *s*, by employing mathematical equations of an elliptical canopy surface. Assuming the tree canopy is elliptical in shape, its surface can be described by the expression:

$$\frac{x^2}{a^2} + \frac{y^2}{b^2} + \frac{z^2}{c^2} = 1 \quad (5.9)$$

where *x*, *y* and *z* are the cartesian co-ordinate axes, *a*, *b* and *c* are the canopy radii across and along the row and in the vertical transect respectively. Many shapes can be generated

by varying the values of *a*, *b* and/or *c*. The above equation, however, describes a hemi-ellipsoidal canopy surface resting on the soil surface, and hence it has to be lifted off the ground by introducing z_o, a distance between the soil surface and the centre of the ellipsoidal tree canopy, in Eq. (5.9).

$$\frac{x^2}{a^2}+\frac{y^2}{b^2}+\frac{\left(z-z_o\right)^2}{c^2}=1 \tag{5.10}$$

The ray coming from the direction of the sun is described by its angular co-ordinates involving azimuth (θ) and zenith (ϕ) angles with its end points at Q (x_q, y_q, z_q) – the point where the beam hits the canopy and P (x_p, y_p, z_p) – the point where the beam is intercepted at certain horizontal surface.

$$\frac{x_q-x_p}{\sin\theta\cos\phi}=\frac{y_q-y_p}{\sin\theta\sin\phi}=\frac{z_q-z_p}{\cos\theta} \tag{5.11}$$

Eqs (5.10) and (5.11) can be combined to eliminate x_q and y_q resulting in a quadratic equation in z_q of the form:

$$uz_q^{\,2}+vz_q+w=0 \tag{5.12}$$

where the coefficients *u*, *v* and *w* are given by:

$$\begin{aligned}
u &= \left(c^2\sin^2\theta\right)(b^2\cos^2\phi+a^2\sin^2\phi)+a^2b^2\cos^2\theta \\
v &= 2[\left(c^2\sin\theta\right)(\cos\theta\cdot(b^2x_p\cos\phi+a^2y_p\sin\phi)-z_p\sin\theta\cdot(b^2\cos^2\phi+a^2\sin^2\phi)] \\
&-(a^2b^2z_o\cos^2\theta) \\
w &= \left(z_pc^2\sin\theta\right)\left[z_p\sin\theta\cdot(b^2\cos^2\phi+a^2\sin^2\phi)-2\cos\theta\cdot(b^2x_p\cos\phi+a^2y_p\sin\phi)\right]+ \\
&\quad \cos^2\theta\cdot\left[c^2b^2x_p^{\,2}+c^2a^2y_p^{\,2}+a^2b^2(z_o^{\,2}-c^2)\right]
\end{aligned} \tag{5.13}$$

If a particular ray penetrates the canopy, then the two roots of the quadratic equation represent the height of entrance (z_q) into the canopy and its exit (z_n) from the canopy. And the path length, *s*, is calculated as follows:

$$s = \frac{z_q - z_n}{\cos\theta} \tag{5.14}$$

If the ray misses the canopy, then the two roots are imaginary. The ray may also pass through more than one canopy before it reaches its destination, and hence the path length, *s*, is calculated as the sum of the individual path lengths traversed through all the canopies. Depending on the row spacing, distance between trees and canopy size, up to five rows of trees and five trees within each row were considered in calculating the path length, *s*. The model is also capable of calculating the path length, *s*, for elliptical canopies with their bases truncated at a height z_b. Annandale *et al*. (2002) have identified three cases for such canopies.

Case 1: $z_q \geq z_b$ and $z_n \geq z_b$. Both roots belong to the canopy and *s* is calculated as in Eq. (5.14).
Case 2: $z_q \geq z_b$ and $z_n < z_b$. z_q belongs to the canopy but z_n is less than z_b and is replaced by z_b in Eq. (5.14).
Case 3: $z_q < z_b$ and $z_n < z_b$. Both roots are less than z_b and hence the ray misses the canopy.

In modelling the transmission of solar irradiance through plant canopies, it is important to discriminate between direct and diffuse components of the solar irradiance because of their differing interactions with the canopy (Campbell and Norman, 1998; Annandale *et al*., 2004). However, it is not common practice to measure these two components separately, but instead solar irradiance is measured. Hence, it is imperative to partition solar irradiance into direct and diffuse irradiances. The method of Weiss and Norman (1985), which estimates direct and diffuse irradiances for the photosynthetically active radiation (PAR) and near infrared (NIR) wavebands from the measured solar irradiance, based on the potential amount of solar irradiance that may reach the earth's surface, is adopted.

Direct irradiance is assumed to originate from a single source and estimation of its transmission to a given grid point through the canopy at a particular time is largely dependent on the direction of the source of the irradiance. The source of diffuse irradiance, on the other hand, could be from all directions and its transmission through the canopy to reach a certain point on a horizontal plane surface is dependent on the size and foliage density of the canopy. The diffuse irradiance transmission coefficient, assumed not to

change throughout the day, is, therefore, estimated as the mean of all the transmissions involving all azimuth and zenith angles for a given size and foliage density of plant canopies. For this estimation the model divides the hemisphere into 24 azimuth and five elevation angles of 15^o each.

The model requires inputs of day of year, time of day, latitude, longitude and elevation of the site, row orientation, row and tree spacing, canopy height, canopy radii, bare stem height, absorptivity, leaf area density as well as measured solar irradiance.

5.3 MATERIALS AND METHODS

The ability of the model to simulate hourly intercepted solar irradiance was validated using data collected at several sites in KwaZulu-Natal, South Africa. Details of location and planting specification of the tree crops used in this experiment are given in Table 5.1. Different tree crops and growth stages were used to test the validity of the model. The tree canopy characteristics used as input parameters to the model during the course of the experiment are also presented in Table 5.2. Canopy dimensions were measured using a calibrated rod whereas row orientation was measured using a compass and corrected to true north for all locations.

Leaf area density (*LAD*) was measured using one of three methods based on convenience: (i) when the leaves were few in number, they were traced and scanned using a LA3100 leaf area meter (Li-Cor, Lincoln, NE). The total leaf area was then divided by the canopy volume to get *LAD*; (ii) an LAI-2000 canopy analyzer (Li-Cor) was used for trees with large number of leaves. This involved making leaf area index (*LAI*) measurements in four quadrants of the tree by fitting the LAI-2000 with a 90^o view cap. The canopy shape and volume for each quadrant were estimated from a vertical and horizontal coordinate system using points at the boundary of the canopy. *LAD* was then estimated from the *LAI*, canopy shape and volume measurements. All *LAI* measurements were conducted when the sky conditions were completely overcast; (iii) destructive measurements of *LAD* were performed when the experiments allowed – most of the experiments were either commercially cultivated or on-going trials for other research purposes.

Table 5.1 Details of tree crops, location and planting specification

Crop	Location	Latitude	Longitude	Altitude (m)	Planting pattern	Row and tree spacing (m)	Row axis
Jatropha (*Jatropha curcas*)	Ukulinga, Pietermaritzburg	29°40′11″S	30°24′50″E	781	Single trees	3 × 3	NW-SE (139-319°)
Jatropha (*Jatropha curcas*)	Ukulinga, Pietermaritzburg	29°40′11″S	30°24′50″E	781	Single trees	5 × 2	NW-SE (139-319°)
Jatropha (*Jatropha curcas*)	Ukulinga, Pietermaritzburg	29°40′11″S	30°24′50″E	781	Tramline	Two rows 1 × 2.5 with 6 m row between tramlines	NW-SE (139-319°)
Leucaena (*Leucaena leucocephela*)	Ukulinga, Pietermaritzburg	29°40′11″S	30°24′50″E	781	Hedgerows	2 × 0.5	NW-SE (156-336°)
Macadamia (*Macadamia integrifolia*)	Wartburg	29°32′26″S	30°26′56″E	874	Single trees	6 × 4	W-E (286-106°)
Wattle (*Acacia mearnsii*)	Seven Oaks	29°12′38″S	30°38′46″E	1115	Hedgerows	3 × 1.5	NW-SE (137-317°)

Solar irradiance below the tree canopy was measured using, depending on row spacing, distance between trees and canopy size, 0.25-, 0.5- and 1-m long tube solarimeters. The tube solarimeters were constructed in the laboratory using glass tubes and copper-constantan thermocouples mounted on veroboard with sections printed matt-black and enamel-white. The bottom half of the glass tubes were filled with silica gel. Apart from the glass, no other filters were used, thereby ensuring that the solarimeter responded to solar wavelenths. The tube solarimeters were calibrated against a standard Kipp and Zonen CM11 solarimeter (Delft, The Netherlands). Solar irradiance was scanned every 10 s and then averaged every 10 min using a CR7X or CR23X datalogger (Campbell Sci., Logan, UT). The tube solarimeters were placed at 0.5 m from each other starting from the base of the tree trunk in four directions, along and perpendicular to the row up to mid-way between trees and rows. The tube solarimeters were usually placed on the ground when the soil beneath the tree crops was bare; otherwise they were elevated to above the height of the understorey crop to avoid interference of radiation transmission through the tree canopy. The tube solarimeters were also inspected regularly during the experiment. This included cleaning glass tubes, recalibrating and replacing sensors when required. Depending on the row spacing and distance between trees, tube solarimeters ranging from five to 22 in number were used for each “tree” experiment.

Above-canopy measurements of solar irradiance were also taken using a LI-200 pyranometer at each site. A CR10X datalogger was used to scan the solar irradiance measurements every 10 s and log the average every 10 min.

The performance of the model in simulating hourly solar irradiance transmission was evaluated using graphical and statistical methods for each node at each experimental site and averaged over all the sites. The graphs allow a quick means of visual evaluation for any systematic behaviour in the model performance. For comparison purposes, the graphs of the results were presented in two ways for the first canopy (Jatropha) stand. These included the trend of estimated and measured transmitted solar irradiance versus day of year for each node, and the estimated versus measured solar irradiance on a one-to-one graph for each node. The former presentation has the advantage of showing the diurnal variation of the modelled and measured solar irradiance transmission and the agreement (or lack of) between the two at certain times. The latter has the advantage of indicating more clearly when the model simulations agree or fail to agree with field measurements. It also

captures a larger number of data points, especially those taken for a certain canopy at different times of the year representing varying canopy characteristics. Moreover, data points from different nodes can be combined into one graph, if need be, to illustrate the performance of the model. Graphs depicting distribution of the estimated versus measured points on a one-to-one line only, therefore, were used for the rest of the canopies.

The statistical indices used also included the coefficient of determination (r^2) – a correlation measure which describes the goodness-of-fit of the model (a square of Pearson's correlation coefficient), Willmott's index of agreement (d) – which reflects the degree to which the observed variable is estimated accurately by the simulated variable (Willmott, 1982), and general absolute standard deviation (*GASD*) – an absolute difference measure which explains the actual magnitude of the error produced by the model (Jørgensen *et al*., 1986). *GASD* is simply the more commonly known mean absolute error (*MAE*) divided by the average of the observed values expressed as percentage. Both r^2 and d vary between zero (worst) and one (best) model performance values, and *GASD* varies between zero (best) and infinity (worst) model performance values. Based on De Jager (1994) acceptable values of these statistical indices for model prediction capability are that: r^2 and d should be greater than 0.8 and *GASD* should be less than 20%.

5.4 RESULTS AND DISCUSSION

5.4.1 Model validation

Ascertaining validity of the model requires checking for its internal consistency and testing the model simulation outputs under conditions comparable with the objectives for which it is developed (CAMASE, 1995; Annandale *et al*., 2004). The model formulations and equations were checked for their consistency using unit analysis. Sensitivity analysis was needed to gain understanding of the sensitivity of the model to uncertainty in various input parameters. Sensitivity analysis tests were carried out for all the sites under the experiment using a 25% decrease and increase of a selected model input parameter, keeping all other parameters constant, during a clear sky day and observing the variations in the model outputs. Input parameters that vary with plant growth were chosen for the sensitivity test. These included (Table 5.2) across (W_x) and along (W_y) the row canopy diameters, canopy height (h), bare stem height (*BSH*) and leaf area density (*LAD*). Solar irradiance transmiss-

Table 5.2 Canopy input parameters during the course of the experiment

Crop	Time period		Canopy status	h (m)	W_x (m)	W_y (m)	BSH (m)	LAD (m^2 m^{-3})
	Year	DOY						
Jatropha only	2006	272-282	Initial	1.50	0.60	0.40	0.10	0.52
	2006	315-326	Full	1.50	0.95	0.85	0.20	3.56
	2006	345-355	Full	1.55	1.25	1.05	0.20	3.21
Jatropha single row	2006/07	356-4	Full	1.70	0.90	0.90	0.20	2.80
	2007	99-109	Full	1.95	1.70	1.40	0.25	2.52
Jatropha tramline	2006	322-327	Full	1.12	0.28	0.28	0.40	1.77
	2007	86-94	Full	1.70	1.25	1.15	0.35	3.39
Macadamia	2007	67-73	Full	3.00	2.20	1.90	0.50	2.67
Leucaena	2007	51-62	Full	2.00	1.00	1.60	0.00	0.78
Black wattle	2007	117-125	Full	4.20	2.80	2.40	0.40	0.28

h: canopy height; W_x: canopy diameter across the row; W_y: canopy diameter along the row; BSH: bare stem height; LAD: leaf area density

ion through and interception by the canopy were also used as model outputs.

Overall average model sensitivity values of -0.50 and 0.43 for interception and 0.11 and -0.08 for transmission were obtained for the 25% decrease and increase in the input parameter values respectively. The negative signs indicate a decrease in the value of the output for a corresponding increase in the input or vice versa. The model sensitivity results indicate that the errors that may be generated in the outputs due to errors in the model inputs are relatively low. From the model input parameters tested, the model was found to be most sensitive, in both the interception and transmission outputs, to W_x and W_y, moderately sensitive to *LAD* and least sensitive to *BSH* and *H*. But the values of W_x and W_y can be easily measured in the field using a calibrated rod and are expected to pose little, if any, uncertainty in the model outputs. Besides, their values do not change over a short period of time (depending on type of vegetation) and can be safely assumed to be constant for such a time period. From all the model inputs, *LAD* is apparently the most difficult parameter to measure and merits special attention in the measurement and data collection processes.

5.4.2 Model performance

5.4.2.1 General observations

The model was evaluated using field measurements of hourly radiant transmittance spanning several days at different locations involving different tree crops. The transmission of solar irradiance at a particular time, between sunrise and sunset, for a given direction and distance from the tree trunk was used for testing model performance.

Ten-minute and hourly averages of incident solar irradiance were used as inputs for the simulation. There was little change in the simulated transmitted solar irradiance from both inputs when the canopy size and leaf area density were small, but a relatively larger difference was observed for trees with larger canopy size and leaf area density, especially for nodes located close to the tree trunk (data not shown). The ten-minute data had the advantage of more accurately capturing the location of the sun relative to the plant canopy. Besides, during the hour the sun rises or sets, average hourly time step input may underestimate the transmitted solar irradiance through the canopy. Therefore, model

simulations were carried out using inputs of ten-minute average incident solar irradiance. For model evaluation, however, hourly-averaged simulations and measurements of transmitted solar irradiance were used.

The model clearly simulated the trend of the solar irradiance that is transmitted through the canopy to reach the ground. The model indicated low levels of transmitted solar irradiance near the tree trunk and increased levels of transmitted solar irradiance away from the trunk in agreement with the actual measurements. It also indicated the presence of more solar irradiance for most of the day for nodes located in the northern direction than for nodes located in the southern direction from the tree trunk.

In general, as shown later for the various canopy types, the agreement between the simulated and observed transmitted solar irradiance was good. There was improved agreement for nodes located further from than near to the tree trunk, and on the northern side of the tree trunk compard to the southern side when the statistical indices of two nodes at equal distance but in opposite direction from the tree trunk were compared. Also the agreement improved for overcast compared with clear-sky conditions under similar canopy characteristics for the same node.

For nodes located further from the tree trunk, and north from the tree trunk (in the southern hemisphere, the sun's location relative to the tree canopies is always in the north), the interference of the canopy in intercepting solar irradiance would be less. Accordingly the errors that might be incurred due to the inherent model assumptions, measurement of *LAD* and estimation of the path length, *s*, will be minimized. The effect of this was more pronounced when contribution of the tree trunk to the interception of solar irradiance relative to the foliage elements was large.

During overcast skies, the transmittance of solar irradiance depends on the canopy size and *LAD*, but during clear days additional factors involving the location of the sun relative to the tree and the transfer of direct-beam irradiance are included in the simulations which contribute to the source of error in the simulation.

5.4.2.2 Jatropha trees

Radiation transmission simulations and measurements were performed concurrently for three periods (from late winter up to summer) comprising different developmental and growth stages and canopy characteristics (Table 5.2). This started in late winter when the trees had few leaves with small canopy dimensions and continued through spring up to summer during which the canopy progressively increased in size and developed more leaves. These presented the chance to test the model with varying canopy dimensions and leaf area densities.

The trend of the simulated and measured hourly transmitted solar irradiance through the Jatropha canopies with various size and leaf area density for nodes located at equal distance from the tree trunk but in opposite directions both along and across the row respectively is given in Figs 5.2 and 5.3. For the same canopy but with data points from m-

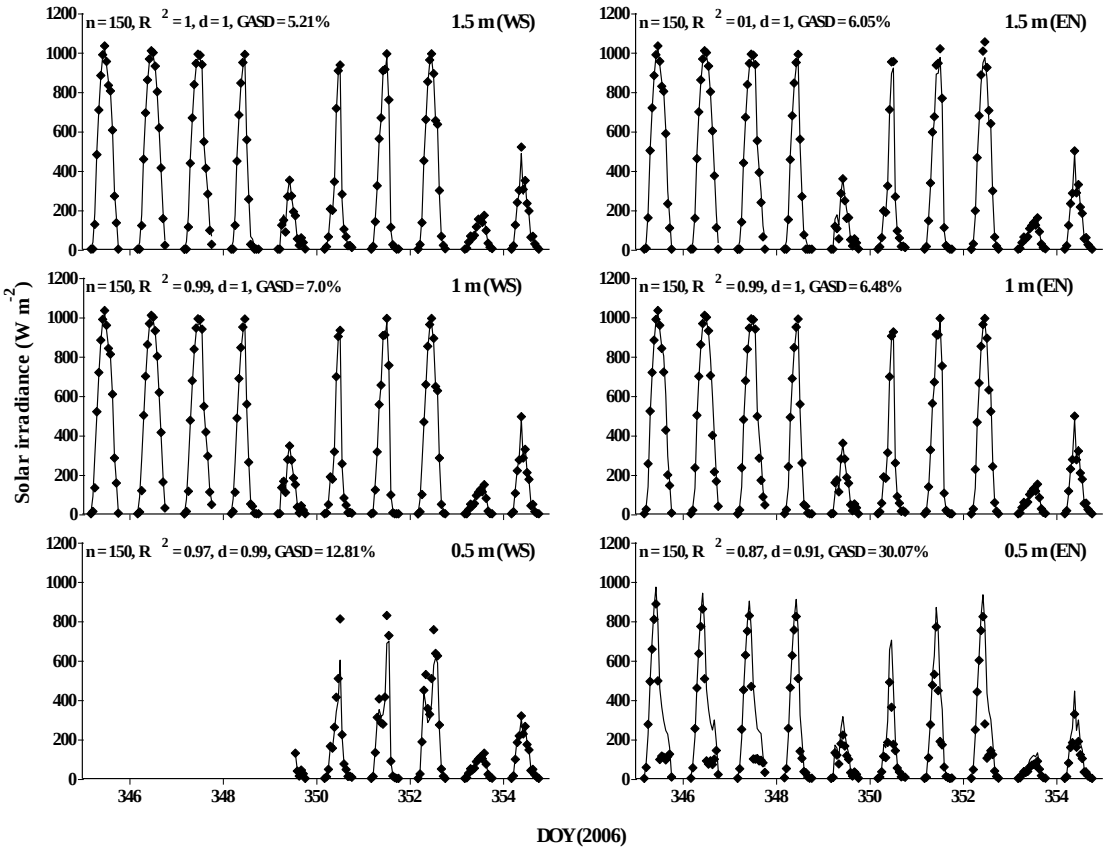

Fig. 5.2 Estimated (lines) and measured (points) hourly transmitted solar irradiance for tube solarimeters positioned on the ground at different distances from the tree trunk across the row on either side of the Jatropha tree from day of year (doy) 345 to 355, 2006 (WS: West of South; EN: East of North)

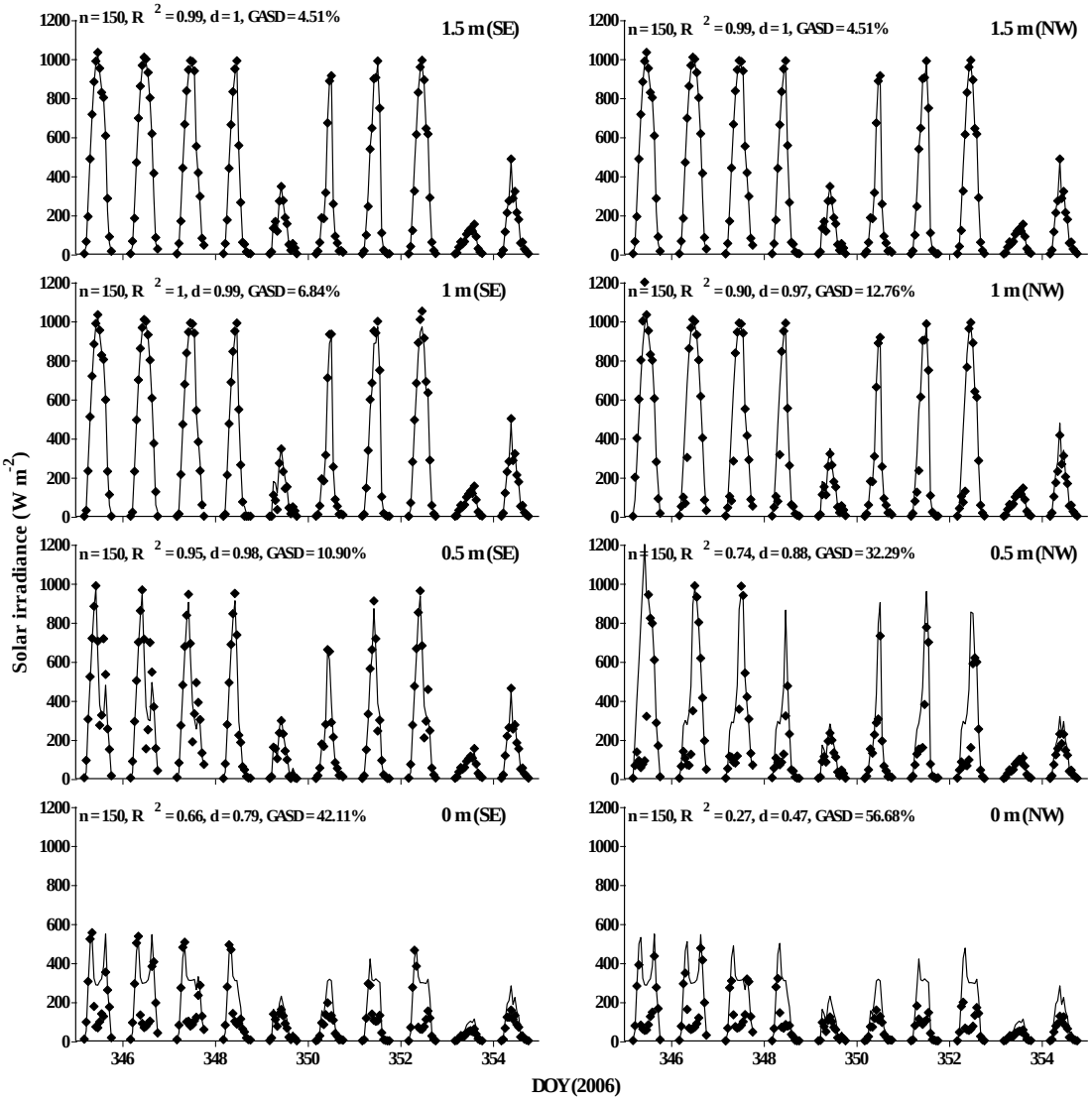

Fig. 5.3 Estimated (lines) and measured (points) hourly transmitted solar irradiance for tube solarimeters positioned on the ground at different distances from the tree trunk along the row on either side of the Jatropha tree from doy 345 to 355, 2006 (SE: South of East; NW: North of West)

ore days involving various canopy characteristics is presented in Figs 5.4 and 5.5 along with a one-to-one line. In general, model predictions of the transmitted solar irradiance at all nodes were in good agreement with actual measurements. The statistical indices achieved were acceptable to allow for an adequate prediction of the transmitted solar irradiance for the canopy at all nodes except the nodes located next to the tree trunk.

With small canopy size and few leaves, the transmitted solar irradiance was predicted very well with little interference by the canopy. With an increase in the canopy size and number of leaves, the model appeared to overestimate the transmitted solar irradiance for nodes lo-

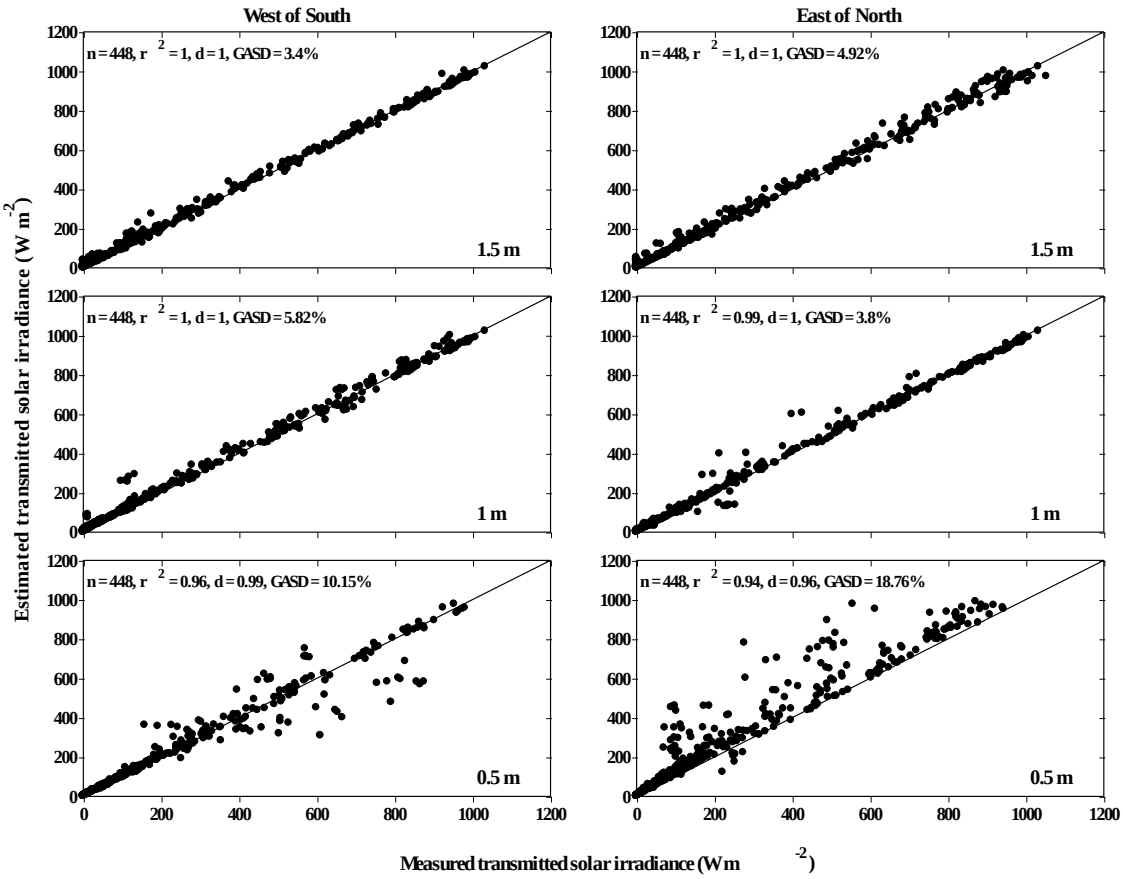

Fig. 5.4 Agreement between estimated and measured hourly transmitted solar irradiance across the row for Jatropha only plants under different canopy characteristics

cated close to the tree trunk, especially along the row. This was attributed to the presence of the tree trunk and the continuous shade it casts on the tube solarimeters throughout the day. As a result, most of the statistical indices achieved for nodes close to the tree trunk were not within the generally accepted range for a model as a means of predicting actual observations.

5.4.2.3 Jatropha trees and Kikuyu grass (single row)

The Jatropha trees were planted in 5 m of row spacing and 2.5 m of tree spacing with Kikuyu grass planted as an understorey crop. Because of the interference of the Kikuyu grass on the measurement of the transmitted solar radiation, the tube solarimeters were elevated by 0.3 m above the ground. Radiation transmission simulations and measurements were carried out concurrently at two periods with varying canopy dimensions (Table 5.2).

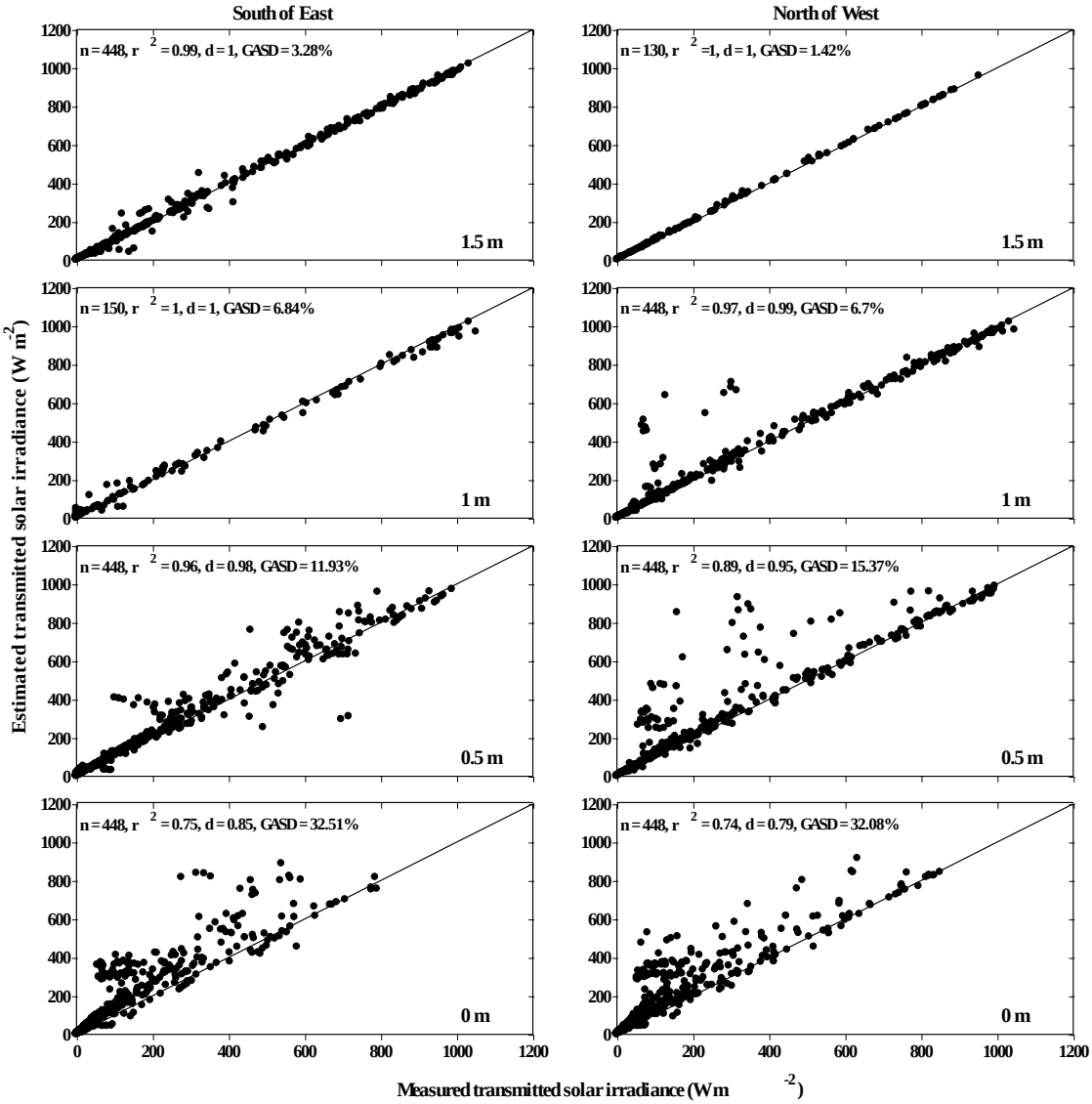

Fig. 5.5 Agreement between estimated and measured hourly transmitted solar irradiance along the row for Jatropha only plants under different canopy characteristics

Figs 5.6 and 5.7 show the estimated versus measured hourly transmitted solar irradiance at equal distance but in opposite directions from the tree trunk both along and across the row for the Jatropha and Kikuyu mixture plot at 0.3 m above the ground. The model generally simulated the trend of transmitted solar irradiance very well. From the two periods of measurement, it was evident that the solar irradiance amount transmitted to the nodes, especially close to the tree trunk, became less as the canopy dimensions increased in size. In the first period, the model overestimated the transmitted solar irradiance at most nodes. In the second period of measurement, the model mainly underestimated in the West of South direction across the row. This was because the tree canopy below which the tube solarimeters were placed was asymmetrical, exhibiting multi-branching with more foliage

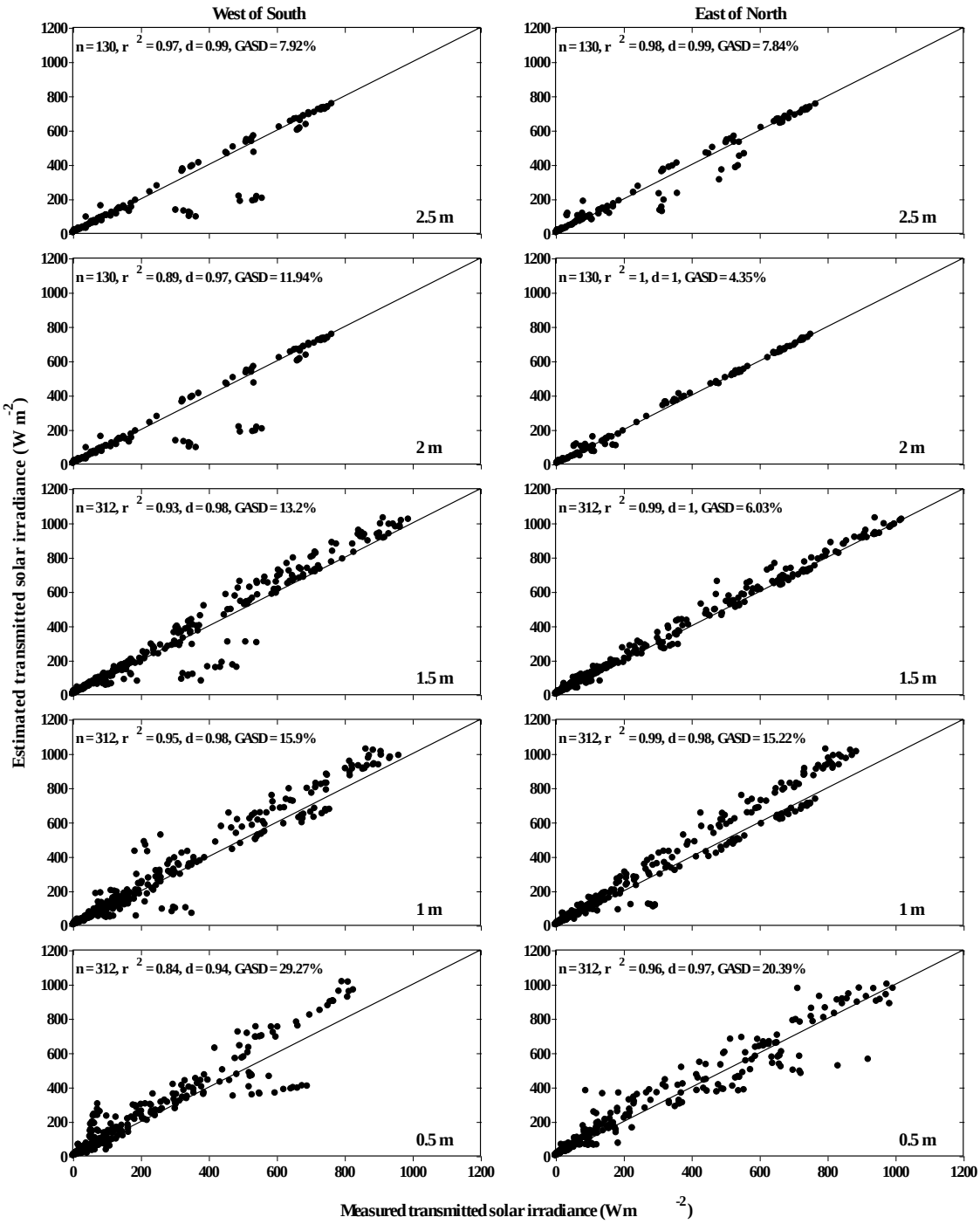

Fig. 5.6 Agreement between estimated and measured hourly transmitted solar irradiance across the row on either side of the Jatropha tree trunk in a the Jatropha and Kikuyu grass mixed plot under different canopy characteristics

on the East of North than on West of South directions from the tree trunk. The radius across the row towards West of South was 0.70 m while towards East of North was 1 m. The highest point of the tree was also leaning more towards East of North. The model, assuming that the canopy was symmetrical, simulated reduced transmission of solar irradiance than the measured amount for the nodes located in the West of South direction

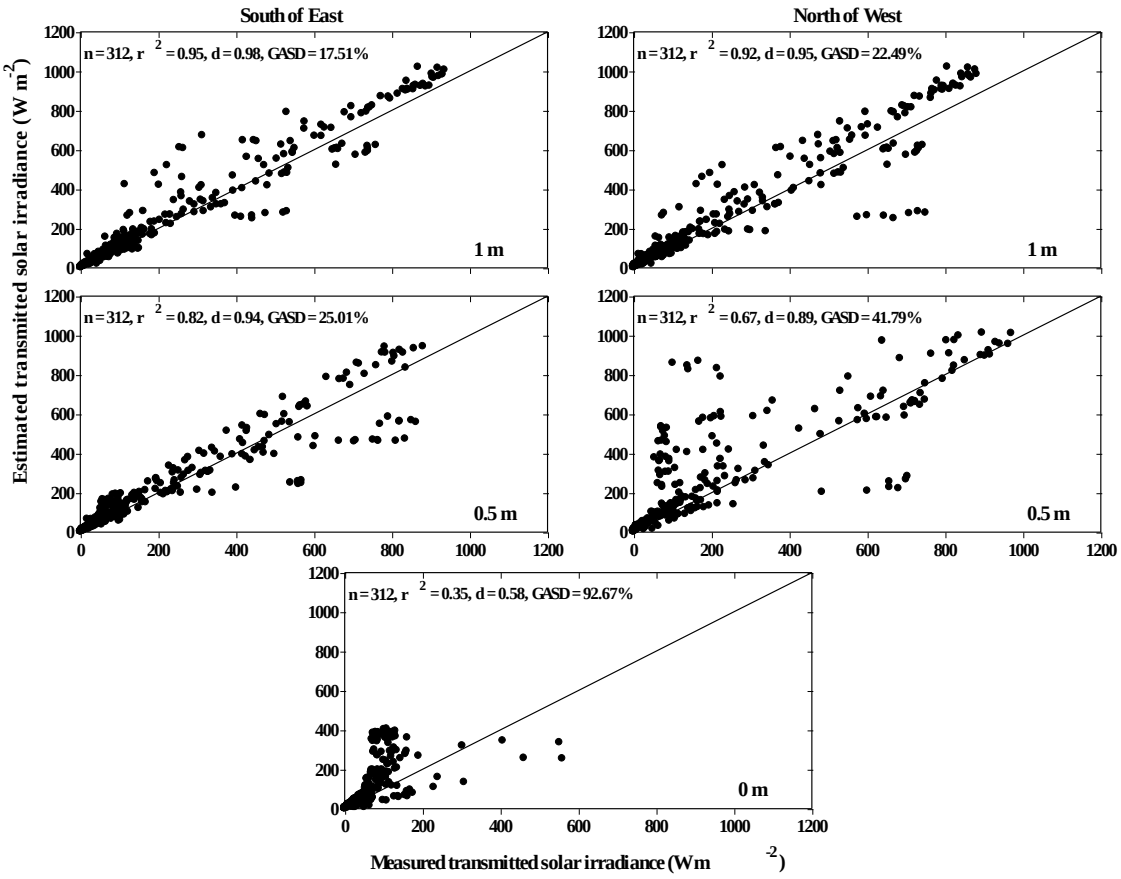

Fig. 5.7 Agreement between estimated and measured hourly transmitted solar irradiance along the row on either side of the Jatropha tree trunk in a Jatropha and Kikuyu grass mixed plot under different canopy characteristics

at some time during the morning. This resulted in some discrepancies between the simulated and measured transmitted solar irradiance. The agreement between the simulated and measured transmission for nodes located in the East of North direction was not affected that much although the canopy radius was larger in that direction. This was because the sun is usually located in the North relative to the tree canopy and thus those nodes in that direction stay illuminated for most of the day. The agreement between the simulated and measured transmitted solar irradiance for the nodes located next and near to the tree trunk was also not as good as for the other nodes. This was because the tree trunk and leaves were close to the tube solarimeters adjacent and near the tree trunks, shading them throughout the day. Consequently, some of the statistical indices achieved for these tube solarimeter positions were not within the generally accepted range, especially the *GASD*. And specifically, for the node located next to the tree trunk, all the statistical indices used, the r^2, *d* and *GASD* were not acceptable for a model as a means of predicting the actual observations.

Along the row, the *GASD* was greater than the acceptable 20% for almost all nodes (Fig. 5.7). The values of the statistical indices for nodes located across the row were slightly better than for nodes located along the row when nodes with similar distance from the tree trunk were considered.

5.4.2.4 Jatropha trees and Kikuyu grass (tramline)

This plot consisted of a tramline of Jatropha trees 2 m apart with a 6-m row spacing between the tramlines and 2.5-m distance between trees along the tramline. Kikuyu grass was planted as an understorey crop. As in the single row, the tube solarimeters were elevated by 0.3 m above the ground to avoid interference by the Kikuyu grass. The tubes were positioned starting from the centre of the tramline to the centre of the 6-m row on either direction across the row, and along the tramlines to mid-way of the tree spacing. The transmission of solar irradiance for the two nodes located at and next to the middle of the 6-m row on either side of the tree was not significantly influenced by the tree canopies.

The comparison between the simulated and measured hourly transmitted solar irradiance for the nodes along and across the row and between the tramlines is given in Figs 5.8 to 5.11. The measurements and simulations for these trees were performed at two periods: when the trees were small in size with few leaves and when the trees grew in size and increased in foliage density. At the initial stage, the interference of the canopy was so small that the agreement between the simulated and measured transmitted solar irradiance was excellent for all nodes, apart from slight overestimations for nodes located next and near to the tree trunk. But with increased canopy size and foliage density, the model overestimated the transmitted solar measurements for nodes located next and near to the tree trunk. This was because the tube solarimeters were placed close to numerous and big leaves which left them shaded for most of the day. Also the tree trunk affected transmission measurements significantly. The trees chosen for the experiment also exhibited asymmetry as the canopy dimensions increased which contributed to some of the discrepancy between the simulations and measurements. For instance, the tree along the left hand lane of the tramline had a smaller radius towards West of South than towards East of North and consequently the model underestimated the transmitted solar irradiance in the West of South direction. Despite this, all the statistical indices achieved were acceptable for a model as a means of predicting the actual observations except for nodes located next

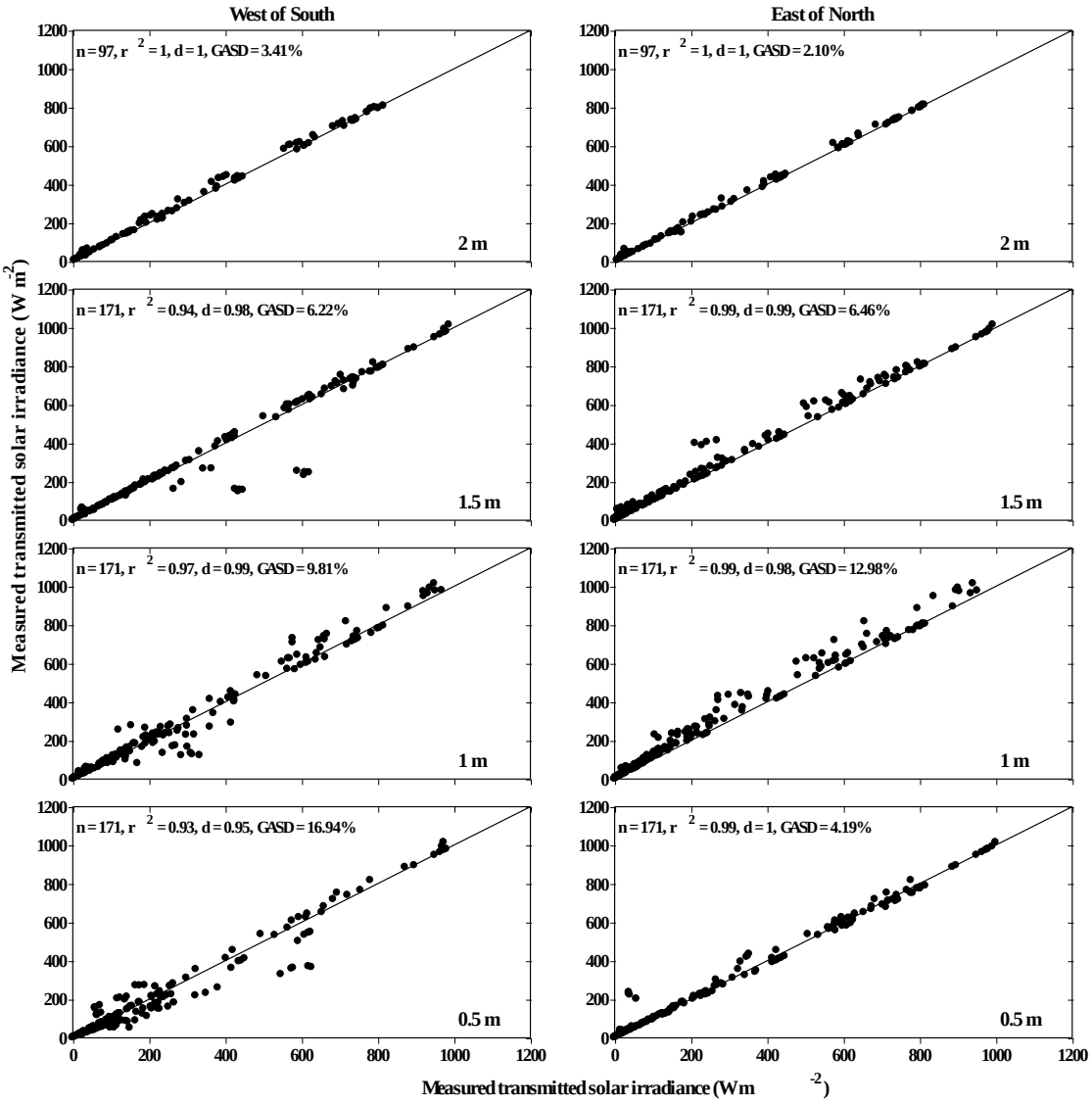

Fig. 5.8 Agreement between estimated and measured hourly transmitted solar irradiance across the row for tube solarimeters placed away from the either side of the tramline Jatropha trees in a Jatropha and kikuyu mixed plots under different canopy characteristics

to the trunk.

5.4.2.5 Leucaena

The Leucaena trees formed a hedgerow along the row. Accordingly, measurements and simulations were carried out for nodes across the row only. In general, there was a good agreement, with the simulated versus measured points fairly distributed along the one-to-one line (Fig. 5.12). All the statistical indices achieved were also acceptable for a model as a means of predicting the actual observations.

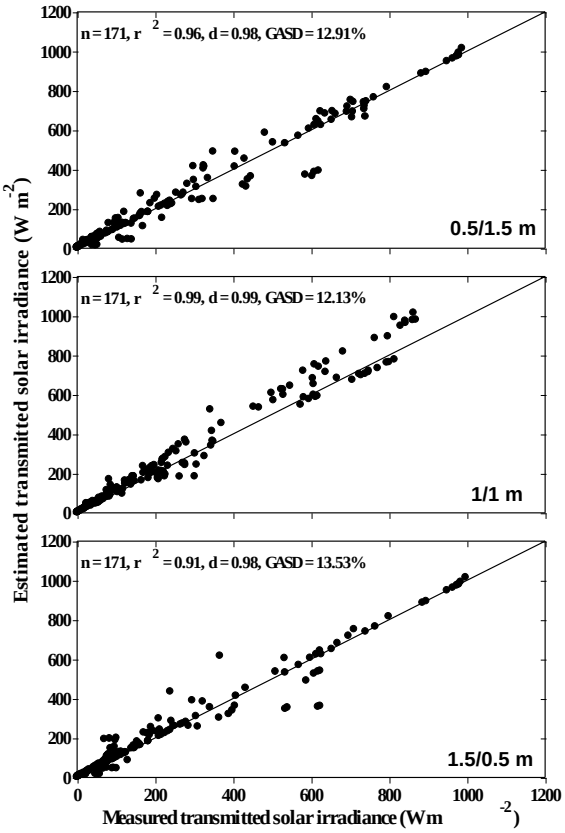

Fig. 5.9 Agreement between estimated and measured hourly transmitted solar irradiance across the row for tube solarimeters placed between the tramline of Jatropha trees in a Jatropha and kikuyu mixed plots under different canopy characteristics

5.4.2.6 Macadamia

The Macadamia trees were three years old at the time of the experiment, planted with a row and tree spacing of six and four meters respectively. They typically formed isolated tree crowns. In general, the simulations of hourly transmitted solar irradiance, for all nodes located across and along the row, agreed well with the actual measurements (Figs 5.13 and 5.14). The model failed to reproduce the hourly transmitted solar radiation for particular nodes during certain periods of the day. This was more pronounced for the node located 0.5 m East of North across the row (Fig. 5.13). The model predicted a larger transmitted amount for a certain period of time during the day but the actual measurements revealed a smaller transmitted amount for that same period of time. This resulted in scatter of the estimated versus measured points around the one-to-one line and was reflected in a relatively low r^2 and higher *GASD*.

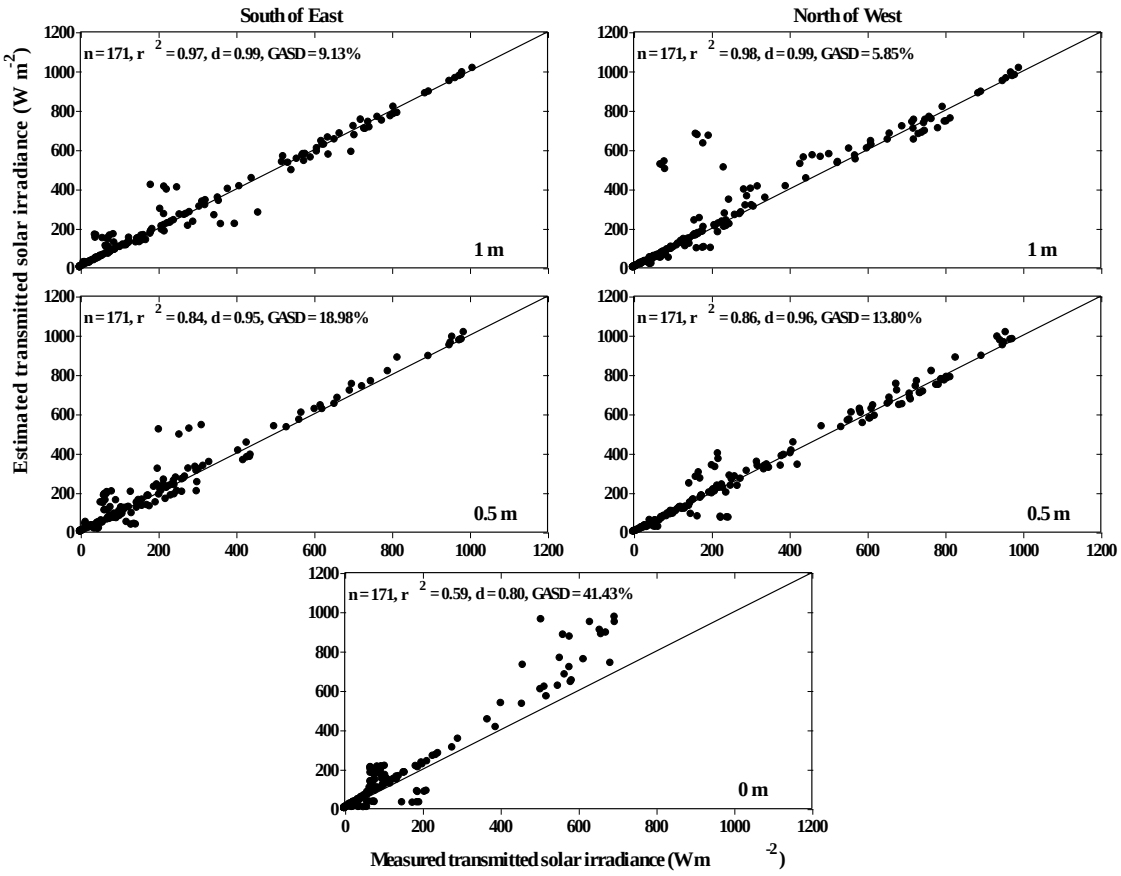

Fig. 5.10 Agreement between estimated and measured hourly transmitted solar irradiance for tube solarimeters placed along the left lane of tramline in a Jatropha and kikuyu mixed plots under different canopy characteristics

This could probably be attributed to the non-uniform height of the maximum horizontal diameter the canopy exhibited.

5.4.2.7 Black Wattle

The black wattle trees were one-year old at the time of the experiment and they formed a distinct hedgerow. The spacing between the rows and trees was 3 and 1.5 m respectively. This stand had about the largest canopy dimensions and smallest leaf area density of all the tree crops used in this experiment (Table 5.2). In general, the model tended to slightly underestimate larger values of transmitted solar irradiance (Figs 5.15 and 5.16). The r^2 and *d* indices achieved for almost all the nodes were acceptable but the *GASD* was slightly larger than the acceptable range for most of the nodes.

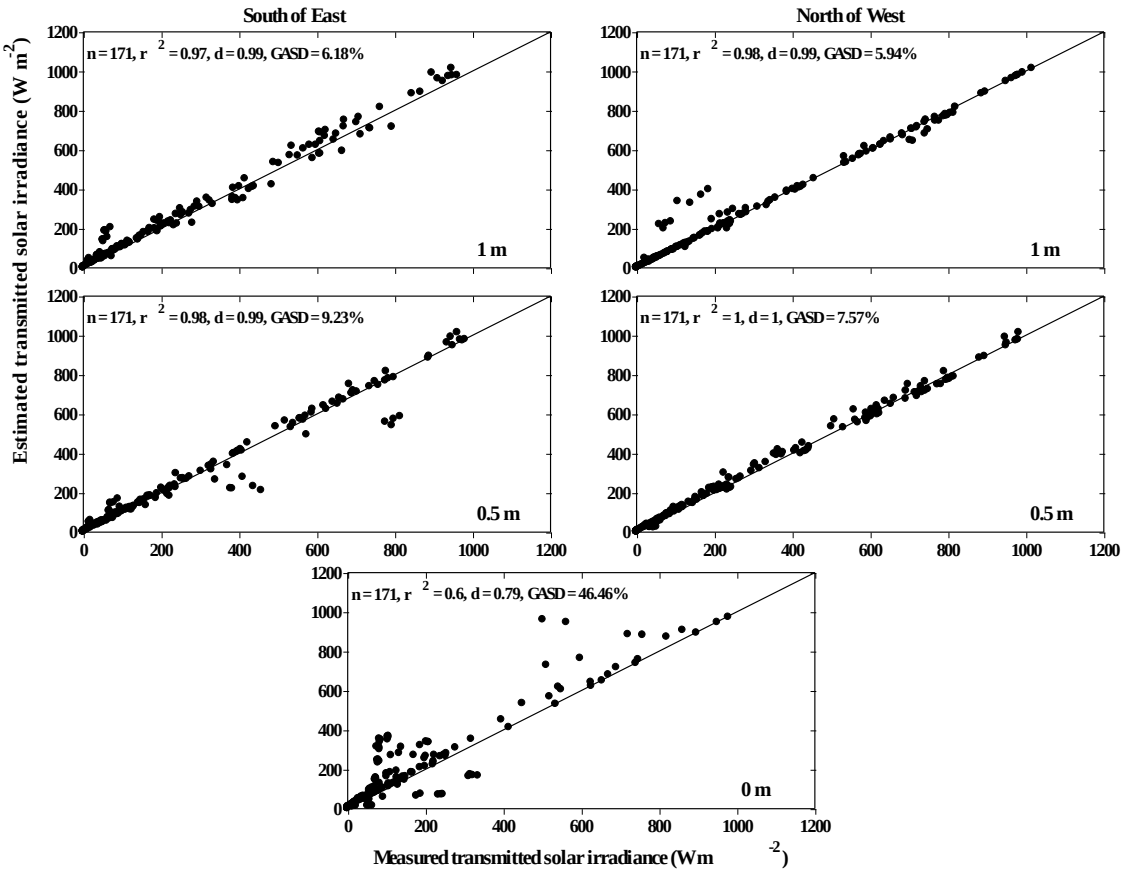

Fig. 5.11 Agreement between estimated and measured hourly transmitted solar irradiance for tube solarimeters placed along right lane of tramline in a Jatropha and kikuyu mixed plots under different canopy characteristics

Because of the canopy dimensions and distance between the trees, there was little difference in the amount of simulated transmitted solar irradiance when the nodes along the row were considered. A two-dimensional model may be adequate for tree crops with such planting specifications based on the assumption that there would be little solar irradiance transmitted to the nodes along the hedges. But the relatively smaller *LAD* of the wattle trees allowed the transmission of solar irradiance to these nodes, and this justifies that a three-dimensional solar irradiance transmission model should be used for plants with such canopy characteristics.

The statistical indices also showed, contrary to the results from the other tree crops, improved agreement for nodes located closer to rather than further from the tree trunk. This could be due to the canopy size and row and tree spacing of the stand. The canopy also had a non-uniform leaf distribution along the height of the canopy, with the upper part of the canopy being denser than the lower part. Therefore, the assumption of uniform *LAD* throughout the canopy could also be another reason why this stand showed a different tre-

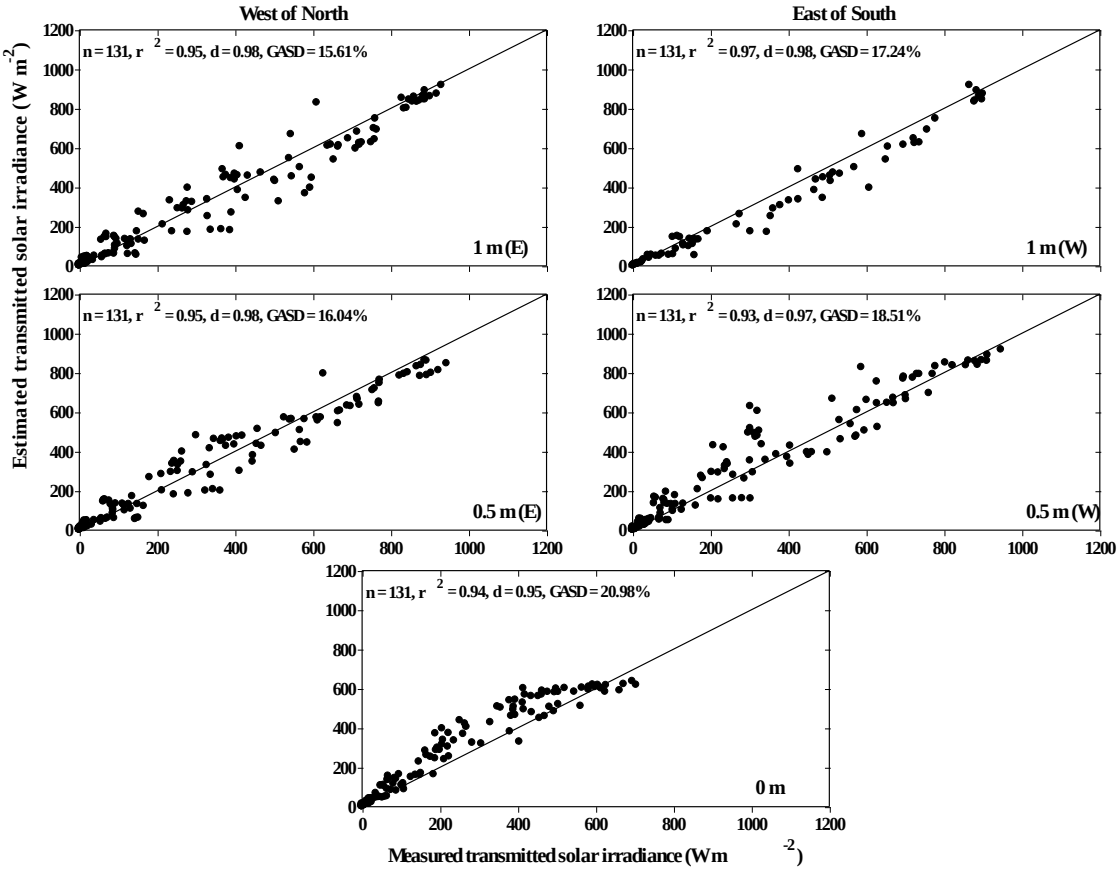

Fig. 5.12 Agreement between estimated and measured hourly transmitted solar irradiance for tube solarimeters placed across the row in on either side of the Leucaena hedges

nd of results compared to the other stands in this experiment. Wang and Jarvis (1990) found an improved agreement between simulated and measured transmitted photosynthetically active radiation (PAR) by assuming variable *LAD* both in the vertical and horizontal directions as opposed to uniform *LAD* throug-hout the canopy.

5.4.2.8 Overall accuracy of the model

The statistical indices achieved by comparing the estimated and measured hourly solar irradiance transmission averaged for all the nodes at all the canopies gave a *slope* = 0.97, *intercept* = 18.10 W m^{-2}, r^2 = 0.91, *d* = 0.96 and *GASD* = 17.66%. These average statistical indices suggest that the model was able to reproduce the transmittance of solar irradiance for a variety of tree canopies and planting patterns with good accuracy. The slope and intercept indicate that the model generally tended to overestimate hourly solar irradiance transmission except at very low values. Using a two-dimensional version of this model, Annandale *et al*. (2004) noted similar observations for a variety of tree canopies. They also

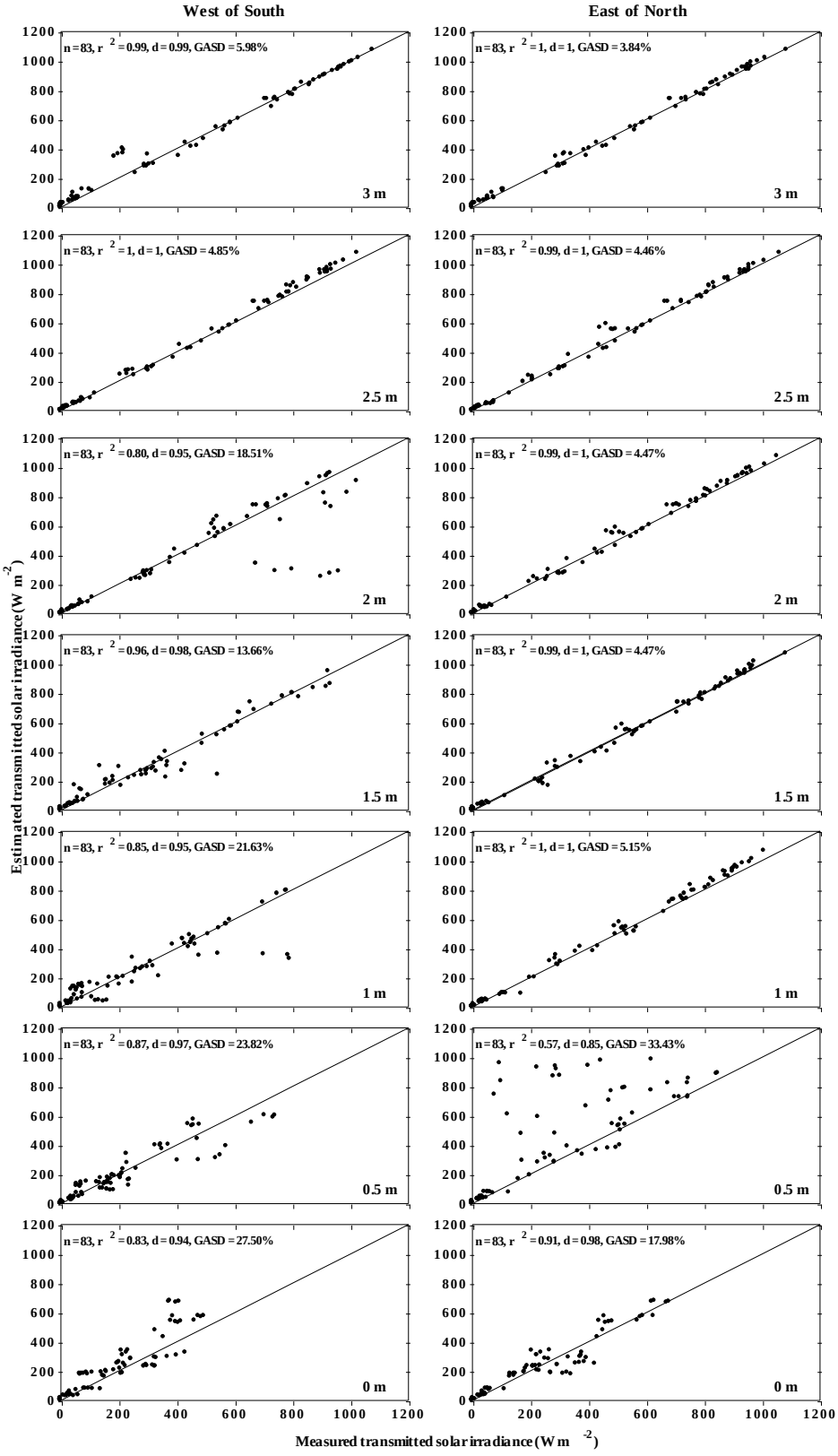

Fig. 5.13 Agreement between estimated and measured hourly transmitted solar irradiance for tube solarimeters placed across the row on either side of the Macadamia

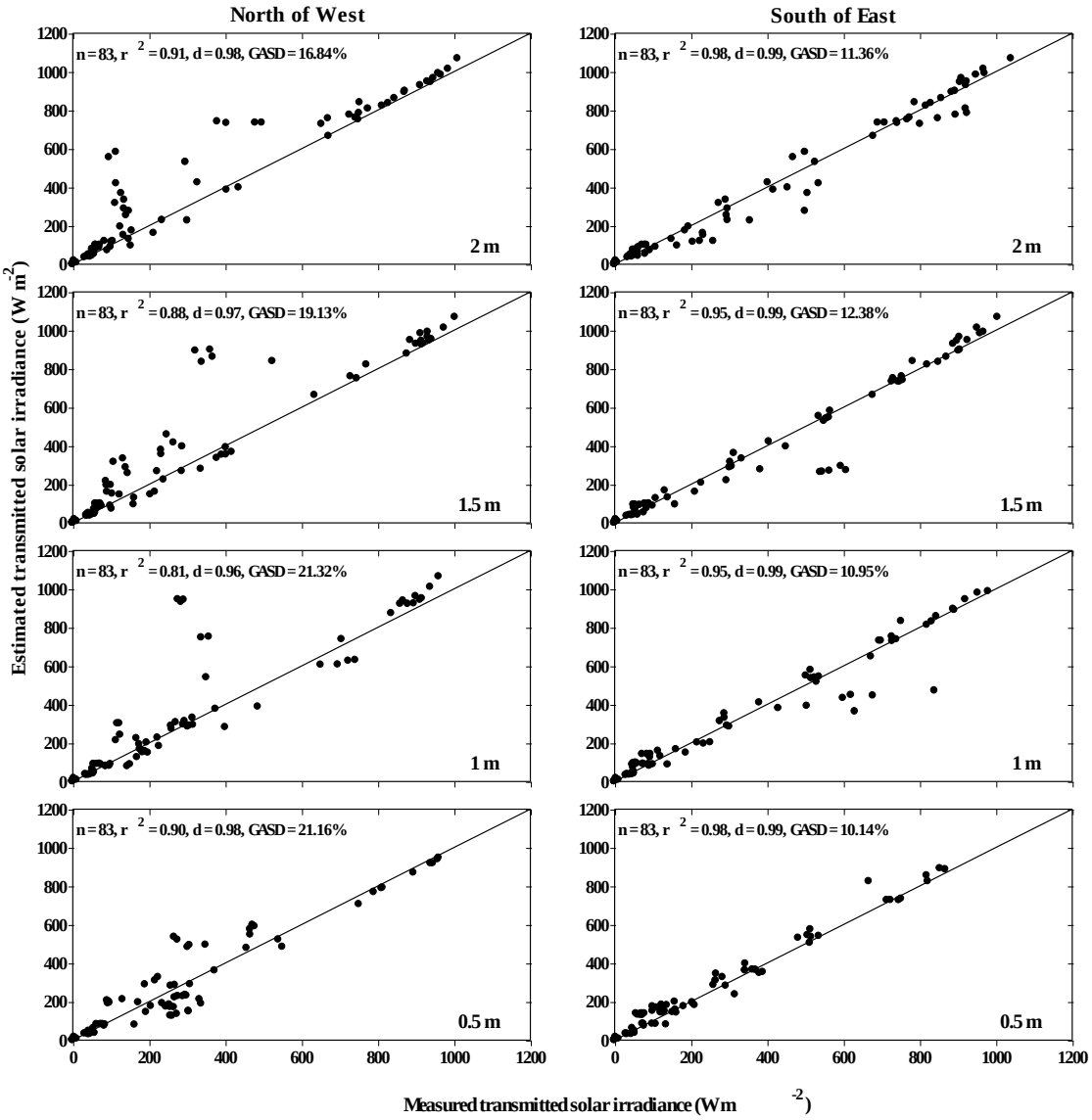

Fig. 5.14 Agreement between estimated and measured hourly transmitted solar irradiance for tube solarimeters placed along the row on either side of the Macadamia tree

reported *slope* = 0.87, *intercept* = 10.90 W m^{-2}, r^2 = 0.76, *d* = 0.93 and *GASD* = 40%. This indicates that the performance of the three-dimensional model used here improved considerably compared with the two-dimensional version. A similar two-dimensional version of this model was also used for estimation of solar irradiance transmission (Charles-Edwards and Thorpe, 1976) and transpiration (Thorpe, 1978) of apple orchards. Oyarzun *et al*. (2007) also used a simplified three-dimensional solar irradiance interception model that assumes a prismatic canopy shape with canopy porosity as a model input. Canopy porosity was estimated from the proportion of sunflecks with the shaded area cast by the trees on the ground. The estimation of this input variable may be subjective considering sunflecks contain full and partially (penumbra) lit areas on the ground. They

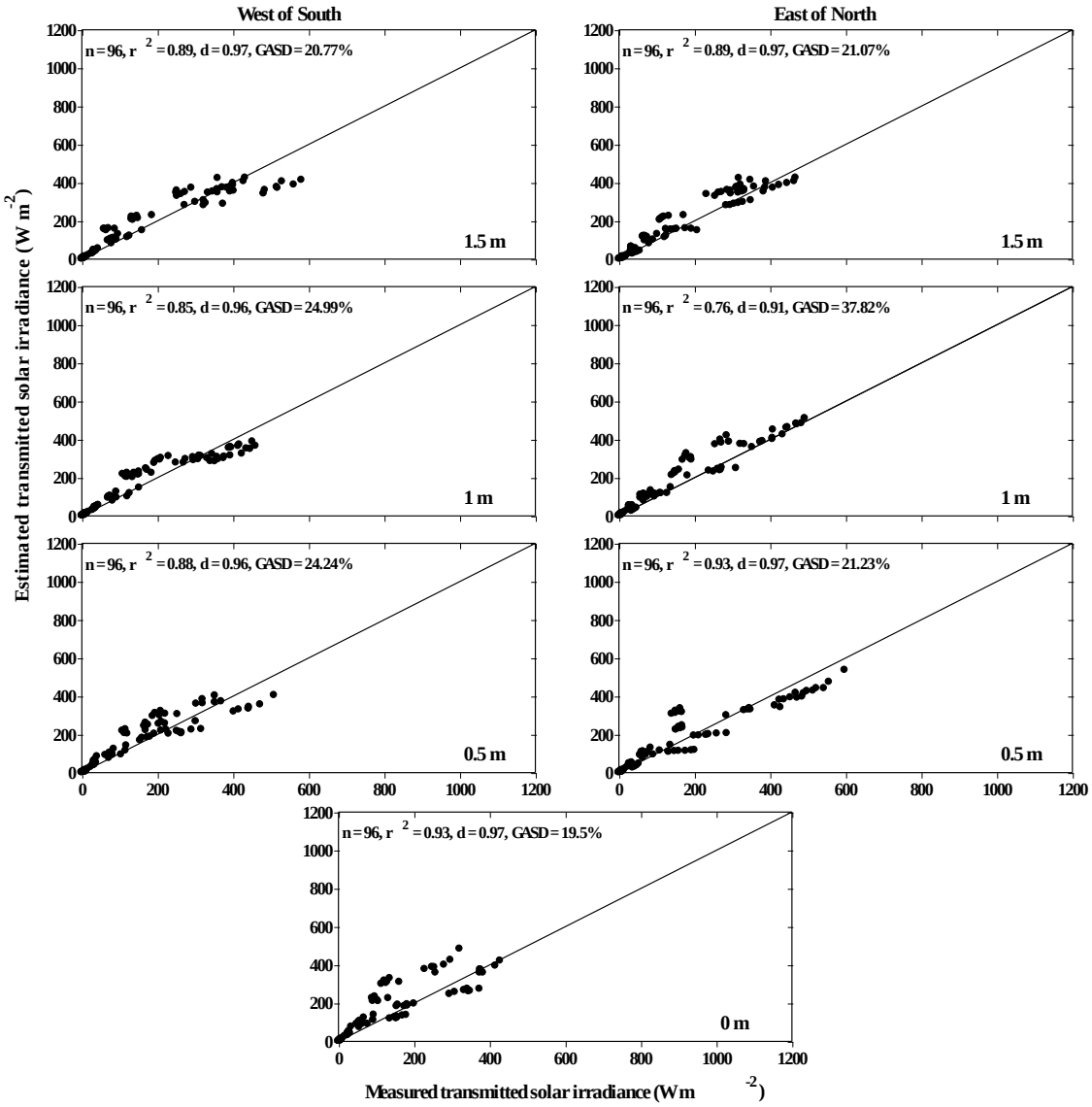

Fig. 5.15 Agreement between estimated and measured hourly transmitted solar irradiance for tube solarimeters placed across the row on either side of the Black Wattle trees

used their model for a variety of orchard canopies and reported a *GASD* = 11.32% and *d* = 0.87 by comparing estimated and measured hourly fraction of PAR interception. They found that their model slightly overestimated the PAR interception. Validation of a similar but more detailed radiation transfer model than used in this study (Wang and Jarvis, 1990) over Sitka spruce and radiata pine resulted in satisfactory predictions of transmitted PAR. The nodes and data points per node that the model considered were fewer than in this study. The statistics were given in mean residual of hourly transmittance averaged over a day and ranged between 1 and 38%. The results cannot be compared directly with the results of the present work because of the difference in radiation wavelength considered in both studies. Green *et al*. (2003) also used a more c omplex three-dimensional model that

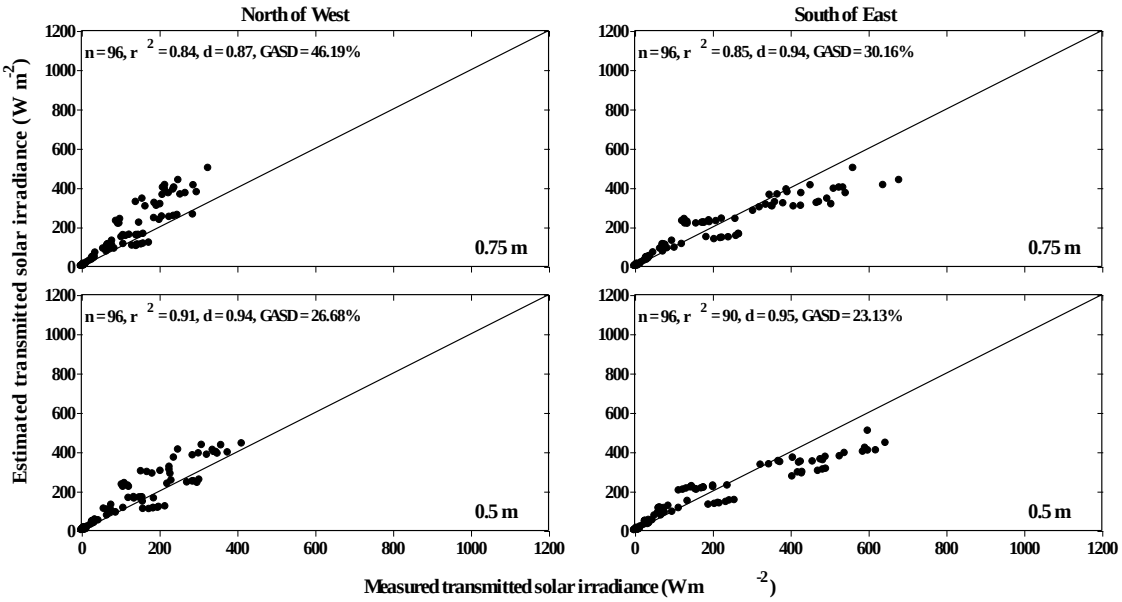

Fig. 5.16 Agreement between estimated and measured hourly transmitted solar irradiance for tube solarimeters placed along the row on either side of the Black Wattle trees

accounts for scattering of solar irradiance within the canopy. They measured the intercepted PAR by two apple canopies using a whirligig radiometer. They reported, on average, *slope* = 0.97, *intercept* = -12.8 μmol s^{-1}, r^2 = 0.98 and standard error of 451 μmol s^{-1} m^{-2} by comparing measured and estimated 10-min PAR interception over two different apple canopies. Considering the above results from the literature, the three-dimensional solar radiation interception model presented here works as well as or better than other similar models.

5.5 CONCLUSIONS

The relatively simple three-dimensional solar irradiance model presented here was validated using data sets comprising different canopy characteristics (canopy size and leaf area density), row orientations, row and tree spacing and sky conditions. Comparison of estimations and measurements of hourly transmitted solar irradiance was performed for nodes located across and along the tree rows in four directions from the tree trunk. In general, the model was able to simulate the spatial and temporal variation of hourly solar irradiance transmission of the tree crops for each node using a range of model input parameters very well. Stronger agreement between simulations and measurements was noted for nodes located further from the tree trunk and on northern compared with the southern side of the tree trunk (the study site being in the southern hemisphere). The

agreement was also better for overcast than for clear-sky conditions when same node locations under similar canopy characteristics were compared. Some discrepancies between estimated and measured hourly solar irradiance transmittance were also observed due to the presence of the tree trunk with a larger influence on transmittance of radiant energy than the foliage elements, tube solarimeters being shaded by leaves and branches of close proximity, asymmetrical canopy shapes, and non-uniform tree canopy sizes and leaf distribution. However, overall r^2 = 0.91, d = 0.96 and $GASD$ = 17.66% were obtained by averaging the statistical indices for all the nodes at all the experimental sites indicating that the model was able to estimate hourly solar irradiance transmission with reasonalbe accuracy.

These results suggest that such a three-dimensional solar irradiance model could be useful in planning and management practices. The model could be used to aid in designing row orientations, row spacing and distance between trees that would result in optimal interception by tree crops and transmission of to the understorey crops and soil for a specific location. It could also be used for the management of thinning and pruning of stands based on the interception of solar irradiance requirements and assessing coloration and sunburn in fruits. The model could also play a major role in estimating evapotranspiration and dry matter production as part of a tree water-use and tree growth and development model.

Acknowledgments

Special thanks to - Mr. N Moyo for calibration and construction of tube solarimeters, and Mr. Livio Tessaro for use of facilities at the Macadamia field site.

6 EVAPORATION ESTIMATION OVER SPARSE VEGETATION USING SINGLE- AND DOUBLE-LAYER MODELS

ABSTRACT

The need for proper and efficient management of water resources in the agricultural sector has signaled the search for less expensive methods of determining water-use. This study was conducted to investigate if the Penman-Monteith (PM) equation and the Shuttleworth and Wallace (SW) model could be used to determine the latent energy flux, and thereby total evaporation, from a sparse vegetation canopy at a daily time scale. The total evaporation from a *Jatropha curcas* plot was determined as a residual of the shortened surface energy balance using measurements of net irradiance, soil heat flux and sensible heat flux, the latter using eddy covariance, assuming energy balance closure is met. The PM equation and SW models were also used to estimate total evaporation from routine automatic weather station observations, resistance parameters and vegetation indices. Beer's law was included in the SW model to estimate the amount of energy that is transmitted through the canopy and absorbed at the soil surface. The PM equation failed to reproduce the 'measured' daily total evaporation during periods of low leaf area index (*LAI*) which was attributed to an inability to account for the fluxes from the soil surface. The SW model, however, using more resistance parameters, produced total evaporation estimates that agreed very well with the 'measured' evaporation with a slope of 0.96, r^2 of 0.91 and root mean square error (*RMSE*) of 0.45 mm for a *LAI* ranging from no leaves to 1.83 m^2 m^{-2}. The SW model also estimated soil evaporation and plant transpiration separately, and about 66% of the cumulative evaporation simulated throughout the study period was attributed to soil evaporation. For a *LAI* ranging between 0 (no leaves) and approximately 1.4 m^2 m^{-2} during the year 2007, the simulated soil evaporation was about 84% of the cumulative evaporation. For a *LAI* between 1.4 and 1.83 m^2 m^{-2} during the 2008 part of the study period, the simulated soil evaporation contributed about 52% of the cumulative evaporation. These statistics signify the importance of soil evaporation in sparse vegetation and suggest that the PM equation should be replaced by the SW model for surfaces that assume a range of *LAI* values during the growing season.

Keywords: Penman-Monteith; Shuttleworth and Wallace; evaporation; shortened energy balance

6.1 INTRODUCTION

The ever-increasing demand for water, nationally and internationally, by the different sectors of the economy has highlighted the need for proper and efficient management of water resources. Realization of this has led nationally to the 1998 Republic of South Africa National Water Act which refers to the possible prescription of methods for determining the amount of water use for purposes of water allocation and charges in the case of activities resulting in stream flow reduction. Forest plantations and agricultural lands have long been known for the significant role they play in water consumption. Therefore, it is imperative to understand the processes on how water is used in vegetated fields, and moreover search for less expensive methods that quantify and determine the water-use more accurately and precisely. Reliable methods that account for the transport of water in the soil, plant and atmosphere continuum can yield the water balance, and hence water-use of a system. Evaporation from the soil and plant surfaces is a chief constituent of the water balance and indicative of usage of water from such lands. This process is usually complex and direct measurements are difficult and often costly (Allen *et al.*, 1998). This, therefore, highlights the need for less expensive and yet accurate and reliable alternative methods for routine evaporation estimation.

Mathematical models have been widely used in the past to estimate evaporation from horizontally homogeneous surfaces, which could take the form of bare soil, open-water bodies or vegetated surfaces. For horizontally homogeneous vegetated surfaces, these models assume that the canopy is a single-layer of vegetation overlying the soil (Monteith, 1965), and hence they are termed single-layer models (Raupach and Finnigan, 1988). The Penman-Monteith (PM) equation, a relatively simple biophysical model for estimating evaporation, is the most commonly-used single-layer model which uses surface energy balance and resistance-based heat and mass transfer equations. The equations employed in such models are not adequate to estimate the total evaporation in mixed or sparse vegetation, especially as the component resistances of the two or more surfaces involved are not well represented in these equations (Lafleur and Rouse, 1990; Stannard, 1993; Farahani and Bausch, 1995). Moreover, the diurnal radiation interception and transmission

characteristics are different from their homogeneous counterparts. The total evaporation in mixed or sparse vegetation is the sum of the contribution of evaporation from the component parts, *viz.* the vegetation cover and the underlying substrate, and can vary depending on the type of plants involved, and the coverage they render to the soil. As water that evaporates directly from the soil is considered as a loss, it becomes important to distinguish between the evaporation arising from the component parts (Kabat *et al.*, 1997). The development of multi-layer models that consider separate mass and energy transfer occurring at different plant canopy layers and the soil can overcome such problems (e.g., Shuttleworth and Wallace, 1985; Choudhury and Monteith, 1988). These models offer the capability of simulating evaporation accurately from canopies that provide differing amount of coverage to the ground, ranging from bare soil to full-canopy.

Shuttleworth and Wallace (1985) developed and extended the one-dimensional single-layer PM equation into a one-dimensional two-layer evaporation model. The model (hereafter called SW) has been used for variety of vegetation types: e.g., wetland sedge (Lafleur and Rouse, 1990), sparse crops of dryland millet (Wallace, 1990; Lund and Soegaard, 2003), sparse wildland vegetation (Stannard, 1993), maize (Farahani and Bausch, 1995), barley (Tourula and Heikinheimo, 1998), row crops of cotton, wheat and maize (Anadranistakis *et al.*, 2000), row crops of sorghum (Kato *et al.*, 2004), vine (Ortega-Farias *et al.*, 2007) and grassland (Zhongmin *et al.*, 2009). Besides comparing the SW model-estimates against measurements, most of these studies also compared evaporation estimates from the SW model against evaporation estimates from the conventional PM equation and found that the estimates were similar at full-canopy, but that the PM equation underestimated for soil cover less than full-canopy.

The objective of this study was to evaluate the applicability of the SW model in estimating the latent energy flux, and hence the evaporation arising from sole stands of *Jatropha curcas* trees and the soil. Total evaporation was calculated as a residual of the shortened surface energy balance from measurements of net irradiance, soil heat flux and sensible heat flux assuming that energy balance closure is met. The performance of the PM equation for the same sparse field was also assessed.

6.2 THEORY

6.2.1 The Penman-Monteith (PM) equation

The PM equation is a single-layer biophysical model that estimates total evaporation from a surface using a combination of radiative energy and resistance equations (Monteith, 1965):

$$E = \left(\frac{\Delta(R_n - G_s) + \rho c_p D / R_a^a}{\Delta + \gamma(1 + R_a^c / R_a^a)} \right) \Big/ \lambda \qquad (6.1)$$

where E is the total evaporation (mm), λ the latent heat of vapourization (kJ kg^{-1}), Δ the slope of the saturation water vapour pressure function of the reference and mean canopy source height temperatures (kPa ^{o}C^{-1}), R_n the net irradiance (W m^{-2}), G_s the soil heat flux (W m^{-2}), ρ the air density (1.14 kg m^{-3}), c_p the specific heat capacity of air at constant pressure (1011 J kg^{-1} K^{-1}), D the atmospheric water vapour pressure deficit (kPa), R_a^a (s m^{-1}) the aerodynamic resistance, R_a^c (s m^{-1}) the canopy resistance and γ the psychrometric constant (kPa ^{o}C^{-1}).

6.2.2 The Shuttleworth and Wallace (SW) model

The SW model is specifically designed to estimate separate energy fluxes that arise from the vegetation and the underlying soil in sparse canopies. The model assumes that the aerodynamic mixing within the canopy is sufficient to allow the assumption of mean canopy wind speed (Thom, 1972) that can be described by meteorological parameters such as air temperature, humidity and wind speed.

The SW model derives the fluxes from the available energy and resistance-based heat and mass transfer at the vegetation and soil components (Fig. 6.1) using the shortened surface energy balance term. The available energy for the canopy (A), soil (A_s) and vegetation (A_c) are, respectively, given by:

$$A = R_n - G_s = \lambda E + H \qquad (6.2)$$

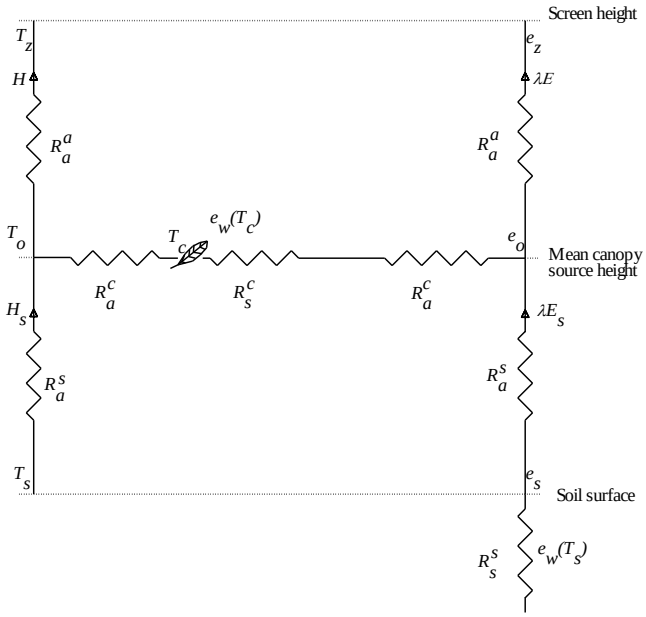

Fig. 6.1 Schematic diagram of resistances and fluxes in the two-layer evaporation model of Shuttleworth and Wallace (1985)

where H and λE are given by:

$$H = \rho c_p \left(T_z - T_o\right) / R_a^a \tag{6.3}$$

$$\lambda E = \rho c_p \left(e_z - e_o\right) / \gamma R_a^a \tag{6.4}$$

$$A_s = R_{ns} - G_s = H_s + \lambda E_s \tag{6.5}$$

where H_s and λE_s are given by:

$$H_s = \rho c_p \left(T_s - T_o\right) / R_a^s \tag{6.6}$$

$$\lambda E_s = \rho c_p \left(e_s - e_o\right) / \gamma \left(R_a^s + R_s^s\right) \tag{6.7}$$

$$A_c = A - A_s = H_c + \lambda E_c \tag{6.8}$$

where H_c and λE_c are given by:

$$H_c = \rho c_p \left(T_c - T_o\right) / R_a^c \tag{6.9}$$

$$\lambda E_c = \rho c_p \left(e_c - e_o\right) / \gamma \left(R_a^c + R_s^c\right) \tag{6.10}$$

where the subscripts *s* and *c* refer to soil and vegetative canopy respectively, H and λE are the sensible heat and latent energy fluxes respectively (W m^{-2}), T_z and T_o are the air temperatures at reference and canopy source heights respectively (^oC), e_z and e_o are the water vapour pressures at reference and canopy source heights respectively (kPa), R_a^a (s m^{-1}) the aerodynamic resistance between canopy source height and reference height, R_a^s (s m^{-1}) the aerodynamic resistance between the soil and canopy source height, R_s^s (s m^{-1}) the surface resistance of the soil component, R_a^c (s m^{-1}) the bulk boundary layer resistance of the vegetative component and R_s^c (s m^{-1}) the bulk stomatal resistance of the vegetative component.

The water vapour pressure deficits at a reference (D) and mean canopy (D_o) source heights are, respectively, defined as:

$$D = e_w(T_z) - e_z \tag{6.11}$$

$$D_o = e_w(T_o) - e_o \tag{6.12}$$

where $e_w(T_z)$ and $e_w(T_o)$ are the saturated water vapour pressures at T_z and T_o respectively. The introduction of Δ, the slope of the saturation water vapour pressure and temperature, into the mean canopy height water vapour pressure yields:

$$D_o = e_w(T_z) - [e_w(T_z) - e_w(T_o)] - e_o \tag{6.13}$$

Substituting Eqs (6.2), (6.3) and (6.4) into Eq. (6.13) enable D_o to be expressed as a function of D as follows:

$$D_o = D + [\Delta A - (\Delta + \gamma)\lambda E]\frac{R_a^a}{\rho c_p} \tag{6.14}$$

Together, these equations form PM-type equations, without the need for having D_o, for separate calculation of evaporation from the soil and the plants in the canopy:

$$\lambda E_s = \frac{\Delta A_s + \frac{\rho c_p}{R_a^s}\left(D + [\Delta A - (\Delta + \gamma)\lambda E]\frac{R_a^a}{\rho c_p} \right)}{\Delta + \gamma(1 + \frac{R_s^s}{R_a^s})} \tag{6.15}$$

$$\lambda E_c = \frac{\Delta(A - A_s) + \frac{\rho c_p}{R_a^c}\left(D + [\Delta A - (\Delta + \gamma)\lambda E]\frac{R_a^a}{\rho c_p} \right)}{\Delta + \gamma(1 + \frac{R_s^c}{R_a^c})} \tag{6.16}$$

Finally the total latent energy flux from the system, λE, is the sum of the latent energy fluxes from soil and plants, and the resultant equation is arranged in the form:

$$\lambda E = C_s PM_s + C_c PM_c \tag{6.17}$$

The PM_s and PM_c are PM-type combination equations for surfaces with bare soil and fully-covered vegetation respectively:

$$PM_s = \frac{\Delta A + \{\rho c_p D - \Delta R_a^s (A - A_s)\} / (R_a^a + R_a^s)}{\Delta + \gamma\left(1 + \frac{R_s^s}{(R_a^a + R_a^s)} \right)} \tag{6.18}$$

$$PM_c = \frac{\Delta A + \{\rho c_p D - \Delta R_a^c A_s\} / (R_a^a + R_a^c)}{\Delta + \gamma\left(1 + \frac{R_s^c}{(R_a^a + R_a^c)} \right)} \tag{6.19}$$

C_s and C_c are coefficients given by:

$$C_s = \left(1 + \frac{R_s R_a}{R_v (R_s + R_a)} \right)^{-1} \tag{6.20}$$

$$C_c = \left(1 + \frac{R_c R_a}{R_s (R_c + R_a)} \right)^{-1} \tag{6.21}$$

R_a, R_s and R_c are given by:

$$R_a = (\Delta + \gamma) R_a^a \tag{6.22}$$

$$R_s = (\Delta + \gamma) R_a^s + \gamma R_s^s \tag{6.23}$$

$$R_c = (\Delta + \gamma) R_a^c + \gamma R_s^c \tag{6.24}$$

Once λE is calculated, it can be used in Eq. (6.14) to determine D_o which in turn can also be used in Eqs (6.15) and (6.16) along with the available energy fluxes both at the canopy and substrate level and resistance parameters to determine λE_s and λE_c. Derivation of two-layer SW model is detailed in Appendix A.

6.2.3 Resistance parameters

The PM equation requires two resistances: the aerodynamic (R_a^a) and canopy (R_a^c) resistances. The aerodynamic resistance is computed following Thom (1972):

$$R_a^a = \frac{u}{u_*^2} + \frac{2}{k u_*} + \psi_m - \psi_h \tag{6.25}$$

where u is the horizontal wind speed, u_* the friction velocity taken as 0.14 × u following Weber (1999), k the von Kármán's constant (0.41), and ψ_m and ψ_h are the stability functions for momentum and heat respectively given as (Dyer and Hicks, 1970):

$$\begin{aligned} \psi_m &= (1 - 16L)^{-0.25} \\ \psi_h &= (1 - 16L)^{-0.5} \end{aligned} \tag{6.26}$$

where L is the Obukhov length.

The canopy resistance is determined in a similar manner as in the SW model and is given in this section under the SW resistance parameters.

The SW model requires two aerodynamic resistances: between the substrate and the mean canopy height, R_a^s, and between the mean canopy height and reference height, R_a^a. These are basically derived from the eddy diffusivity resistance above and within the canopy.

Assuming that the air flow within sparse canopies is adequately described by the *K*-theory, the eddy diffusion coefficient, K (m^2 s^{-1}), at a height z above the canopy can be described as (Thom, 1971; Dolman and Wallace, 1991):

$$K = ku_*(z-d), \quad (z > h) \tag{6.27}$$

where h is the canopy height and d the displacement height of the vegetation given as $0.56h$. It is also assumed that K decreases exponentially with height (Thom, 1971), thus:

$$K = K_h \exp\left(-n\left(1-{}^{z}\!/_{h}\right)\right) \quad (z < h) \tag{6.28}$$

where K_h is the value of K at the top of the crop, ku_* (h - d), and n the eddy diffusivity decay constant for a closed canopy assumed to be 2.5. Both R_a^a and R_a^s are then integrated from the reciprocal of the eddy diffusion coefficient and the decay of the eddy diffusion coefficient equations, over the heights zero to d + z_o and d + z_o to h respectively as (Shuttleworth and Gurney, 1990):

$$R_a^s = \frac{h\exp(n)}{nK_h}\left[\exp(-nz_o'/h) - \exp\left(-n(z_o+d)/h\right)\right] \tag{6.29}$$

$$R_a^a = \frac{1}{ku_*}\ln\left(\frac{z-d}{h-d}\right) + \frac{h}{nK_h}\left[\exp\left\{n\left(1-\frac{z_o+d}{h}\right)\right\}-1\right] \tag{6.30}$$

where z_o' and z_o are the roughness length of the total vegetation ($0.1h$) and the soil (0.01 m) respectively.

Assuming the leaf area index (*LAI*) is uniformly distributed with height and the eddy diffusion of momentum and energy is similar throughout the canopy, the bulk boundary layer resistance, R_a^c, is calculated by integrating the leaf boundary layer conductance over the canopy height (Choudhury and Monteith, 1988; Shuttleworth and Gurney, 1990; Lhomme *et al*., 1994a, 1997).

$$R_a^c = \frac{2.5 \cdot \left(w_l / u_h \right)^{0.5}}{4 \cdot LAI \cdot 0.005 \cdot \left(1 - \exp(-n/2) \right)} \tag{6.31}$$

where w_l is the average canopy leaf width and u_h the wind speed at the top of the canopy.

The canopy resistance, in soil-plant-atmosphere models, is commonly empirically related to independent environmental conditions that are known to affect stomatal opening. Jarvis (1976) proposed a multi-variate multiplicative model that relates the response of stomatal conductance, g_s, to important meteorological factors at the leaf scale and the available soil water. The general Jarvis-type relation can be expressed as follows:

$$g_s = g_{\max} f_1(\delta q) f_2(I_s) f_3(T) f_4(\delta\theta) \tag{6.32}$$

where g_{max} (m s^{-1}) is the maximum stomatal conductance under non-limiting conditions and $f_1(\delta q)$, $f_2(I_s)$, $f_3(T)$ and $f_4(\delta\theta)$ are functions of specific humidity deficit (g kg^{-1}), solar irradiance (W m^{-2}), air temperature (^{o}C), and soil water deficit (mm) respectively. The response functions, $f(i)$ where i represents a potentially limiting factor, vary between 0 and 1. The stomatal conductance, g_s, takes the value of the g_{max} as long as the environmental conditions are at their optimum, in which case each individual response function, $f(i)$, becomes unity. But g_s starts to decline when these conditions fall below optimal, in which case the $f(i)$ assume values less than unity which is then multiplied by g_{max} resulting in g_s less than g_{max}. Following Stewart (1988) and Dolman *et al*. (1991), the individual limiting response functions are given by:

$$\begin{aligned}
f_1(\delta q) &= \exp(-a_1 \delta q) \\
f_2(I_s) &= \frac{I_s / (a_2 + I_s)}{1100 / (1100 + a_2)} \\
f_3(T) &= \frac{(T - T_l)(T_h - T)^t}{(a_3 - T_l)(T_h - a_3)^t} \\
f_4(\delta\theta) &= \min\left\{ (\theta - \theta_w) / (\theta_c - \theta_w), 1 \right\}
\end{aligned} \tag{6.33}$$

where I_s = 1100 W m^{-2} corresponds to $f_1(I_s) = 1$, $t = (T_h - a_3)/(a_3 - T_l)$, T_l (^{o}C) and T_h (^{o}C) are the lower and upper air temperature limits for transpiration respectively, taken as 0 and

40 ^{o}C, a_1, a_2 and a_3 are parameters that are derived by non-linear optimization. The wilting (θ_w) and critical (θ_c) soil water contents are taken as 340 and 250 mm respectively. For the purpose of this work, g_s was calculated by inverting the Penman-Monteith equation (Penman, 1965) following a day after rain had occurred when the *LAI* was at its maximum. Non-linear optimization was then used to derive the model parameters, and the resulting values of the optimization are presented in Table 6.1. The stomatal resistance was then calculated as a reciprocal of the stomatal conductance, and up-scaled to canopy resistance following Shuttleworth and Wallace (1985) as follows:

$$R_s^c = r_s / 2LAI \tag{6.34}$$

Soil resistance is also one of the parameters that are explicitly presented in two-layer SW models. Numerous formulations have been proposed in the literature that attempt to relate volumetric soil water content to soil resistance. The soil resistance was determined by inverting the PM equation for a time period when the plots were bare or with minimal *LAI*. This was then used to derive parameter values for surface soil resistance for several equations that were deduced from the literature and summarized by Farahani and Ahuja (1996). However, the existing parameters from the literature appeared to yield a better agreement between the simulated and measured (as a residual of the shortened energy balance) latent energy flux based on slope, coefficient of determination (r^2) and root mean square error (*RMSE*) than the newly derived parameters, and were used for further simulation. For the purpose of this study, a better result was achieved from a functional soil resistance formulae that was applied by Farahani and Bausch (1995) as follows:

$$R_s^s = 39\left(\theta / \theta_s\right)^{-2.59} \tag{6.35}$$

where θ and θ_s are the actual and saturated water contents respectively.

Table 6.1 Parameters values resulting from the optimization procedure of the Jarvis-type surface conductance model

g_{max} (m s^{-1})	a_1	a_2	a_3
26.04 ± 3.33	60 ± 18	1483 ± 959	23.14 ± 3.39

6.2.4 Net irradiance: above and below the canopy

Net irradiance above the canopy was estimated from solar irradiance measurements according to Doorenbos and Pruitt (1992). The corresponding soil heat flux was estimated from the resulting net irradiance as 20% and 10% during bright and cloudy days respectively. The available energy flux below the canopy was determined from a relatively simple three-dimensional tree-canopy radiation interception model based on the works of Charles-Edwards and Thornley (1973) which considers the earth-sun relationship, the geometry of the plant canopy, planting pattern, row orientation and solar irradiance transfer equations (see Chapter 5). The model assumes that trees are elliptical in shape with uniform leaf distribution, and that solar irradiance attenuation within the canopy follows Beer's law. As solar irradiance can be obstructed by neighbouring trees, the model considers several trees around the tree of interest. The model divides the ground below the canopy into 0.5 m squares and determines the solar irradiance transmitted to each area by calculating the path length traversed through the tree canopy to reach a point within the area at a particular time. It also makes use of inputs of geographic location, altitude, row orientation, row and tree spacing, canopy size, leaf area density and solar irradiance. The transmitted irradiance is then used to further estimate the net irradiance and soil heat flux received at the soil surface for each square according to the method of Doorenbos and Pruitt (1992). The soil and plant available energy values were then used as input to the SW model to estimate the latent energy flux, and thereby the evaporation, for each square and then averaged over the entire plot.

6.3 MATERIALS AND METHODS

The experiment was conducted over sole stands of *J. curcas* in a 50 m × 60 m plot at Ukulinga (29°40′11″S, 30°24′50″E and 781 masl), Pietermaritzburg, KwaZulu-Natal, South Africa. The trees were about two and half years old at the start of the experiment time with tree height, *h*, on average ranging from 1 to 2 m during the experiment. The trees were planted in 3 m × 3 m row and tree spacing. The area between trees was weeded to keep it devoid of vegetation. The study comprised data from late spring when the trees had no leaves (LAI = 0 m^2 m^{-2}) to summer when the trees attained maximum LAI (1.83 m^2 m^{-2}).

Net radiometers and soil heat flux plates were set up to measure the available energy flux. One net radiometer (NR LITE, Kipp and Zonen, Delft, The Netherlands) was placed 3 m from the ground directly above and facing the trees, and a second net radiometer (model Q*7.1, REBS, Seattle, WA) was placed 3 m from the ground directly above the space between the trees facing the bare soil. The average net irradiance was then used for computation of the available energy.

A pair of soil heat flux plates (HFT-S, REBS, Seattle, WA) were buried 80 mm below the soil surface, with one of them placed directly below a tree and the other one between trees, were used to determine the soil heat flux. The soil heat stored above the soil heat flux plates was accounted for by using a system of parallel thermocouples (type E) that were placed above the plates at depths of 20 and 60 mm from the surface. The soil heat flux at the soil surface was then determined by adding the stored heat at 20 and 60 mm above the plates to the soil heat flux measured by the plates at the 80 mm depth (Tanner, 1960). A Campbell CS615 time domain reflectometer (TDR) was also used to measure the volumetric soil water content in the upper 60 mm. All measurements were sampled every 10 s and averaged every 10 minutes using a Campbell CR23X datalogger (Campbell Scientific Inc., Logan, UT). Sensible heat flux was determined using a three-dimensional sonic anemometer (Model 81000, RM Young, Traverse City, MI) mounted at 2.3 m above the ground from measurements of vertical wind speed and virtual temperature. The measurements were done differentially at 10 Hz frequency and the data were logged every 2 and 30 min using a Campbell CR5000 datalogger. The latent energy flux was then calculated as a residual of the shortened surface energy balance involving the available energy and sensible heat flux assuming that closure is met.

Standard automatic weather station measurements were also made at about 10 m away from the edge of the Jatropha plot. Measurements of solar irradiance (LI-200 pyranometer), air temperature and relative humidity (CS500 Vaisala), wind speed and direction (Model 03001, RM Young) and rainfall (TE525MM tipping bucket rain gauge, Texas Electronics Inc., Dallas, TX) were obtained. A Campbell CR10X datalogger was used to sample measurements every 10 s and log averages every 10 min.

Soil water content was also measured to a depth of 1000 mm using CS100 TDRs from the surface at 200 mm intervals. Measurements were sampled every 1 min and then 60 min average was logged using a Campbell CR1000 datalogger.

Measurements of *LAI* were conducted on a bimonthly basis, using an LAI-2000 canopy analyzer (Li-Cor, Lincoln, NE). Measurements were made along diagonal transects between tree rows using a 45^{o} view cap with four replications. Leaf area density (*LAD*) was also measured using an LAI-2000 canopy analyzer. This involved making *LAI* measurements using a 90^{o} view cap by placing the sensor next to the tree trunk in all four quadrants of the tree. The canopy shape and volume for each quadrant were estimated from a vertical and horizontal coordinate system using points at the boundary of the canopy. The *LAD* was then estimated from *LAI*, canopy shape and volume measurements. All *LAI* and *LAD* measurements were conducted when the sky conditions were completely overcast.

All data were recomputed to 10 min averages to serve as model inputs. The outputs from the 10 min averages were also subsequently averaged over a period of half hour and integrated over a day to serve for model validation purposes.

6.4 RESULTS AND DISCUSSION

The pattern of the measured daily net irradiance (R_n), soil heat flux density (G) and sensible heat flux (H) along with the calculated (as a residual of the shortened surface energy balance - which would be referred to as the 'measured' throughout this study) and modelled (using the SW model) latent energy flux (λE) starting from late spring up to mid-summer are shown in Fig. 6.2 using a moving average with a period of ten days. Also shown in the figure are, for the same time period, the *LAI* trend and rainfall distribution.

The study period coincided with the onset of the rainy season in late spring during which time the plants started as bare leaved trees and then grew progressively to achieve maximum *LAI* by mid-summer. Both the rainfall distribution and the progressive growth of the trees had a significant influence on the partitioning of the energy balance components. Rainy days were associated with clouds which limit the ingress of solar irradiance into the atmosphere resulting in less R_n being received at the surface. A larger proportion of the R_n was also utilized, during the study period, to evaporate water from the surface rather than

to heat the surface and this resulted in λE greater than H throughout the study period. The period during which the H peaked was associated with absence of rain and/or high R_n (although the dryness was not that acute to result in H greater than λE). In general, the pattern of the sensible heat and latent energy flux components responded to the changes in the R_n, rainfall distribution and also the structure of the canopy.

Measured and modelled (using the PM equation) daily total evaporation for the Jatropha trees is given in Fig. 6.3. The total daily evaporation was largely underestimated during the stage when the trees were devoid of leaves but then started to increase and match the measured total evaporation as the trees grew progressively and increased in *LAI*. Similar results have also been found in the literature (e.g., Lafleur and Rouse, 1990; Stannard, 1993; Farahani and Bausch, 1995; Kato *et al*., 2004) and were attributed to the the inability of the PM equation to account for evaporation that arises from the soil. This is because the surface resistance used in the equation considers the canopy only, which happens to be rather large at this stage, and ignores the soil. To overcome such problems encountered in sparse vegetation, most researchers employ a surface resistance that combines both the soil

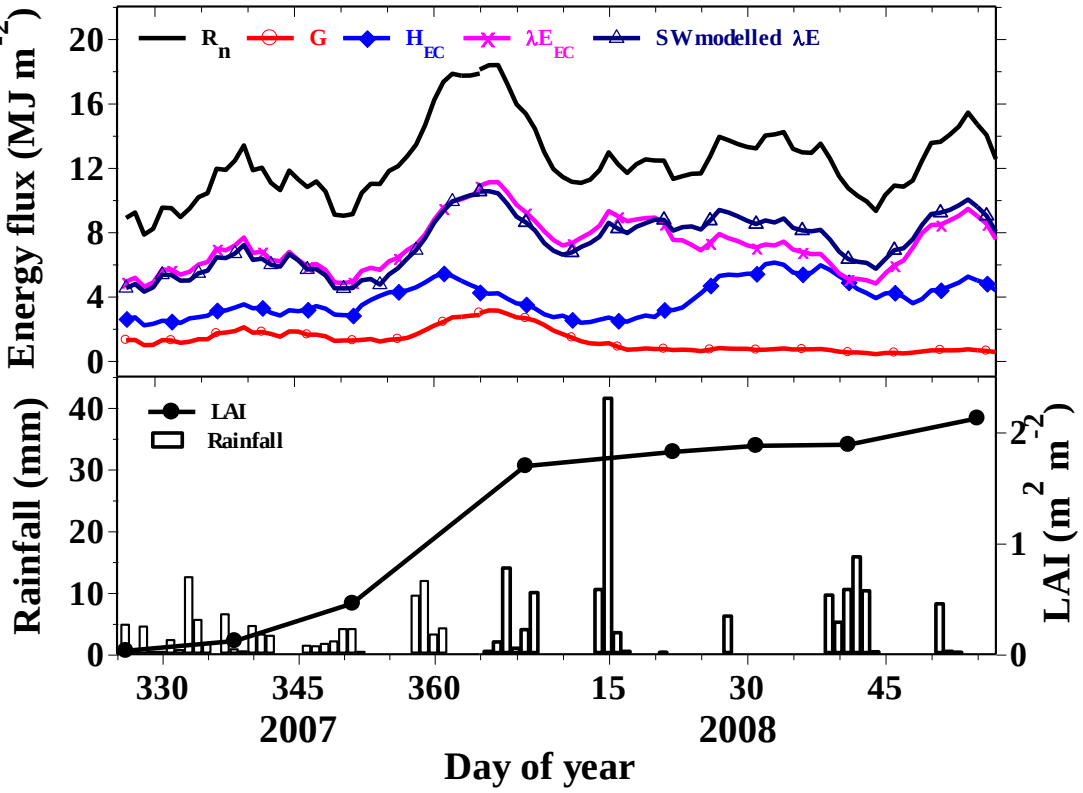

Fig. 6.2 Variation of daily energy balance components, including modelled (SW) total evaporation, during 2007/2008 using a moving average with a period of 10 days. Also shown is the trend of *LAI* and rainfall distribution for the same time period

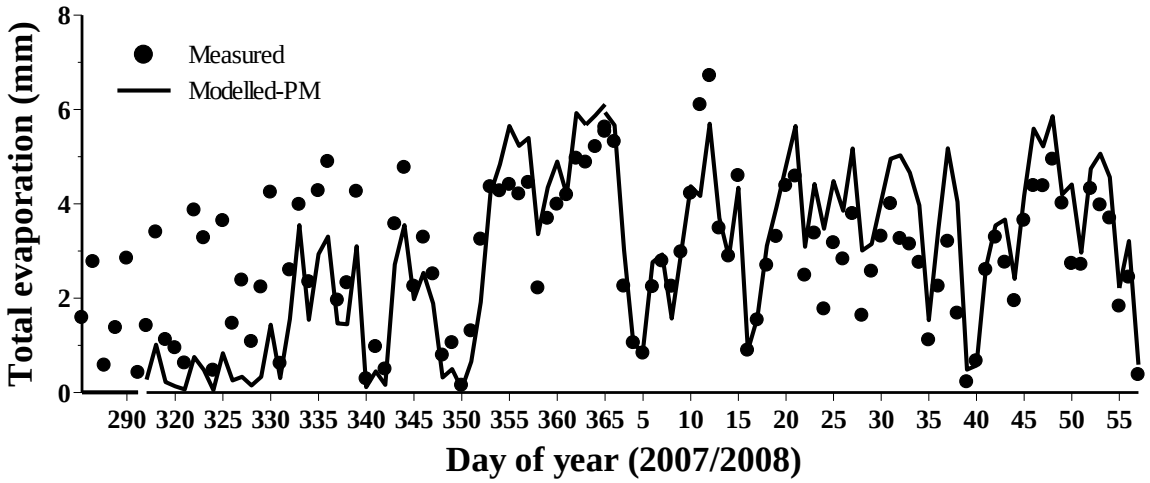

Fig. 6.3 Measured and modelled (PM) daily total evaporation for day of year (doy) 286 (2007) to 56 (2008)

and plant resistances. But it is difficult to measure or relate, either empirically or physically, to other routine meteorological variables. More often, the surface resistance is determined from independent measurements of surface energy fluxes and/or available energy, vapour pressure deficit and air temperature at a reference height (Raupach and Finnigan, 1988).

Towards the end of the study period, the PM equation consistently overestimated the daily total evaporation (Fig. 6.3). The surface resistance parameters were determined by inverting the PM equation for a similar *LAI* at this stage which reflects a weighted average of the soil and canopy resistance. Hence the estimates of the total evaporation from the PM equation were expected to agree closely with the measured total evaporation. The discrepancy between the measured and modelled evaporation values at this stage might be attributed to these parameters resulting in overestimation of the stomatal conductance.

Measured and modelled (SW model) daily total evaporation for the Jatropha trees is also shown in Fig. 6.4. Overall, the agreement between the measured and modelled total evaporation was very good, especially for the first two thirds of the study period starting from the time when the trees had no leaves until they attained a considerable *LAI*. The model overestimated the measured daily total evaporation on a few days during the last one third of the study period. The stomatal resistance parameters used for this simulation were determined by inverting the PM equation, which assumes a homogeneous surface, as opposed to deriving them from measurements. Days following rainy events were used for

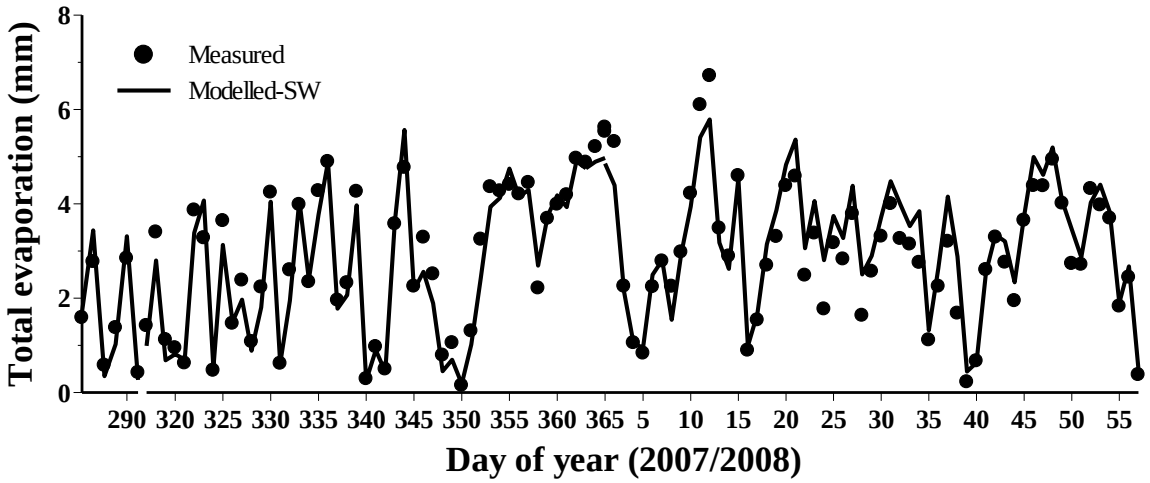

Fig. 6.4 Measured and modelled (SW) daily total evaporation for doy 286 (2007) to 56 (2008)

derivation of the parameters but the discrepancy occurred during the time when the rain events were scarce and the soil water content was low compared to the rest of the study period. This might have contributed towards the discrepancy between the measured and modelled daily total evaporation. Besides, as mentioned earlier, these parameters might have resulted in an overestimated stomatal conductance that could give rise to an overestimation of the modelled daily total evaporation.

The agreement between the modelled (SW model) and measured daily total evaporation is also presented as a scatter-plot in Fig. 6.5. Shown in the graph are the one-to-one (solid) and linear best-fit (broken) lines. The points are well scattered along the one-to-one line with a regression slope of 0.96, r^2 of 0.91 and *RMSE* of 0.45 mm. The model underestimated two large data points of total evaporation that had occurred during the study period. In the same site, daily total evaporation estimated from temperature-variance (TV) and surface renewal (SR) methods resulted in r^2 and *RMSE* of 0.95 and 0.38 mm (TV) and 0.98 and 0.22 mm (SR) respectively for the same data points used in the model evaluation (recalculated from Chapter 4). Both these methods are data intensive in that they calculate H from high frequency measurements of air temperature, and compute the λE, and hence the total evaporation, as a residual of the shortened surface energy balance assuming that energy balance closure is met.

Considering the data required to run the model and the empiricism and uncertainty involved in deriving certain parameters of the model, the r^2 and *RMSE* achieved from the SW model are arguably good compared to those achieved from the TV and SR methods.

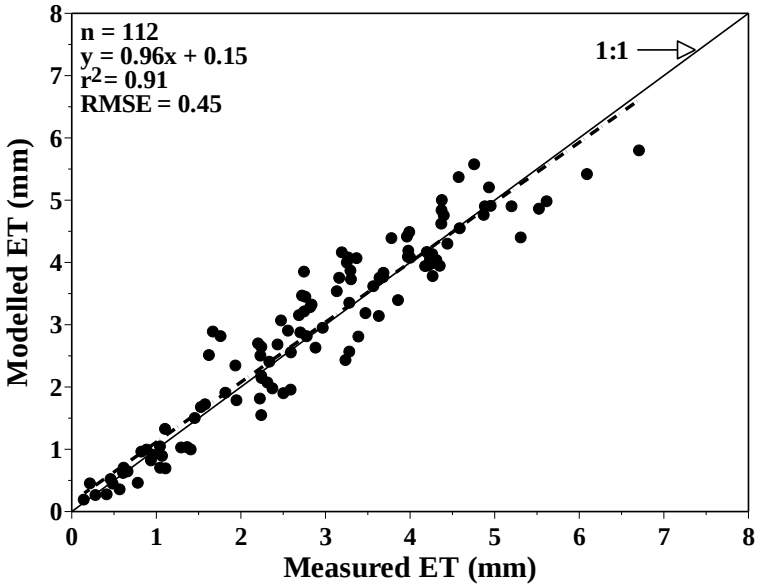

Fig. 6.5 Modelled (SW) versus measured (as a residual of the shortened surface energy balance) daily total evaporation (ET). The broken line is the best-fit while the solid line represents the one-to-one relationship

Other related studies have also compared estimates of daily total evaporation from the SW model against measurements. Lafleur and Rouse (1990), for instance, reported a *RMSE* of about 0.42 mm for evaporation measured using the Bowen ratio energy balance (BREB) method over subarctic wetland. Dolman *et al*. (1991) obtained a slope ranging between 0.79 and 0.94 and r^2 between 0.81 and 1.04 for different vegetation biomes. Stannard (1993) found a slope of 1.09 and r^2 of 0.85 for model-estimated total evaporation against measurements using the EC method over sparse wildland vegetation. Anadranistakis *et al*. (2000) obtained a slope of 0.92, r^2 of 0.97 and *RMSE* of 0.48 mm for total evaporation measured using soil water profile measurements for maize, wheat and cotton fields. Kato *et al*. (2004) found a *RMSE* of 0.95 mm by comparing modelled and BREB-measured total evaporation over sparse sorghum. Ortega-Farias *et al*. (2007) also reported a slope of 0.71, r^2 of 0.71 and *RMSE* of 0.42 mm for total evaporation measured using an eddy covariance method over vine. The results achieved in this study are comparable to that reported in the literature.

The main advantage of the SW model is its ability to partition the total evaporation into soil and plant evaporation. The trend of the modelled daily soil and plant evaporation for the Jatropha trees is shown in Fig. 6.6. Although there is no independent data to verify this, the data make sense in that the soil evaporation was by far greater than the plant

transpiration when the trees were devoid of leaves and/or with small *LAI*. But as the foliage started to appear in the summer, the plant evaporation progressively increased to become slightly greater than the soil evaporation. With the maximum *LAI* and *LAD* that was observed during the study period, however, the trees were not wide and dense enough to prevent the solar irradiance from reaching the soil, and therefore the contribution of the soil towards the total evaporation was considerable. The soil evaporation is strongly dependent on surface wetness throughout the study period. The soil evaporation was obser ved to increase when the surface conditions were wet even during periods when the vegetation had acquired a considerable *LAI*. Of the total evaporation simulated throughout the study period, about 66% was attributed to soil evaporation. For a *LAI* ranging between 0 (no leaves) and approximately 1.4 m^2 m^{-2} during the year 2007, the simulated soil evaporation was about 84% of the total evaporation. For a *LAI* between 1.4 and 1.83 m^2 m^{-2} during the 2008 part of the study period, the simulated soil evaporation accounted for about 52% of the total evaporation while plant transpiration accounted for about 48%. These data demonstrate the importance of soil evaporation in sparse vegetation especially during a rainy season.

It should be kept in mind, though, that the modelled daily total evaporation were compared with those calculated as a residual of the shortened surface energy balance from measurements of net irradiance, soil heat flux and EC-sensible heat flux assuming that closure is met. A general lack of energy balance closure is prevalent in most vegetation types, with a mean imbalance in the order of 10 to 30% between measured values of the available energy flux (R_n - G) and the turbulent energy fluxes (H + λE) (e.g., Twine *et al*., 2000; Wilson *et al*., 2002; Barr *et al*., 2006; Oncley *et al*., 2007; Castellvi *et al*., 2008). Savage (2009) had compared H_{EC} against independent H measurements of MOST based surface layer scintillometry and found that the EC did not underestimate H. This gives confidence in calculating λE as a residual of the shortened energy balance equation. Uncertainties regarding to surface energy balance closure and EC underestimation of surface energy fluxes (H and λE) are discussed in Chapter 2, Section 2.1.5, 2.3; and Chapter 3, Section 3.4.2.

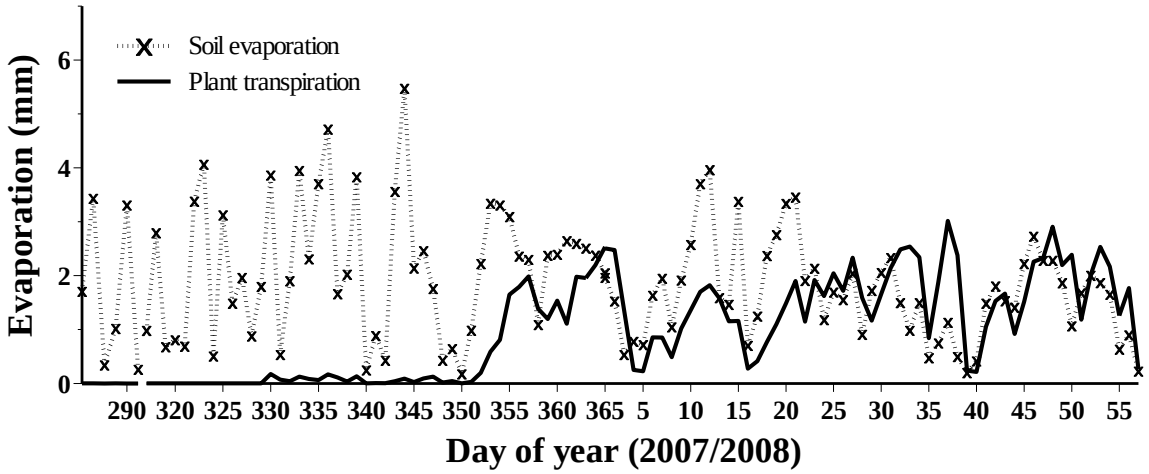

Fig. 6.6 The trend of SW-simulated soil (x) and plant (-) evaporation for doy 286 (2007) to 56 (2008)

6.5 CONCLUSIONS

This study investigated the ability of the Penman-Monteith (PM) equation and the Shuttleworth and Wallace (SW) model to estimate evaporation from sparse vegetation. The latent energy flux, and hence evaporation, estimated using the PM equation and the SW model were compared with those calculated as a residual of the shortened surface energy balance from measurements of net irradiance, soil heat flux and EC-measured sensible heat flux assuming that energy balance closure is met. The total evaporation from the SW model agreed very well with measurements for *LAI* ranging between 0 (no leaves) and 1.83 m^2 m^{-2}. Both, the measured and modelled total evaporation, were sensitive to the energy and amount of water available to the surface and the canopy structure. The PM equation significantly underestimated total evaporation during the stages when the trees had zero or small *LAI*. This was because the surface resistances employed in the PM equation did not account for the evaporation that arises from the soil. The SW model, on the other hand, accounted explicitly for the different resistances which enabled it to estimate and account for the evaporation from both the soil and plant components. This also enabled the SW model to estimate the soil evaporation and plant transpiration separately, and revealed that the soil was the sole contributor of evaporation during the stages when the trees had zero or small *LAI*, and that the contribution of evaporation from the soil and the plants was similar in the latter stages of the experiment as the soil was not fully covered by the trees. The difference in total evaporation between the PM equation and the SW model decreased during the latter stages of the experiment. This was because the SW model reflects the PM equation as the canopy starts to close. Therefore, these findings indicate that that the

conventional PM equation should be replaced by a multi-source model for long-term modelling of evaporation that accommodates changes in *LAI* with time. However, simple practical methods of specifying and determining the canopy and soil resistances, required in the SW model, need to be developed. The SW model can also be coupled, integrated or linked with a soil water balance and growth models to serve as a complete tree growth model.

For a better evaluation of the models, the model-estimations should be compared against more direct measurements of total evaporation. Furthermore, the partitioning of the total evaporation into the soil evaporation and plant transpiration should be validated through independent measurements, for example - microlysimetric and sap-flow methods respectively.

Acknowledgments

Profile soil water data from S Ghezehei is gratefully acknowledged.

7 ESTIMATING SENSIBLE HEAT FLUX FROM RADIOMETRIC TEMPERATURE OVER SPARSE TREE CROPS

ABSTRACT

Accurate determination of evaporation from land surfaces into the atmosphere is crucial for purposes of water resource management. This study estimated evaporation as a residual term of the shortened surface energy balance equation over sparse vegetation of *Jatropha curcas*, which requires accurate and precise measurement of the sensible heat flux (*H*). The *H* was estimated using (i) a two-layer Shuttleworth and Wallace model that was further developed to include remotely-sensed surface radiometric temperature measurements; (ii) a one-layer model, but with the excess resistance that arises due to the replacement of the aerodynamic temperature with a radiometric temperature estimated by linking the one- and two-layer models; and (iii) the two-layer Shuttleworth and Wallace model that does not require radiometric temperature measurements. A composite surface radiometric temperature input that is required in (i) and (ii) was represented by an area-weighting of soil and foliage surface radiometric temperatures. Independent simultaneous measurements of *H* were also made using a three-dimensional sonic anemometer. The agreement between estimated and measured *H*, using 10-min data, was in general good with root mean square errors (*RMSE*) (W m^{-2}) of 45.11, 43.77 and 39.86 for the three models respectively. The linear regressions that resulted from models (i) and (ii), by comparing the estimated and measured *H*, were similar with large underestimation at lower values and overestimation at higher values. The comparative results achieved from (iii) were better than those in (i) and (ii) for the 10-min data; but this was not translated into the daily data as all models appeared to have a tendency to underestimate *H*. This underestimation of *H* would result in overestimation of the latent energy flux, and hence evaporation, calculated as a residual of the shortened surface energy balance. The resulting *RMSE*s for the daily *H* data for the three models were (MJ m^{-2}) 1.16, 1.17 and 1.18 respectively. It appears that similar or better agreement between measured and estimated *H* can be obtained without the need for surface radiometric temperature measurements.

Keywords: one- and two-layer; modelling; sensible heat flux; radiometric surface temperature

7.1 INTRODUCTION

Knowledge of mass and energy exchange between the land surface and the atmosphere has important implications in water resource management and atmospheric circulation studies (Prueger and Kustas, 2005). The available energy at the surface-atmosphere interface is usually utilized, neglecting advected energy and physical and biochemical energy storage, in heating or cooling the surface convectively (sensible heat flux) and/or evaporating water from or condensing water to the surface (latent energy flux). Specification of these energy flux components is imperative for estimation of total evaporation from vegetation and soil surfaces. The latent energy flux, and thereby evaporation, from a surface could be determined, assuming that energy balance closure is met, as a residual term of the shortened surface energy balance equation arranged in the form:

$$\lambda E = R_n - G - H \tag{7.1}$$

where λ is the latent energy of vapourization (J kg^{-1}), E the water vapour flux density (kg s^{-1} m^{-2}), R_n the net irradiance (W m^{-2}), G the soil heat flux density (W m^{-2}) and H the sensible heat flux density (W m^{-2}). The R_n and G terms can either be independently measured or estimated from standard meteorological observations. But the logistics that are required for measuring or estimating H often make its determination very difficult. Therefore, the success of using the residual method for estimation of evaporation relies on how accurately and critically H is determined. To this end, remotely-sensed surface radiometric temperature measurements, along with measurements of weather variables and resistance parameters, have been widely used to infer H (e.g., Jackson *et al.*, 1985; Choudhury *et al.*, 1986; Huband and Monteith, 1986; Kustas *et al.*, 1989; Chehbouni *et al.*, 1997; Lhomme *et al.*, 1997; Troufleau *et al.*, 1997; Lhomme *et al.*, 2000).

Remotely-sensed surface radiometric temperature measurements are used in place of the aerodynamic surface temperature (air temperature at canopy source height) in the classical equation for estimating H from a homogeneous surface. Jackson *et al.* (1985) reported

good agreement between net irradiance measured using net radiometers and estimated with the use of thermal infrared thermometers over wheat fields of varying soil water content. But some studies showed that there could be large differences between the radiative and aerodynamic surface temperatures. This problem becomes critical when H has to be estimated using surface radiometric temperature measurements over sparse and heterogeneous canopies (Choudhury *et al*., 1986; Huband and Monteith, 1986) leading to erroneous, usually greater, estimation of H (Kustas *et al*., 1989; Stewart *et al*., 1989; Kalma and Jupp, 1990) for unstable conditions. This has led some researchers to conclude that the surface radiometric temperature measurements are not good enough to result in sufficiently accurate estimates of H (e.g., Hall *et al*., 1992).

Other workers introduced an excess resistance, r_r, that is added to the aerodynamic resistance and reported an improved agreement between modelled and measured H (e.g., Kustas *et al*., 1989; Chehbouni *et al*., 1997; Lhomme *et al*., 1997; Troufleau *et al*., 1997; Lhomme *et al*., 2000). This r_r arises due to the replacement of the aerodynamic temperature by the radiometric temperature and is parameterized as a function of a dimensionless factor kB^{-1}(where k is von Kármán constant and B^{-1} is dimensionless bulk parameter introduced by Owen and Thomson (1963) and used by Chamberlain (1968) and Thom (1972)). However, few of these studies agree on the value or a commonly accepted way of determining the 'radiometric' kB^{-1} (Troufleau *et al*., 1997). Kustas *et al*. (1989), in a study of surface energy balance of sparse vegetation in an arid climate, reported values of kB^{-1} ranging from 1 to 10. They also proposed parameterizing kB^{-1} as a function of wind speed at reference height, radiometric and air temperature as $u_z (T_r - T_a)$. Stewart *et al*. (1994) also reported values of kB^{-1} ranging from 3.4 to 12.4 for eight semi-arid sites and suggested that it may be possible to use an optimal value of kB^{-1} for arid and semi-arid areas. Lhomme *et al*. (1997) and Troufleau *et al*. (1997), however, showed that the 'radiometric' kB^{-1} was not constant for a given canopy but varied with the vegetation, surface resistances and meteorological conditions. This has led Lhomme *et al*. (1997) to suggest that the kB^{-1} parameter is not an appropriate tool to correctly estimate H from the surface radiometric temperature over sparse vegetation in an operational manner. Lhomme *et al*. (2000) also proposed a polynomial function for deriving a generic value of kB^{-1} as a function of LAI, for various view angle classes of infrared thermometers. The difficulty of determining the kB^{-1} parameter has led some workers to seek for a relation between the different temperatures involved in sparse vegetation (e.g., Chehbouni *et al*., 1997;

Troufleau *et al*., 1997) that would enable them to estimate *H* in sparse vegetation without the need for estimating kB^{-1}. But such procedures would have little application outside the time and site for which they were derived for.

The two-layer evaporation model of Shuttleworth and Wallace (hereafter called SW) (1985) has also been modified to accommodate surface radiometric temperature (e.g., Kustas, 1990; Lhomme *et al*., 1994a; Norman *et al*., 1995), and was applied for estimation of *H* over sparse crops. Lhomme *et al*. (1994a) assumed the surface radiometric temperature to be an area-weighted mean of the soil and foliage temperatures. This allowed them to estimate *H* as a function of the difference between the radiometric and air temperature as corrected by temperature difference between the soil and foliage surfaces. Similarly, Norman *et al*. (1995) also estimated *H* as a function of the difference between the radiometric and air temperature. But the correction factor involved calculation of the soil and foliage temperature from radiometric temperature measured at two different view angles along with resistance parameters. Lhomme *et al*. (1994a) also used provisions for estimation of the aerodynamic temperature as illustrated by Shuttleworth and Gurney (1990) to estimate *H* from separate surface temperature measurements involved. Furthermore, Lhomme *et al*. (1997) linked the one- and two-layer models to arrive at a method for estimating kB^{-1} from weather variables and resistance parameters for use in the one-layer model formulation.

This work investigates the use of a one-dimensional two-layer SW evaporation model, originally developed by Shuttleworth and Wallace (1985) and later modified by Lhomme *et al*. (1994a) to accommodate surface radiometric temperature, for estimation of *H* over sparse vegetation of *Jatropha curcus*. The use of a one-layer model in estimating *H* is also investigated, with the r_r estimated by linking a one-layer and two-layer component models (Lhomme *et al*., 1997). An additional objective of this study is to estimate *H* using the two-layer SW evaporation model without the need for surface radiometric temperature measurements. The model-estimated *H* was evaluated against *H* obtained using eddy covariance.

7.2 THEORY

7.2.1 The two-layer SW model approach

In sparse vegetation represented by the two-layer SW model proposed by Shuttleworth and Wallace (1985) (Fig. 7.1), the sensible heat flux for the soil (H_s), vegetation (H_c) and the whole canopy (H) are, respectively, given by:

$$H_s = \rho c_p \left(T_s - T_o\right) / R_a^s \tag{7.2}$$

$$H_c = \rho c_p \left(T_c - T_o\right) / R_a^c \tag{7.3}$$

$$H = \rho c_p \left(T_o - T_z\right) / R_a^a \tag{7.4}$$

where the subscripts *s* and *c* refer to the soil and vegetation canopy respectively, the subscripts *o* and *z* refer to canopy source and reference (screen) heights respectively, ρ the air density (1.14 kg m^{-3}), c_p the specific heat capacity of air at constant pressure (1011 J kg^{-1} K^{-1}), T the temperature (^{o}C), R_a^s (s m^{-1}) the aerodynamic resistance between the soil and canopy source height, R_a^c (s m^{-1}) the bulk boundary layer resistance of the vegetative component and R_a^a (s m^{-1}) the aerodynamic resistance between canopy source height and height *z*.

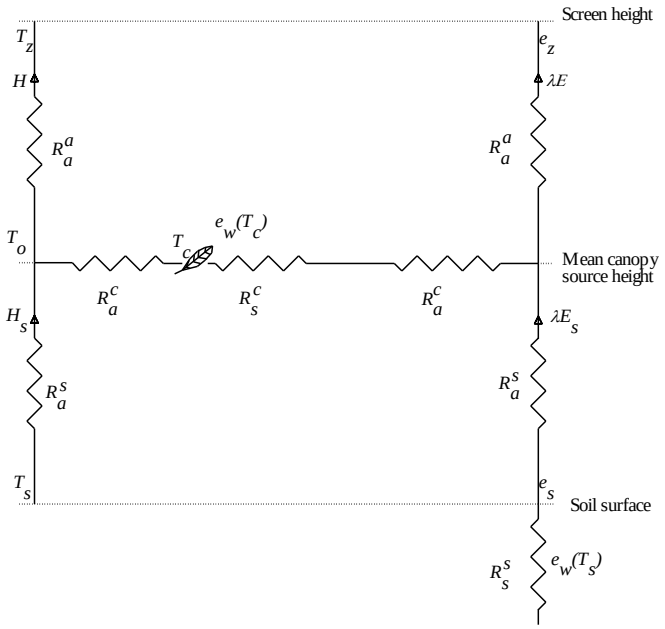

Fig. 7.1 Schematic diagram of resistances and fluxes in the two-layer evaporation model of Shuttleworth and Wallace (1985)

Lhomme *et al*. (1994a), by adding Eqs (7.2) and (7.3) together, derived an expression for H as follows:

$$H = \rho c_p \left(T_e - T_o\right) / r_e \tag{7.5}$$

where T_e, the resistance-weighted temperature of each layer, and r_e, the equivalent resistance, are respectively defined as $T_e = \frac{R_a^c T_s + R_a^s T_c}{R_a^c + R_a^s}$ and $r_e = \frac{R_a^c R_a^s}{R_a^c + R_a^s}$.

Lhomme *et al*. (1994a) also combined Eqs (7.4) and (7.5) to determine H from soil and foliage surface temperatures represented by a two-layer model:

$$H = \frac{\rho c_p \left(T_e - T_z\right)}{R_a^a + r_e} \tag{7.6}$$

If surface radiometric temperature measurements were made separately for the soil and foliage components, then Eq. (7.6) might be used to determine the total H. But more often a single surface radiometric temperature measurement, T_r, made from vertically above the surface, is used. In such instances T_r is considered to be the area-weighted mean of the soil and foliage temperatures (Choudhury, 1989; Kalma and Jupp, 1990). Assuming a_c represents the fractional area of the soil surface covered by foliage, T_r is given by:

$$T_r = \left(1 - a_c\right) T_s + a_c T_c \tag{7.7}$$

Lhomme *et al*. (1994a), realizing that T_e in Eq. (7.6) cannot be directly measured from T_r, developed a relationship between T_r and T_e using the definitions of both terms:

$$T_e - T_r = -c\left(T_s - T_c\right) \tag{7.8}$$

where $c = \frac{R_a^s}{R_a^s + R_a^c} - a_c$

Hence the H in Eq. (7.6) can finally be written as:

$$H = \rho c_p \left[\left(T_r - T_z \right) - c(T_s - T_c) \right] / \left(R_a^a + r_e \right) \tag{7.9}$$

Shuttleworth and Gurney (1990) also derived an expression for T_o from the soil, foliage and air temperatures, and their corresponding resistances:

$$T_o = \frac{T_z g_a^a + T_s g_a^s + T_c g_a^c}{g_a^a + g_a^s + g_a^c} \tag{7.10}$$

where g (m s^{-1}) is the for conductance, reciprocal of resistance, and the superscripts and subscripts assume their original definitions. Eq. (7.10) can be used in place of T_o in Eq. (7.4) to determine the total H. The derivation of these equations is detailed in Appendices A and B.

7.2.2 Linking the one-layer and two-layer approaches

The formulations and derivations in this section are mainly taken from Lhomme *et al.* (1997). Details of the derivation are presented in the Appendix C. The total H can be expressed as a function of surface radiometric temperature using the classical one-layer Ohm's law type formulation as follows:

$$H = \rho c_p \left(T_r - T_z \right) / \left(R_a^a + r_r \right) \tag{7.11}$$

where r_r is the excess resistance that is introduced due to the replacement of the aerodynamic temperature, T_o, with the radiometric temperature, T_r. Combining Eqs (7.9) and (7.11), and considering the definition of T_r from Eq. (7.7), r_r can be expressed as:

$$r_r = \frac{B^{-1}}{u_*} = \frac{r_e + R_a^a c \big/ \left(q - a_c \right)}{1 - c \big/ \left(q - a_c \right)}, \text{defining } q = \left(T_s - T_z \big/ T_s - T_c \right) \tag{7.12}$$

where u_* (m s^{-1}) is the friction velocity. Applying the energy balance equation to the substrate and foliage layers and the whole canopy, and linearising the saturated water

vapour pressure curve between the soil surface and mean canopy height, and the foliage elements and mean canopy height respectively leads to:

$$\begin{aligned} T_s - T_o &= \omega_s \left[\left(R_a^s + R_s^s \right) \left(A_s / \rho c_p \right) - D_o / \gamma \right] \\ T_c - T_o &= \omega_f \left[\left(R_a^c + R_s^c \right) \left(\left(A - A_s \right) / \rho c_p \right) - D_o / \gamma \right] \end{aligned} \tag{7.13}$$

with

$$\omega_s = \left[1 + \frac{\Delta}{\gamma} + \frac{R_s^s}{R_a^s} \right]^{-1} \text{ and } \omega_f = \left[1 + \frac{\Delta}{\gamma} + \frac{R_s^c}{R_a^c} \right]^{-1} \tag{7.14}$$

where A_s, A_c and A are the available energy fluxes at the substrate and foliage layers and the whole canopy respectively, D_o the water vapour pressure deficit at mean canopy source height, γ the psychrometeric constant and Δ the slope of the saturation vapour pressure function of – T_s and T_o for ω_s, and T_c and T_o for ω_f. Combining the expression for $T_s - T_o$ from Eq. (7.13) and for $T_o - T_z$ from Eq. (7.4) leads to:

$$T_s - T_z = \omega_s \left[\left(R_a^s + R_s^s \right) \frac{A_s}{\rho c_p} - \frac{D_o}{\gamma} \right] + \left(A - \lambda E \right) \frac{R_a^a}{\rho c_p} \tag{7.15}$$

Subtracting the expression for $T_c - T_o$ from $T_s - T_o$ in Eq. (7.13) results in:

$$T_s - T_c = \omega_s \left(R_a^s + R_s^s \right) \frac{A_s}{\rho c_p} - \omega_f \left(R_a^c + R_s^c \right) \frac{A - A_s}{\rho c_p} - \frac{D_o}{\gamma} \left(\omega_s - \omega_f \right) \tag{7.16}$$

These expressions can aid in estimating the total H and/or its components. The expressions for $T_s - T_o$ and $T_c - T_o$ in Eq. (7.13) can be used in Eqs (7.2) and (7.3) to estimate H_s and H_c respectively, and thereby the total H. Eqs (7.15) and (7.16) can also be used to estimate r_r which can then be used in Eq. (7.11) to estimate the total H. But all of these expressions require D_o and λE which themselves are difficult to estimate. Eqs (7.15) and (7.16) can further be manipulated to eliminate D_o and λE to yield equations that involve weather variables and elementary resistance parameters only in the form of:

$$T_s - T_z = \nu_1\left(\frac{AR_a^a}{\rho c_p}\right) + \nu_2\left(\frac{A_s R_a^a}{\rho c_p}\right) + \nu_3\left(\frac{D}{\gamma}\right) \tag{7.17}$$

$$\text{where } \nu_1 = \left(1 - \frac{\Delta}{\gamma}\omega_s + \Delta\left(C_c\phi_c + \frac{C_s\phi_s R_a^a}{R_a^a + R_a^s}\right)\right)\left(\omega_s\left(1 + \frac{\Delta}{\gamma}\right) - 1\right)$$

$$\nu_2 = \Delta\left(\frac{C_c\phi_c R_a^s}{R_a^a + R_a^s} - \frac{C_s\phi_s R_a^c}{R_a^a + R_a^c}\right)\left(\omega_s\left(1 + \frac{\Delta}{\gamma}\right) - 1\right) + \omega_s\left(\frac{R_a^s + R_s^s}{R_a^a}\right) \tag{7.18}$$

$$\nu_3 = \gamma\left(\frac{C_c\phi_c}{R_a^a + R_a^c} + \frac{C_s\phi_s}{R_a^a + R_a^s}\right)\left(\omega_s\left(1 + \frac{\Delta}{\gamma}\right) - 1\right)R_a^a - \omega_s$$

$$T_s - T_c = \delta_1\left(\frac{AR_a^a}{\rho c_p}\right) + \delta_2\left(\frac{A_s R_a^a}{\rho c_p}\right) + \delta_3\left(\frac{D}{\gamma}\right) \tag{7.19}$$

$$\text{where } \delta_1 = \left(\omega_f - \omega_s\right)\left(\frac{\Delta}{\gamma} - \Delta\left(1 + \frac{\Delta}{\gamma}\right)\left(C_c\phi_c - \frac{C_s\phi_s R_a^a}{R_a^a + R_a^s}\right)\right) - \omega_f\left(\frac{R_a^c + R_s^c}{R_a^a}\right)$$

$$\delta_2 = \omega_s\frac{R_a^s + R_s^s}{R_a^a} + \omega_f\frac{R_a^c + R_s^c}{R_a^a} + \Delta\left(1 + \frac{\Delta}{\gamma}\right)\left(\omega_f - \omega_s\right)\left(\frac{C_c\phi_c R_a^c}{R_a^a + R_a^c} - \frac{C_s\phi_s R_a^s}{R_a^a + R_a^s}\right) \tag{7.20}$$

$$\delta_3 = \left(\omega_f - \omega_s\right)\left(1 - \left(\gamma + \Delta\right)R_a^a\left(\frac{C_c\phi_c}{R_a^a + R_a^c} + \frac{C_s\phi_s}{R_a^a + R_a^s}\right)\right)$$

with C_s and C_c defined as:

$$C_s = \left[1 + \frac{R_s R_a}{R_c(R_s + R_a)}\right]^{-1}, \text{ and } C_c = \left[1 + \frac{R_c R_a}{R_s(R_c + R_a)}\right]^{-1} \tag{7.21}$$

$$\text{where } \quad R_s = \left(\Delta + \gamma\right)R_a^s + \gamma R_s^s,\ R_c = \left(\Delta + \gamma\right)R_a^c + \gamma R_s^c, \text{ and } R_a = \left(\Delta + \gamma\right)R_a^a \tag{7.22}$$

ϕ_s and ϕ_c also defined as:

$$\phi_s = \left[\Delta + \gamma\left(1 + \frac{R_s^s}{R_a^a + R_a^s}\right)\right]^{-1}, \text{ and } \phi_c = \left[\Delta + \gamma\left(1 + \frac{R_s^c}{R_a^a + R_a^c}\right)\right]^{-1} \tag{7.23}$$

7.2.3 Resistance parameters

The SW model requires two aerodynamic resistances: between the substrate and the mean canopy height, R_a^s, and between the mean canopy height and reference height, R_a^a. These are basically derived from the eddy diffusivity resistance above and within the canopy. Assuming that the air flow within sparse canopies is adequately described by the *K*-theory, the eddy diffusion coefficient, *K* (m^2 s^{-1}), at a height *z* above the canopy can be described as (Thom, 1971; Dolman and Wallace, 1991):

$$K = ku_*(z-d), \quad (z > h) \tag{7.24}$$

where *k* is von Kármán constant (0.41), *d* the displacement height of the vegetation given as 0.56*h* for sparse vegetation and *h* the crop height. It is also assumed that *K* decreases exponentially with height (Thom, 1971), thus:

$$K = K_h \exp\left(-n\left(1-{}^{z}\!/_{h}\right)\right), \quad (z < h) \tag{7.25}$$

where K_h is the value of *K* at the top of the crop, ku_* (*h* - *d*), and *n* the eddy diffusivity decay constant for a closed canopy assumed to be 2.5. Both R_a^a and R_a^s are then integrated from the reciprocal of the eddy diffusion coefficient and the decay of the eddy diffusion coefficient equations, over the heights zero to $d + z_o$ and $d + z_o$ to *h* respectively as (Shuttleworth and Gurney, 1990):

$$R_a^s = \frac{h\exp(n)}{nK_h}\left[\exp(-nz_o'/h) - \exp\left(-n(z_o+d)/h\right)\right] \tag{7.26}$$

$$R_a^a = \frac{1}{ku_*}\ln\left(\frac{z-d}{h-d}\right) + \frac{h}{nK_h}\left[\exp\left\{n\left(1-\frac{z_o+d}{h}\right)\right\} - 1\right] \tag{7.27}$$

where z_o' and z_o are the roughness length of the canopy (0.1*h*) and the soil (0.01 m) respectively.

Assuming the leaf area index (*LAI*) is uniformly distributed with height and the eddy diffusion of momentum and energy is similar throughout the canopy, the bulk boundary layer resistance, R_a^c, is calculated by integrating the leaf boundary layer conductance over the canopy height (Choudhury and Monteith, 1988; Shuttleworth and Gurney, 1990; Lhomme *et al*., 1994a, b, 1997):

$$R_a^c = \frac{2.5 \cdot \left(w_l / u_h \right)^{0.5}}{4 \cdot LAI \cdot 0.005 \cdot \left(1 - \exp(-n/2) \right)} \tag{7.28}$$

where w_l is the leaf width and u_h the wind speed at the top of the crop canopy.

The canopy resistance, in soil-plant-atmosphere models, is commonly empirically related to independent environmental conditions that are known to affect stomatal opening. Jarvis (1976) proposed a multi-variate multiplicative model that relates the response of stomatal conductance, g_s, to important meteorological variables at the leaf scale and the available soil water. The general Jarvis-type relation can be expressed as follows:

$$g_s = g_{\max} f_1(\delta q) f_2(I_s) f_3(T) f_4(\delta\theta) \tag{7.29}$$

where g_{max} (m s^{-1}) is the maximum stomatal conductance under non-limiting conditions and $f_1(\delta q)$, $f_2(I_s)$, $f_3(T)$ and $f_4(\delta\theta)$ are functions of specific humidity deficit (g kg^{-1}), solar irradiance (W m^{-2}), air temperature (^oC), and soil water deficit (mm) respectively. The response functions, $f(i)$ where i represents a potentially limiting factor, vary between 0 and 1. The stomatal conductance, g_s, takes the value of the g_{max} as long as the environmental conditions are at their optimum, in which case each individual response function, $f(i)$, becomes unity. But g_s starts to decline when these conditions fall below optimal, in which case the $f(i)$ assume values less than unity which is then multiplied by g_{max} resulting in g_s less than g_{max}. Following Stewart (1988) and Dolman *et al*. (1991), the individual limiting response functions are given by:

$$
\begin{aligned}
f_1(\delta q) &= \exp(-a_1 \delta q) \\
f_2(I_s) &= \frac{I_s/(a_2 + I_s)}{1100/(1100 + a_2)} \\
f_3(T) &= \frac{(T - T_l)(T_h - T)^t}{(a_3 - T_l)(T_h - a_3)^t} \\
f_4(\delta\theta) &= \min\left\{(\theta - \theta_w)/(\theta_c - \theta_w), 1\right\}
\end{aligned}
\tag{7.30}
$$

where I_s = 1100 W m^{-2} corresponds to $f_1(I_s) = 1$, $t = (T_h - a_3)/(a_3 - T_l)$, T_l (°C) and T_h (°C) are the lower and upper air temperature limits for transpiration respectively, taken as 0 and 40 °C, a_1, a_2 and a_3 are parameters that are derived by non-linear optimization. The wilting (θ_w) and critical (θ_c) soil water contents are taken as 340 and 250 mm respectively. For the purpose of this work, g_s was calculated by inverting the Penman-Monteith (hereafter called PM) equation (Penman, 1965) following a day after rain had occurred when the *LAI* was at its maximum. Non-linear optimization was then used to derive the model parameters, and the resulting values of the optimization are presented in Table 7.1. The stomatal resistance was then calculated as a reciprocal of the stomatal conductance, and up-scaled to canopy resistance following Shuttleworth and Wallace (1985) as follows:

$$R_s^c = r_s / 2LAI \tag{7.31}$$

Soil resistance is also one of the parameters that are explicitly presented in two-layer models. Numerous formulations have been proposed in the literature that attempt to relate volumetric soil water content to soil resistance. The soil resistance was determined by inverting the PM equation for a time period when the plots were bare or with minimal *LAI*. This was then used to derive parameter values for surface soil resistance for several equations that were deduced from the literature and summarized by Farahani and Ahuja (1996). However, the existing parameters from the literature appeared to yield a better agreement between the simulated and measured (as a residual of the shortened energy balance) latent energy flux based on slope, coefficient of determination (r^2) and root mean square error (*RMSE*) than the newly derived parameters, and were used for further simulation. For the purpose of this study, a better result was achieved from a functional soil resistance formulae that was applied by Farahani and Bausch (1995) as follows:

Table 7.1 Optimized parameter values of the Jarvis-type surface conductance model

g_{max} (m s^{-1})	a_1	a_2	a_3
26.04 ± 3.33	60 ± 18	1483 ± 959	23.14 ± 3.39

$$R_s^s = 39\left(\theta / \theta_s\right)^{-2.59} \tag{7.32}$$

where θ and θ_s are the actual and saturated water contents respectively.

7.2.4 Net irradiance: above and below the canopy

Net irradiance above the canopy was estimated from solar irradiance measurements according to Doorenbos and Pruitt (1992). The corresponding soil heat flux was estimated from the resulting net irradiance as 20% and 10% during bright and cloudy days respectively. The available energy flux below the canopy was determined from a relatively simple three- dimensional tree-canopy radiation interception model based on the works of Charles-Edwards and Thornley (1973) which considers the earth-sun relationship, the geometry of the plant canopy, planting pattern, row orientation and solar irradiance transfer equations (see Chapter 5). The model assumes that trees are elliptical in shape with a uniform leaf distribution, and that solar irradiance attenuation within the canopy follows Beer's law. As solar irradiance can be obstructed by neighbouring trees, the model considers several trees around the tree of interest. The model divides the ground below the canopy into 0.5 m squares and determines the solar irradiance transmitted to each area by calculating the path length traversed through the tree canopy to reach a point within the area at a particular time. It also makes use of inputs of geographic location, altitude, row orientation, row and tree spacing, canopy size, leaf area density and solar irradiance. The transmitted irradiance is then used to further estimate the net irradiance and soil heat flux received at the soil surface for each square according to the method of Doorenbos and Pruitt (1992). The soil and plant available energy values were then used as input to the SW model that was modified to accommodate surface radiometric temperature in order to estimate the sensible heat flux for each square and then averaged over the entire plot.

7.3 MATERIALS AND METHODS

The experiment was conducted over stands of *J. curcas* in a 50 m × 60 m plot at Ukulinga (29°40′11″S, 30°24′50″E and 781 masl), Pietermaritzburg, KwaZulu-Natal, South Africa. The trees were about two and half years old at the start of the experiment with tree height, *h*, on average ranging from 1 to 1.85 m during the experiment. The trees were planted in 3 m × 3 m row and tree spacing. The area between trees was weeded and kept devoid of vegetation. The study comprised data from late spring when the trees had no leaves (*LAI* = 0 m^2 m^{-2}) to summer when the trees attained a considerable *LAI* (1.52 m^2 m^{-2}).

Soil and foliage surface temperatures were measured using two nadir-looking infrared thermometers (IRTs) (Model 4000 BL, Everest Interscience Inc., Tucson, AZ), with a 4° field of view. One IRT was mounted 1 m directly above bare soil covering a diameter of about 0.10 m on the ground, and the second was placed directly above a tree facing the foliage. The height of the second IRT was kept at about 0.5 m above the highest leaf on the tree, covering a diameter of about 0.07 m. A composite temperature was then computed on the basis of the weight of the percent cover of the soil and foliage components. To prevent shading of the surface of interest, both IRTs were mounted on an arm extending towards the north direction (in Southern Hemisphere) from a stand. The IRTs were calibrated according to the method detailed in Savage and Heilman (2009). The emissivity of both the soil and foliage was assumed to be one. A 21X datalogger (Campbell Scientific Inc., Logan, UT) was used to sample measurements every 10 s and log averages every 10 minutes.

Sensible heat flux was determined using a three-dimensional sonic anemometer (Model 81000, RM Young, Traverse City, MI) mounted at 2.3 m above the ground from measurements of vertical wind speed and virtual temperature. The measurements were done differentially at 10 Hz frequency and the data were logged every 2 and 30 min using a Campbell CR5000 datalogger.

Net radiometers and soil heat flux plates were set up to measure the available energy flux. One net radiometer (NR LITE, Kipp and Zonen, Delft, The Netherlands) was placed 3 m from the ground directly above and facing the trees, and a second net radiometer (model Q*7.1, REBS, Seattle, WA) was placed 3 m from the ground directly above the space

between the trees facing the bare soil. The average net irradiance was then used for computation of the available energy.

A pair of soil heat flux plates (HFT-S, REBS, Seattle, WA) were buried 80 mm below the soil surface, with one of them placed directly below a tree and the other one between trees, were used to determine the soil heat flux. The soil heat stored above the soil heat flux plates was accounted for by using a system of parallel thermocouples (type E) that were placed above the plates at depths of 20 and 60 mm from the surface. The soil heat flux at the soil surface was then determined by adding the stored heat at 20 and 60 mm above the plates to the soil heat flux measured by the plates at the 80 mm depth (Tanner, 1960). A Campbell CS615 time domain reflectometer (TDR) was also used to measure the volumetric soil water content in the upper 60 mm. All measurements were sampled every 10 s and averaged every 10 minutes using a Campbell CR23X datalogger (Campbell Scientific Inc., Logan, UT). Soil water content was also measured to a depth of 1000 mm using CS100 TDRs from the surface at 200 mm intervals. Measurements were sampled every 1 min and then averages logged every 60 min using a Campbell CR1000 datalogger.

Standard automatic weather station measurements were also made at about 10 m away from the edge of the Jatropha plot. Measurements of solar irradiance (LI-200 pyranometer), air temperature and relative humidity (CS500 Vaisala), wind speed and direction (Model 03001, RM Young) and rainfall (TE525MM tipping bucket rain gauge, Texas Electronics Inc., Dallas, TX) were obtained. A Campbell CR10X datalogger was used to sample measurements every 10 s and log averages every 10 min.

Measurements of *LAI* were conducted on a bimonthly basis, using an LAI-2000 canopy analyzer (Li-Cor, Lincoln, NE). Measurements were made along diagonal transects between tree rows using a 45^{o} view cap with four replications. Leaf area density (*LAD*) was also measured using an LAI-2000 canopy analyzer. This involved making *LAI* measurements using a 90^{o} view cap by placing the sensor next to the tree trunk in all four quadrants of the tree. The canopy shape and volume for each quadrant were estimated from a vertical and horizontal coordinate system using points at the boundary of the canopy. The *LAD* was then estimated from *LAI*, canopy shape and volume measurements. All *LAI* and *LAD* measurements were conducted when the sky conditions were completely overcast.

The foliage canopy diameters along the x- and y-axes were also used to determine the foliage area coverage (a_c), and thereby soil area coverage (a_s).

All data were recomputed to 10 min averages to serve as model inputs. The outputs from the 10-min averages were also aggregated into daily totals to serve for model validation purposes.

7.4 RESULTS AND DISCUSSION

7.4.1 *H* estimated using surface radiometric temperatures

7.4.1.1 The two-layer SW model

In this section Eqs (7.4), (7.6) and (7.9) were used to determine the total *H*. The model outputs from Eqs (7.4) and (7.6) were a carbon copy of each other; and they were also found to be very close to 10-min model-outputs achieved from Eq. (7.9) with slightly greater values, especially for higher values of *H*, and slightly smaller values for lower values of *H*. The discrepancies between the two model-outputs were hardly noticeable when the 10-min outputs were aggregated into daily values. This should be expected as the second equation was derived using the first equation, and then the resulting equation was used to derive the third equation. Therefore, considering that the outputs were similar, only a single result representing the two-layer SW models will be discussed.

The modelled and measured daily total *H* along with the rainfall that occurred during the study period is given in Fig. 7.2. The model estimates appeared to be good for the first few days when the surface was devoid of vegetation but then underestimated for most of the rest of the study period, with a few overestimations. Lhomme *et al*. (1994a, b) presented scatter-plot graphs to depict the agreement between 20-min modelled and measured *H* values but did not give such trends. From their graphs, it was evident that the agreement was better when the *LAI* was small, becoming more scattered as *LAI* increased. The agreement between the modelled and measured 10-min and daily *H* values along with some statistics for this study is given in Fig. 7.3(a) and (b) respectively. Also given in the graphs are the one-to-one line and the best linear-fit (broken lines). In Fig. 7.3(a) the scatter of the points appear to be large, especially for small and large values of *H*, but the

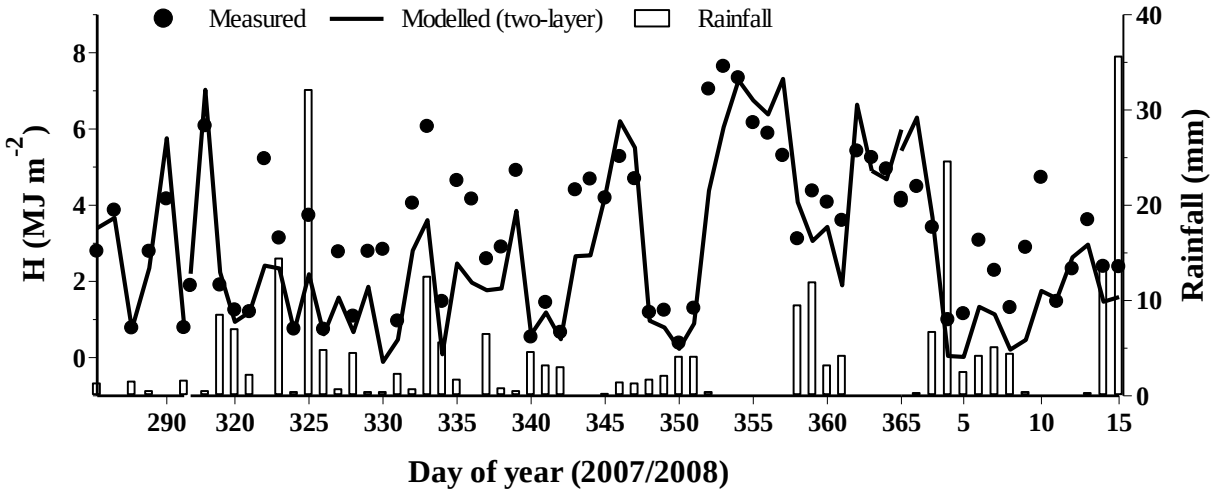

Fig. 7.2 The modelled and EC-measured (with two-layer model using radiometric temperature) daily *H* along with rainfall during the study period

under- and over-estimation seem to cancel out each other which is reflected in a good slope (0.95). But the large scatter also resulted in a rather small r^2 (0.71). Lhomme *et al*. (1994a) found the slope resulting from the modelled and measured *H* for the sparse millet site to be 1, 0.84 and 0.83 for three stages during the growing season respectively. They also found the r^2 to be 0.69, 0.63 and 0.51 for the same site during the three growing season stages. Lhomme *et al*. (1994a, b) also reported a *RMSE* of, on average, about 52 W m^{-2} and 59 W m^{-2} for measurements conducted over fallow savannah and millet respectively. In this study, a *RMSE* of about 45 W m^{-2} was achieved but for more data points and smaller time scale than has been used in Lhomme *et al*. (1994a, b). Based on the statistics achieved, it can be concluded that the two-layer SW model estimated *H* reasonably well. It should be noted that the underestimation of *H* would have the opposite effect on evaporation calculated as a residual of the shortened surface energy balance.

The total *H* that is calculated by Eq. (7.9) is determined mainly by T_r - T_z and then corrected by T_s - T_c according to Lhomme *et al*. (1994a). But further manipulation of Eq. (7.9) reveals that the fractional foliage cover does not have any bearing on the determination of total *H*. No matter what value (between 0 and 1) of this fractional cover is used, the resulting total *H* remains the same for a given input. This is because the fractional foliage cover would eventually cancel out in the equation. Replacing the expressions for T_r from Eq. (7.7) and for *c* from Eq. (7.8) in Eq. (7.9) leads to:

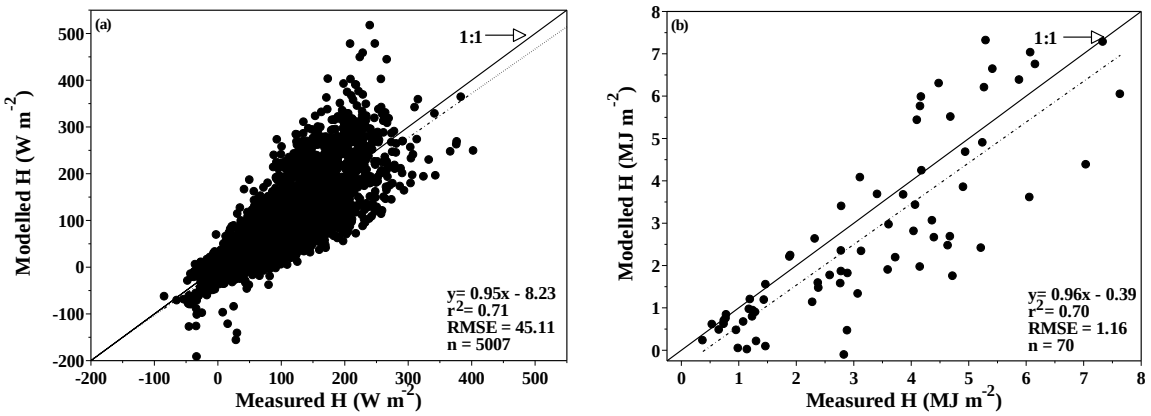

Fig. 7.3 The agreement, for the period of day of year (doy) 260 (2007) to 15 (2008), between modelled and EC-measured (using two-layer models) *H* values along with a one-to-one line and relevant statistics (a) 10 minutes, and (b) daily

$$
\begin{aligned}
H &= \rho c_p \left[\left(a_c T_c + a_s T_s - T_z \right) - \left(\left(\frac{R_a^s}{R_a^s + R_a^c} - a_c \right) (T_s - T_c) \right) \right] / \left(R_a^a + r_e \right) \\
H &= \rho c_p \left[\left(a_c T_c + a_s T_s - T_z \right) - \left(\frac{T_s R_a^s}{R_a^s + R_a^c} - a_c T_s - \frac{T_c R_a^s}{R_a^s + R_a^c} + a_c T_c \right) \right] / \left(R_a^a + r_e \right) \\
H &= \rho c_p \left[\cancel{a_c T_c} + \cancel{a_s T_s} - T_z - \frac{T_s R_a^s}{R_a^s + R_a^c} + T_s - \cancel{a_s T_s} + \frac{T_c R_a^s}{R_a^s + R_a^c} - \cancel{a_c T_c} \right] / \left(R_a^a + r_e \right) \\
H &= \rho c_p \left[T_s - T_z - \frac{R_a^s}{R_a^s + R_a^c} \left(T_s - T_c \right) \right] / \left(R_a^a + r_e \right)
\end{aligned}
\tag{7.33}
$$

where $a_s = 1 - a_c$

From this it is evident that the total *H* is mainly determined by T_s - T_z and corrected by T_s - T_c.

A closer examination in trend of the daily total *H* reveals that, for most of the time, the measured was greater than the modelled *H*. This was because of a lag that is created in heating and cooling the soil surface. The soil surface heats up slowly following an increase in net irradiance especially following rainy days compared to the air temperature, resulting in a smaller modelled *H* than measured. It should be noted that rainfall was abundant during most of the study period (Fig. 7.2). In such instances, T_s - T_z was not large enough to result in an *H* that matched the measured. The soil surface also cools slowly following a decrease in net irradiance and/or the occurrence of rain compared to air temperature following a dry spell, resulting in a larger difference between T_s and T_z and hence a

modelled *H* greater than the measured *H*. This explains why the modelled *H* was smaller sometimes than the measured *H* and vice versa.

7.4.1.2 Linked one- and two-layer models and excess resistance

The total *H* and its component parts were also estimated by linking a one-layer and two-layer models. The two-layer model also involved the estimation of radiation interception, and thereby the net irradiance; above and below the vegetation canopy from measurements of solar irradiance and structural attributes of the canopy. Eq. (7.11) was used with the excess resistance, r_r, a term estimated either from Eqs (7.15) and (7.16) or Eqs (7.17) and (7.19) (Lhomme *et al*., 1997). The derivations are detailed in Appendix C. Eqs (7.15) and (7.16) require D_o and λE as a prerequisite, but could further be manipulated to eliminate the D_o and λE terms to arrive at Eqs (7.17) and (7.19) which involve climatic variables and resistance parameters only. The outputs from using both sets of equations for estimating *H* were similar, but the latter set would be preferred to the former as it does not involve the D_o and λE terms.

Graphical presentation of the modelled and measured 10-min *H* values resulting from Eq. (7.11) are given in Fig. 7.4(a). The results achieved from this model were very similar to those achieved from using a composite radiometric temperature in the two-layer models in Section 7.4.1.1, which did not involve the radiation interception module. The slight difference between the outputs from the two models can better be detected by comparing

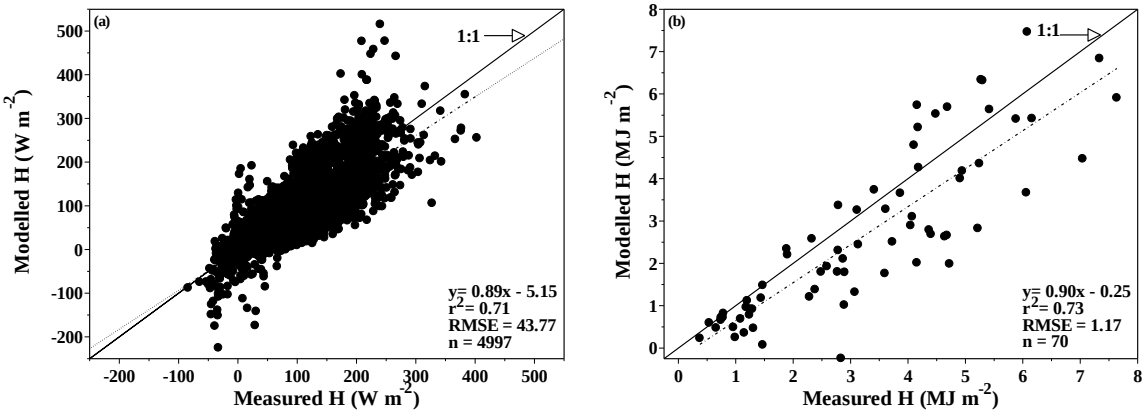

Fig. 7. 4 The agreement, for the period of day of year (doy) 260 (2007) to 15 (2008), between modelled and EC-measured (using Eq. (7.11)) *H* values along with a one-to-one graph and resulting statistics. (a) 10 minutes, and (b) daily

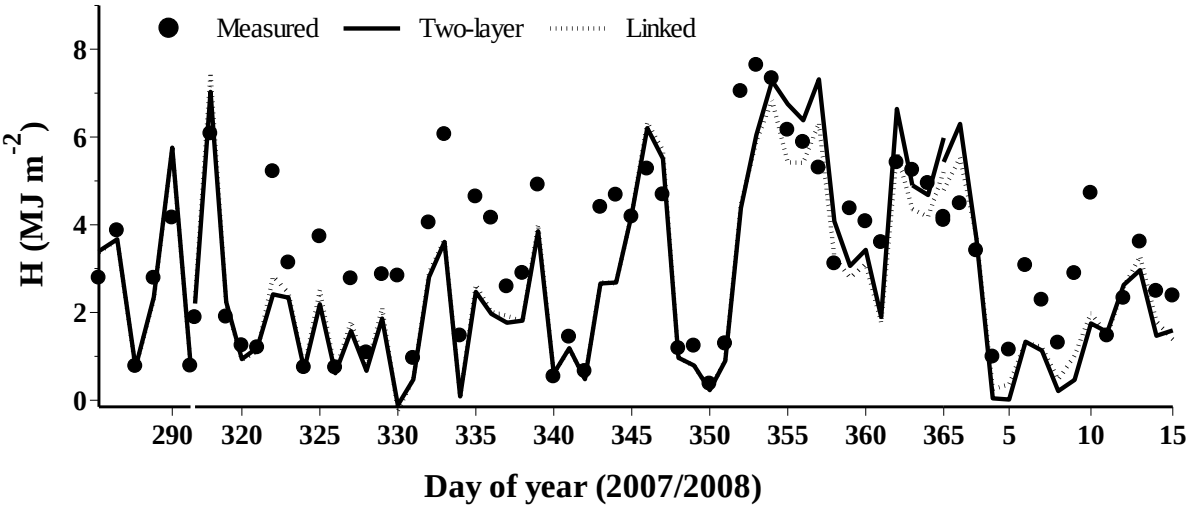

Fig. 7.5 The trend of modelled and EC-measured (solid line for the two-layer model that included surface radiometric temperature and broken lines for the linked model) daily *H* during the study period

the daily scatter-plots (Figs 7.3(b) and 7.4(b)) and trends (Fig. 7.5) of both. The model used here was relatively more complex as it involved the radiation interception module and estimation of the extra resistance in the form of r_r. Despite the complexities in this model, the improvement achieved in terms of agreement between modelled and measured *H* was small. But still the agreement is good, especially compared to similar work done by Lhomme *et al*. (1997) over a fallow savannah who reported a *RMSE* of 81 W m^{-2}, although they made a number of assumptions towards the estimation of *H*.

7.4.2 *H* estimated without using surface radiometric temperature measurement

The two-layer SW model used here also involved the estimation of radiation interception, and thereby the net irradiance; above and below the vegetation. In this section, T_s - T_o and T_c - T_o were calculated from the two-layer SW model as in Eq. (7.13) and then used in Eqs (7.2) and (7.3) to estimate the *H* arising from the soil and vegetation layers, without the need for having surface radiometric temperature measurements, respectively (Lhomme *et al*., 1997). The *H* from both the soil and foliage were then summed to give the total *H*. Comparison of the modelled and measured 10-min *H* values is given in Fig. 7.6(a). The agreement is good especially compared to the models in Section 7.4.1. Although underestimation of lower and higher values of *H* was common, the scatter-plots were more compact with no outliers as was witnessed in Section 7.4.1, and the *RMSE* (40 W m^{-2}) achieved is less than what was achieved from the models in Section 7.4.1. But when these

values were aggregated to daily values, the model tended to underestimate and did not preserve the improved statistics that it showed in the 10-min data (Fig. 7.6(b)). The model's consistent underestimation was prevalent towards the end of the study period which coincided with relatively higher *LAI* (Fig. 7.7). Contrary to this, the models in Section 7.4.1 (also included in Fig. 7.7 for comparison purposes) mainly underestimated when the *LAI* was small.

It should also be noted that the foliage surface temperature measurements, T_c, could be contaminated by the soil surface temperature measurements, T_s, especially when the *LAI* was small. It was inevitable that the IRT sensors that were placed directly above the trees

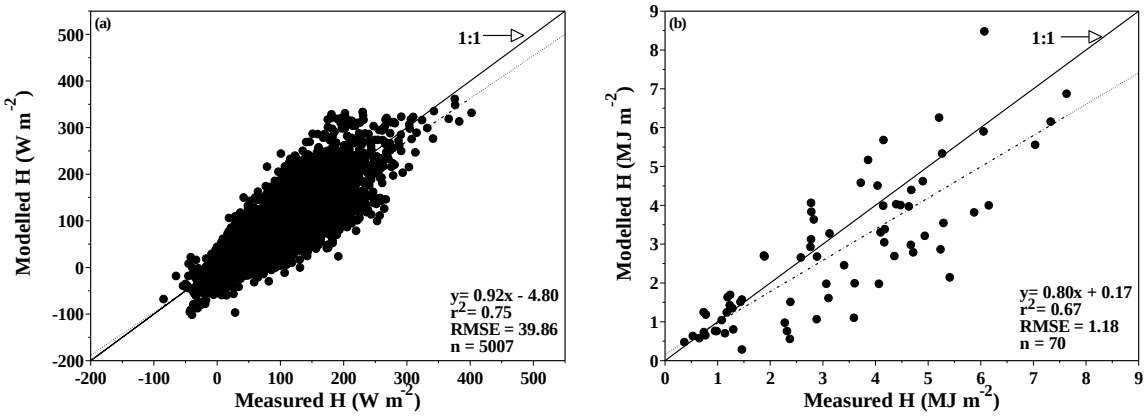

Fig. 7.6 The agreement, for a period of day of year (doy) 260 to 365 (2007) and doy 1 to 15 (2008), between measured and modelled (using Eqs (7.2) and (7.3)) *H* values along with a one-to-one graph and resulting statistics. (a) 10 minutes, and (b) daily

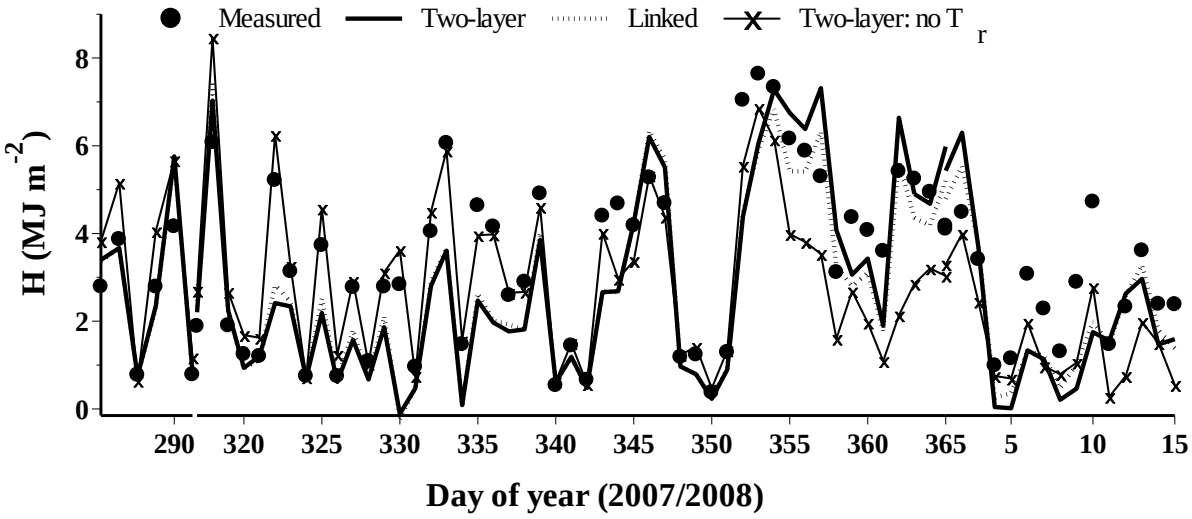

Fig. 7.7 Measured and modelled (solid line- two-layer using surface radiometric temperature, broken lines- linked and thin lines marked with x's- two-layer without surface radiometric temperature) daily *H* during the study period

would see part of the soil when the *LAI* was small and the foliage not dense enough to fully cover the ground beneath. Determining the area covered by the foliage canopy using the x- and y-axes diameters of the canopy at such instances may cause a_c to be greater than was actually (and automatically a_s to be less than the actual). During the day, H_c was usually negative, probably due to ample soil water content, for most of the time. Therefore, assigning a greater foliage area would make H_c more negative and this implies that the total *H* would be underestimated compared to measured. This underestimation, when *LAI* was small, was observed with the models in Sections 7.4.1.1 and 7.4.1.2 that used surface radiometric temperature. The foliage cover was used only in the latter model. The two-layer SW model in Section 7.4.2, that involved Eq. (7.13), did not show underestimation of the total *H* during this period because there was no surface radiometric temperature involved and hence no element of area coverage in the equation. This suggests that the model in Section 7.4.1.2 that used Eq. (7.11) could have resulted in a better estimation if the foliage cover were determined more precisely.

7.5 CONCLUSIONS

Sensible heat flux (*H*) or its component parts from a sparse tree crop canopy, *J. curcas*, were determined in two ways: (a) from inputs of measurements of surface radiometric temperature using (i) two-layer SW models that use either separate or composite surface temperature, and (ii) linked one- and two-layer models; and (b) two-layer SW model without the need for surface radiometric temperature measurement.

The estimates of *H* from the two-layer models, using separate or composite surface temperatures, were similar to each other and agreed reasonably well with *H* measured using eddy covariance (*RMSE* of 45 W m^{-2} for 10-min and 1.16 MJ m^{-2} for daily). In the two-layer models that involved composite surface temperature, it was found that calculating the composite temperature based on the soil and foliage area coverage had no bearing on the outcome of the total *H*. Further manipulation of the equation revealed that it was the temperature difference between the soil surface and reference height as corrected by the temperature difference between the soil and foliage that was important in estimating *H*.

The two-layer model was also linked with the one-layer model and used a composite surface radiometric temperature instead of air temperature at canopy source height in the classical flux-gradient equation and accordingly an excess resistance, r_r, was introduced in the equation. This excess resistance was determined using solar irradiance, resistance parameters and weather variables. The agreement between measured and modelled *H*, in this case, was also reasonably good (*RMSE* of 44 W m^{-2} for 10 min and 1.17 MJ m^{-2} for daily). The complexity of this model did not guarantee an improvement in the agreement between the modelled and measured *H* compared to the simpler models that did not involve radiation interception. The results achieved from this model were similar to those achieved from the two-layer models that did not involve radiation interception, both in terms of the scatter-plots and statistics. Both models underestimated higher values of *H* when the *LAI* was small, with better agreement for higher values of *H* when the *LAI* was relatively larger.

The two-layer SW model was also manipulated, using inputs of solar irradiance, resistance parameters and weather variables, to determine the temperature difference between the soil surface and canopy source height, and between the foliage layer and canopy source height to estimate the *H* arising from the soil and foliage layers respectively, without the need for radiometric temperature measurements. The agreement between modelled and measured *H* for the 10-min data (*RMSE* of 40 W m^{-2}) was better than for the other two models which used surface radiometric temperature measurements but this was not translated into the daily data (*RMSE* of 1.18 MJ m^{-2}). The daily trend also revealed, contrary to the models that used surface radiometric temperature measurement, that the agreement was very good when leaves were absent or the *LAI* was small, but it underestimated when the *LAI* was relatively larger towards the end of the study period.

At low *LAI*, the foliage surface temperature may be contaminated by soil surface temperature, implying a greater foliage area than was actual which in turn may imply underestimation of the total *H*. The linked one- and two-layer model that used surface radiometric temperature measurement may have been a victim of this incidence as the modelled *H* was underestimated at low *LAI*. This suggests that this model could have resulted in a better estimation of *H* if the foliage cover were determined more precisely. The two-layer models, although it was shown that fractional area had no bearing on the outcome of *H*, also showed underestimation of *H* at low *LAI*. The model that did not use

surface radiometric temperature measurement was not affected by this since it did not involve any element of soil area/foliage coverage in its equations, and the agreement between modelled and measured appeared good at low *LAI*.

In general, all three models showed a tendency to underestimate *H*. This will have the opposite effect (overestimate) in latent energy flux, and thereby evaporation, calculated as the residual term of the shortened surface energy balance equation. The model which did not use extra surface temperature measurements also produced similar or better agreement between modelled and measured *H* compared to models that used surface temperature measurements.

Acknowledgements

Profile soil water data from S Ghezehei is gratefully acknowledged.

8 GENERAL CONCLUSIONS AND RECOMMENDATIONS FOR FUTURE RESEARCH

8.1 CONCLUSIONS

The main focus of the work was on estimating and modelling sensible heat flux (H) and latent energy flux (λE), and hence total evaporation (ET), accurately using simple low-cost methods. The temperature-variance (TV) and surface renewal (SR) methods that use high frequency (typically 2 to 10 Hz) air temperature measurements, without the need for turbulent wind velocity measurements, were used for estimation of H. From this λE, and hence ET, was calculated as a residual of the shortened surface energy balance involving H from TV (H_{TV}) and SR (H_{SR}) and measurements of net irradiance (R_n) and soil heat flux (G), assuming energy balance closure is met. Single- and double-layer models were also used to estimate ET from routine meteorological observations. Extended versions of these models were used to estimate H using additional inputs of radiometric surface temperature. All estimations of H were compared against H obtained from eddy covariance (H_{EC}); and λE, and hence ET, were compared with those calculated using the residual surface energy balance from measurements of R_n, G and H_{EC}.

The TV method estimated H, using universal constants, over sparse vegetation of *Jatropha curcas*, mixed grassland community and bare fallow land, without and with adjustments for skewness (actual and estimated) of air temperature (s_k) under different atmospheric stability conditions. The atmospheric stability conditions were identified using sensor height (z) and Obukhov length (L) obtained from EC and air temperature difference between two thermocouple measurement heights. Improved agreement in terms of slope, coefficient of determination (r^2) and root mean square error (*RMSE*), over almost all surfaces used, was noted when air temperature difference between two measurement heights rather than the z/L criterion of identifying stability conditions was used. The near-neutral H_{TV} values were not reproduced very well. The H_{TV} estimates adjusted for actual s_k resulted in better agreement in terms of slope and *RMSE* for almost all surfaces compared to those not adjusted or adjusted using estimated s_k within the respective means of identifying stability condition of the atmosphere when compared with H_{EC}. The r^2 barely changed whether adjustments for s_k were made or not. Also, H_{TV} adjusted for estimated s_k

showed an improved agreement over the unadjusted estimates. This suggests that H_{TV} estimates should be adjusted for actual s_k when available, and for estimated s_k in the absence of actual s_k. The TV method offers a reasonably accurate and relatively low-cost means of estimating H over variety of different surfaces.

Season-long high frequency air temperature data collected over *J. curcas* allowed estimation of seasonal H using the TV and SR methods. This enabled seasonal λE, and hence ET, to be calculated as a residual of the shortened surface energy balance equation along with measurements of R_n and G. The seasonal estimates of H and ET from the TV and SR methods agreed reasonably well with those obtained from EC. The SR method needs calibration but gives more accurate estimates, and hence is less suitable for routine applications; whereas the TV method can use universal constants which give less accurate estimates – but is more suitable for routine application compared to SR method. Overall, the seasonal ET total for the EC, TV and SR methods were 626, 673 and 640 mm respectively with a total rainfall of 690 mm. Energy flux and rainfall thorough the season also revealed that ET is governed by the available energy, rainfall amount and vegetation canopy structure. The ET increased with increases in R_n and leaf area index (LAI) and vice versa. A footprint analysis also indicated that greater than 80% of the measured H under most atmospheric stability conditions originated from the surface of interest. These findings ensure that H can routinely be estimated over vegetation surfaces with reasonable accuracy from high frequency air temperature measurements using the relatively low-cost TV and SR methods. Long-term water-use can then be calculated as a residual of the shortened surface energy balance along with measurements of R_n and G assuming that energy balance closure is met.

The Penman-Monteith (PM) equation and the Shuttleworth and Wallace (SW) model, representing single- and double-layer models respectively, were used to determine evaporation from sparse vegetation of *J. curcas*. Routine meteorological observations, vegetation indices and/or soil water content were used as inputs in both cases. The double-layer SW model used a three-dimensional solar irradiance interception as sub-model to determine the available energy above and below the plant canopy. Model estimates of evaporation were compared with those obtained as a residual of the energy balance equation from measurements of R_n, G and H_{EC}. The PM equation significantly underestimated total evaporation during the stages when the trees had small or zero LAI,

with improved agreement with increased *LAI*. This was because of lack of appropriate representation of soil surface resistances in the PM equation. The total evaporation from the SW model, however, agreed very well with measurements with a slope of 0.96, r^2 of 0.91 and *RMSE* of 0.45 mm for the range of *LAI* encountered during the experiment. The explicit representation of surface resistance parameters also allowed the SW model to estimate the soil evaporation and plant transpiration separately. The model results indicated that soil evaporation was the sole contributor at low *LAI* and continued to contribute significantly to the total evaporation as long as the soil was not fully covered covered by the vegetation. About 66% of the modelled cumulative evaporation for the study period was attributed to soil evaporation. For the time period when the trees had no leaves until they attained a *LAI* of approximately 1.4 m^2 m^{-2}, the modelled soil evaporation was about 84% of the total evaporation. For a *LAI* ranging between 1.4 and 1.83 m^2 m^{-2}, the modelled soil evaporation accounted for about 52% of the total evaporation. As the canopy starts to close the SW model aligns more closely with the PM equation, hence the difference in total evaporation between the PM equation and the SW model at the latter stages of the experiment was smaller. The findings of this study suggest that the PM-type models should be superceded by the SW-type models for long-term modelling of evaporation over sparse vegetation surfaces.

Extended versions of the SW model were also used to estimate *H* and/or its component parts over sparse *J. curcas* trees. The *H* was determined using (i) double-layer SW model requiring either separate or composite additional surface temperature input, (ii) linked one- and two-layer model, requiring additional composite surface radiometric temperature input and (iii) double-layer SW model without the need for surface radiometric temperature measurement. The models in (ii) and (iii) required a three-dimensional solar irradiance interception as a sub-model to estimate the available energy above and below the plant canopy in order to estimate *H*.

Using model (i), the modelled and measured *H* agreed reasonably well with *RMSE* of 45 W m^{-2} for 10-min and 1.16 MJ m^{-2} for daily data. There was no significant difference in the modelled *H* whether separate or composite surface temperature inputs were used. In fact, it was found that using the composite surface temperature as input based on the soil and foliage area coverage had no bearing on the outcome of the total *H*. It was the temperature

difference between the soil surface and reference height as corrected by the temperature difference between the soil and foliage that was important in estimating *H*.

Model (ii) required an excess resistance in the form of r_r due to the replacement of the aerodynamic temperature by radiometric temperature in the classic flux-gradient equation. The results achieved from this model were similar to those achieved from (i) both in terms of the scatter-plots and statistics with *RMSE* of 44 W m^{-2} for 10-min and 1.17 MJ m^{-2} for daily data. Both models underestimated higher values of *H* when the *LAI* was small, with improved agreement for higher values of *H* when the *LAI* was larger. The additional complexity of model (ii) was not translated into improved agreement compared to results achieved from model (i).

Using model (iii), the agreement between modelled and measured *H* for the 10-min data was better (*RMSE* of 40 W m^{-2}) than for the other two models which used surface radiometric temperature measurements, but this was not reflected in the daily data (*RMSE* of 1.18 MJ m^{-2}). The daily trend also exhibited, contrary to the models that used additional surface temperature inputs, a good agreement when leaves were absent or the *LAI* was small, but underestimation when *LAI* was relatively larger.

In general, all three models showed a tendency to underestimate *H*. This will have the opposite effect (overestimate) in λE, and hence *ET*, calculated as the residual term of the shortened surface energy balance equation. The model which did not use extra surface temperature measurements also produced similar or better agreement between modelled and measured *H* compared to models that used surface temperature measurements.

Evaporation and biomass production from sparse vegetation requires accurate estimation of the available energy above and below the canopy. This was needed to be addressed in the double-layer SW models so far used (except for the one that estimated *H* using additional surface temperature inputs). A relatively simple three-dimensional solar irradiance model was developed and validated using data sets comprising different canopy characteristics (canopy size and leaf area density), row orientations, row and tree spacing and sky conditions for use in the double-layer SW models.

Measurements of solar irradiance above and below the canopy were made using LI-200 and tube solarimeters respectively. The tube solarimeters were placed 0.5 m from each other starting from the base of a tree trunk in four directions, along and perpendicular to the row up to mid-way between trees and rows. Comparison of modelled and measured hourly transmitted solar irradiance was performed for each node. In general, the model reproduced the spatial and temporal variation of hourly solar irradiance transmission of the tree crops for each node for a range of model input parameters very well. An overall average of r^2 = 0.91, Willmott's index of agreement, d = 0.96 and general absolute standard deviation, $GASD$ = 17.66% was obtained for measurements conducted on isolated tree crowns, hedgerows and tree canopies arranged in tramline mode. An improved agreement between modelled and measured values was noted for nodes located further from than near to the tree trunk and in north than in the south side of the tree trunk (in southern hemisphere). The agreement was also improved for overcast than for clear sky conditions when same node locations under similar canopy characteristics were compared. Tree trunks (especially for trees with low *LAI*), leaves and branches in close proximity with tube solarimeters, asymmetrical canopy shapes, and non-uniform tree canopy sizes and leaf distribution violate the basic assumptions of the model and hence affected its performance negatively. The model was successfully used as a sub-module in the double-layer SW model for estimating *ET* and *H*.

8.2 RECOMMENDATIONS FOR FUTURE RESEARCH

Most H_{TV} estimations are performed for unstable atmospheric conditions. Hence identification of atmospheric stability is of utmost importance. Therefore, more rigorous means of identifying stability conditions, other than through the air temperature difference between two heights that is used in this study, that do not involve complex measurements is still needed. In this regard, air temperature structure function that is employed in the surface renewal method might be a viable option. This study has also shown that estimates under stable and neutral conditions are promising and hence future research should concentrate on finding appropriate constants or refining the existing ones.

Future studies should also concentrate on the right height of air temperature sensor/s deployment above the ground and/or vegetation for H_{TV} computations. Theoretically, H_{TV} estimations should be conducted from sensors mounted in the inertial sublayer as the

method is MOST based, but equally good or better results have been obtained from sensors mounted in the roughness sublayer. The issue of identifying the heights of the roughness and inertial sublayers for a given surface has also a huge effect on H_{TV} estimations, and hence requires due attention.

High frequency air temperature measurements, ranging from 2 to 10 Hz, are traditionally used for H_{TV} estimations. H_{TV} estimations from different air temperature measurement frequencies should be conducted to establish the minimum data frequency required for H_{TV} estimation without compromising accuracy.

The mathematical computations that are involved in the SR equation have prohibited its adoption by the agricultural community for determination of H and λE, and therefore, the equations involved need to be simplified to be of use to the average agriculturalist. Besides, the equations that are involved sometimes fail to find a real solution resulting in a loss of data. Iterative procedures that are promising in this regard are developed and should be used in place of the traditionally used program or spreadsheet (M J Savage, pers. comm., 2009). More importantly future studies should concentrate on elimination of the need for calibration of the SR method against standard measurements.

In terms of estimating water-use, research should focus on using the TV and SR methods to determine evaporation directly from high frequency water vapour measurements. Moreover, the usefulness of these methods for estimation of other fluxes or trace gases like carbon dioxide and methane should be explored.

It is established here that the SW-type models should be used for sparse vegetation. However, these models require more detailed knowledge of the resistance parameters and simple means of acquiring these resistance parameters should be developed in the future. Adequate representation of the combined soil and plant resistance also poses a challenge in using the PM-type equations successfully for sparse vegetation, and hence deserves some attention. The applicability of the Priestley-Taylor equation for such vegetation cover should also be evaluated in line with the PM equation and SW model.

The challenge in using a one dimensional radiation interception model in sparse vegetation is in finding an extinction coefficient that adequately accounts for the leaf grouping and

clumping that are inherent to such vegetation surfaces. Future radiation interception models should consider developing a simple methodology that adequately determines the extinction coefficient for sparse vegetation.

The estimated (TV and SR methods) and modelled evaporation in this study were compared with total evaporation obtained as a residual of the shortened surface energy balance equation, assuming closure is met, from measurements of R_n, G and H_{EC}. In the future, comparisons of estimates should be made against more direct measurements of evaporation. Solving the issues surrounding the surface energy balance closure and underestimation of surface fluxes by the EC method would also be invaluable in validating the TV and SR methods, and the SW model. Moreover, the soil evaporation and plant transpiration partitioned using the double-layer SW model should be tested further using independent measurements, for example – microlysimetric and sap-flow methods respectively. Finally, the feasibility of coupling, integrating or linking the double-layer SW and the three-dimensional radiation interception models with soil water balance and growth models to create a complete tree growth model should be investigated.

APPENDIX

A. The Shuttleworth and Wallace (SW) model

In sparse vegetation represented by the two-layer model proposed by Shuttleworth and Wallace (1985) (Fig. 7.1), the total available energy for the canopy (A), using the shortened energy balance term, is given by:

$$A = R_n - G = H + \lambda E \qquad \text{A1}$$

where H, the sensible heat flux, and λE, the latent energy flux, are given as:

$$H = -\rho c_p (T_z - T_o) / R_a^a \Rightarrow T_z - T_o = -HR_a^a / \rho c_p \qquad \text{A2}$$

$$\lambda E = -\rho c_p (e_z - e_o) / \gamma R_a^a \Rightarrow e_z - e_o = -\lambda E \gamma R_a^a / \rho c_p \qquad \text{A3}$$

The available energy for the soil (A_s) is also given by:

$$A_s = R_{ns} - G = H_s + \lambda E_s \qquad \text{A4}$$

where H_s and λE_s are given by:

$$H_s = \rho c_p (T_s - T_o) / R_a^s \qquad \text{A5}$$

$$\lambda E_s = \rho c_p (e_s - e_o) / \left[\gamma \left(R_a^s + R_s^s \right) \right] \qquad \text{A6}$$

The available energy for the vegetation (A_c) is also given by:

$$A_c = A - A_s = H_c + \lambda E_c \qquad \text{A7}$$

where H_c and λE_c are given by:

$$H_c = \rho c_p (T_c - T_o) / R_a^c \qquad \text{A8}$$

$$\lambda E_c = \rho c_p (e_c - e_o) / \left[\gamma \left(R_a^c + R_s^c \right) \right] \qquad \text{A9}$$

where the subscripts *s* and *c* refer to soil and vegetative canopy respectively, the subscripts *z* and *o* also refer to reference and canopy source heights respectively, ρ is the air density (1.14 kg m^{-3}), c_p the specific heat capacity of air at constant pressure (1011 J kg^{-1} K^{-1}), R_n the net irradiance, *G* the soil heat flux, *T* the temperature, *e* the water vapour pressures, R_a^a (s m^{-1}) the aerodynamic resistance between canopy source height and reference height, R_a^s (s m^{-1}) the aerodynamic resistance between the soil and canopy source height, R_s^s (s m^{-1}) the surface resistance of the soil component, R_a^c (s m^{-1}) the bulk boundary layer resistance of the vegetative component and R_s^c (s m^{-1}) the bulk stomatal resistance of the vegetative component.

The vapour pressure deficits at a reference (*D*) and mean canopy (D_o) source heights and the slope of the saturated vapour pressure (Δ) are, respectively, defined as:

$$D = e_w(T_z) - e_z \qquad \text{A10}$$

$$D_o = e_w(T_o) - e_o \qquad \text{A11}$$

$$\Delta = \frac{e_w(T_z) - e_w(T_o)}{T_z - T_o} \Rightarrow e_w(T_o) = e_w(T_z) - \Delta\left(T_z - T_o\right) \qquad \text{A12}$$

Substituting the first part of Eq. A12 in Eq. A11 allows D_o to be expressed as:

$$D_o = e_w(T_z) - \left[e_w(T_z) - e_w(T_o)\right] - e_o \qquad \text{A13}$$

Using the expression for $e_w(T_z)$ from Eq. A10 into Eq. A13; replacing the terms in square brackets from Eq. A12 and rearranging gives:

$$D_o = D - \Delta\left(T_z - T_o\right) + e_z - e_o \qquad \text{A14}$$

Now using the expressions for $T_z - T_o$ from Eq. A2 and for $e_z - e_o$ from Eq. A3 and replacing these in Eq. A14 leads to:

$$D_o = D - \Delta\left(HR_a^a / \rho c_p\right) - \left(\lambda E \gamma R_a^a / \rho c_p\right) \Rightarrow D_o = D + \frac{R_a^a}{\rho c_p}\left(\Delta H - \lambda E \gamma\right) \quad \text{A15}$$

Adding $\Delta\lambda E - \Delta\lambda E$ to the variables in the bracket gives:

$$D_o = D + \frac{R_a^a}{\rho c_p}\left(\Delta\left(H + \lambda E\right) - \lambda E\left(\Delta + \gamma\right)\right) \quad \text{A16}$$

Finally D_o can be written as:

$$D_o = D + \frac{R_a^a}{\rho c_p}\left(\Delta A - \lambda E\left(\Delta + \gamma\right)\right) \quad \text{A17}$$

Separate equations for calculation of evaporation from the soil (λE_s) and the vegetation (λE_c) in the canopy can be deduced from the PM (Penman-Monteith) equation as follows:

$$\lambda E_s = \left(\Delta A_s + \rho c_p D_o / R_a^s\right) / \left[\Delta + \gamma\left(1 + R_s^s / R_a^s\right)\right] \quad \text{A18}$$

$$\lambda E_c = \left(\Delta\left(A - A_s\right) + \rho c_p D_o / R_a^c\right) / \left[\Delta + \gamma\left(1 + R_s^c / R_a^c\right)\right] \quad \text{A19}$$

Substituting Eq. A17 in Eqs A18 and A19 and adding λE_s and λE_c together to get the total λE gives:

$$\lambda E = \frac{\Delta A_s R_a^s + \rho c_p\left(D + \left[\Delta A - \left(\Delta + \gamma\right)\lambda E\right] R_a^a / \rho c_p\right)}{\left(\Delta + \gamma\right) R_a^s + \gamma R_s^s} + \frac{\Delta\left(A - A_s\right) R_a^c + \rho c_p\left(D + \left[\Delta A - \left(\Delta + \gamma\right)\lambda E\right] R_a^a / \rho c_p\right)}{\left(\Delta + \gamma\right) R_a^c + \gamma R_s^c} \quad \text{A20}$$

Eq. A20 rearranged for terms in λE leads to:

$$\begin{aligned}
&\lambda E\left[\begin{array}{l}\left\{\left(\Delta+\gamma\right)R_a^s+\gamma R_s^s\right\}\left\{\left(\Delta+\gamma\right)R_a^c+\gamma R_s^c\right\}\\ +\left(\Delta+\gamma\right)R_a^a\left[\left\{\left(\Delta+\gamma\right)R_a^c+\gamma R_s^c\right\}+\left\{\left(\Delta+\gamma\right)R_a^s+\gamma R_s^s\right\}\right]\end{array}\right]\\
&=\left(\Delta A_s R_a^s+\rho c_p D+\Delta A R_a^a\right)\left\{\left(\Delta+\gamma\right)R_a^c+\gamma R_s^c\right\}\\
&+\left(\Delta\left(A-A_s\right)R_a^c+\rho c_p D+\Delta A R_a^a\right)\left\{\left(\Delta+\gamma\right)R_a^s+\gamma R_s^s\right\}
\end{aligned} \qquad \text{A21}$$

Defining

$$\begin{aligned}
R_s&=\left(\Delta+\gamma\right)R_a^s+\gamma R_s^s\\
R_c&=\left(\Delta+\gamma\right)R_a^c+\gamma R_s^c\\
R_a&=\left(\Delta+\gamma\right)R_a^a
\end{aligned} \qquad \text{A22}$$

and adding the terms $\Delta A R_a^s-\Delta A R_a^s$ to the first expression in brackets right after the equal sign of Eq. A21 and then substituting the expressions of Eq. A22 into Eq. A21 gives:

$$\begin{aligned}
&\lambda E\left(R_s R_c+R_c R_a+R_s R_a\right)=\left\{\Delta A\left(R_a^a+R_a^s\right)+\rho c_p D-R_a^s\Delta\left(A-A_s\right)\right\}R_c\\
&+\left\{\Delta A\left(R_a^a+R_a^c\right)+\rho c_p D-R_a^c\Delta\left(A_s\right)\right\}R_s
\end{aligned} \qquad \text{A23}$$

with

$$\begin{aligned}
R_s+R_a&=\left(\Delta+\gamma\right)\left(R_a^a+R_a^s\right)+\gamma R_s^s\\
R_c+R_a&=\left(\Delta+\gamma\right)\left(R_a^a+R_a^c\right)+\gamma R_s^c
\end{aligned} \qquad \text{A24}$$

now multiplying the first expression of Eq. A23 following the equal sign by the identity $\left(R_s+R_a/R_s+R_a\right)$ and the second expression by the identity $\left(R_c+R_a/R_c+R_a\right)$ and then dividing the numerator and denominator of the resulting expressions by $\left(R_a^a+R_a^s\right)$ and $\left(R_a^a+R_a^c\right)$ respectively leads to:

$$\lambda E\left(R_s R_c+R_c R_a+R_s R_a\right)=PM_s R_c\left(R_s+R_a\right)+PM_c R_s\left(R_c+R_a\right) \qquad \text{A25}$$

with PM_s and PM_c defined as:

$$PM_s = \frac{\Delta A + \left\{\rho c_p D - \Delta R_a^s \left(A - A_s\right)\right\} / \left(R_a^a + R_a^s\right)}{\Delta + \gamma\left(1 + R_s^s / \left(R_a^a + R_a^s\right)\right)} \quad \text{A26}$$

$$PM_c = \frac{\Delta A + \left\{\rho c_p D - \Delta R_a^c A_s\right\} / \left(R_a^a + R_a^c\right)}{\Delta + \gamma\left(1 + R_s^c / \left(R_a^a + R_a^c\right)\right)} \quad \text{A27}$$

Finally

$$\lambda E = C_s PM_s + C_c PM_c \quad \text{A28}$$

with C_s and C_c defined as:

$$\begin{aligned} C_s &= R_c(R_s + R_a) / (R_s R_c + R_c R_a + R_s R_a) \\ C_c &= R_s(R_c + R_a) / (R_s R_c + R_c R_a + R_s R_a) \end{aligned} \quad \text{A29}$$

B. Estimation of Sensible heat flux from radiometric temperature measurements

The development of the two-layer SW model has also opened a way for expressing the sensible heat flux components over sparse and heterogeneous vegetation from remotely-sensed surface radiometric temperature measurements. To this end, Lhomme and co-workers have expanded the derivation of the SW model towards the estimation of the sensible heat flux components from separate (for overstorey and understorey components) or composite surface temperature measurements. The derivations follow:

The T_o term that exists in the expression of the sensible heat flux components (Eqs A2, A5 and A8) cannot be easily determined, and hence it has either to be eliminated from the equations or derived from simpler measurable terms if the sensible heat flux components were to be determined from surface radiometric temperature measurements. The following derivations, following Lhomme *et al*. (1994a, b; 1997) strive towards both: elimination or replacement of T_o in the equation and calculation of T_o from relatively easily measureable variables.

The total H can be represented as the sum of Eqs A5 and A8:

$$H = \frac{\rho c_p \left[R_a^s \left(T_c - T_o \right) + R_a^c \left(T_s - T_o \right) \right]}{R_a^s R_a^c} \qquad \text{B1}$$

multiplying the terms in brackets and collecting like terms gives:

$$H = \frac{\rho c_p \left[R_a^s T_c + R_a^c T_s - T_o \left(R_a^s + R_a^c \right) \right]}{R_a^s R_a^c} \qquad \text{B2}$$

now multiplying the right hand side (RHS) of the equation by the identity $\left(R_a^s + R_a^c \right) / \left(R_a^s + R_a^c \right)$ gives:

$$H = \frac{\rho c_p \left(R_a^s + R_a^c \right)}{R_a^s R_a^c} \left[\frac{R_a^s T_c + R_a^c T_s}{R_a^s + R_a^c} - T_o \right] \qquad \text{B3}$$

defining $T_e = \frac{R_a^s T_c + R_a^c T_s}{R_a^s + R_a^c}$ and $r_e = \frac{R_a^s R_a^c}{R_a^s + R_a^c}$ leads to:

$$H = \frac{\rho c_p \left(T_e - T_o \right)}{r_e} \qquad \text{B4}$$

now equating Eqs A2 and B4 leads to:

$$\frac{\left(T_o - T_z \right)}{R_a^a} = \frac{\left(T_e - T_o \right)}{r_e}$$
$$T_o = \frac{R_a^a T_e + r_e T_z}{R_a^a + r_e} \qquad \text{B5}$$

Substituting the above expression of T_o in Eq. B4 gives:

$$H = \frac{\rho c_p \left(T_e - T_z \right)}{R_a^a + r_e} \qquad \text{B6}$$

It is difficult to measure or calculate the T_e term in Eq. B6 especially when only a single surface radiometric temperature measurement, T_r, made from vertically above the surface, is available. To overcome such a problem, Lhomme *et al*. (1994a) assumed that the T_r is an area weighted mean of the substrate and foliage temperatures following Choudhury (1989) and Kalma and Jupp (1990). Assuming a_c represents the fractional area covered by foliage, T_r is calculated as follows:

$$T_r = (1-a_c)T_s + a_c T_c \qquad \text{B7}$$

Lhomme *et al*. (1994a) developed a relationship between T_r and T_e based on their respective definitions as follows:

$$\begin{aligned}
T_e - T_r &= \frac{R_a^c T_s + R_a^s T_c}{R_a^c + R_a^s} - \left(a_c T_c + (1-a_c)T_s\right) \\
T_e - T_r &= \frac{\cancel{R_a^c T_s} + R_a^s T_c - \cancel{R_a^c T_s} - R_a^s T_s}{R_a^c + R_a^s} + a_c\left(T_s - T_c\right) \\
T_e - T_r &= \frac{R_a^s\left(T_c - T_s\right)}{R_a^c + R_a^s} + a_c\left(T_s - T_c\right) \\
T_e - T_r &= \left(\frac{R_a^c + R_a^s}{R_a^s}\right)^{-1}\left(T_c - T_s\right) + a_c\left(T_s - T_c\right) \\
T_e - T_r &= -\left(\frac{1}{1 + R_a^c / R_a^s}\right)\left(T_s - T_c\right) + a_c\left(T_s - T_c\right) \\
T_e - T_r &= \left(-\left(\frac{1}{1 + R_a^c / R_a^s}\right) + a_c\right)\left(T_s - T_c\right) \\
&\text{defining } c = \left(\frac{1}{1 + R_a^c / R_a^s}\right) - a_c \\
T_e - T_r &= -c\left(T_s - T_c\right)
\end{aligned} \qquad \text{B8}$$

Finally taking the expression of T_e from the above and putting it in place of T_e in Eq. B4 leads to an expression of total H that does not involve the T_o term, as follows:

$$H = \rho c_p \left[\left(T_r - T_z\right) - c(T_s - T_c)\right] / \left(R_a^a + r_e\right) \qquad \text{B9}$$

The total H can also be estimated from Eq. A2 by relating the aerodynamic temperature (T_o) to the air, soil and foliage temperature measurements and the associated resistances. Equating the sum of Eqs A5 and A8 against A2 leads to (Shuttleworth and Gurney, 1990):

$$\frac{(T_o - T_a)}{R_a^a} = \frac{(T_s - T_o)}{R_a^s} + \frac{(T_c - T_o)}{R_a^c} \qquad \text{B10}$$

Changing the resistances to conductance parameters and solving for T_o gives:

$$T_o = \frac{g_a^s T_s + g_a^c T_c + g_a^a T_z}{g_a^s + g_a^c + g_a^a} \qquad \text{B11}$$

This expression of T_o can be used in Eq. A2 to solve for H. Furthermore, in the absence of separate measurements of T_c and T_s, T_o can be solved by assuming $T_c \approx T_z$, and that the composite surface radiometric temperature (T_r) is an area weighted average of the soil (T_s) and foliage (T_c) temperatures (Eq. B7). Solving Eq. B7 for T_s and putting the resulting expression in Eq. B11 in place of T_c, as well as replacing T_c with T_z gives:

$$T_o = \frac{\left(g_a^a + g_a^c\right) T_z + g_a^s \left(\frac{T_r - a_c T_z}{1 - a_c} \right)}{g_a^s + g_a^c + g_a^a} \qquad \text{B12}$$

Similarly the above expression can be used in place of T_o in Eq. A2 to aid in the determination of the total H.

C. Linking the single- and double-layer models

The total sensible heat flux can empirically be expressed as a function of surface radiometrtic measurement, T_r, either directly measured or calculated from Eq. B7 as area weighed mean, using the classical Ohm's law type formulation. But the replacement of the aerodynamic temperature with the radiometric temperature results in an excess resistance, r_r, that has to be added to the aerodynamic resistance.

$$H = \rho c_p \left(T_r - T_z\right) / \left(R_a^a + r_r\right) \qquad \text{C1}$$

Determination of r_r has been the subject of many articles, with some studies regarding its value as a constant and in other cases as a function of other variables. In this study, the method used by Lhomme *et al*. (1997), which estimates r_r as a function of easily measurable climatic variables and resistance parameters, is adopted.

Equating Eqs B9 and C1 leads to:

$$\frac{T_r - T_z}{R_a^a + r_r} = \frac{\left(T_r - T_z\right) - c\delta T}{R_a^a + r_e}$$
$$r_r = \frac{\cancel{\left(T_r - T_z\right)R_a^a} + \left(T_r - T_z\right)r_e - \cancel{\left(T_r - T_z\right)R_a^a} + c\delta T R_a^a}{\left(T_r - T_z\right) - c\delta T} \qquad \text{C2}$$

now dividing the numerator and denominator of the RHS of the equation by $T_r - T_z$ results in:

$$r_r = \frac{r_e + c\delta T R_a^a \Big/ \left(T_r - T_z\right)}{1 - \left(T_r - T_z\right) \Big/ c\delta T}, \text{ defining } m = \frac{\delta T}{\left(T_r - T_z\right)} \qquad \text{C3}$$
$$r_r = \frac{r_e + R_a^a cm}{1 - cm}$$

but if r_r were determined from routine meteorological observations, then the T_r term should be eliminated from m. This is achieved by replacing the T_r term in m with the expression from Eq. B7.

$$m = \frac{\delta T}{(T_s - T_z) - a_c (T_s - T_c)}, \text{ dividing all parts by } \delta T$$

$$m = \frac{1}{\left(T_s - T_z \middle/ \delta T\right) - a_c}, \text{ defining } \left(T_s - T_z \middle/ \delta T\right) = q \qquad \text{C4}$$

$$r_r = \frac{r_e + R_a^a c \middle/ (q - a_c)}{1 - c \middle/ (q - a_c)}$$

Now it is possible to express the ratio q, and accordingly r_r, as a function of the variables that exist in the two layer SW model, namely resistance parameters and climatic inputs. The details of the derivation follow:

Eq. A29 can be rewritten as (simply by using the reciprocal of Eq. A29 and raising the resultant to the power of -1):

$$C_s = \left[1 + \frac{R_s R_a}{R_c (R_s + R_a)}\right]^{-1}$$
$$C_c = \left[1 + \frac{R_c R_a}{R_s (R_c + R_a)}\right]^{-1} \qquad \text{C5}$$

Defining the denominators of Eqs A26 and A27, respectively, as:

$$\phi_s = \left[\Delta + \gamma\left(1 + \frac{R_s^s}{R_a^a + R_a^s}\right)\right]^{-1}$$
$$\phi_c = \left[\Delta + \gamma\left(1 + \frac{R_s^c}{R_a^a + R_a^c}\right)\right]^{-1} \qquad \text{C6}$$

and then λE in Eq. A28 can be rewritten as:

$$\lambda E = C_s \phi_s \frac{\Delta A + \left(\rho c_p D - \Delta R_a^s (A - A_s)\right)}{R_a^a + R_a^s} + C_c \phi_c \frac{\Delta A + \left(\rho c_p D - \Delta R_a^c A_s\right)}{\left(R_a^a + R_a^c\right)} \qquad \text{C7}$$

For the sensible heat flux arising from the substrate, substituting Eqs A5 and A6 into Eq. A4 gives:

$$A_s = \rho c_p \left(T_s - T_o\right) / R_a^s + \rho c_p \left(e_w\left(T_s\right) - e_o\right) / \gamma \left(R_a^s + R_s^s\right) \qquad \text{C8}$$

The Δ between the soil surface and mean canopy height is given by:

$$\Delta = \frac{e_w(T_s) - e_w(T_o)}{T_s - T_o} \Rightarrow e_w(T_s) = e_w(T_o) + \Delta\left(T_s - T_o\right) \qquad \text{C9}$$

Introducing the above expression into Eq. C8 and dividing both sides by ρc_p:

$$\frac{A_s}{\rho c_p} = \frac{T_s - T_o}{R_a^s} + \frac{\Delta\left(T_s - T_o\right)}{\gamma\left(R_a^s + R_s^s\right)} + \frac{e_w(T_o) - e_o}{\gamma\left(R_a^s + R_s^s\right)} \qquad \text{C10}$$

Using Eq. A11 in Eq. C8 and solving the equation for $T_s - T_o$ gives:

$$T_s - T_o = \frac{\left(A_s / \rho c_p\right) - D_o / \left(\gamma\left(R_a^s + R_s^s\right)\right)}{\left(1 / R_a^s\right) + \Delta / \left(\gamma\left(R_a^s + R_s^s\right)\right)} \qquad \text{C11}$$

Multiplying the RHS of Eq. C11 by the identity $\left(R_a^s + R_s^s\right) / \left(R_a^s + R_s^s\right)$ gives:

$$\begin{aligned} T_s - T_o &= \frac{\left(R_a^s + R_s^s\right)\left(A_s / \rho c_p\right) - D_o / \gamma}{\left(R_a^s + R_s^s\right) / R_a^s + \Delta / \gamma} \\ &= \frac{\left(R_a^s + R_s^s\right)\left(A_s / \rho c_p\right) - D_o / \gamma}{1 + R_s^s / R_a^s + \Delta / \gamma} \end{aligned} \qquad \text{C12}$$

Defining

$$\omega_s = \left[1 + \frac{R_s^s}{R_a^s} + \frac{\Delta}{\gamma}\right]^{-1} \qquad \text{C13}$$

and then finally Eq. A5 can be written as:

$$H_s = \rho c_p \omega_s \left[\left(R_a^s + R_s^s \right) \frac{A_s}{\rho c_p} - \frac{D_o}{\gamma} \right] / R_a^s \qquad \text{C14}$$

In the same manner, for the sensible heat flux arising from the overstorey foliage elements can be derived by substituting Eqs A8 and A9 into Eq. A7:

$$A_c = A - A_s = H_c + \lambda E_c = \frac{\rho c_p \left(T_c - T_o \right)}{R_a^c} + \frac{\rho c_p \left(e_w(T_c) - e_o \right)}{\gamma \left(R_a^c + R_s^c \right)} \qquad \text{C15}$$

The Δ between the foliage elements and mean canopy height is given by:

$$\Delta = \frac{e_w(T_c) - e_w(T_o)}{T_c - T_o} \Rightarrow e_w(T_c) = e_w(T_o) + \Delta \left(T_c - T_o \right) \qquad \text{C16}$$

Introducing the above expression in Eq. C15 and dividing both sides by ρc_p:

$$\frac{A - A_s}{\rho c_p} = \frac{T_c - T_o}{R_a^c} + \frac{\Delta \left(T_c - T_o \right)}{\gamma \left(R_a^c + R_s^c \right)} + \frac{e_w \left(T_o \right) - e_o}{\gamma \left(R_a^c + R_s^c \right)} \qquad \text{C17}$$

Using Eq. A11 in Eq. C17 and solving the equation for $T_c - T_o$ gives:

$$T_c - T_o = \frac{\left(\left(A - A_s \right) / \rho c_p \right) - D_o / \left(\gamma \left(R_a^c + R_s^c \right) \right)}{\left(1 / R_a^c \right) + \Delta / \left(\gamma \left(R_a^c + R_s^c \right) \right)} \qquad \text{C18}$$

Multiplying the RHS of Eq. C18 by the identity $\left(R_a^c + R_s^c \right) / \left(R_a^c + R_s^c \right)$ gives:

$$T_c - T_o = \frac{\left(R_a^c + R_s^c \right) \left(\left(A - A_s \right) / \rho c_p \right) - D_o / \gamma}{1 + R_s^c / R_a^c + \Delta / \gamma} \qquad \text{C19}$$

Defining

$$\omega_f = \left[1 + \frac{\Delta}{\gamma} + \frac{R_s^c}{R_a^c}\right]^{-1} \quad \text{C20}$$

and then finally Eq. A8 can be written as:

$$H_c = \rho c_p \omega_f \left[\left(R_a^c + R_s^c\right)\frac{\left(A - A_s\right)}{\rho c_p} - \frac{D_o}{\gamma}\right] / R_a^c \quad \text{C21}$$

Mathematical expressions in terms of energy and resistance parameters for $T_s - T_z$ and $T_s - T_c$ can also be derived from the above equations. $T_s - T_z$ can be written as $T_s - T_o + T_o - T_z$. By substituting the expression for $T_o - T_z$ from Eq. A2 and for T_s - T_o from Eqs C12 and C13 leads to:

$$T_s - T_z = \omega_s \left[\left(R_a^s + R_s^s\right)\frac{A_s}{\rho c_p} - \frac{D_o}{\gamma}\right] + \left(A - \lambda E\right)\frac{R_a^a}{\rho c_p} \quad \text{C22}$$

Similarly, mathematical expressions for $T_s - T_c$ can be obtained by subtracting Eq. C19 from Eq. C12, yielding:

$$T_s - T_o - \left(T_c - T_o\right) = \omega_s \left(R_a^s + R_s^s\right)\frac{A_s}{\rho c_p} - \omega_f \left(R_a^c + R_s^c\right)\frac{A - A_s}{\rho c_p} - \frac{D_o}{\gamma}\left(\omega_s - \omega_f\right) \quad \text{C23}$$

At this stage, the expressions from Eqs C2 and C19 can be used in Eqs A5 and A8, respectively, to enable the estimation of separate sensible heat flux components arising from the soil and vegetation. In a similar manner, Eqs C22 and C23 can also be used to estimate q, thereby r_r, and then use Eq. C1 to estimate the total H. But the problem with both means of estimating the total H is that they involve terms like D_o and λE which themselves are difficult to estimate.

To eliminate such terms, Eq. C23 can be expanded by substituting D_o with the expression from Eq. A17

$$T_s - T_z = \omega_s \left(R_a^s + R_s^s\right)\frac{A_s}{\rho c_p} - \frac{\omega_s}{\gamma} D \frac{\omega_s}{\gamma}\frac{R_a^a}{\rho c_p}\Delta A + \frac{\omega_s}{\gamma}\frac{R_a^a}{\rho c_p}\lambda E\left(\Delta+\gamma\right) + \frac{R_a^a}{\rho c_p} A - \frac{R_a^a}{\rho c_p}\lambda E \quad \text{C24}$$

collecting like terms in λE together gives:

$$T_s - T_z = \omega_s \left(R_a^s + R_s^s\right)\frac{A_s}{\rho c_p} - \frac{\omega_s}{\gamma} D - \frac{\omega_s}{\gamma}\frac{R_a^a}{\rho c_p}\Delta A + \lambda E \frac{R_a^a}{\rho c_p}\left(\omega_s\left(1+\frac{\Delta}{\gamma}\right)-1\right) + \frac{R_a^a}{\rho c_p} A \quad \text{C25}$$

and replacing the expression of C7 in place of λE gives:

$$T_s - T_z = \omega_s \left(R_a^s + R_s^s\right)\frac{A_s}{\rho c_p} - \frac{\omega_s}{\gamma} D - \frac{\omega_s}{\gamma}\frac{R_a^a}{\rho c_p}\Delta A + + \frac{R_a^a}{\rho c_p} A$$
$$+\left[\frac{R_a^a}{\rho c_p} C_c \phi_f \Delta A + C_c \phi_f \frac{D R_a^a}{R_a^a + R_a^c} - C_c \phi_f \frac{\Delta A_s R_a^c}{R_a^a + R_a^c}\frac{R_a^a}{\rho c_p} - C_s \phi_s \Delta A \frac{R_a^a}{\rho c_p} + C_s \phi_s \frac{D R_a^a}{R_a^a + R_a^s} - C_s \phi_s \frac{\Delta A R_a^s}{R_a^a + R_a^s}\frac{R_a^a}{\rho c_p} + C_s \phi_s \frac{\Delta A R_a^s}{R_a^a + R_a^s}\frac{R_a^a}{\rho c_p}\right] \quad \text{C26}$$
$$\left(\omega_s\left(1+\frac{\Delta}{\gamma}\right)-1\right)$$

collecting like terms within the square bracket leads to:

$$T_s - T_z = \omega_s \left(R_a^s + R_s^s \right) \frac{A_s}{\rho c_p} - \frac{\omega_s}{\gamma} D - \frac{\omega_s}{\gamma} \frac{R_a^a}{\rho c_p} \Delta A + \frac{R_a^a}{\rho c_p} A$$
$$+ \left[\frac{\Delta A R_a^a}{\rho c_p} \left(C_c \phi_c + \frac{C_s \phi_s R_a^a}{R_a^a + R_a^s} \right) + \frac{\Delta A_s R_a^a}{\rho c_p} \left(\frac{C_s \phi_s R_a^s}{R_a^a + R_a^s} - \frac{C_c \phi_c R_a^c}{R_a^a + R_a^c} \right) + D R_a^a \left(\frac{C_c \phi_c}{R_a^a + R_a^c} + \frac{C_s \phi_s}{R_a^a + R_a^s} \right) \right] \left(\omega_s \left(1 + \frac{\Delta}{\gamma} \right) - 1 \right) \quad \text{C27}$$

collecting like terms in A, A_s and D and accordingly dividing the equation into three parts and solving for T_s - T_z gives:

$$T_s - T_z = \frac{A R_a^a}{\rho c_p} \left[\left(1 - \frac{\Delta}{\gamma} \omega_s + \Delta \left(C_c \phi_c + \frac{C_s \phi_s R_a^a}{R_a^a + R_a^s} \right) \right) \left(\omega_s \left(1 + \frac{\Delta}{\gamma} \right) - 1 \right) \right]$$
$$+ \frac{A_s R_a^a}{\rho c_p} \left[\Delta \left(\frac{C_c \phi_c R_a^s}{R_a^a + R_a^s} - \frac{C_s \phi_s R_a^c}{R_a^a + R_a^c} \right) \left(\omega_s \left(1 + \frac{\Delta}{\gamma} \right) - 1 \right) + \omega_s \left(\frac{R_a^s + R_s^s}{R_a^a} \right) \right] \quad \text{C28}$$
$$+ \frac{D}{\gamma} \left[\gamma \left(\frac{C_c \phi_c}{R_a^a + R_a^c} + \frac{C_s \phi_s}{R_a^a + R_a^s} \right) \left(\omega_s \left(1 + \frac{\Delta}{\gamma} \right) - 1 \right) R_a^a - \omega_s \right]$$

The terms in square brackets are defined as ν_1, ν_2 and ν_3 respectively; and finally T_s - T_z can be written as:

$$T_s - T_z = \nu_1 \left(\frac{A R_a^a}{\rho c_p} \right) + \nu_2 \left(\frac{A_s R_a^a}{\rho c_p} \right) + \nu_3 \left(\frac{D}{\gamma} \right) \quad \text{C29}$$

In a similar manner Eq. C23 can be expanded by substituting D_o with the expression from Eq. A17

$$T_s - T_c = \omega_s \left(R_a^s + R_s^s\right)\frac{A_s}{\rho c_p} + \omega_f \left(R_a^c + R_s^c\right)\frac{A_s}{\rho c_p} - \omega_f \left(R_a^c + R_s^c\right)\frac{A}{\rho c_p} + \frac{\left(\omega_f - \omega_s\right)D}{\gamma} + \left(\omega_f - \omega_s\right)\frac{\Delta}{\gamma}\frac{AR_a^a}{\rho c_p} - \left(\omega_f - \omega_s\right)\left(1 - \frac{\Delta}{\gamma}\right)\frac{\lambda E R_a^a}{\rho c_p} \quad \text{C30}$$

and replacing λE with the expression in C7 gives:

$$\begin{aligned} T_s - T_c = {} & \omega_s \left(R_a^s + R_s^s\right)\frac{A_s}{\rho c_p} + \omega_f \left(R_a^c + R_s^c\right)\frac{A_s}{\rho c_p} - \omega_f \left(R_a^c + R_s^c\right)\frac{A}{\rho c_p} + \frac{\left(\omega_f - \omega_s\right)D}{\gamma} + \left(\omega_f - \omega_s\right)\frac{\Delta}{\gamma}\frac{AR_a^a}{\rho c_p} \\ & - \left(\omega_f - \omega_s\right)\left(1 + \frac{\Delta}{\gamma}\right)\left[\frac{\Delta A R_a^a}{\rho c_p}\left(C_c\phi_c - \frac{C_s\phi_s R_a^a}{R_a^a + R_a^s}\right) + \frac{\Delta A_s R_a^a}{\rho c_p}\left(\frac{C_s\phi_s R_a^s}{R_a^a + R_a^s} - \frac{C_c\phi_c R_a^c}{R_a^a + R_a^c}\right) + DR_a^a\left(\frac{C_c\phi_c}{R_a^a + R_a^c} + \frac{C_s\phi_s}{R_a^a + R_a^s}\right)\right] \end{aligned} \quad \text{C31}$$

Collecting like terms in A, A_s and D and accordingly dividing the equation into three parts and solving for $T_s - T_c$ gives:

$$\begin{aligned} T_s - T_c = {} & \frac{AR_a^a}{\rho c_p}\left[\left(\omega_f - \omega_s\right)\left(\frac{\Delta}{\gamma} - \Delta\left(1 + \frac{\Delta}{\gamma}\right)\left(C_c\phi_c - \frac{C_s\phi_s R_a^a}{R_a^a + R_a^s}\right)\right) - \omega_f\left(\frac{R_a^c + R_s^c}{R_a^a}\right)\right] \\ & + \frac{A_s R_a^a}{\rho c_p}\left[\omega_s\frac{R_a^s + R_s^s}{R_a^a} + \omega_f\frac{R_a^c + R_s^c}{R_a^a} + \Delta\left(1 + \frac{\Delta}{\gamma}\right)\left(\omega_f - \omega_s\right)\left(\frac{C_c\phi_c R_a^c}{R_a^a + R_a^c} - \frac{C_s\phi_s R_a^s}{R_a^a + R_a^s}\right)\right] \\ & + \frac{D}{\gamma}\left[\left(\omega_f - \omega_s\right)\left(1 - \left(\gamma + \Delta\right)R_a^a\left(\frac{C_c\phi_c}{R_a^a + R_a^c} + \frac{C_s\phi_s}{R_a^a + R_a^s}\right)\right)\right] \end{aligned} \quad \text{C32}$$

The terms in square brackets are defined as δ_1, δ_2 and δ_3 respectively; and finally $T_s - T_c$ can be written as:

$$T_s - T_c = \delta_1 \left(\frac{AR_a^a}{\rho c_p} \right) + \delta_2 \left(\frac{A_s R_a^a}{\rho c_p} \right) + \delta_3 \left(\frac{D}{\gamma} \right) \qquad \text{(C33)}$$

Now Eqs C29 and C33 can be used to for estimation of q, and hence r_r, without the need for D_o and λE terms and ultimately r_r can be used in Eq. C1 to aid in estimating the total H.

REFERENCES

Albertson JD, Parlange MB, Katul GG, Chu C-R, Stricker H, Tyler S (1995) Sensible heat flux from arid regions: A simple flux-variance method. Water Resour Res 31:969–973.

Allen RG, Pereira LS, Raes D, Smith M (1998) Crop evapotranspiration: guidelines for computing crop water requirements. FAO Irrigation Drain Pap No. 56, 300pp.

Allen SJ, Roberts JM, Smith SM, Jackson NA (1998) Modelling the modification of crop microclimate by spaced tree canopies. Chapter 7, 62–70. In: Annual report (July 1996-June 1997) Agroforestry Modelling and Research Co-ordination Project Report to DFID-FRP.

Anadranistakis M, Liakatas A, Kerkides P, Rizos S, Gavanosis J, Poulovassilis A (2000) Crop water requirements model tested for crops grown in Greece. Agric Water Manag 45:297–316.

Annandale JG, Jovanovic NZ, Benadé N, Du Sautoy N, Mpandeli NS, Lobit P (2002) Two-dimensional water balance and energy interception model for fruit trees. Water Resources Commission Report No. 945/1/02, 217 pp, Pretoria, South Africa. ISBN 1 86845 8695.

Annandale JG, Jovanovic NZ, Campbell GS, Du Sautoy N, Lobit P (2004) Two-dimensional solar radiation interception model for hedgerow fruit trees. Agric Forest Meteorol 121:207–225.

Arya SP (2001) Introduction to Micrometeorology. Second Edition. Academic Press. London, UK. 420 pp.

Baldocchi D, Meyers T (1998) On using eco-physiological, micrometeorological and biogeochemical theory to evaluate carbon dioxide, water vapor and trace gas fluxes over vegetation: a perspective. Agric Forest Meteorol 90:1–25.

Baldocchi DD, Collineau S (1994) The physical nature of light in heterogeneous canopies: spatial and temporal attributes. In: Caldwell MM, Pearcy RW (Eds), Exploitation of Environmental Heterogeneity by Plants: Ecophysiological Processes Above and Below Ground. Academic Press. San Diego, CA, pp. 21–72.

Barr AG, Morgenstern K, Black TA, McCaughey JH, Nesic Z (2006) Surface energy balance closure by the eddy-covariance method above three boreal forest stands and implications for the measurement of the CO_2 flux. Agric Forest Meteorol 140:322–337.

Blyth EM, Harding RJ (1995) Application of aggregation models to surface heat flux from the Sahelian tiger bush. Agric Forest Meteorol 72:213–235.

Boast CW (1986) Evaporation from bare soil measured with high spatial resolution. In A. Klute (ed.) Methods of soil analysis, Part 1. Amer Soc Agron, Inc, and Soil Sci Soc Am, Inc., Madison, WI, USA.

Bowen IS (1926) The ratio of heat losses by conduction and by evaporation from any water surface. Phys Rev 27:779–787.

Brutsaert WH (1982) Evaporation Into the Atmosphere. Theory, History and Applications. D. Reidel Publishing Co, Dordrecht, Holand. 299 pp.

Brutsaert WH (2005) Hydrology: An Introduction. Cambridge University Press, UK. 605 pp.

Businger JA, Yaglom AM (1971) Introduction to Obukhov's paper on 'turbulence in an atmosphere with a non-uniform temperature'. Boundary-Layer Meteorol 2:3–6.

CAMASE (1995) Newsletter of Agro-ecosystems Modelling, extra edition. AB-DLO Publisher, Wageningen, The Netherlands, November 1995.

Campbell GS (1986) Extinction coefficients for radiation in plant canopies calculated using an ellipsoidal inclination angle distribution. Agric Forest Meteorol 36:317–321.

Campbell GS, Norman JM (1998) An Introduction to Environmental Biophysics, 2nd ed. Springer, New York. 286 pp.

Castellvi F (2004) Combining surface renewal analysis and similarity theory: a new approach for estimating sensible heat flux. Water Resour Res 40: W05201, doi: 10.1029/2003WR002677.

Castellvi F, Martínez-Cob A (2005) Estimating sensible heat flux using surface renewal analysis and the flux variance method: A case study over olive trees at Sastago (NE of Spain). Water Resour Res 41: W09422, doi:10.1029/2005WR004035, 1-10.

Castellvi F, Martínez-Cob A, Pérez-Coveta O (2006). Estimating sensible and latent heat fluxes over rice using surface renewal. Agric Forest Meteorol 139:164–169.

Castellvi F, Snyder RL, Baldocchi DD (2008) Surface energy-balance closure over rangeland grass using the eddy covariance method and surface renewal analysis. Agric Forest Meteorol 148:1147–1160.

Chamberlain AC (1968) Transport of gases to and from surfaces with bluff and wave-like roughness elements. Q J R Meteorol Soc 94:318–332.

Charles-Edwards DA, Thornley JHM (1973) Light interception by an isolated plant. A simple model. Ann Bot 37:919–928.

Charles-Edwards DA, Thorpe MR (1976) Interception of diffuse and direct-beam radiation by a hedge-row apple orchard. Ann Bot 40:603–613.

Chehbouni A, Lo Seen D, Njoku EG, Lhomme JP, Monteny B, Kerr YH (1997). Estimation of sensible heat flux over sparsely vegetated surfaces. J. Hydro 188–189:855–868.

Chen SG, Ceulemans R, Impens I (1994) A fractal based Populus canopy structure model for the calculation of light interception. Forest Ecol Manag 69:97–110.

Chen W, Novak MD, Black TA, Lee X (1997a) Coherent eddies and temperature structure functions for three contrasting surfaces. Part I: Ramp model with finite micro front time. Boundary-Layer Meteorol 84:99–123.

Chen W, Novak MD, Black TA, Lee X (1997b) Coherent eddies and temperature structure functions for three contrasting surfaces. Part II: Renewal model for sensible heat flux. Boundary-Layer Meteorol 84:125–147.

Choudhury BJ (1989) Estimating evaporation and carbon assimilation using infrared temperature data. In: Asrar G (Ed) Theory and Applications of Optical Remote Sensing. Wiley, New York, pp. 628–690.

Choudhury BJ, Monteith JL (1988) A four-layer model for the heat budget of homogeneous land surfaces. Q J R Meteorol Soc 114:373–398.

Choudhury BJ, Reginato RJ, Idso SB (1986) An analysis of infrared temperature observations over wheat and calculation of latent heat flux. Agric Forest Meteorol 37:75–88.

Dabberdt WT, Lenschow DH, Horst TW, Zimmerman PR, Oncley SP, Delaney AC (1993) Atmosphere surface exchange measurements. Science 260:1472–1481.

Dauzat J (1993) Simulated plants and radiative transfer simulations. In: Varlet-Grancher C, Bonhomme R, Sinoquet H (Eds), Crop Structure and Light Microclimate: Characterization and Applications. INRA, Paris, pp. 271–278.

de Bruin HAR, Hartogensis OK (2005) Variance method to determine turbulent fluxes of momentum and sensible heat in the stable atmospheric surface layer. Boundary-Layer Meteorol 116:385–392.

de Bruin HAR, Kohsiek W, van den Hurk BJJM (1993) A verification of some methods to determine the fluxes of momentum, sensible heat and water vapour using standard

deviation and structure parameter of scalar meteorological quantities. Boundary-Layer Meteorol 63:231–257.

De Jager JM (1994) Accuracy of vegetation evaporation ratio formulae for estimating final wheat yield. Water SA 20:307–315.

De Pury DGG, Farquhar GD (1997) Simple scaling of photosynthesis from leaves to canopies without the errors of big-leaf models. Plant Cell Environ 20:537–557.

Deardorff JW (1978) Observed characteristics of the outer layer. AMS course on the planetary boundary layer. Boulder, Colo. (Unpublished manuscript).

Dolman AJ (1993) A multiple-source land surface energy balance model for use in general circulation models. Agric Forest Meteorol 65:21–45.

Dolman AJ, Gash JHC, Roberts J, Shuttleworth WJ (1991) Stomatal and surface conductance of tropical rainforest. Agric Forest Meteorol 54:303–318.

Dolman AJ, Wallace JS (1991) Lagrangian and K-theory approaches in modelling evaporation from sparse canopies. Q J R Meteorol Soc 117:1325–1340.

Doorenbos J, Pruitt WO (1992) Crop water requirements. FAO Irrig Drain Paper No. 24. FAO, Rome, Italy.

Drexler JZ, Snyder RL, Spano D, Paw U KT (2004) A review of models and micrometeorological methods used to estimate wetland evapotranspiration. Hydrol Process 18:2071–2101.

Duce P, Spano D, Snyder RL (1998) Effects of different fine-wire thermocouple design on high frequency temperature measurement. In: AMS 23rd Conf on Agric Forest Meteorol Albuquerque, NM, Nov. 2–6, pp. 146–147.

Duce P, Spano D, Snyder RL, Paw U KT (1997) Surface renewal estimates of evapotranspiration. Short canopies. Acta Hort 449:57–62.

Duursma RA, Mäkelä A (2007) Summary models for light interception and light-use efficiency of non-homogeneous canopies. Tree Physiol 27:859–870.

Dyer AJ, Hicks BB (1970) Flux gradient relationship in the constant flux layer. Q J R Meteorol Soc 96:715–721.

Farahani HJ, Ahuja LR (1996) Evaporation modeling of partial canopy/residue-covered fields. Trans ASAE 39:2051–2064.

Farahani HJ, Bausch WC (1995) Performance of evapotranspiration models for maize – bare soil to closed canopy. Trans ASAE 38:1049–1059.

Foken T, Wichura B (1996) Tools for quality assessment of surface based flux measurements. Agric Forest Meteorol 78:83–105.

Francis G, Edinger R, Becker K (2005) A concept for simultaneous wasteland reclamation, fuel production, and socio-economic development in degraded areas in India: Need, potential and perspectives of Jatropha plantations. Natural Resources Forum 29:12–24.

Gao W, Shaw RH, Paw U KT (1989) Observation of organized structure in turbulent flow within and above a forest canopy. Boundary-Layer Meteorol 47:349–377.

Garratt JR (1992) The Atmospheric Boundary Layer. Cambridge University Press, Cambridge. 316 pp.

Green SR, McNaughton K, Wunsche JN, Clothier B (2003) Modeling light interception and transpiration of apple tree canopies. Agron J 95:1380–1387.

Gübitz GM, Mittelbach M, Trabi M (1999) Exploitation of the tropical oil seed plant *Jatropha curcas* L. Bioresource Technology 67:73–82.

Guo X, Zhang H, Cai X, Kang L, Zhu T, Leclerc MY (2009) Flux-variance method for latent heat and carbon dioxide fluxes in unstable conditions. Boundary-Layer Meteorol 131:363–384.

Hall FG, Huemmrich KF, Goetz SJ, Sellers PJ, Nickeson JE (1992) Satellite remote sensing of surface energy balance: success, failures and unresolved issues in FIFE. J Geophys Res 97:19061–19089.

Ham JM, Heilman JL (2003) Experimental test of density and energy-balance corrections on carbon dioxide flux as measured using open-path eddy covariance. Agron J 95:1393–1403.

Hao Y, Wang Y, Huang X, Cui X, Zhou X, Wang S, Niu H, Jiang G (2007) Seasonal and interannual variation in water vapor and energy exchange over a typical steppe in Inner Mongolia, China. Agric Forest Meteorol 146:57–69.

Heller, J (1996) Physic nut. *Jatropha curcas* L. Promoting the conservation and use of underutilized and neglected crops. 1. Institute of Plant Genetics and Crop Plant Research, Gatersleben/ International Plant Genetic Resources Institute, Rome. ISBN 92-9043-278-0

Horst TW, Weil JC (1992) Footprint estimation for scalar flux measurements in the atmospheric surface-layer. Boundary-Layer Meteorol 59:279–296.

Hsieh C-I, Katul G, Chi T (2000) An approximate analytical model for footprint estimation of scalar fluxes in thermally stratified atmospheric flows. Adv Water Resour 23:765–772.

Hsieh C-I, Katul GG, Schieldge J, Sigmond J, Knoerr KR (1996) Estimation of momentum and heat fluxes using dissipation and flux-variance methods in the unstable surface layer. Water Resour Res 32:2453–2462.

Hsieh C-I, Lai M-C, Hsia Y-J, Chang T-J (2008) Estimation of sensible heat, water vapour and CO_2 fluxes using the flux-variance method. Int J Biometeorol 52:521–533.

Huband NDS, Monteith JL (1986) Radiative surface temperature and energy balance of a wheat crop. Boundary-Layer Meteorol 36:1–17.

Humphreys ER, Black TA, Ethier GJ, Drewitt GB, Spittlehouse DL, Jork E-M, Nesic Z, Livingston NJ (2003) Annual and seasonal variability of sensible and latent heat fluxes above a coastal Douglas-fir forest, British Columbia, Canada. Agric Forest Meteorol 135:190–201.

Huntingford C, Allen SJ, Garding RJ (1995) An intercomparison of single and dual-source vegetation-atmosphere transfer models applied to transpiration from Sahelian Savannah. Boundary-Layer Meteorol 74:397–418.

Jackson RD, Pinter PJ, Reginato RJ (1985) Net radiation calculated from remote multispectral and ground station meteorological data. Agric Forest Meteorol 35:153–164.

Jarvis P (1976) The interpretation of the variations in leaf water potentials and stomatal conductances found in canopies in the field. Philos Trans R Soc London Ser B 273:593–610.

Jørgensen SE, Kamp-Nielsen L, Christensen T, Windolf-Nielsen J, Westergaard B (1986) Validation of a prognosis based upon a eutrophication model. Ecol Model 35:165–182.

Kabat P, Dohnan AJ, Elbers JA (1997) Evaporation, sensible heat and canopy conductance of fallow savannah and patterned woodland in the Sahel. J Hydro 188–189:494–515.

Kaimal JC, Finnigan JJ (1994) Atmospheric Boundary Layer Flows, Their Structure and Measurement. Oxford University Press, New York. 289 pp.

Kalma, JD, Jupp, DLB (1990) Estimating evaporation from pasture using infrared thermometry: evaluation of a one-layer resistance model. Agric Forest Meteorol 51:223–246.

Kanda M, Inagaki A, Letzel MO, Raacsh S, Watanabe T (2004) LES study of the energy imbalance problem with eddy covariance fluxes. Boundary-Layer Meteorol 110:381–404.

Kato T, Kimura R, Kamichika M (2004) Estimation of evapotranspiration, transpiration ratio and water-use efficiency from a sparse canopy using a compartment model. Agric Water Manag 65:173–191.

Katul G, Goltz SM, Hsieh C-I, Cheng Y, Mowry F, Sigmond J (1995) Estimations of surface and momentum fluxes using the flux-variance method above uniform and non-uniform terrain. Boundary-Layer Meteorol 74:237–260.

Katul G, Hsieh C-I, Oren R, Ellsworth D, Phillips N (1996) Latent and sensible heat flux predictions from a uniform pine forest using surface renewal and flux variance methods. Boundary-Layer Meteorol 80:249–282.

Kljun N, Calanca P, Rotach MW, Schmid HP (2004) A simple parameterisation for flux footprint predictions. Boundary-Layer Meteorol 112:503–523.

Kustas WP (1990) Estimates of evapotranspiration with a one- and two-layer model of heat transfer over partial canopy cover. J Appl Meteorol 29:704–715.

Kustas WP, Blanford H, Stannard DI, Daughtry CST, Nichols WD, Weltz MA (1994) Local energy flux estimates for unstable conditions using variance data in semiarid rangelands. Water Resour Res 30:1351–1361.

Kustas WP, Choudhury BJ, Kunkel KE, Gay LW (1989) Estimate of the aerodynamic roughness parameters over an incomplete canopy cover of cotton. Agric Forest Meteorol 46:91–105.

Kustas WP, Norman JM (1999) Evaluation of soil and vegetation heat flux predictions using simple two-source model with radiometric temperatures for partial canopy cover. Agric Forest Meteorol 94:13–29.

Lafleur PM, Rouse WR (1990) Application of energy combination model for evaporation from sparse canopies. Agric Forest Meteorol 49:135–153.

Leclerc MY, Shen SH, Lamb B (1997) Observations and large-eddy simulation modeling of footprints in the lower convective boundary layer. J Geophys Res Atmos 102:9323–9334.

Leclerc MY, Thurtell GW (1990) Footprint prediction of scalar fluxes using a markovian analysis. Boundary-Layer Meteorol 52:247–258.

Lee X, Finnigan J, Paw U KT (2004) Coordinate systems and flux bias error. In: Lee X, Massman W, Law BE (Eds) Handbook of Micrometeorology. A Guide for Surface Flux Measurement and Analysis. Kluwer Academic Press, Dordrecht. pp. 33–66.

Lemeur R, Blad BL (1974) A critical review of light models for estimating the shortwave radiation regime of plant canopies. Agric Meteorol 14:255–286.

Lhomme JP, Chehbouni A (1999) Comments on dual-source vegetation-atmosphere transfer models. Agric Forest Meteorol 94:269–273.

Lhomme JP, Chehbouni A, Monteny B (2000) Sensible heat flux-radiometric surface temperature relationship over sparse vegetation: Parameterizing B^{-1}. Boundary-Layer Meteorol 97:431–457.

Lhomme JP, Troufleau D, Monteny B, Chehbouni A, Bauduin S (1997) Sensible heat flux and radiometric surface temperature over sparse Sahelian vegetation II. A model for the kB^{-1} parameter. J Hydro 188–189:839–854.

Lhomme, JP, Monteny B, Amadou M (1994a) Estimating sensible heat flux from radiometric temperature over sparse millet. Agric Forest Meteorol 68:77–91.

Lhomme, JP, Monteny B, Chehbouni A, Troufleau D (1994b) Determination of sensible heat flux over sahelian fallow savannah using infra-red thermometry. Agric Forest Meteorol 68:93–105.

Lloyd CR, Culf AD, Dolman AJ, Gash JHC (1991) Estimates of sensible heat flux from observations of temperature fluctuations. Boundary-Layer Meteorol 57:311–322.

Lund MR, Soegaard H (2003) Modelling of evaporation in a sparse millet crop using a two-source model including sensible heat advection within the canopy. J Hydro 280:124–144.

Mahrt L (1998) Flux sampling errors for aircraft and towers. J Atmos Oceanic Technol 15:416–429.

Mahrt L (2000) Surface heterogeneity and vertical structure of the boundary layer. Boudary-Layer Meteorol 96:33–62.

Mann JE, Curry GL, De Michele DW, Baker DN (1980) Light penetration in a row crop of random plant spacing. Agron J 72:131–142.

Mengistu MG (2008) Heat and energy exchange above different surfaces using surface renewal. PhD thesis, University of KwaZulu-Natal, 151 pp.

Meyers TP, Baldocchi DD (2005) Current micrometeorological flux methodologies with applications in agriculture. In: Hatfield JL, Baker JM (Eds) Micrometeorology in

Agricultural Systems. Agronomy Monograph no. 47. ASA, CSSA, SSSA Publishers, Madison, Wisconsin, USA. pp. 381–405.

Monin AS, Obukhov AM (1954) Basic laws of turbulent mixing in the atmosphere near the ground. Trudy Akad Nauk SSSR 24(151):163–187.

Monin AS, Yaglom AM (1971) Statistical Fluid Mechanics: Mechanics of Turbulence. Vol 1. MIT Press, Cambridge, Massachusetts, 769 pp.

Monsi M, Saeki T (1953) Uber den Liechfaktor in den pflanzengesellschaften und seine bedeutung für die stoffproduktion. Jpn J Bot 14:22–52.

Monteith JL (1965) Evaporation and the environment. Symp Soc Exp Biol 19:206–234.

Myneni RB, Ross J, Asrar G (1989) A review on the theory of photon transport in leaf canopies. Agric Forest Meteorol 45:1–153.

Nair PKR (1991) State of the art of agroforestry systems. Forest Ecol Manag 45:5–29.

Norman JM (1975) Radiative transfer in vegetation. In: de Vries DA, Afgan NH (Eds) Heat and Mass Transfer in the Biosphere. I. Transfer Processes in Plant Environment. Scripta Book Company, Washington, DC, pp. 187–205.

Norman JM, Campbell GS (1983) Application of a plant–environment model to problems in irrigation. Adv Irrig 2:155–188.

Norman JM, Kustas WP, Humes KS (1995) Source approach for estimating soil and vegetation energy fluxes in observations of directional radiometric surface temperature. Agric Forest Meteorol 77:263–293.

Norman JM, Welles JM (1983) Radiative transfer in an array of canopies. Agron J 75:481–488.

Oncley SP, Foken T, Vogt R, Kohsiek W, de Bruin HAR, Bernhofer C, Christen A, van Gorsel E, Grantz D, Feigenwinter C, Lehner I, Liebethal C, Liu H, Mauder M, Pitacco A, Ribeiro L, Weidinger T (2007) The Energy Balance Experiment EBEX-2000. Part I: overview and energy balance. Boundary-Layer Meteorol 123:1–28.

Openshaw K (2000) A review of *Jatropha curcas*: an oil plant of unfulfilled promise. Biomass and Bioenergy 19:1–15.

Ortega-Farias S, Carrasco M, Olioso A, Acevedo C, Poblete C (2007) Latent heat flux over Cabernet Sauvignon vineyard using the Shuttleworth and Wallace model. Irrig Sci 25:161–170.

Owen PR, Thomson WR (1963) Heat transfer across rough surfaces. J Fluid Mech 15:321–324.

Oyarzun RA, Stockle CO, Whiting MD (2007) A simple approach to modeling radiation interception by fruit-tree orchards. Agric Forest Meteorol 142:12–24.

Padro J (1993) An investigation of flux-variance methods and universal functions applied to three land-use types in unstable conditions. Boundary-Layer Meteorol 66:413–425.

Panofsky HA, Dutton JA (1984) Atmospheric Turbulence: Models and Methods for Engineering Applications. John Wiley & Sons. New York. 397 pp.

Pasquill, F (1972) Some aspects of boundary layer description. Q J R Meteorol Soc 98:469–494.

Paw U KT, Brunnet Y, Collineau S, Shaw RH, Maitani T, Qui J, Hipps L (1992) On coherent structure in turbulence within and above agricultural plant canopies. Agric Forest Meteorol 61:55–68.

Paw U KT, Qiu J, Su HB, Watanabe T, Brunet Y (1995) Surface renewal analysis: a new method to obtain scalar fluxes without velocity data. Agric Forest Meteorol 74:119–137.

Paw U KT, Snyder RL, Spano D, Su HB (2005) Surface renewal estimates of scalar exchange. In: Hatfield JL, Baker JM (Eds) Micrometeorology in Agricultural Systems. Agronomy Monograph no. 47. ASA, CSSA, SSSA Publishers, Madison, Wisconsin, USA. pp. 455-483.

Pielke RA, Sr, Avissar R, Raupach M, Dolman AJ, Zeng X, Denning AS (1998) Interactions between the atmosphere and terrestrial ecosystems: influence on weather and climate. Global Change Bio 4:461–475.

Prueger JH, Kustas WP (2005) Aerodynamic methods for estimating turbulent fluxes. In: Hatfield JL, Baker JM (Eds.) Micrometeorology in Agricultural Systems. Agronomy Monograph no. 47. ASA, CSSA, SSSA Publishers, Madison, Wisconsin, USA. pp. 407–436.

Prueger JH, Kustas WP, Hipps LE, Hatfield JL (2004) Aerodynamic parameters and sensible heat flux estimates for a semi-arid ecosystem. J Arid Environ 57:87–100.

Raupach MR, Finnigan JJ (1988) 'Single-layer models of evaporation from plant canopies are incorrect but useful, whereas multilayer models are correct but useless': Discuss. Aust J Plant Physiol 15:705–716.

Raupach MR, Finnigan JJ, Brunet Y (1989) Coherent eddies in vegetation canopies. In: Proc. 4th Australasian Conference on Heat and Mass Transfer, Christchurch, New Zealand, May 9-12. Bergell House, New York. pp. 75–90.

Republic of South Africa (1998) National Water Act. Act No 36 of 1998. South African Government Printer. 90 pp.

Ritchie JT (1972) Model for predicting evaporation from a row crop with incomplete cover. Water Resour Res 8:1204-1213.

Rosenberg NJ, Blad BL, Verma SB (1983) Microclimate: The Biological Environment. Second Edition. John Wiley & Sons. New York. 495 pp.

Ross J (1975) Radiative transfer in plant communities. In: Monteith JL (Ed) Vegetation and the Atmosphere. Volume 1. Academic Press Inc. London, pp. 13–55.

Savage MJ (2007) Sensible heat estimation using a high frequency temperature-based method above various canopies. Proc 13th S Afr Nat Com of the Int Assoc of Hydro Sci (SANCIAHS) Symp, Sept 6–7, Cape Town, Republic of South Africa.

Savage MJ (2009) Estimation of evaporation using dual-beam surface layer scintillometer and component energy balance measurements. Agric Forest Meteorol 149:501–517.

Savage MJ, Everson CS, Metelekamp BR (1997) Evaporation measurement above vegetated surfaces using micrometeorological techniques. Water Research Commission Report No. 349/1/97, 248 pp, Pretoria, South Africa. ISBN 1 86845 363 4.

Savage MJ, Everson CS, Metelekamp BR (2009) Bowen ratio evaporation measurement in a remote montane grassland: Data integrity and fluxes. J Hydro 376:249–260.

Savage MJ, Everson CS, Odhiambo GO, Mengistu MG, Jarmain C (2004) Theory and practice of evapotranspiration measurement, with special focus on SLS as an operational tool for the estimation of spatially-averaged evaporation. Water Research Commission Report No.1335/1/04, 204 pp, Pretoria, South Africa. ISBN 1-77005-247-X.

Savage MJ, Graham AND, Lightbody KE (2000) An investigation of the stem steady heat energy balance technique in determining water-use by trees. Water commission Report No. 348/1/00, 181 pp, Pretoria, South Africa. ISBN 1-86845-617-X.

Savage MJ, Heilman JL (2009) Infrared calibration of net radiometers and infrared thermometers. Agric Forest Meteorol 149:1279–1293.

Savage MJ, Mclnnes KJ, Heilman JL (1995) Placement height of eddy correlation sensors above a short turfgrass surface. Agric Forest Meteorol 74:195-204.

Schmid HP (2002) Footprint modeling for vegetation atmosphere exchange studies: a review and perspective, Agric Forest Meteorol 113:159–183.

Schuepp PH, Leclerc MY, Macpherson JI, Desjardins RL (1990) Footprint prediction of scalar fluxes from analytical solutions of the diffusion equation. Boundary-Layer Meteorol 50:353–373.

Sellers PJ, Mintz Y, Sud YC, Dalcher A (1986) A simple biosphere model (SiB) for use within General Circulation Models. J Atmos Sci 43:505–531.

Shaw RH, Pereira AR (1982) Aerodynamic roughness of a plant canopy: a numerical experiment. Agric Meteorol 26:51–65.

Shuttleworth WJ, Gurney RJ (1990) The theoretical relationship between foliage temperature and canopy resistance in sparse crops. Q J R Meteorol Soc 116:497–519.

Shuttleworth WJ, Wallace JS (1985) Evaporation from sparse crops – an energy combination theory. Q J R Meteorol Soc 111:839–855.

Sinoquet H (1993) Modelling radiative transfer in heterogeneous canopies and intercropping system. In: Varlet-Grancher C, Bonhomme R, Sinoquet H (Eds), Crop Structure and Light Microclimate: Characterization and Applications. INRA, Paris, pp. 229–252.

Sinoquet H, Moulia B, Bonhomme R (1991) Estimating the three-dimensional geometry of maize crop as input to radiation models: Comparison between three-dimensional digitizing and plant profiles. Agric Forest Meteorol 55:233–249.

Sinoquet H, Stephan J, Sonohat G, Lauri PÉ, Monney Ph (2007) Simple equations to estimate light interception by isolated trees from canopy structure features: assessment with three-dimensional digitized apple trees. New Phytologist 175:94–106.

Snyder RL, Paw U KT, Spano D, Duce P (1997) Surface renewal estimates of evapotranspiration. Theory. Acta Hort 449:49–56.

Snyder RL, Spano D, Duce P, Paw U KT, Rivera M (2008) Surface renewal estimation of pasture evapotranspiration. J Irrig Drain Eng 134:716–721.

Snyder RL, Spano D, Paw U KT (1996) Surface renewal analysis for sensible heat and latent heat flux density. Boundary-Layer Meteorol 77:249–266.

Sogachev A, Lloyd JJ (2004) Using a one-and-a-half order closure model of the atmospheric boundary layer for surface flux footprint estimation. Boundary-Layer Meteorol 112:467–502.

Sogachev A, Sedletske A (2006) SCADIS ‘‘footprint calculator’’: operating manual. In: Kulmala M, Lindroth A, Ruuskanen T (Eds), Proceedings of BACCI, NECC and FCoE Activities 2005, Book B. Report Series in Aerosol Science, vol. 81B, pp. 543–553.

Spano D, Duce P, Snyder RL, Paw U KT (1997a) Surface renewal estimates of evapotranspiration. Tall canopies. Acta Hort 449:63–68.

Spano D, Snyder RL, Duce P, Paw U KT (1997b) Surface renewal analysis for sensible heat flux density using structure functions. Agric Forest Meteorol 86:259–271.

Spano D, Snyder RL, Duce P, Paw U KT (2000) Estimating sensible and latent heat flux densities from grape vine canopies using surface renewal. Agric Forest Meteorol 104:171–183.

Stannard DI (1993) Comparison of Penman-Monteith, Shuttleworth-Wallace, and modified Priestley-Taylor evapotranspiration models for wildland vegetation in semiarid rangeland. Water Res Res 5:622–633.

Stewart JB (1988) Modelling surface conductance of pine forest. Agric Forest Meteorol 43:19–35.

Stewart JB, Kustas WP, Humes KS, Nichols WD, Moran MS, de Bruin HAR, (1994) Sensible heat flux-surface radiometric temperature relationship for eight semi-arid areas. J Appl Meteorol 33:1110–1117.

Stewart JB, Shuttleworth WJ, Blyth K, Lloyd CR (1989) FIFE: a comparison between aerodynamic surface temperature and surface radiometric temperature over sparse prairie grass. 19th Conf Agric Forest Meteorol, Charleston, South Carolina, March 1989, pp. 144–146.

Stull RB (1988) An Introduction to Boundary Layer Meteorology. Kluwer Academic Publishers, Dordrecht, 666 pp.

Sugita M, Kawakubo N (2003) Surface and mixed-layer variance methods to estimate regional sensible heat flux at the surface. Boundary-Layer Meteorol 106:117–145.

Swift LW (1976) Algorithm for solar radiation on mountain slopes. Water Resour Res 12:108–112.

Swinbank WC (1951) Measurement of vertical transfer of heat and water vapour by eddies in the lower atmosphere. J Meteorol 8:135–145.

Tanner CB (1960) Energy balance approach to evapotranspiration from crops. Soil Sci Proc Amer 24:1–9.

Thom AS (1971) Momentum absorption by vegetation. Q J R Meteorol Soc 97:414–428.

Thom AS (1972) Momentum, mass and heat exchange of vegetation. Q J R Meteorol Soc 98:124–134.

Thorpe MR (1978) Net radiation and transpiration of apple trees in rows. Agric Meteorol 19:41–57.

Tillman JE (1972) The indirect determination of stability, heat and momentum fluxes in the atmospheric boundary layer from simple scalar variables during dry unstable conditions. J Appl Meteorol 11:783–792.

Tourula T, Heikinheimo M (1998) Modelling evapotranspiration from a barley field over the growing season. Agric Forest Meteorol 91:237–250.

Troufleau D, Lhomme JP, Monteny B, Vidal A (1997) Sensible heat flux and radiometric surface temperature over sparse Sahelian vegetation. I. An experimental analysis of the kB^{-1} parameter. J Hydro 188–189:815–838.

Twine TE, Kustas WP, Norman JM, Cook DR, Houser PR, Meyers TP, Prueger JH, Starks PJ, Wesely ML (2000) Correcting eddy-covariance flux underestimates over a grassland. Agric Forest Meteorol 103:279–300.

United Nations (2006) Water: a Shared Responsibility. The 2nd United Nations world water development report. UNESCO publishing, Paris, France and Berghahn Books, New York, USA.

United Nations (2009a) World Population Prospects: The 2008 Revision. Department of Economics and Social Affairs, Population Division, New York, 2009.

United Nations (2009b) Water in a changing world. The 3rd United Nations world water development report. UNESCO publishing, Paris, France and Earthscan, London, UK.

Unland HE, Houser PR, Shuttleworth WJ, Yang Z-L (1996) Surface flux measurement and modeling at a semi-arid Sonoran Desert site. Agric Forest Meteorol 82:119–153.

van Atta CW (1977) Effect of coherent structures on structure functions of temperature in the atmospheric boundary layer. Arch Mech 29:161–171.

Vesala T, Kljun N, Rannik U, Rinne J, Sogachev A, Markkanen T, Sabelfeld K, Foken T, Leclerc MY (2008) Flux and concentration footprint modelling: State of the art, Environ Pollution 152:653–666.

Vugts HF, Waterloo MJ, Beekman FJ, Fruhmau KF, Bruijnzeel LA (1993) The temperature variance method, a powerful tool in the estimation of actual evapotranspiration rates. IAHS Publ 216:251–260.

Wallace JS (1997) Evaporation and radiation interception by neighbouring plants. Q J R Meteorol Soc 123:1885–1905.

Wallace JS, Batchelor CH, Dabeesing DN, Soopramanien GC (1990) The partitioning of light and water in drip irrigated plant cane with maize intercrop. Agric Forest Meteorol 17:235–256.

Wallace JS, Roberts JM, Sivakumar MVK (1990) The estimation of transpiration from sparse dryland millet using stomatal conductance and vegetation indices. Agric Forest Meteorol 51:35–49.

Wang K-Y, Kellomaki S, Zha T, Peltola H (2004) Seasonal variation in energy and water fluxes in a pine forest: an analysis based on eddy covariance and an integrated model. Ecol Model 179:259–279.

Wang YP, Jarvis PG (1990) Description and validation of an array model – MAESTRO. Agric Forest Meteorol 51:257–280.

Weaver HL (1990) Temperature and humidity flux-variance relations determined by one-dimensional eddy correlation. Boundary-Layer Meteorol 53:77–91.

Weber RO (1999) Remarks on the definition and estimation of friction velocity. Boundary–Layer Meteorol 93:197–209.

Weiss A, Norman JM (1985) Partitioning solar radiation into direct and diffuse, visible and near-infrared components. Agric Forest Meteorol 34:205–213.

Wesely ML (1988) Use of variance techniques to measure dry airsurface exchange rates. Boundary-Layer Meteorol 44:13–31.

Wesson KH, Katul G, Lai C-T (2001) Sensible heat flux estimation by flux-variance and half-order time derivative methods. Water Resour Res 37: 2333–2343.

Wever LA, Flanagan LB, Carlson PJ (2002) Seasonal and interannual variation in evapotranspiration, energy balance and surface conductance in a northern temperate grassland. Agric Forest Meteorol 112:31–49.

Willmott C J (1981) On the validation of models. Phys Geog 2:184–194.

Willmott CJ (1982) Some comments on the evaluation of model performance. Bull Am Met Soc 63:1309–1313.

Wilson K, Goldstein A, Falge E, Aubinet M, Baldocchi D, Berbigier P, Bernhofer C, Ceulemans R, Dolman H, Field C, Grelle A, Ibrom A, Law BE, Kowalski A, Meyers T, Moncrieff J, Monson R, Oechel W, Tenhunen J, Valentini R, Verma S (2002) Energy balance closure at FLUXNET sites. Agric Forest Meteorol 113:223–243.

Wilson KB, Baldocchi DD (2000) Seasonal and interannual variability of energy fluxes over a broadleaved temperate deciduous forest in North America. Agric Forest Meteorol 100:1–18.

Wilson KB, Baldocchi DD, Marc A, Berbigier P, Bernhofer C, Dolman H, Falge E, Field C, Goldstein A, Granier A, Grelle A, Halldor T, Hollinger D, Katul G, Law BE, Lindroth A, Meyers T, Moncrieff J, Monson R, Oechel W, Tenhunen J, Valentini R, Verma S, Vesala T, Wofsy S (2002) Energy partitioning between latent and sensible heat flux during the warm season at FLUXNET sites. Water Resour Res 38:1294-1295, doi:10.1029/2001WR000989, 2002.

Wyngaard JC, Cote OR, Izumi Y (1971) Local free convection, similarity and the budgets of shear stress and heat flux. J Atmos Sci 28:1171–1182.

Zapta N, Martínez-Cob A (2001) Estimation of sensible and latent heat flux from natural sparse vegetation surfaces using surface renewal. J Hydro 254: 215–228.

Zhongmin H, Guirui Y, Yanlian Z, Xiaomin S, Yingnian L, Peili S, Yanfen W, Xia S, Zemei Z, Li Z, Shenggong L (2009) Partitioning of evapotranspiration and its controls in four grassland ecosystems: application of a two-source model. Agric Forest Meteorol 149:1410–1420.